JUSTUS-LIEBIG-
UNIVERSITÄT
GIESSEN

JAZF1: a novel p400/TIP60/NuA4 complex member involved in the acetylation of H2A.Z

Dissertation

zur Erlangung des Doktorgrades der Naturwissenschaften

(Dr. rer. nat.)

vorgelegt von

Tara Procida

aus Frankfurt am Main

Justus-Liebig-Universität Giessen

Fachbereich 08 – Biologie und Chemie

Institut für Genetik

Leitung: Prof. Dr. rer. nat. Sandra B. Hake

2021

Eidesstattliche Versicherung

Ich erkläre: Ich habe die vorgelegte Dissertation selbstständig und ohne unerlaubte fremde Hilfe und nur mit den Hilfen angefertigt, die ich in der Dissertation angegeben habe. Alle Textstellen, die wörtlich oder sinngemäß aus veröffentlichten Schriften entnommen sind, und alle Angaben, die auf mündlichen Auskünften beruhen, sind als solche kenntlich gemacht. Ich stimme einer evtl. Überprüfung meiner Dissertation durch eine Antiplagiat-Software zu. Bei den von mir durchgeführten und in der Dissertation erwähnten Untersuchungen habe ich die Grundsätze guter wissenschaftlicher Praxis, wie sie in der „Satzung der Justus-Liebig-Universität Gießen zur Sicherung guter wissenschaftlicher Praxis" niedergelegt sind, eingehalten.

Statement of authorship

I declare that I have completed this dissertation single-handedly without the unauthorized help of a second party and only with the assistance acknowledged therein. I have appropriately acknowledged and cited all text passages that are derived verbatim from or are based on the content of published work of others, and all information relating to verbal communications. I consent to the use of an anti-plagiarism software to check my thesis. I have abided by the principles of good scientific conduct laid down in the charter of the Justus Liebig University Giessen „Satzung der Justus-Liebig-Universität Gießen zur Sicherung guter wissenschaftlicher Praxis" in carrying out the investigations described in the dissertation.

Gießen, 06.10.2021   _____

Ort, Datum   (Tara Procida)

DANKSAGUNG

An dieser Stelle möchte ich mich bei allen Kollegen, Kollaborationspartnern, Freunden und meiner Familie bedanken, die wesentlich zum Gelingen der hier vorliegenden Arbeit beigetragen haben. *Aus tiefstem Herzen danke ich dir…*

…Sandra B. für deine Unterstützung, deine Betreuung, deine Herzlichkeit, deine Hilfsbereitschaft, deinen wissenschaftlichen Input und vieles mehr. Besonders danke ich dir dafür, dass ich Teil deines tollen Teams sein durfte und meine Arbeit bei dir anfertigen konnte. Du bist eine ganz tolle Chefin mit sehr viel Menschlichkeit und den besten wissenschaftlichen Präsentationen aller Zeiten!

…Marek für deine tatkräftige Unterstützung bei dem Projekt, die bioinformatischen Analysen, die vielen tollen Diskussionen und für die Begutachtung meiner Thesis als Zweitgutachter.

…Klonierungsexperte Jörg für deine kompetente Hilfe im Labor und deine überaus aufschlussreichen Anekdotenerzählungen.

…Nadine für deine stetige Hilfe, dein Engagement und deine Zuverlässlichkeit. Wann immer ich deine Hilfe benötigt habe, du warst für mich da.

…Labmanagerin Sonja für deine Beharrlichkeit in sämtlichen Angelegenheiten die das Labor betreffen. Aber auch danke dafür, dass du mir tagtäglich den Tag versüßt hast mit deiner positiven Einstellung.

…Anna für deine klugen Ratschläge und Lebensweisheiten sowie deine Mithilfe bei allen organisatorischen Aufgaben.

…Tim für deine Hilfsbereitschaft, deine Geduld, deine lustige Art und viele tolle Gespräche! Ohne dich wäre es sicher nur halb so schön im Lab gewesen.

…Sandy für deine immerwährende Hilfsbereitschaft sowohl in privaten wie auch in wissenschaftlichen Belangen.

…Andreas für deine Hilfe bei vielen wissenschaftlichen Fragen und Problemen.

…Lena Vogel für deine Unterstützung im Labor sowie vielen geselligen Gesprächen während unserer kleinen Päuschen.

…Tobi für deinen Support bei allen bioinformatischen Analysen und Fragen. Ich konnte dich zu jeder Zeit kontaktieren!

…Kostja for your motivation, your scientific input and for always being positive.

…Carlotta für deine unaufhörliche Fröhlichkeit, die auch mich ab und zu angesteckt hat. Du bist und bleibst der Sonnenschein des Instituts.

…Lena W. für deine motivierende Art und deinen moralischen Beistand in jeglicher Situtation.

…Mama & Papa für eure stetige Unterstützung!

…Philip & Ira für einfach alles!!!

Ein herzliches Dankeschön geht auch an die Justus-Liebig-Universität Giessen für die finanzielle Förderung meines Promotionsvorhabens über das Graduierten-stipendium. Auch den übrigen derzeitigen und ehemaligen Mitgliedern der Arbeitsgruppe, sowie all meinen Gießener Freunden und meinen Alsfelder Girls möchte ich danken, die immer an mich geglaubt haben und für mich da waren.

TABLE OF CONTENTS

SUMMARY

In the nucleus of eukaryotic cells, the DNA occurs with histone proteins that package the DNA into the repeating subunit of chromatin, the nucleosome. This basic functional entity consists of two copies of each canonical histone H2A, H2B, H3 and H4, where the DNA is wrapped around. In order to allow DNA-related processes to gain access to the compacted DNA, different epigenetic regulatory mechanisms have evolved, in which the exchange of canonical histones with their specific variants is one possibility. The evolutionary conserved histone protein H2A.Z is one of the most intensively studied H2A variants that is involved in several biological processes such as transcriptional regulation with sometimes contrasting functions. To accomplish its diverse and at the same time controversial roles, H2A.Z requires the concerted action of unique multi-subunit histone variant-specific exchangers, responsible for its dedicated loading – and removal – into specific chromatin regions. In metazoans, H2A.Z incorporation is tightly regulated by the multifunctional p400/TIP60/NuA4 (p400) and SRCAP chaperone/remodelling complexes. However, it is still unclear, whether other, not yet identified proteins, are also implicated in the chromatin deposition of H2A.Z. Hence, a quantitative mass spectrometry (qMS) approach was employed to gain more insights into H2A.Z's chromatin-free interactome. Besides all members of both known chaperone complexes, also new interactors were identified that were formerly not related to H2A.Z deposition. Among others, the proposed transcriptional regulator Juxtaposed with another zinc finger 1 (JAZF1) was discovered as a novel member of an H2A.Z-specific p400 sub-complex that contains MBTD1 but excludes ANP32E. Since JAZF1 is functionally poorly characterized and has frequently been linked to human diseases such as sarcomas, I aimed to unravel the functions of JAZF1, especially with regard to the role it may play within the H2A.Z-specific p400 complex. First preliminary data hint towards a role of JAZF1 in the regulation of DNA damage repair processes, as it has already been shown for other p400 complex components. Moreover, RNA-seq experiments demonstrated that depletion of the putative transcription factor JAZF1 results in the deregulation of several genes involved not only in DNA repair, but also above all in ribosome biogenesis. To identify the underlying molecular mechanism by which JAZF1 might control transcriptional regulation of genes, the genome-wide level of H2A.Z and H2A.Zac upon JAZF1 depletion via ChIP-seq analyses were evaluated. Remarkably, >1.000 genomic sites that were significantly deregulated in H2A.Zac levels upon loss of JAZF1 were identified, while H2A.Z levels and locations remained unaffected. Since depletion of TIP60, the histone acetyltransferase of the p400 complex, also

SUMMARY

causes decreased acetylation of H2A.Z at some JAZF1-targeted regulatory enhancer regions, it is possible that JAZF1's function in gene regulation might depend on the enzymatic activity of the TIP60-containing p400 complex. Therefore, I propose JAZF1 as a chromatin modulator, which orchestrates acetylation of the histone variant H2A.Z via recruiting the enzymatic active p400 complex to respective sites, thereby controlling expression of target genes. Altogether, this study contributes to a better understanding of the largely unknown functions of JAZF1 and may thus provide a starting point for future research to clarify its putative role in the development of diseases such as human sarcomas.

ZUSAMMENFASSUNG

Im Zellkern eukaryotischer Zellen tritt die DNA mit Histonproteinen auf, welche die DNA in die sich wiederholende Untereinheit des Chromatins verpacken, dem Nukleosom. Diese grundlegende funktionelle Einheit besteht aus zwei Kopien jedes kanonischen Histons H2A, H2B, H3 und H4, um welche die DNA gewunden ist. Um DNA-basierten Prozessen den Zugang zur kompaktierten DNA zu ermöglichen, enstanden verschiedene epigenetische Regulationsmechanismen, wovon der Austausch von kanonischen Histonen durch eine spezifische Variante eine Möglichkeit darstellt. Das evolutionär konservierte Histonprotein H2A.Z ist eine der am intensivsten untersuchten H2A Varianten, das an einer Vielzahl biologischer Prozesse wie der Transkriptionsregulation, mit teilweise gegensätzlichen Funktionen, beteiligt ist. Um seine vielfältigen und zum Teil kontroversen Aufgaben erfüllen zu können, erfordert H2A.Z die aufeinander abgestimmte Aktion einzigartiger, multimerer Chaperon- und Remodellierungskomplexe, die für den koordinierten Einbau – oder Ausbau – von H2A.Z in bestimmte Chromatinregionen verantwortlich sind. Bei Metazoen wird dieser Prozess durch zwei multifunktionelle Komplexe, dem p400/TIP60/NuA4 (p400) und dem SRCAP Komplex, streng reguliert. Es ist jedoch unklar, ob weitere, noch nicht identifizierte Proteine ebenfalls am Austausch von H2A.Z beteiligt sind. Daher wurde quantitative Massenspektromterie (qMS) angewendet, um mehr Einblicke in das chromatinfreie Interaktom von H2A.Z zu erhalten. Neben allen Mitgliedern beider bekannter H2A.Z-spezifischen Chaperonkomplexe, wurden auch neue Interaktoren detektiert, die bisher nicht mit dem H2A.Z-Einbau in Zusammenhang standen. Unter anderem wurde das als Transkriptionsregulator vorgeschlagene Protein Juxtaposed with another zinc finger 1 (JAZF1) als ein neues Mitglied eines H2A.Z-spezifischen p400 Subkomplexes, der MBTD1 enthält, jedoch ANP32E ausschließt, identifiziert. Da JAZF1 funktionell unzureichend untersucht ist und häufig mit humanen Erkrankungen wie Sarkomen in Verbindung gebracht wurde, war das Ziel meines Forschungsvorhabens, die Charakterisierung der Funktionen von JAZF1, insbesondere im Hinblick auf die Rolle, die JAZF1 innerhalb des H2A.Z-spezifischen p400 Komplexes spielen könnte. Erste vorläufige Daten deuten darauf hin, dass JAZF1 in der Regulation von DNA-Reparaturprozessen involviert ist, wie es bereits für andere p400 Komplexmitglieder bewiesen werden konnte. Darüber hinaus zeigten RNA-seq Experimente, dass die Depletion des mutmaßlichen Transkriptionsfaktors JAZF1 zur Deregulierung mehrerer Gene führt, die nicht nur an der DNA-Reparatur, sondern vor allem auch an der Ribosomenbiogenese beteiligt sind. Um den zugrundeliegenden molekularen

ZUSAMMENFASSUNG

Mechanismus aufzudecken, durch den JAZF1 die Transkription von Genen steuert, wurde die genomweite Anreicherung von H2A.Z sowie H2A.Zac nach der Herrunterregulierung von JAZF1 mit Hilfe von ChIP-seq Analysen bewertet. Bemerkenswerterweise führte der Verlust von JAZF1 zu einer Deregulierung der Acetylierung von H2A.Z an >1.000 genomischen Stellen, während das Level und die Lokalisierung von H2A.Z unverändert blieben. Da die Depletion der Histonacetyltransferase TIP60 des p400 Komplexes auch eine verminderte Acetylierung von H2A.Z an einigen JAZF1-spezifischen regulatorischen Enhancer-Regionen verursachte, ist es möglich, dass JAZF1's spezifische Funktion in der Genregulation von der enzymatischen Aktivität des TIP60-enthaltenden p400 Komplexes abhängt. Daher schlage ich JAZF1 als ein Chromatinmodulator vor, der die Acetylierung der Histonvariante H2A.Z durch die Rekruitierung des enzymatisch aktiven p400 Komplexes zu spezifischen Regionen koordiniert und dadurch die Expression von Zielgenen steuert. Insgesamt trägt diese Studie zu einem besseren Verständnis der weitgehend unbekannten Funktionen von JAZF1 bei und könnte somit einen Ansatzpunkt für zukünftige Forschungen bieten, um die Beteiligung von JAZF1 an der Entstehung von Erkrankungen wie menschlicher Sarkome klären zu können.

1 INTRODUCTION

1.1 The basic structure of chromatin

DNA is the fundamental carrier of genetic information [1] that provides essential instructions for all living organisms including cell metabolism, development and genetic inheritance [2]. It acts as a repository and versatile coding device [3] by its special composition, structure and its unique shape. Over 60 years ago, DNA was identified as a right-handed double helix structure consisting of two helical chains that coil around the same axis [4]. These two chains are connected by complementary base pairing of purine (adenine, guanine) and pyrimidine bases (cytosine, thymine) [4]. One of the four nucleobases, together with a phosphate group and a sugar moiety, form a nucleotide - the basic unit of DNA [5]. The chemical linkage between these molecules leads to the polymerization of a long nucleic acid chain of repetitive nucleotides that bear the genetic information [6]. The human genome, for instance, consists of approximately three billion base pairs of DNA [7–9] and is predominantly organized into chromosomes which are stored within the cells nucleus [10]. If the DNA of one human cell is stretched to its full length, it would reach a total length of about two meters [5, 10, 11]. However, a mammalian nucleus has an average diameter of only 6 µm [12, 13]. Raising the question of how DNA fits into the nucleus of a eukaryotic cell. Here chromatin comes into play, which was first described and termed by Walter Flemming in 1882 [14, 15]. In eukaryotes, the DNA is not present as a naked and relaxed molecule but occurs with small proteins that package the DNA into structural units, the so-called nucleosomes [16, 17] (Figure 1). These DNA-binding proteins, better known as histone proteins [18] (Figure 1A), form nucleoprotein complexes to compress the eukaryotic genetic material into a compact and dynamic functional organization that can fit into the cells nucleus [19]. Basically, chromatin exists as a repeating structure of nucleosomes [17, 20, 21] (Figure 1B), which in turn consist of approximately 146 base pairs of left-handed DNA that is wrapped 1.65 times around a disk-shaped, octameric histone core composed of two copies of each of the canonical histones H2A, H2B, H3 and H4 [22–26] (Figure 1C).
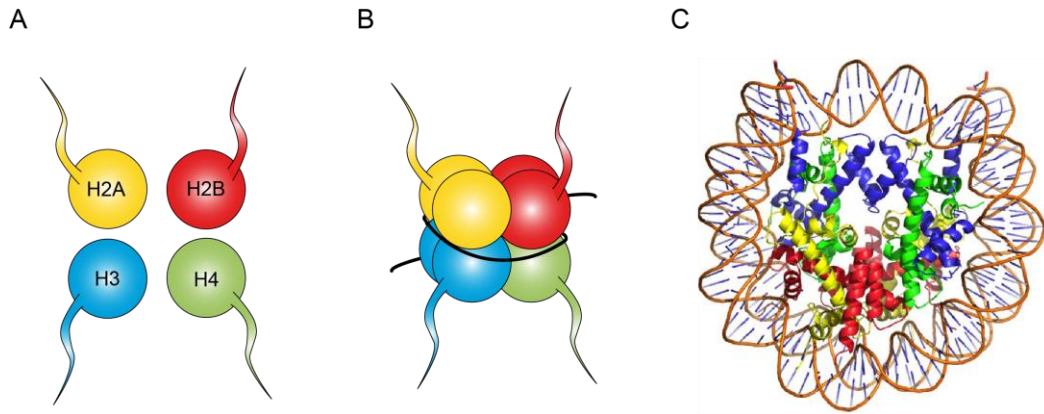
Figure 1: Schematic representation and crystal structure of the repeating unit of chromatin. (**A**) Depiction of the canonical core histone proteins. H2A is shown in yellow, H2B in red, H3 in blue and H4 in green. (**B**) The superhelical DNA (black) is wrapped around a histone octamer consisting of two copies of each histone H2A (yellow), H2B (red), H3 (blue) and H4 (green). Such a formation of histone octamer and DNA is referred to as nucleosome/nucleosome core particle (NCP). The N-terminal tails of the core histones, which extend from the histone octamer surface, are favourite point for posttranslational modifications. (**C**) Crystal structure of a nucleosome as described in (B). The DNA is depicted in orange, H2A in yellow, H2B in red, H3 in blue and H4 in green. Figure C is adapted and reprinted from Nature Scientific Reports [26].

This fundamental and functional building block is known as the nucleosome core particle (NCP) [27], whose assembly is facilitated by interactions of two structurally and functionally distinct regions of the core histones: the histone fold domain (HFD) and the histone tail [28]. Although sequence similarities are missing, the HFDs of the four canonical histones have a structural motif in common that mediates the interplay between histones and DNA [29]. The HFDs are shaped by three alpha-helices (α1-α3) connected by two short loops, L1 and L2 [30]. In solution, the core histones accumulate to heterodimers, where H2A only pairs with H2B and H3 only with H4 [29]. While H3 and H4 form a tetramer of two H3-H4 dimers via a four-helix bundle arrangement of the H3 HFDs, H2A and H2B, in contrast, aggregate to H2A-H2B dimers, which exhibit only minor contacts to the second H2A-H2B heterodimer [29]. In the presence of DNA or under high salt conditions, two H2A-H2B dimers and one (H3-H4)$_2$ tetramer are able to assemble and persist as an octamer, which is supported by the formation of a four-helix bundle that connects H2B and H4 [29]. In order to guarantee further stability, a second interaction is formed between the unstructured C-terminus of H2A (docking domain) and H3 [29]. The interplay between DNA and core histones is not base-specific but rather occurs as a result of extensive electrostatic and hydrogen-bonding interactions [31, 32]. The minor groove of the DNA, which possesses a highly negative charge due to its phosphate backbone,

interacts at 14 positions with the histone octamer [28, 29, 33]. In addition, the positively charged N-terminal tails of histones are able to associate with the DNA as well as with the histone octamer surface of neighbouring nucleosomes [28, 31, 34]. Accordingly, these disordered histone tails are particularly involved in stabilizing the DNA within a NCP and organizing higher-order chromatin structures [31, 32, 35–38]. It is therefore not surprising, that posttranslational modifications (PTMs) of histone proteins, like acetylation or phosphorylation, play a key role in nucleosome stability and dynamics by altering the energy landscape of histone-DNA and histone-histone interactions [32].

The linkage of NCPs is achieved by short DNA segments (referred to as linker DNA), which mediate the arrangement and the connection of NCPs with each other to constitute a primary chromatin structure, the so-called 'beads on a string' nucleosome array [16, 17, 39] (Figure 2). This functional and dynamic organization can be observed as a nucleosomal chain of about 10 nm in diameter by electron microscopy, where the nucleosomes appear as the 'beads' and the nucleosome-separating linker DNA as the 'string' [40].
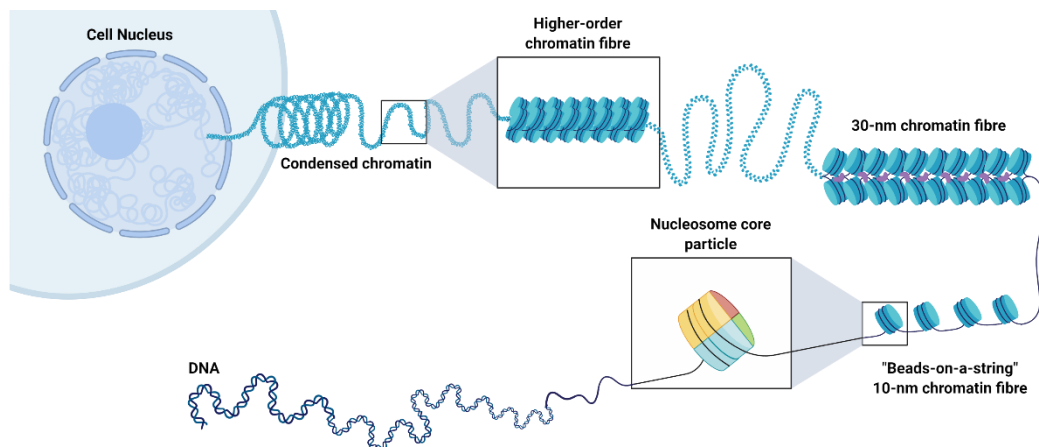
Figure 2: Schematic representation of different structural chromatin states. The DNA is tightly packed into the functional organization of chromatin, with the nucleosome core particle as its fundamental building block. Based on the degree of compaction, different structural states of chromatin exist. Nucleosomes, which are connected via linker DNA, form the primary so-called 'beads on a string' structure. Further organization of the nucleosome array by short-range interactions leads to the generation of the proposed secondary chromatin structure, termed 30-nm chromatin fibre. Subsequent interactions between the chromatin fibres contribute to the formation of higher-order chromatin fibres (tertiary chromatin structure) that finally condense to build the entire chromosome (not shown) [36]. Histone H2A is shown in yellow, H2B in red, H3 in blue, H4 in green and H1, which binds internucleosomal linker DNA, in purple. Figure created with BioRender.com.

Moreover, the nucleosome-associated histone H1 binds internucleosomal linker DNA and promotes further compaction of the chromatin fiber by binding 20 additional bp of DNA, which flank the entry/exit site in the nucleosome [41] (Figure 2). Such an arrangement of one histone octamer, a linker histone H1 and a total of approximately 166 bp of DNA is referred to as the chromatosome [42, 43]. In addition, there are numerous architectural chromatin-binding proteins, such as Heterochromatin protein 1 (HP1), Methyl-CpG-binding protein 2 (MeCP2) or Polycomb group proteins, which can modulate chromatin structure as well [44]. *In vitro* data suggest that under physiological salt concentrations the chromatin fiber can be further reversibly folded into a secondary chromatin conformation, which is characterized by a diameter of approximately 30 nm [45–47] (Figure 2). However, thus far no *in vivo* evidence of the 30-nm fiber could be obtained nor could the exact structure be solved. Currently two competing models for the proposed chromatin arrangement exist: the solenoid and the zigzag model [48]. For more detailed and comprehensive informations see [39, 49–52].

The structural organization of chromatin not only plays a role in packaging the DNA into a nucleus of an eukaryotic cell, but it also regulates the accessibility of DNA for various DNA-related processes [53]. Both, the architectural proteins as well as the briefly mentioned N-terminal tails of histones and their posttranslational modifications, are crucial for chromatin compaction and for maintaining higher-order chromatin states, thereby influencing DNA packaging dynamics. However, there are also other ways to ensure DNA accessibility for all processes that require direct access to the DNA. In the following section various mechanisms regulating chromatin structure are described in more detail.

1.2   The epigenetics of chromatin complexity

The eukaryotic DNA is tightly packaged into the highly dynamic organization of chromatin that has an inhibitory effect on all DNA-related processes. Based on the degree of compaction, two major functional states of chromatin exist: eu- and heterochromatin [54]. While euchromatin is less condensed and in general more transcriptionally active, heterchromatin, in contrast, has been shown to be more densely packed, and can be further subdivided into permanently (constitutive) or temporarily transcriptionally silent (facultative) chromatin [55, 56]. In addition to transcription, DNA accessibility must be guaranteed for other DNA-associated processes such as replication, DNA damage repair or recombination [53]. Prompting

the question of how alteration of those chromatin states is achieved. Here the term epigenetics comes into play that was first characterized by Waddington in 1942 [57]. It describes functional changes to the genome without altering the DNA sequence itself [58]. Instead, DNA packaging dynamics and chromatin conformations are modulated via several epigenetic mechanisms including DNA methylation, long noncoding RNAs (lncRNAs), ATP-dependent chromatin remodelling, PTMs of histone proteins and incorporation of histone variants [59] (Figure 3).
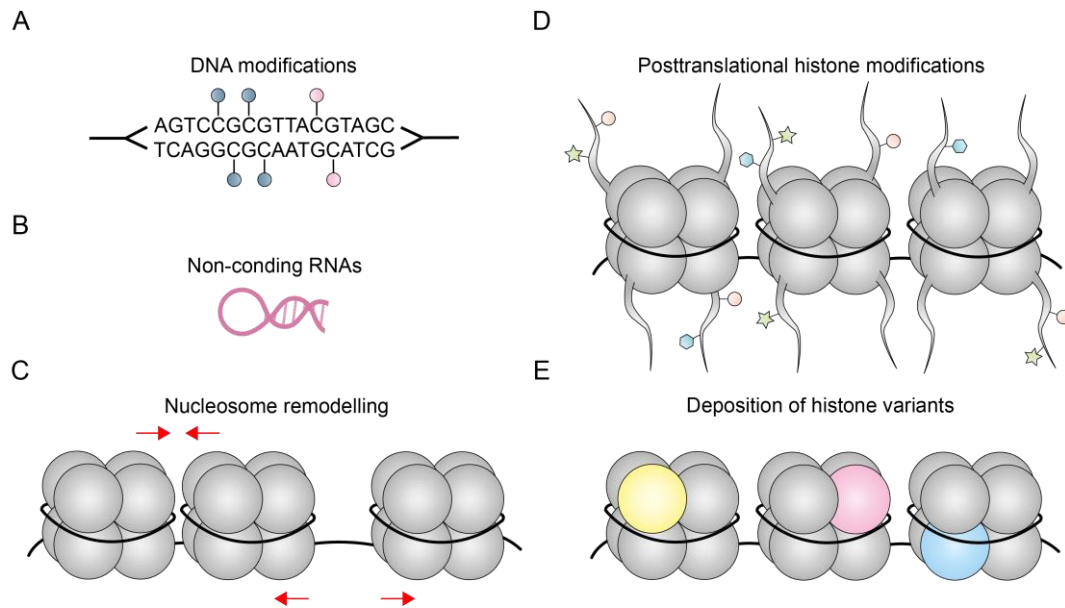
Figure 3: Different types of chromatin regulatory mechanisms. Chromatin structure can be modulated by (**A**) DNA methylation (blue dot) or hydroxymethylation (red dot), (**B**) non-coding regulatory RNAs (ncRNAs), (**C**) nucleosome remodelling such as sliding of nucleosomes (red arrows), (**D**) posttranslational modifications (PTMs) of histone proteins such as acetylation (orange circle), methylation (blue hexagon) or phosphorylation (green star), among many others, (**E**) exchange of canonical core histones with their variants e.g. H2A.Z (light yellow), testis-specific TSH2B (light red) or H3.3 (light blue).

1.2.1 Methylation, the most famous mark of DNA

In mammals, one of the major epigenetic processes regulating chromatin architecture is DNA methylation that occurs mainly at cytosine residues (5-methylcytosine, 5mC) especially in a CpG (cytosine-phosphate-guanine) dinucleotide context [60] (Figure 3A). The attachment of methyl groups to CpG-dense promoter regions leads to the impeded binding of transcription factors and probably even more important, it also acts as a platform for several proteins that modify histones to grant the formation of transcriptionally inactive heterochromatin [61, 62]. For this reason, DNA methylation is mainly associated with gene silencing [63], but in addition to gene regulation, it is

also linked to other essential biological processes such as genomic imprinting, X-chromosome inactivation or cell differentiation [59]. The establishment and maintenance of CpG methylation is ensured by two distinct groups of DNA methyltransferases (DNMTs) [64]. The *de novo* methyltransferases DNMT3A and DNMT3B are responsible for the establishment of DNA methylation [65], whereas DNMT1 is critical for the preservation of methyl groups of the progeny strand during DNA replication [66]. Therefore, both groups of enzymes are essential for the establishment of the transcriptional repressive epigenetic mark and, moreover, they contribute to the maintenance of the cellular phenotype by carrying on the methylation patterns into subsequent generations [63, 67]. In contrast, DNA demethylation can occur either passively by inhibiting DNMT1 activity during cell division, thereby reducing overall methylation levels, or actively, independently of DNA replication [68–70]. Active DNA demethylation is mediated by the Ten-eleven translocation (Tet) enzymes (Tet1, Tet2, Tet3), which oxidize 5mC to 5-hydroxymethyl-cytosine (5hmC), which in turn can be further iteratively converted into 5-formyl-cytosine (5fC) and then to 5-carboxy-cytosine (5caC) [69] followed by base excision repair (BER) and cytosine replacement [70]. Since 5hmC has been shown to impair the binding of the repressive methyl-binding protein MeCP2, which usually promotes chromatin condensation and inactivation, thereby regulating gene expression, it is proposed that 5hmC does not only function as an intermediate in DNA demethylation [69, 71–74]. Overall, it is therefore not surprising that deregulation of these tightly controlled processes, leading to aberrant DNA methylation patterns, has been associated with human diseases such as cancer [75].

1.2.2 Long noncoding RNA (lncRNA) as key regulatory molecules

In addition to DNA methylation, another mechanism has evolved to regulate chromatin structure relying on long noncoding RNAs (lncRNAs) [76] (Figure 3B), which are typically defined as non-protein coding transcripts whose lengths exceed 200 nucleotides [77–79]. It is suggested that lncRNAs contribute to the regulation of chromatin structure by either recruiting histone modifying enzymes (see chapter 1.2.4) or DNMTs, which modify chromatin by posttranslational histone modifications or DNA methylation, respectively [78, 80]. Furthermore, RNA-mediated regulation of chromatin architecture can also be realized by controlling nucleosome positioning (see chapter 1.2.3) [78]. A large number of lncRNAs exist, which are often expressed in a temporal and spatial manner [81]. One example for mediating changes in

chromatin dynamics through lncRNAs is conveyed by the Hox transcript antisense RNA (HOTAIR), which induces a repressive chromatin state across the HOXD locus via recruiting the Polycomb repressive complex 2 (PRC2) for transcriptional silencing [81].

1.2.3 Machineries of chromatin remodelling

The occlusion of DNA in nucleosomes provides an obstacle for diverse biological processes such as transcription, replication or DNA damage repair. To resolve these limitations, nucleosomes have to be remodelled to gain access to the DNA, thereby allowing binding of various regulatory proteins. One way of chromatin regulation is realized by ATP-dependent nucleosome remodelling complexes [82] (Figure 3C). These macromolecular, often multiprotein, machines are able to modify chromatin structure by using ATP hydrolysis as a source of energy [83]. Nucleosome modulation can be conducted in different ways including evicting or unwrapping of nucleosomes, sliding of nucleosomes along the DNA or changing the nucleosomal composition by replacing core histones with their variants [84, 85]. Several nucleosome remodelling complexes exist, which are classified into different subfamilies according to their catalytic ATPase domain structure [86]. Currently, the best known subfamilies, in terms of function and formation, are the Switch/Sucrose non-fermentable (SWI/SNF), Imitation switch (ISWI), Chromodomain helicase DNA-binding protein (CHD) and Inositol-requiring 80 (INO80) families [86]. The enzymatic ATPase subunit is structurally specific for each complex and responsible for nucleosome remodelling activities [86, 87]. This subunit interacts with a large number of different proteins, thereby forming the multiple chromatin remodelling complexes, which differ in their characteristic, composition, functioning and remodelling activities [86]. Each of these activities results in the alteration of DNA accessibility, which is indispensable for DNA-related nuclear processes [88]. The members of the INO80 subfamily are unique among ATP-dependent remodelling complexes because of their ability to catalyze the exchange of canonical H2A-H2B from the nucleosome structure with a variant-containing H2A.Z-H2B dimer [88]. In mammals, three complexes of the INO80 subfamiliy exist named INO80, Snf2 related CREBBP activator protein (SRCAP) and p400/NuA4/Tip60 (p400) [89]. Due to the special importance for this thesis, the different members of the INO80 subfamily and their comprehensive functions are described in more detail in the section 1.3.1 below.

1.2.4 A landscape of histone modifications

As already mentioned, not only DNA but also histone proteins can be covalently modified (Figure 3D) to regulate structural and dynamic changes in nucleosome positioning, which takes place in various ways, thereby allowing DNA-associated complexes to bind their target sites and exercise their functions [32]. To date, a large number of posttranslational histone modifications exist: acetylation, phosphorylation, methylation and ubiquitinylation of histones are the best known PTMs, whereas e.g. sumoylation, ADP ribosylation, glycosylation, propionylation, butrylation, formylation, crotonylation, deamination, succinylation, malonylation and lactylation of histones are not very well-studied [90–94]. Histone proteins can possess plenty of different PTMs that, in combination, encode the controversial 'histone code' [95]. The establishment of those reversible marks is tightly regulated and their interpretation into biological functions accomplished through a dynamic interplay between several proteins, which are referred to as histone 'writers', 'erasers' and 'readers' [95, 96]. While 'writers' deposit the respective modification, 'erasers', in contrast, can remove those marks [97]. There are two different ways – either directly or indirectly – how histone PTMs can influence chromatin structures [98]. The above-mentioned 'readers' have the potential to indirectly affect chromatin dynamics. They recognize and bind PTM-marked histones to mediate changes in nucleosome structure by recruiting other chromatin-associated factors [32]. Moreover, chaperones as well as chromatin remodellers are able to spot PTMs and modulate chromatin landscapes [32, 99–101]. The second way of modulating chromatin structure via histone PTMs is mediated directly through charge differences of histone residues, leading to extensive changes of electrostatic histone-DNA interactions [32]. Basically, the addition of PTMs to histone amino-acid residues either removes a positive charge – in case of acetylation – or introduces a negative charge – in case of phosphorylation –, thereby altering the energy landscape of interactions within the interfaces between DNA and histone proteins [32, 102]. Simply put, these functionally dynamic changes, which are a direct consequence of the addition or removal of PTMs, are caused by the formation or disruption of interactions between DNA and the nucleosomal components, which in turn influences positioning and stability of nucleosome structures [32]. While posttranslational histone modifications arise primarily on the unstructured N-terminal tail of histones, they can, on the other hand, also be found on the histone core domains [103]. Since this thesis mainly focuses on modifications of histone tails, only these structural domains and their best-studied PTMs will be further discussed.

However, there are a myriad of data available that partially unraveled the functions of core histone modifications [104–106].

The disordered histone tails protrude from the nucleosome core [107] and can be modified in various ways. Methylation of histone proteins is, among others, a well-examined modification that occurs on lysine (mono-, di- and trimethylation) and arginine residues (mono- and symmetric or asymmetric dimethylation) exhibiting different effects on gene activity [108]. Depending on the residues that are modified and the degree of modification, methylation can serve either as an active or repressive mark in regulating gene expression [108]. For instance, trimethylation of histone H3 lysine 4 (H3K4) and lysine 36 (H3K36) are typically gene-activating marks, while H3K4me3 is found to be enriched on promoters, H3K36me3 in turn is associated with gene bodies [108–110]. H3K4 can also be monomethylated (H3K4me1), which commonly marks enhancers [111]. Moreover, trimethylation of histone H3 lysine 27 (H3K27) and lysine 9 (H3K9) are generally linked to gene repression via the formation of facultative or constitutive hetechromatic landscapes, respectively [112, 113]. Beside its role in transcriptional regulation, histone methylation also plays an important role in DNA damage repair [114]. The dynamic methylation patterns are tightly regulated by lysine methyltransferases (KMTs) such as Enhancer of zeste homolog 2 (EZH2) [115], which have the potential to methylate target histone proteins, and by lysine demethylases (KDMs) such as members of the Jumonji domain-containing 2 (JMJD2) family [116], which, in contrast, remove those modifications [108]. Finally, Plant homeodomain (PHD), Tudor, Chromo, Malignant brain tumor (MBT) or Pro-trp-trp-pro (PWWP) domain-containing histone methylation 'reader' proteins such as HP1 or p53-binding protein (53BP1) can recognize methylation-marked histones and orchestrate actions on chromatin in order to regulate transcription or facilitate DNA damage repair [116].

In addition to methylation, histone proteins can also be phosphorylated on serine, threonine and tyrosine residues, thereby introducing a negative charge to the modified histone amino acid residue, which is catalyzed by a large number of protein kinases such as Aurora B, while the eviction of those groups takes place by phosphatases [117–119]. 14-3-3, BRCA1 C-terminus (BRCT) or Baculovirus inhibitor of apoptosis protein repeat (BIR) domain-containing 'reader' proteins such as Breast cancer type 1 susceptibility protein (BRCA1) or Survivin in turn recognize phospho-specific histone proteins and act in concert with complexes to orchestrate chromatin-associated processes [116, 119–121]. The phosphorylation of histones is an important modification that plays a major role in diverse processes including transcriptional regulation (e.g. phosphorylation of H3S10, H3S28 and H2BS32),

chromosome compaction during mitosis (phosphorylation of H3S10 and H3S28) and meiosis (phosphorylation of H4S1 and H2BS10), apoptosis (e.g. phosphorylation of H2BS10 and H3T45) and DNA damage repair (phosphorylation of H2A.XS139) [117, 122].

By far one of the most intensely studied histone modifications that plays a crucial role in this study, is the acetylation of the N-terminal histone ends [123]. In general acetylation takes place on conserved positively charged lysine amino acid residues present in the histone tails, which unlike to methylation leads to changes in electrostatic properties by charge neutralization, thereby reducing the affinity of histone proteins for negatively charged DNA [119, 124]. Additionally, it is assumed that acetylation alters histone interactivities of adjacent nucleosomes and abates interactions with other regulatory factors [32, 123]. This is believed to facilitate open chromatin structures whereby acetylation can be linked to transcriptionally active chromatin [123, 125]. The readout of this PTM is achieved by Bromodomain-containing (BRD) 'reader' proteins such as members of the Bromo- and extra-terminal (BET) family, with many of them involved in regulating transcription [119, 126]. The establishment and the elimination of acetylation patterns is tightly regulated by two different types of enzymes. Histone acetyltransferases (HATs), or alternatively called lysine acetyltransferases (KATs) [127], are essential for the setting of acetyl groups to lysines, while histone/lysine deacetylases (HDACs/KDACs), in contrast, are crucial for removing those marks [128]. A sizable number of KATs exist, which are grouped into five distinct subfamilies according to their catalytic domain [128–130]. The best-studied group of KATs belongs to the MYST family, which is named after its founding members: Monocytic leukemia zinc-finger protein-related factor (Morf), Something about silencing protein 3 (Ybf2/Sas3), Something about silencing protein 2 (Sas2) and TAT-interactive protein 60 kDa (TIP60) [129]. A key member of this family is TIP60 also referred to as Lysine acetyltransferase 5 (KAT5), which belongs to a multiprotein complex, namely the p400 chaperone/remodelling complex of the above-mentioned INO80 chromatin remodeller subfamily and functions in a countless number of cellular processes such as regulation of gene expression, cell cycle progression, chromatin structure, genomic stability and stem cell differentiation [129, 131]. Due to its enzymatic activity, TIP60 is able to acetylate several target histone proteins such as histone H2A on K5, H3 on K14, and histone H4 on K5, K8, K12, K16 [129] and, additionally, it is proposed to acetylate the histone variants H2A.Z and H2A.X (see chapter 1.3.1) [132, 133]. Besides the involvement of TIP60 in a variety of biological processes through its diverse acetylation activity of histones and non-histone substrates such as p53, it also plays an essential role in DNA damage repair [129] as

well as in the nucleosomal exchange of the histone variant H2A.Z (see chapter 1.3.1) [134]. As TIP60 and its broad functions within the p400 complex and its relation to the histone variant H2A.Z are of greatest interest for this thesis, they are explained in greater detail in the section 1.3.1 below.

1.2.5 Diversity of histone variants

As already indicated, histone variants play a crucial role in regulating chromatin dynamics (Figure 3E); thereby creating even more variety of chromatin regulatory mechanisms. For each canonical core histone (except of H4, here only one hominidae-specific histone variant was recently found [135]) a substantial number of histone variants exist (Figure 4).
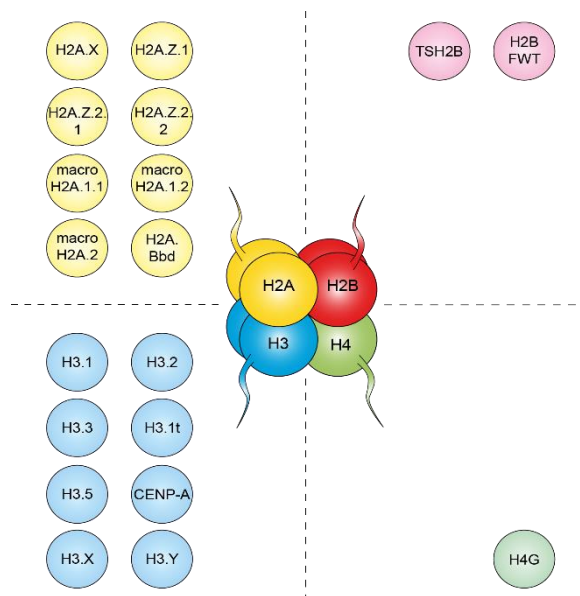
Figure 4: Human core histone variants. Histone variants for H2A (light yellow), H2B (light red), H3 (light blue) and the previously discovered variant of H4 (light green) are shown. For simplification, the large histone variant family of the linker histone H1 is not illustrated.

Histone variants differ in many aspects from their canonical counterparts, which includes differences in primary sequences, genomic distribution and organisation of the genes, expression and deposition timing, RNA processing and genomic occupancy [136]. The exchange of core histones with their specific variants at defined genomic locations results in an altered nucleosomal composition, which can contribute to changes in nucleosome structure and stability due to distinct binding affinities of the variants [137, 138]. Furthermore, histone variants can be

posttranslational modified in different ways than their canonical siblings, thus allowing other regulatory factors to bind and to recruit alternative 'readers', which in turn can affect chromatin landscapes and dynamics [137]. In addition to their metabolic chromatin functions, this divergence confers each histone variant specific roles in distinct biological processes such as transcriptional regulation, chromosome segregation, DNA repair, meiotic recombination or DNA replication [139–141].

Histone variants can deviate substantially from the main isoforms in regard to their gene and amino acid sequences [137, 139], whereby minimal but also huge structural differences in their domains can occur [142]. Depending on the degree of deviation, they can be grouped either into homomorphous, where only a few amino acid substitutions arise (e.g. H3.1, H3.2 or H3.3), or heteromorphous families, which involve larger differences, even up to the exchange of whole domains (e.g. H2A.X, H2A.Z, H2A.Bbd or CENP-A) [139, 143, 144]. Furthermore, histone variants differ in their cellular abundance as compared to their canonical counterparts. In order to supply the high demand of histone proteins for packaging freshly synthesized DNA behind the replication fork, the genes that encode the five different canonical histone proteins are present in multiple gene copies [145, 146]. These genes typically cluster together in the genome of all eukaryotic species to ensure rapid expression during the S-phase of the cell cycle [146]. In contrast to the replication-dependent expression of the canonical histone gene cluster, genes of histone variants are arranged outside of this array and exist only as single-, or two-copy genes [147]. The expression of these genes occurs continuously throughout the cell cycle, in a manner that is independent of replication and the gene products are deposited at specific genomic locations, deposited where they are needed by variant-specific histone chaperone/remodelling complexes [148]. Not only the histone genes, their genomic organisation and their time point of expression, but also the generated transcripts exhibit striking differences. Compared to histone variant mRNAs, the transcripts of canonical histone genes possess a unique stem-loop motif at the 3'-end, but lack polyadenylation as well as non-coding intron regions, whereas some histone variant intron segments can potentially give rise to different splice isoforms [146, 149]. Collectively, this versatile divergence between canonical and non-canonical histone proteins is a fundamental aspect contributing to the large diversity of chromatin regulatory mechanisms. In the following sections, the five major histone families and their variants are described briefly.

1.2.5.1 Histone H1 variants

The histone H1 family exhibits the largest number of histone variants, that are functionally highly redundant [150]. To date in humans alone, eleven different linker histones have been discovered [151] including seven somatic (H1.1, H1.2, H1.3, H1.4, H1.5, $H1^0$, H1X) and four germ-line specific (H1t, H1T2, HILS1, H1foo) variants [139, 152–156]. The abundance of these variants is species-, tissue-, and developmental-specific [148, 150] and in addition to their essential role in chromatin compaction, some H1 variants have been shown to affect gene expression by acting as transcriptional repressors or sometimes even as activators of transcription [150, 157].

1.2.5.2 Histone H3 variants

In humans, the histone H3 family consists of two canonical histones, namely H3.1 and H3.2, and six variants including H3.3, CENP-A, H3.X, H3.Y and the testis-specific H3.1t and H3.5 variants, whose functions remain poorly understood [138, 158, 159]. Interestingly, H3.3 differs from the canonical histones, H3.1 and H3.2, in only four- or five amino acid residues [160, 161], thereby belonging to the group of homomorphic variants [139]. It is suggested, that these amino acid substitutions are responsible for specific H3.3 functionality and deposition [161, 162]. While chromatin incorporation of H3.3 is achieved by either Histone regulatory homolog A (HIRA) or Death domain-associated protein/alpha-thalassemia/Mental retardation syndrome X-linked protein (DAXX/ATRX) chaperone complexes [161], canonical H3 histones are deposited via the Chromatin assembly complex 1 (CAF-1) [163]. H3.3 is specifically enriched in actively transcribed genomic sites, but also occurs at repressive chromatin regions, including the telomers [164] and plays crucial roles in different biological processes such as transcription, replication or spermatogenesis [165–167]. Moreover, only H3.3 possesses a unique serine residue at position 31, which is not only phosphorylated during a few stages during mitosis [168], it can also be stimulation-induced phosphorylated to enable rapid transcription of several genes in mouse macrophages [169]. In contrast to H3.3 and although H3.1 and H3.2 vary in just one amino acid, the canonical histone H3.2 is mostly linked to facultative heterochromatin, whereas H3.1 exhibits a mixture of both active and repressive marks [170, 171]. The heteromorphic histone CENP-A is one of the most specialized variants that is incorporated into centromeric chromatin regions, where it supports the formation of centromeres during mitosis by the assembly of kinetochores, therefore it is indispensable for cell survival

[140, 172–175]. Not so long ago, two novel primate-specific histone H3 variants, H3.X and H3.Y, were identified [171]. Both variants are present in specific, human brain regions and are expressed in malignant and in several normal tissues such as bone, breast or lung [171]. Some studies showed, that H3.Y, and hypothetically H3.X as well, is integrated at transcriptional start sites (TSSs) of transcriptionally active genes leading to a more open chromatin conformation [176–178].

1.2.5.3 Histone H4 variant

So far, only one histone H4 variant has been recently described in higher eukaryotes, which, surprisingly, shares only 85% protein sequence similarities with the evolutionarily highly conserved histone H4 [135]. The hominidae-specific variant H4G is expressed in many human cell lines and in some cancer tissues [135]. It is primarily located in the nucleoli, where it is supposedly involved in rDNA transcription and ribosome biogenesis by affecting nucleolar chromatin structures [135, 179].

1.2.5.4 Histone H2B variants

In contrast to the large heteromorphous histone families H1, H3 and H2A, the human histone H2B family exhibits a higher amino acid identity, but also comprises only two testis-specific variants, called TSH2B and H2BFWT, whose functions are largely unknown [143, 180]. During spermatogenesis, the human sperm variant TSH2B negatively influences the stability of histone octamers, which are undistinguishable from canonical H2B-containing particles due to their high similarity in function and structure [181, 182]. The primate-specific variant H2BFWT is also expressed in testis, where it is potentially involved in telomere formation although it is not able to interact with chromatin modulating factors, but rather functions as a specific marker for telomeric identity [183, 184]. Interestingly, a third H2B variant was recently identified in mice, namely H2BE, which replaces canonical H2B exclusively in inactive olfactory chemosensory neurons resulting in neuronal cell death, thereby regulating the life span of these cells [185].

1.2.5.5 Histone H2A variants

Among the five major histone families, the histone H2A family contains the highest number of variants with the most variations [186]. To date, eight different H2A variants exist in humans: H2A.X, macroH2A.1.1, macroH2A.1.2, macroH2A.2, H2A.Bbd (Barr

body deficient), H2A.Z.1, H2A.Z.2.1 and H2A.Z.2.2 [187]. All of these H2A variants exhibit the greatest sequence differences in their C-terminal region, which is important for intra- and internucleosomal interactions, supporting nucleosome stability as well as linker histone H1 binding for higher-order chromatin structure [188–190]. Hence, it is no surprise, that incorporation of H2A variants has the potential to regulate chromatin dynamics by altering histone-interactions and giving rise to different structural outcomes.

In mammals, the histone variant H2A.Bbd shares only 50% amino acid identity with canonical H2A and is lacking both the C-terminal tail and a portion of the docking domain [188, 191]. It can, therefore, be deduced that the replacement of canonical H2A with H2A.Bbd results in an altered nucleosomal organization, which is characterized by a more relaxed structure in which DNA is less tightly ordered [188, 192]. Indeed, several studies revealed that H2A.Bbd incorporation is related to an open chromatin structure and H2A.Bbd-harbouring nucleosomes are enriched within actively transcribed genes, arguing for its role in promoting transcription [190, 193–195]. However, H2A.Bbd's function in reducing nucleosome stability is limited to certain tissues since it is almost exclusively expressed in testis, where it was shown to play a crucial role in mouse spermatogenesis and, to a much lesser extent in brain, although its function here is largely elusive [196, 197].

In contrast to the extraordinarily small histone H2A.Bbd, the histone variant macroH2A is nearly three times larger than canonical H2A and exhibits a unique domain structure, in which the histone fold domain is additionally connected to a large, highly conserved, non-histone macro domain via a linker segment [188, 198]. In vertebrates, macroH2A is present in three isoforms: macroH2A.1.1 and macroH2A.1.2 are generated by alternative splicing, while macroH2A.2 is encoded by another independent gene [199]. In general, macroH2A is linked to transcriptional repression by negatively affecting histone acetylation, as well as chromatin association of transcription factors and nucleosome remodelling complexes [200]. Through these mechanisms, macroH2A regulates multiple, distinct biological processes such as transcriptional regulation, chromatin remodelling, DNA repair or X-chromosome inactivation [188, 200–204]. However, there are also conflicting results on the functions of macroH2A, which indicate that it is not only involved in transcriptional repression, but also positively influences the transcription of several target genes [205].

The histone protein H2A.X is an outstanding variant with specialized functions in DNA damage repair processes [186]. Compared to conventional H2A, H2A.X comprises an additional motif in the C-terminus whose serine on position 139 becomes rapidly

phosphorylated upon DNA damage, thereby stimulating a DNA damage repair signalling cascade [186, 206, 207]. In mammals, phosphorylation of the histone variant H2A.X (commonly referred to as γH2A.X [208]) is catalyzed by three kinases named Ataxia telangiectasia mutated (ATM), Ataxia telangiectasia and rad3 related (ATR) and DNA-dependent protein kinase (DNA-PK), whose activation depends on the type of DNA damage [209, 210]. One of the most deleterious DNA lesions are DNA double-strand breaks (DSBs) [211]. As a first response to DSBs, the histone variant H2A.X gets promptly phosphorylated by ATM and spreads bidirectionally over several megabases surrounding DNA lesions [117, 209, 212], thereby creating a platform for several regulatory factors involved in modulating chromatin structures in order to facilitate repair processes at sites of actions [210]. Finally, the large number of various interacting proteins such as BRCA1 or 53BP1 mediate the repair of DSBs by non-homologous end joining (NHEJ) or homologous recombination (HR) [213]. Along with other complexes, the members of the INO80 subfamily play a decisive role in DSB repair [213, 214] that will be discussed in more detail in section 1.3.1. Apart from its role as a specific DSB marker, H2A.X is also involved in other cellular processes such as mitosis, stem cell development, cellular senescence, chromosome segregation, chromosome inactivation and regulation of transcription [215, 216].

Since the histone variant H2A.Z is the main focus of this thesis, it will be described in greater detail in the next chapter.

1.3 The histone variant H2A.Z

Among all histone variants, H2A.Z is one of the best-studied. H2A.Z is evolutionary conserved, but shares only 60% sequence identity to canonical H2A within the same species, indicating potentially unique and vitally important functions of H2A.Z [188, 217]. Indeed, first studies have been shown that H2A.Z is one of few variants that is indispensable for survival especially in *Drosophila melanogaster*, *Tetrahymena thermophile* and *Xenopus laevis* [139, 218–223]. Subsequent studies evidenced its significance in mammals by performing knock-out mice experiments, which clearly demonstrated that H2A.Z is required for early mammalian development as depletion of H2A.Z results in embryonic lethality of the organism [218, 224, 225]. This fact makes the importance of the key regulator H2A.Z in establishing chromatin structures, which are pivotal for normal mammalian development, even plainer, and therefore it is not surprising that dysregulation of H2A.Z has been associated with multiple diseases such as cancer [226–228].

INTRODUCTION

In vertebrates, different isoforms of H2A.Z exist that are encoded by two non-allelic genes, *H2AFZ* (H2A.Z.1) and *H2AFV* (H2A.Z.2) [188, 229]. Surprisingly, despite significant differences in their nucleotide sequence, both generated protein products, H2A.Z.1 and H2A.Z.2, are highly similar and differ in only three amino acids from each other [229]. Moreover, it has been recently discovered that the human primary transcript of *H2AFV* undergoes alternative splicing leading to one additional isoform [230, 231]. Accordingly, apart from the main isoform H2A.Z.2.1 (formerly H2A.Z.2), the variant H2A.Z.2.2 exists, which is found only in primates and in a lower abundance in most tissues as compared to H2A.Z.2.1 [230].

From a structural point of view, H2A.Z-containing nucleosomes are almost identical to the conventional ones [232]. However, conspicuous features differing between both structures appear especially in the L1 region and the docking domain, which can potentially lead to an altered nucleosome stability [232]. It is assumed that the incorporation of H2A.Z into an H2A-containing nucleosome (heterotypic nucleosome) leads to a strong destabilization of the core particle due to a steric clash of their distinct L1 loops [232]. This putative weakening effect of H2A.Z is further supported by the hypothesis that the integration of H2A.Z results in a loss of hydrogen bonds between the docking domain of H2A.Z and H3, thus altering the sites of histone interactions within the octamer [232]. Overall, these H2A.Z-mediated changes in nucleosome stability are mainly caused by its L1 region and the docking domain, which exhibit distinct properties to canonical H2A, thereby facilitating H2A.Z's destabilizing functions. Interestingly, chromatin incorporation of the splice-variant H2A.Z.2.2 leads to structural changes, which strongly reduce the stability of a nucleosome caused by its unique docking domain and special features [230]. Nevertheless, it should be clearly highlighted that many studies intensively investigated the impact of H2A.Z on nucleosome stability obtaining contrasting results [217]. Several studies reported a stabilizing [233, 234] and others a destabilizing [232, 235] effect of H2A.Z incorporation on nucleosome structure. Even so, an explanation for these contradictory results remains elusive as they can have multitude of reasons (as reviewed in [188]). Principally, it is not sensible to merely consider H2A.Z and its influence on nucleosome dynamics alone, H2A.Z should rather be looked at in its entirety. In fact, the structural effect of H2A.Z is probably not the only important factor responsible for changes in nucleosome stability, but it potentially derives from a combination of posttranslational modifications, the nucleosome composition and/or the interacting determinants of H2A.Z. It is therefore conceivable, that these addressed H2A.Z-related influences on chromatin can lead to highly distinct functional outcomes. In agreement with H2A.Z's function in affecting nucleosome stability as a

result of the nucleosomal composition, it was shown that nucleosomes containing both histone variants H2A.Z and H3.3 are highly unstable [236]. Furthermore, homotypic H2A.Z nucleosomes are more stable than heterotypic H2A.Z/H2A nucleosomes due to the steric properties of their L1 loop regions [237]. In contrast to its potential destabilizing character, it is also suggested that H2A.Z promotes higher-order chromatin structures by influencing internucleosomal interactions [238]. Compared to canonical H2A, H2A.Z contains an extended acidic patch that increases the affinity of the N-terminal tail of H4 to adjacent nucleosomes, thereby mediating chromatin fiber compaction [232, 239]. Additionally, the chromatin binding protein Heterochromatin protein 1 alpha (HP1α) interacts specifically with H2A.Z to reinforce chromatin fiber folding at constitutive heterochromatic regions [239]. These studies provide notable examples of H2A.Z's role in stabilizing chromatin conformations, although all reports on H2A.Z's structural features are somehow conflicting.

To further complicate H2A.Z's functioning, it is subjected to several posttranslational modifications, such as acetylation, sumoylation and ubiquitinylation, with different functional outcomes [188, 240]. Sumoylation of H2A.Z was reported to act as a specific chromatin mark for chromosome relocation during DNA damage repair processes in *S. cerevisiae* [241]. Ubiquitinylated H2A.Z is associated with a repressive chromatin state at facultative heterochromatin regions and was shown to locate to the inactive X-chromosome of female mammalian cells [242]. While acetylation of H2A.Z destabilizes nucleosomes and is generally linked to transcriptional activation [233]. Acetylation of H2A.Z occurs on the N-terminal tail on residues K4, K7 and/or K11, and is predominantly found at TSSs of actively transcribed genes but also occurs, to a much lesser extent, at enhancers and intergenic regions [243–248]. While acetylation of H2A.Z is achieved by TIP60 in yeast and drosophila, recent studies proposed that TIP60 is also responsible for H2A.Z acetylation in mammalian cells [132, 249–251]. In general, it is suggested that the dynamic acetylation patterns of H2A.Z are correlated with activating (destabilizing) functions, while non-acetylated H2A.Z nucleosomes are associated with repressive (stabilizing) chromatin states in which DNA is more tightly bound [240].

At the functional level, the role of H2A.Z is also highly controversial, which has been reflected in its structural discrepancies [139]. Generally, H2A.Z is predominately described as a histone variant that positively regulates transcription and promotes open chromatin conformations, however, several contrasting functions of H2A.Z are addressed by its participation in transcriptional repression as well as in the formation of pericentric and centromeric heterochromatin regions [239, 252–256]. Besides its role in influencing chromatin structure and gene transcription and silencing, H2A.Z is

also involved in DNA damage repair, genome stability, mitosis, telomere integrity, chromosome segregation and development [140, 188, 217, 253, 257]. Nevertheless, how H2A.Z exactly performs its versatile and ambiguous functions in so many DNA-related biological processes continues to remain unresolved. It should be taken into account that the functional divergence is not only dictated by H2A.Z alone, but rather requires the coordinated interplay of PTMs, other histone proteins, nucleosomal binding factors and H2A.Z-specific remodelling complexes at sites of action. The totality of those mechanisms can help to explain the vast diversity of structural and functional discrepancies of H2A.Z. Therefore, it is possible that nucleosomal H2A.Z requires the help of diverse proteins/complexes, which recognize H2A.Z within its specific locations to assist H2A.Z in accomplishing its functions and depending on H2A.Z's chromatin context, different functional outcomes may occur.

In order to gain more insights into the H2A.Z-specific chromatin network, the Hake group uncovered the nucleosomal interactome of H2A.Z by label-free quantitative mass spectrometry (qMS) [227, 258]. Beside members of the already known H2A.Z-specific chaperone/remodelling complexes SRCAP and p400, they also found histone-modifying complexes involved in both, gene activation and repression, supporting the theory of H2A.Z function as a platform for many complexes, thereby contributing to the different outcomes of gene regulation [258]. Interestingly, they also identified novel H2A.Z-specific chromatin interactors [258]. One of those was PWWP domain-containing protein 2A (PWWP2A), which has been shown to preferentially bind to H2A.Z-containing nucleosomes at promoters of highly transcribed genes and participate in the regulation of transcription [258]. Moreover, depletion of PWWP2A in *Xenopus laevis* led to cranial facial defects caused by impaired neural crest cell differentiation and migration, thereby highlighting the importance of the novel H2A.Z-specific chromatin binder PWWP2A in early frog development [258]. However, as rescue experiments with human PWWP2A RNA restored the wild type phenotype, PWWP2A's developmental functions seem to be evolutionary conserved [258]. The rescuing activity of PWWP2A depends on its C-terminal (IC) domain, which mediates H2A.Z-specificity, suggesting that PWWP2A performs its developmental functions in context of H2A.Z-containing sites in the genome [258].

As investigations of the nucleosomal H2A.Z interactome provided greater insights into H2A.Z's specific chromatin-associated binding factors, thereby contributing to a better understanding of H2A.Z's functioning, its chromatin-free interaction partners have become increasingly important in the last years due to their ability to regulate the genome-wide distribution of H2A.Z by its concerted deposition or eviction into specific

chromatin regions. Since this is a fundamental point in this study, the different human H2A.Z-specific remodelling complexes are explained in more detail below.

1.3.1 H2A.Z-specific chaperone/remodelling complexes

To fulfil its diverse functions at defined chromosome locations, H2A.Z requires the concerted action of specific multi-subunit, histone-variant exchangers, which are responsible for loading (and removal) of H2A.Z into chromatin [259]. In higher eukaryotes, H2A.Z deposition is achieved by two ATP-dependent remodelling machineries [257]. Both, the SRCAP and p400 complexes have unique functions in regulating nucleosome composition by catalyzing the exchange of a canonical H2A-H2B dimer with a variant-containing H2A.Z-H2B dimer [88, 243]. In contrast, H2A.Z eviction is performed by the INO80 complex [260] or by the p400 complex member Acidic leucine-rich nuclear phosphoprotein 32 family member E (ANP32E), especially in context of DNA-damage [257, 261]. The multifactor complexes, SRCAP and p400, have several proteins in common, such as Vacuolar protein sorting-associated protein 72 homolog (YL1/VPS72), DNA methyltransferase 1-associated protein 1 (DMAP1), RuvB-like 1 (RUVBL1), RuvB-like 2 (RUVBL2), Actin-like protein 6A (ACTL6A) and YEATS domain-containing protein 4 (YEATS4) [262] (Figure 5). The H2A.Z-specific histone chaperone member YL1 is the major determinant responsible for the transfer of H2A.Z into nucleosomes [262, 263], arguing for a similar H2A.Z-replacing mechanism being utilized by both complexes.
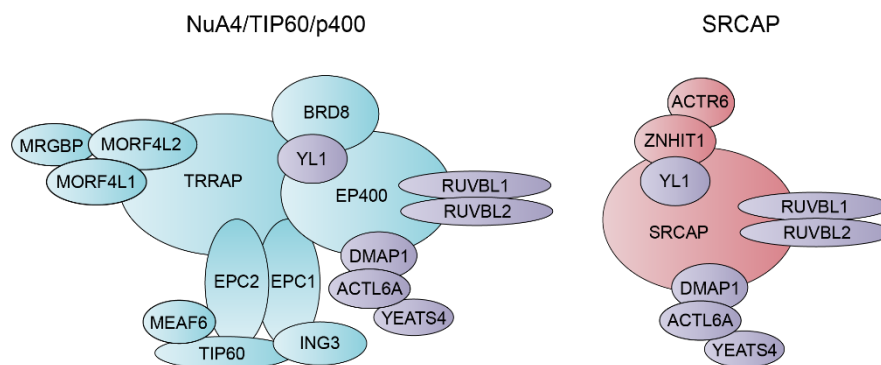
Figure 5: Schematic representation of the human H2A.Z-specific chaperone complexes. H2A.Z deposition is achieved by the two ATP-dependent remodelling complexes NuA4/TIP60/p400 (p400) and SRCAP. Members of the p400 complex are depicted in blue, members of the SRCAP complex in red and shared members of both complexes in purple.

INTRODUCTION

In humans, the histone variant H2A.Z is predominately positioned at the -1 and +1 nucleosomes that flank the nucleosome-depleted region (NDR) of TSSs of promoters, mostly of active genes [257, 264]. Additionally, H2A.Z localizes to other regulatory regions such as enhancers and silencers, where it is proposed to facilitate DNA accessibility for transcription factors [265], however, it is hardly present at transcribed coding regions [257]. This gives rise to the question of how the H2A.Z-specific remodelling complexes are targeted to these specific chromatin sites? It is suggested that a large number of different transcription factors such as TFIIF [266] interact with subunits of the H2A.Z deposition machineries to recruit them to sites of action [259]. The recognition of PTMs at specific regions through different complex-containing 'reader' proteins might also be involved in targeting sites for H2A.Z deposition [259]. Moreover, H2A.Z incorporation is stimulated by the acetylation of H2A and H4 histone tails, which is conducted by the histone acetyltransferase TIP60, a specific p400 complex member, indicating that functional differences between both complexes exist, since the SRCAP complex does not show any histone acetyltransferase activity [134, 259, 267]. Nevertheless, the SRCAP and p400 complexes, share compositional and functional similarities, and therefore one obvious question remains - why are there two different H2A.Z-specific chaperone complexes in mammals? To date, it is not known why H2A.Z is integrated into chromatin through two complexes. It is, however, conceivable that both complexes are potentially involved in different classes of H2A.Z incorporation, which depend on the cellular state and the chromatin context [243]. Moreover, it is evident that both machineries have specialized features, thereby possibly leading to different H2A.Z deposition mechanisms. Since the p400 complex is of particular interest for this study, its properties are highlighted in the next section. The mammalian multimeric p400 complex harbours at least 16 subunits, four of which exhibit catalytic functions [213]. The enzymatic activities reside in the TIP60 histone acetyltransferase, the EP400 SWI/SNF-class DNA-dependent ATPase and the RUVBL1 and RUVBL2 DNA helicase proteins [213, 268–270]. Furthermore, the complex possesses structural DNA binding activities [268]. The essential EP400 motor ATPase alters DNA-histone interactions and thus, facilitates the integration of H2A.Z into specific chromatin regions, especially in gene promoters [213, 271]. As mentioned earlier, the multifunctional histone acetyltransferase TIP60 is a key enzyme, which functions to acetylate histone H4, H2A, H2A.Z and H2A.X, thereby, creating docking sites for 'reader' proteins at specific chromatin environments [272]. The Bromodomain-containing protein 8 (BRD8), a p400 complex member, recognizes these acetylated lysine residues and may potentially work in recruiting/stabilizing the p400 complex on chromatin [273]. A further p400 complex member is

Transformation/transcription domain-associated protein (TRRAP), a scaffold protein with an important role in mediating p400 complex formation [213]. Due to its large diversity of functionally specialized protein members (which are too numerous to mention all of them here), the p400 complex participates in a variety of cellular processes such as nucleosome remodelling, histone and non-histone protein acetylation, transcriptional regulation, cell cycle progression, DNA damage repair and apoptosis [213, 272–274]. The regulation of gene expression through the p400 complex is realized by its H2A.Z-exchange and/or its acetylation activities of target proteins, as well as by interactions with several transcription factors like c-Myc [271, 275–277]. In case of DNA damage such as DSBs, several p400 complex components are recruited to sites of DNA injury, where TIP60 rapidly acetylates the ATM kinase and accordingly activates the previously mentioned DNA-damage repair signalling cascade, in which phosphorylation events of H2A.X, DNA repair and cell-cycle control proteins take place [213, 278, 279]. Moreover, TIP60 hyperacetylates histone H2A, H4 and H2A.X at sites of action to promote an open, relaxed chromatin structure, which is required for DSB repair by facilitating the access and the binding of DNA repair machinery proteins like 53BP1 [213, 214, 279]. However, the exact mechanism by which the p400 complex alters chromatin structures in a DNA damage-occuring environment is not fully understood and need to be further clarified [213].

In general, it is largely unknown how these two complexes exactly perform their functions and whether other, not yet identified proteins are also involved in H2A.Z deposition. Therefore, several studies have been focused on the identification of proteins responsible for the incorporation of H2A.Z into chromatin in order to gain more insights into the H2A.Z-related functioning of those complexes. Thusly, more and more proteins were identified that were formerly unrelated to H2A.Z deposition pathways. Our group was one of many others that previously identified new H2A.Z-specific chaperone/remodelling complex members and thereby provided more insights into H2A.Z's chromatin-free interactome [257].

1.3.2 The nuclear chromatin-free H2A.Z interactome

It is largely unknown how H2A.Z exactly performs its variety of distinct functions. In order to gain further insights into the H2A.Z chaperone network, the Hake group identified its specific chromatin-free interacting proteins responsible for its deposition into chromatin by quantitative mass spectrometry (qMS) [257], similar to the approach which was previously used to solve the interactome of several histone H2A and H3

variants [176, 230]. MS experiments were performed by Clemens Bönisch and Antonia Jack, two former PhD students in the Hake group, in cooperation with Hans Christian Eberl from the group of Matthias Mann (MPI Munich). To this end, HeLa Kyoto (HK) cells stably expressing enhanced green fluorescence protein (GFP) or GFP-tagged H2A.Z.1 were used for stable isotope labelling using amino acids in cell culture (SILAC). Afterwards, soluble nuclear chromatin-free fractions were generated followed by immunoprecipitations (IPs) with GFP-Trap magnetic Dynabeads to precipitate GFP-tagged proteins and their associated binding factors that were identified via MS [257] (Figure 6). Unsurprisingly, GFP-H2A.Z.1 specifically interacted with all members of the p400 and SRCAP complexes. These findings are in line with previous reports on H2A.Z.2.1 and H2A.Z.2.2 chaperone complexes [188, 257], verifying the practicability of the method. The specificity of the approach was also confirmed by the observed interaction of GFP-H2A.Z.1 with ANP32E, a previously reported p400 complex member involved in the eviction of nucleosomal H2A.Z, especially in context of DNA damage [261, 280–282].
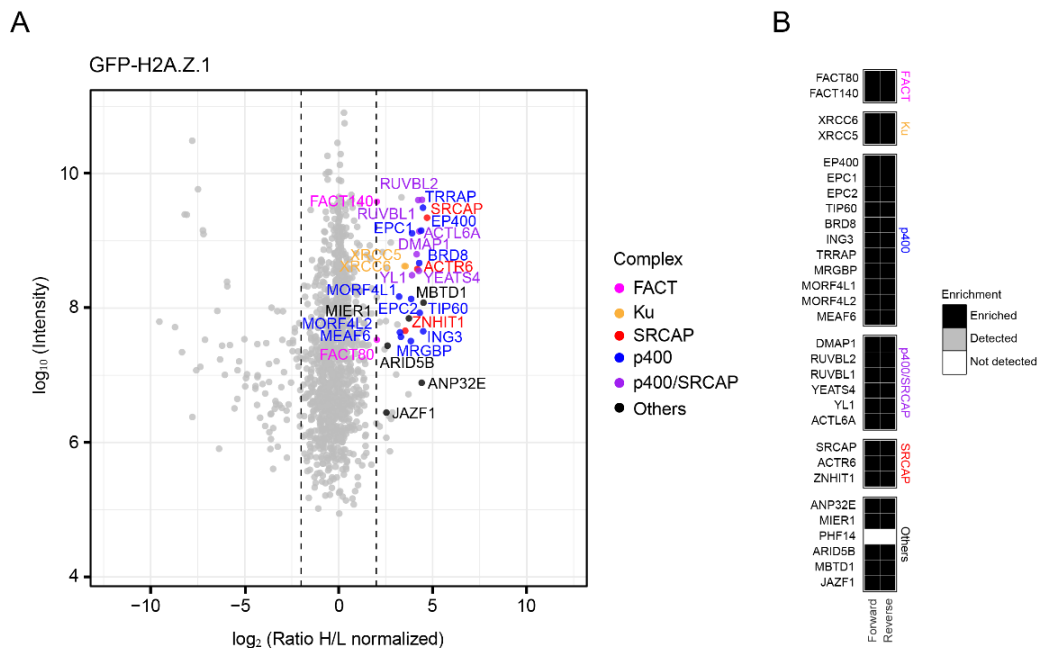
Figure 6: JAZF1 and MBTD1 are specific chromatin-free H2A.Z-interacting proteins.
(**A**) Scatter-plot of GFP-H2A.Z.1 pull-downs. HeLa Kyoto (HK) cells stably expressing GFP or GFP-H2A.Z.1 were SILAC-labelled and the soluble nuclear fraction subjected to immunoprecipiations using GFP-Trap magnetic Dynabeads. Identification of GFP-H2A.Z.1 binding partners was carried out by quantitative mass spectrometry (qMS). Members of the FACT complex are depicted in magenta, members of the Ku complex in orange, members of the SRCAP complex in red, members of the p400 complex in blue and shared members of the p400 and SRCAP complexes in purple. Other proteins are plotted in black. Significantly enriched proteins are highlighted with names according to the respective color. (**B**) Heatmap of all identified GFP-H2A.Z.1-interacting proteins that were enriched (black), detected but not enriched (gray) or not detected (white). Data published in [257].

Moreover, GFP-H2A.Z.1 was also found to associate with the FACT and Ku complexes, which are implicated in DNA damage repair processes [282, 283] and are able to interact with almost all H2A histone variants [257]. Interestingly, among other proteins, the transcriptional repressor Juxtaposed with another zinc finger 1 (JAZF1, also referred to as TIP27 or ZNF802) and the Malignant brain tumor domain containing 1 (MBTD1) proteins were identified as novel, specific chromatin-free GFP-H2A.Z-interacting proteins (similar results were obtained for GFP-H2A.Z.2.1 and GFP-H2A.Z.2.2), since they were not found in pull-downs of canonical H2A or other H2A histone variants [257]. Also note that JAZF1 and MBTD1 were not detected in the previously solved nucleosomal interactome of H2A.Z [258], suggesting that JAZF1 and MBTD1 are specific chromatin-free H2A.Z-interacting proteins and thus do not interact with H2A.Z-containing nucleosomes on chromatin.

1.3.3 JAZF1 and MBTD1 as novel chromatin-free H2A.Z-binding proteins

After the identification of JAZF1 and MBTD1 as chromatin-free H2A.Z-associated proteins, the question arose whether JAZF1 and/or MBTD1 belong to the H2A.Z-specific p400 and/or SRCAP chaperone complexes or if they interact independently of these complexes with H2A.Z alone. To address this question, additional qMS experiments (similar to the above mentioned one) were performed in which the soluble nuclear binding factors of GFP-JAZF1 and -MBTD1 were identified by quantitative SILAC-MS [257] (Figure 7). Surprisingly, GFP-JAZF1 and -MBTD1 interacted with all members of the p400 complex and with shared members of the p400 and SRCAP complexes, but did not associate with SRCAP complex-specific components. Moreover, GFP-JAZF1 pulled-down endogenous MBTD1 and conversely, GFP-MBTD1 associated with endogenous JAZF1. These results suggest that yet another p400 sub-complex exists in mammals, which exhibits both JAZF1 and MBTD1, but excludes ANP32E, since GFP-JAZF1 and -MBTD1 pull-downs did not contain this p400 complex-specific component [257].
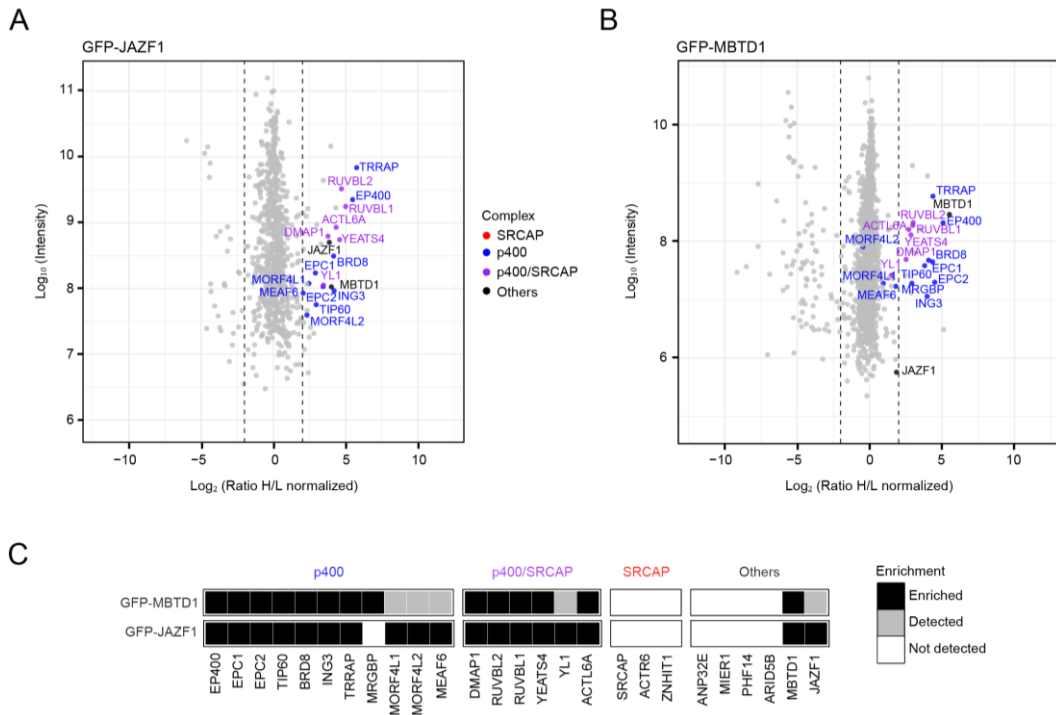
Figure 7: JAZF1 and MBTD1 are novel members of a p400 sub-complex. Scatter-plot of (**A**) GFP-JAZF1 and (**B**) GFP-MBTD1 pull-downs. HeLa Kyoto (HK) cells transiently expressing GFP, GFP-JAZF1 or -MBTD1 were SILAC-labelled and subsequently used for preparation of soluble, nuclear extracts followed by immunoprecipitations with GFP-Trap magnetic Dynabeads. Identification of JAZF1- and MBTD1-associated factors was carried out using MS. Members of the SRCAP complex are depicted in red, of the p400 complex in blue and shared members of both complexes in purple. Other proteins are plotted in black. Significantly enriched proteins are highlighted with names according to the respective color. (**C**) Heatmap of GFP-MBTD1 (upper) and GFP-JAZF1 (lower) interacting proteins that were enriched (black), detected but not enriched (gray) or not detected (white). Data partially published in [257].

1.3.3.1 MBTD1

Recently, MBTD1 has already been reported as a stable subunit of the p400 complex with special features in regulating transcription and promoting DSBs repair by HR [284, 285]. The MBTD1 protein contains a FCS (phe-cys-ser) zinc finger at the N-terminus that presumably binds to regulatory RNAs, and four MBT repeats [286–288] (Figure 8). The MBT1 and MBT2 domains have been reported to be crucial for the interaction with the transcription factor YY1 [286, 289], whereas the MBT4 repeat is responsible for the recognition of mono- and/or dimethylated lysine residues of histone proteins [286, 288].
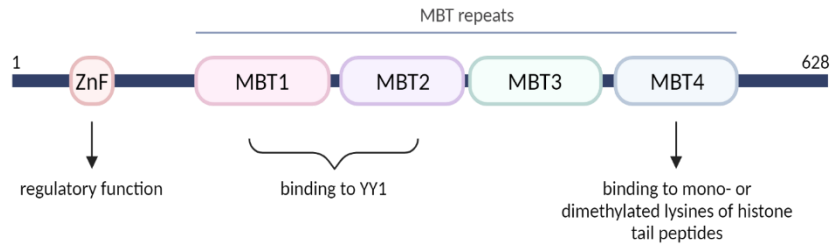
Figure 8: Schematic domain organization and binding features of the human MBTD1 protein. MBTD1 consists of a zinc finger (ZnF, orange), which has been proposed to bind to regulatory RNAs and four MBT repeats: MBT1 is depicted in pink, MBT2 in purple, MBT3 in green and MBT4 in blue. Figure created with BioRender.com.

MBTD1's histone methyl-lysine reading module has been shown to strongly bind to H4K20me1/2, and thus mediates the recruitment of the histone acetyltransferase TIP60 to a specific subset of promoter sites to regulate the transcription of associated genes [284]. Moreover, MBTD1 regulates the binding of 53BP1 to DSBs during DNA damage response, probably by recognizing the same H4K20 methylation patterns, thereby affecting the formation and stability of 53BP1 foci after the occurrence of DNA damage in order to orchestrate the choice of DSB repair pathway [284]. The Enhancer of polycomb homolog 1 (EPC1) subunit of the p400 complex mediates the association of MBTD1 with the complex [284, 286]. Interestingly, several studies have also shown that mutations of *MBTD1* and at least one further gene can lead to the generation of specific fusion proteins, which have been found in human endometrial stromal sarcomas (ESSs) and leukemia [285, 290, 291]. However, the underlying mechanisms by which MBTD1-containing fusion proteins contribute to these diseases are largely unknown. Furthermore, the general functions of intact MBTD1 are so far poorly understood.

1.3.3.2 JAZF1

JAZF1 is mainly described as a putative transcriptional co-regulator involved in various cellular metabolic energy processes such as gluconeogenesis, lipid metabolism, and insulin sensitivity [292, 293]. The human *JAZF1* gene encodes a 27 kDa nuclear protein, which contains a nuclear orphan receptor TAK1/TR4 interacting domain (TID) and three putative C2H2-type zinc finger motifs [292] (Figure 9). At least one alternatively splice variant has been described, which codes for another JAZF1 isoform [292].
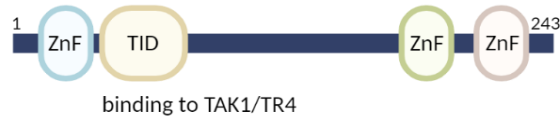
Figure 9: Schematic domain structure of the human JAZF1 protein. JAZF1 consists of a nuclear orphan receptor TAK1/TR4 interacting domain (TID, yellow) required for the interaction with TAK1/TR4 and three putative zinc finger motifs (ZnF) shown in blue, green and brown. Figure created with BioRender.com.

In mice and humans JAZF1 is expressed in multiple tissues, including liver, muscle, fat and testis, while the latter two exhibit the highest level of protein expression [294]. Several mice studies revealed that regulation of JAZF1 expression is modulated by different metabolic disorders [292]. Furthermore, in humans a large number of single nucleotide polymorphisms (SNPs) of JAZF1 exist, which are proposed to be associated with insulin-resistance-related diseases such as type 2 diabetes mellitus (T2DM) [292]. JAZF1 was originally identified as a novel corepressor of the Nuclear receptor subfamily 2 group C member 2 (TAK1/TR4/NR2C2) protein, which plays a crucial role in the receptor-mediated repression and activation of gene expression [295]. The interaction of both proteins is specifically mediated through the TID domain of JAZF1 and is known to be central to maintaining glucose homeostasis in mice by repressing the transcriptional activity of TAK1/TR4 [292, 296]. Numerous studies uncovered that JAZF1 associates with a large number of metabolic-related proteins and acts as a specific regulator of these factors by modulating their gene expression and activity [292–299]. Therefore, it is assumed that JAZF1 is closely related to various metabolic processes and disorders.

In addition, and more interestingly, not only MBTD1 but also JAZF1 is linked to human endometrial stromal tumors, in which chromosomal aberrations involving the *JAZF1* gene occur in the vast majority of ESS cases [300–302]. Besides JAZF1 and MBTD1, fusion proteins with other p400 complex members (including EPC1, MEAF6 or EP400) have also been identified in human sarcomas [303–305], suggesting a potentially disturbed p400 complex-affiliated mechanism, which could contribute to the development of the disease. A recent study in primary human endometrial stromal cells (hEnSCs) revealed that JAZF1 is a new NuA4-interacting protein and that the most prominent aberrant fusion JAZF1-SUZ12 is suspected to mediate an unusual interaction between the PRC2 and the NuA4 complexes [306], which might be one of many possible causes prompting the development of the disease. Indeed, the biological consequences of these fusion proteins in various human sarcomas have

not yet been sufficiently studied. To date, one of the most frequently mutated proteins found in human ESSs is JAZF1, which, together with the p400 complex, plays a potentially critical role as a dynamic driver of the disease. However, although many studies have been focused on identifying the functions of JAZF1 as transcription factor, there is no knowledge about which role and function JAZF1 assumes within the p400 complex. Determining the function of this protein could provide additional insights into JAZF1 and p400 chaperone complex-related disorders. Therefore, further studies are still required to determine potential influences of JAZF1 on p400 complex-associated processes.

1.4   Objectives

In this thesis, I aimed to unravel the chromatin functions of JAZF1, especially in terms of its role within the H2A.Z-specific p400 chaperone complex. Therefore, I first verified the results received from the SILAC-MS approach by immunoprecipitations in order to ascertain whether JAZF1 associates with TIP60, a catalytic subunit of the p400 complex. Afterwards, I purposed to decipher JAZF1's involvement in p400 complex-related processes through knockdown studies. Since MBTD1 was already identified as a specific p400 complex subunit, with a crucial role in DNA damage repair processes, I first set out to analyse whether JAZF1 also affects DSB repair by determining the level of γH2A.X upon JAZF1 depletion via immunoblotting and ChIP-qPCR. Further, to gain deeper insights into JAZF1's implication in transcriptional regulation, I performed RNA-seq experiments. Potential deregulated genes upon loss of JAZF1 were validated via RT-qPCR and immunofluorescence analyses were conducted to reveal spatial relationships between gene regulation and the cellular localization of JAZF1. To identify the underlying molecular mechanism by which JAZF1 might influence gene expression, I evaluated the consequences of JAZF1 depletion on H2A.Z deposition and its acetylation using ChIP-seq. Finally, I assessed whether the putative transcription factor JAZF1 and the histone acetyltransferase TIP60 might act in concert on chromatin via ChIP-qPCR.

2 MATERIAL AND METHODS

2.1 Materials

2.1.1 Technical devices

Table 2.1: List of devices

Description	Supplier
Accuri C6 Plus Flow Cytometer	Becton Dickinson BD Biosciences
Axiocam 506 mono system	Carl Zeiss
Bioruptor Next Gen	Diagenode
Cell culture hood	Thermo Fisher Scientific
Centrifuges	Beckman Coulter Allegra X-30 Beckman Coulter Allegra X-30R Eppendorf 5424 R Eppendorf 5430 R Eppendorf 5417 R
CFX96 Real-Time cycler	Bio-Rad
CL-1000 Ultraviolet Crosslinker	UVP
Countess automated cell counter	Invitrogen
Developer machine ECL Chemostar	Intas
Electrophoresis chamber (nucleic acids)	VWR Peqlab
Electrophoresis chamber (proteins)	Bio-Rad
Fragment Analyzer	Agilent
Freezer (-20°C)	Bosch Privileg Liebherr
Freezer (-80°C)	Thermo Fisher Scientific
Fridge	Beko Liebherr
Gel documentation printer	Mitsubishi
GelStick touch documentation system	Intas
Handcast gel system	Bio-Rad
H_2O purification system	Millipore
Incubator (bacteria)	Infors
Incubator (tissue culture)	Heraeus
Magnetic rack	Diagenode Permagen
Magnetic stirrer	IKA
Microscopes	Carl Zeiss Axio Observer.Z1 Carl Zeiss Telaval 31 Leica DM IL LED
Microwave	Clatronic International Privileg
NanoPhotometer NP80	Implen
pH meter	Xylem Analytics
Pipetboy	Neolab

Pipette set	Labgene Scientific
Power supply unit (microscope)	Eplax
Power supply unit (nucleic acids)	Phase
Power supply unit (proteins)	Bio-Rad
QIAcube	Qiagen
Qubit 4 Fluorometer	Invitrogen
Roller mixer	LLG Labware
Rotating wheel	Heidolph Instruments
Scale	Mettler
Semi-dry blotting system	Bio-Rad
Shaker	Heidolph
Tabletop centrifuge	StarLab
Thermocycler (PCR)	Eppendorf Mastercycler gradient SensoQuest
Thermomixer comfort	Eppendorf 5436
UV-lamp (microscope)	EXFO X-cite series 120
Vacuum pump	LLG Labware
Vortex shaker	Genie
Water bath	Köttermann
White light plate	Kaiser slimlite plano
xCELLigence Real-Time Cell Analyzer	Agilent

2.1.2 Consumables

Table 2.2: List of consumables

Description	Supplier
1.5 ml and 2 ml reaction tubes	Eppendorf
1.5 ml low binding tubes	Sarstedt
15 ml and 50 ml centrifuge tubes	Greiner
15 ml conical hard plastic tubes	Sarstedt
96-well PCR plate	Sarstedt
Cell culture plates (6-well and 24-well)	Greiner
Cell culture plates (10 cm and 14.5 cm)	Greiner
Cellulose paper Whatman	GE Healthcare Life Sciences
Cryotubes	Carl Roth
Disposable needle	B. Braun Melsungen
Disposable scalpel	B. Braun Melsungen
Disposable syringe	Henke-Sass, Wolf
E-plate 16-well	Agilent
Filter tips	Nerbe
Glass pipettes	HBG Henneberg-Sander
Glassware	Schott
Laboratory bunsen burner	Campingaz
Laboratory sealing film (Parafilm)	Sigma-Aldrich
Measuring cylinder (plastic)	Brand
Microscope cover glasses (coverslips)	Paul Marienfeld

Microscope slides	Carl Roth
Mr. Frosty freezing container	Thermo Fisher Scientific
Nitrile gloves	StarLab
Nitrocellulose	GE Healthcare Life Sciences
Pasteur pipettes	Merck Millipore
PCR reaction tubes	Carl Roth
Pipette tips	Ratiolab
Qubit assay tubes	Invitrogen
Sealing foil	Bio-Rad
Serological pipettes	Sarstedt
Tissues lint-free	Kimberly-Clark Professional

2.1.3 Chemicals

Table 2.3: List of chemicals

Description	Supplier
4-(2-hydroxyethyl)-1-piperazineethanesulfonic acid (HEPES)	Carl Roth
4-hydroxytamoxifen (4-OHT)	Sigma-Aldrich
Acetic acid (CH_3COOH)	Carl Roth
Acetone	Carl Roth
Agar	Carl Roth
Agarose	Carl Roth
Albumin fraction V (BSA)	Carl Roth
Ammonium persulfate (APS)	Carl Roth
Ampicillin	Carl Roth
AMPure XP beads	Beckman Coulter
Aprotinin	AppliChem
Bromophenol blue sodium salt	Carl Roth
Calcium chloride dihydrate ($CaCl_2$ 2 x H_2O)	Carl Roth
Coomassie Brilliant Blue R-250	Fluka
Disodium hydrogen phosphate dihydrate (Na_2HPO_4 2 x H_2O)	Carl Roth
Dimethylsulfoxid (DMSO)	Carl Roth
Dithiotheitol (DTT)	Carl Roth
Dulbecco's modified Eagle medium (DMEM)	Gibco
Dynabeads (Protein G)	Invitrogen
Ethanol absolute (EtOH)	Carl Roth
Ethanol denatured (EtOH)	Carl Roth
Ethylenediaminetetraacetic acid (EDTA)	Carl Roth
Ethylene glycol-bis(β-aminoethyl ether)-N,N,N′,N′-tetraacetic acid (EGTA)	Carl Roth
Fetal bovine serum (FBS)	Thermo Fisher Scientific
Fluoromount-G mounting medium	VWR International
Formaldehyde (37%)	Thermo Fisher Scientific
FuGENE HD transfection reagent	Promega

MATERIAL AND METHODS

GFP-Trap Dynabeads	Chromotek
Glycerol	Carl Roth
Glycine	Carl Roth
Glycogen	Thermo Fisher Scientific
Hoechst bisbenzimide H33342	Sigma-Aldrich
Hydrochloric acid (HCl)	Carl Roth
Immersion oil "Immersol" 518 F	Th. Geyer
Isopropanol	Carl Roth
Kanamycin	Carl Roth
Leupeptin	AppliChem
L-glutamine	Gibco
Lithium chloride (LiCl)	Sigma-Aldrich
Magnesium chloride (MgCl$_2$)	Carl Roth
Magnesium sulfate heptahydrate (MgSO$_4$ 7 x H$_2$O)	Carl Roth
Methanol (MeOH)	Carl Roth
Non-fat dry milk	Carl Roth
Nonidet P-40 substitute (NP 40)	Sigma-Aldrich
Oligofectamine transfection reagent	Invitrogen
Opti-MEM	Gibco
Orange G	Merck Millipore
Paraformaldehyde (PFA)	Carl Roth
Penicillin/streptomycin	Gibco
Pepstatin	AppliChem
Phenylmethanesulfonyl fluoride (PMSF)	Carl Roth
Potassium chloride (KCl)	Carl Roth
Potassium dihydrogen phosphate (KH$_2$PO$_4$)	Carl Roth
Proteinase K	Thermo Fisher Scientific
Propidium iodide (PI)	Sigma-Aldrich
Rotiphorese acrylamide/bisacrylamide mix (37.5:1 ratio)	Carl Roth
Shield1	Takara
Sodium chloride (NaCl)	Carl Roth
Sodiumdeoxycholate	Sigma-Aldrich
Sodium dodecyl sulfate (SDS)	Carl Roth
Sodium hydroxide (NaOH)	Carl Roth
Sulfuric acid (H$_2$SO$_4$)	Carl Roth
Tet System Approved FBS	Takara
Trichloroacetic acid (TCA)	Merck Millipore
Tetramethylethylenediamine (TEMED)	Carl Roth
Trident femto Western HRP substrate	GeneTex
Tris(hydrxymethyl)aminomethan (Tris)	Carl Roth
Triton X-100	Carl Roth
Tryptone/Peptone	Carl Roth
Tween20	Carl Roth
Yeast Extract	Carl Roth

2.1.4 Enzymes

Table 2.4: List of enzymes

Description	Supplier
DNase I (RNase-free)	Thermo Fisher Scientific
RNase A (DNase-free)	Thermo Fisher Scientific
SYBR Green master mix	Bio-Rad
Trypsin	Gibco

2.1.5 Markers

Table 2.5: List of markers

Description	Supplier
FastRuler High Range DNA Ladder	Thermo Fisher Scientific
GeneRuler 1 kb DNA Ladder	Thermo Fisher Scientific
GeneRuler 50 bp DNA Ladder	Thermo Fisher Scientific
GeneRuler 100 bp DNA Ladder	Thermo Fisher Scientific
PageRuler Plus Prestained Protein Ladder	Thermo Fisher Scientific

2.1.6 Kits

Table 2.6: List of kits

Description	Supplier
HS Small Fragment Kit	Agilent
Illustra GFX PCR DNA and Gel Band Purification Kit	GE Healthcare Life Sciences
MicroPlex Library Preparation Kit	Diagenode
MinElute PCR Purification Kit	Qiagen
QIAprep Spin Miniprep Kit	Qiagen
QIAGEN Plasmid Midi Kit	Qiagen
QuantSeq 3' mRNA-Seq Library Prep Kit	Lexogen
Qubit dsDNA HS Assay Kit	Invitrogen
RNA Kit	Agilent
RNase-free DNase Set	Qiagen
RNeasy Mini Kit	Qiagen
Trancriptor First Strand cDNA Synthesis Kit	Roche

2.1.7 Software

Table 2.7: List of Software

Description	Version
Adobe Illustrator	24.0.1
BD Accuri C6 Software	V1.0
Bio-Rad CFX Manager Software	2.1
ChemoStar Touch	V2.1
Citavi 6	2018-02-20
Fiji/Image J	1.51n
Fragment Analyzer System Software	1.2.0.11
Integrative Genomics Viewer (IGV)	2.8.0
Intas GDS Touch 2	V1.0.1.5
Microsoft Office	2016
NCBI	web-based browser
PhosphoSitePlus	web-based browser
Primer3	web-based browser
Real-Time Cell Analyzer (RTCA) Software	2.2.1
SnapGene Viewer	V5.1.5
UCSC	web-based browser
Zeiss microscope Software	Zen 3.1 (blue edition)

2.1.8 Antibodies

2.1.8.1 Primary antibodies

Table 2.8: List of primary antibodies used for immunoblotting (IB), immunofluorescence (IF) or chromatin immunoprecipitation (ChIP) applications

Antibody	Order number	Host species	Application	Dilution	Supplier
α-alpha Tubulin	39527	mouse	IB	1:1000	Active Motif
α-Coilin	-	mouse	IF	-	Gift from Graham Dellaire, DAL, Nova Scotia, CA
α-Fibrillarin	NB300-269	mouse	IF	1:100	Novus Biologicals
α-GFP	11814460001	mouse	IB	1:1000	Sigma-Aldrich
α-H2A.Z	39944	rabbit	IB ChIP	1:1000 5 µg/ChIP	Active Motif
α-H2A.Zac (K5, K7, K11)	ABE1363	rabbit	IB ChIP	1:1000 1 µg/ChIP	Merck Millipore
α-H2A.XS139ph	39117	rabbit	IB IF ChIP	1:1000 1:100 5 µg/ChIP	Active Motif
α-H2AK5ac	39108	rabbit	IB	1:1000	Active Motif

α-H3	ab1791	rabbit	IB	1:5000	Abcam
α-H3K14ac	39599	rabbit	IB	1:1000	Active Motif
α-H4K5ac	39700	rabbit	IB	1:1000	Active Motif
α-H4K16ac	39167	rabbit	IB	1:1000	Active Motif
α-JAZF1	animal 1	rabbit	IB	1:500	Produced by Pineda
α-JAZF1	HPA066967	rabbit	IF	1:100	Atlas Antibodies
α-ZNHIT1	HPA019043	rabbit	IB	1:1000	Sigma-Aldrich

2.1.8.2 Secondary antibodies

Table 2.9: List of secondary antibodies used for immunoblotting (IB) or immunofluorescence (IF) applications

Antibody	Order number	Application	Dilution	Supplier
α-mouse Alexa 488	A-11017	IF	1:200	Thermo Fisher Scientific
α-mouse Alexa 594	A-11020	IF	1:200	Thermo Fisher Scientific
α-rabbit Alexa 488	A-11070	IF	1:200	Thermo Fisher Scientific
α-rabbit Alexa 594	A-11072	IF	1:200	Thermo Fisher Scientific
α-mouse HRP	31430	IB	1:20000	Thermo Fisher Scientific
α-rabbit HRP	31460	IB	1:20000	Thermo Fisher Scientific

2.1.9 Human cell lines

Table 2.10: List of human cell lines

Name	Origin	Source/Supplier
HeLa Kyoto (HK)	Cervical cancer, human	Gift from Heinrich Leonhardt, LMU
U2OS 2-6-3 DSB reporter cells [307]	Osteosarcoma, human	Gift from Jessica Downs, ICR, London, UK [308, 309]

2.1.10 Oligonucleotides

2.1.10.1 Oligonucleotides for quantitative PCR of cDNA

Table 2.11: List of oligonucleotides used for quantitative polymerase chain reaction (qPCR) in 5' to 3'. All primer sets were received from Thermo Fisher Scientific.

Name	Sequence forward	Sequence reverse
BIRC3	TCAGACAGCCCAGGAGATGA	CACGGCAGCATTAATCACAGG
CAPN2	CCCTAAACCAGAGCTTCCAGG	CATCCACCACCACCTCCAC
HPRT1	AAGGGTGTTTATTCCTCATGGA	AATCCAGCAGGTCAGCAAAG
ITGB8	AGAAGGAGGTTTTGACGCCAT	TGTCATCACCAGCAGCAATCT

JAZF1_1	CAGATTCGTGTCCGCAAACC	AATTGATTGTGTGGTGCCGC
JAZF1_2	CCGGTGTCGGCTGAGATTAT	AGCAACTGCTGGTGAGGATT
LSM7	GGACGGCACCATTGAGTACA	GAAGGGGTTGGGGATGGC
TIP60_1	GAAGATGGCGGAGGTGGTG	CGGCAGCCCTCGATTATCTC
TIP60_2	AGGGGGAGATAATCGAGGGC	CTTCACGCTCAGGATCTCGG

2.1.10.2 Oligonucleotides for quantitative PCR of ChIP DNA

Table 2.12: List of oligonucleotides used for ChIP quantitative PCR (ChIP-qPCR) in 5' to 3'. gb, gene body; +, +1 nucleosome; -, -1 nucleosome. All primer sets were received from Thermo Fisher Scientific.

Name	Sequence forward	Sequence reverse
ctrl1TP	GGCCCTTGGAAGAGAATGCT	ACATCTGAGGACATTGCCCG
MMP12_gb	TTCTTGTCCCCTAGTCCAATGC	GACGTGTGACTCTGGGCAA
PARS2+	GGGATGCAAGTGGGAAAAC	ATTGCGGTAGGTGAACGTG
PARS2-	AGACGCCTTTATTACAGTGCCC	TCTACGTGGTAGCAGCTCAAAA
p2	GCTGGTGTGGCCAATGC	TGGCAGAGGGAAAAAGATCTCA
p3	GGCATTTCAGTCAGTTGCTCAA	TTGGCCGATTCATTAATGCA
RBMS1_gb	GTCAAGGTGGGAGAACTGCTTA	CACACCACCACATGCAGTTAATT
RPL11_2gb	ACAGCTTTGGGTGATGCAGT	TTGTTGGACCAAAACACGGC

2.1.10.3 Oligonucleotides for RNAi

Table 2.13: List of siRNA oligonucleotides used for RNAi in 5' to 3'. siRNA pools were designed and received from Dharmacon, while individual siRNAs were designed and prevalidated as described in [258, 310] and obtained from Eurofins MWG.

Name	Sequence (sense)	Description
Luciferase (siLuci)	CUUACGCUGAGUACUUCGAUU	-
JAZF1 siRNA pool (siJAZF1)	GGCAUAAAGUAUCACGCUA ACAGAUUCGUGUCCGCAAA GAUACAGAUCCACGGGUUU GAUCCAGACAUGAGACGCA	ON-TARGETplus SMARTpool
JAZF1 #2 (siJAZF1 #2)	AGAAGAAGATTCAGCCGAA	-
JAZF1 #4 (siJAZF1 #4)	ACAGATTCGTGTCCGCAAA	-
Non-target siRNA control pool (siNTC)	UGGUUUACAUGUCGACUAA UGGUUUACAUGUUGUGUGA UGGUUUACAUGUUUUCUGA UGGUUUACAUGUUUUCCUA	ON-TARGETplus SMARTpool
TIP60 #1 (siTIP60 #1)	GGAGAAAGAAUCAACGGA	-
TIP60 #2 (siTIP60 #2)	CAACAAACGUCUGGAUGA	-

2.1.11 Plasmids

Table 2.14: List of plasmids. Retransformation of plasmids was performed in chemical competent *E. coli* (DH5α) cells and plasmids isolated with a Mini- or Midiprep Kit (Qiagen).

Plasmid	Source	Resistance	Description
GFP (empty)	Clontech	Kanamycin	pEGFP-N2 mammalian expression vector backbone
GFP-JAZF1 (full-length)	Gift from Anton Jetten, NIH, USA [295]	Kanamycin	pEGFP-N2 mammalian expression vector backbone
GFP-JAZF1 ΔC164	Antonia Jack (former PhD student in the Hake group)	Kanamycin	pEGFP-N2 mammalian expression vector backbone
GFP-JAZF1 ΔN101	Antonia Jack (former PhD student in the Hake group)	Kanamycin	pEGFP-N2 mammalian expression vector backbone
GFP-JAZF1 ΔN163	Antonia Jack (former PhD student in the Hake group)	Kanamycin	pEGFP-N2 mammalian expression vector backbone
GFP-TIP60 (full-length)	Gift from Benoit de Crombrugghe, UT, USA [311]	Kanamycin	pEGFP-C1 mammalian expression vector backbone

2.1.12 Buffers and solutions

Table 2.15: List of buffers and solutions

Buffer/solution	Components
Coomassie destaining solution	10% Acetic acid (v/v) 30% Methanol (v/v)
Coomassie staining solution	10% Acetic acid (v/v) 50% Methanol (v/v) 0.1% Coomassie Brilliant Blue R-250 (w/v)
Ethidium bromide stock solution	10 mg/ml Ethidium bromide (Carl Roth)
Laemmli buffer (10x)	1.29 M Glycine 0.25 M Tris 1% SDS (v/v)
Laemmli sample buffer (5x)	0.5 M DTT 250 mM Tris 0.02% Bromphenol blue (w/v) 30% Glycerol (v/v) 10% SDS (v/v)
LB agar	1.5% LB agar (v/v)
LB medium	1% NaCl (w/v) 1% Tryptone/Peptone (w/v) 0.5% Yeast extract (w/v)
Orange G loading dye buffer (6x)	0.01 M TE (pH 7.6) 60% Glycerol (v/v) 10% Orange G (w/v)

PBS (10x)	0.02 M KCl 0.014 M KH_2PO_4 0.1 M Na_2HPO_4 2 x H_2O 1.37 M NaCl pH 7.4 adjusted with NaOH
Protease inhibitor mix	1:1000 Aprotinin (1 mg/ml) 1:1000 Leupeptin (1 mg/ml) 1:1000 Pepstatin (0.7 mg/ml) 1:1000 0.2 M PMSF 1:1000 1 M DTT
Semi-dry transfer buffer (1x)	39 mM Glycine 48 mM Tris 20% Methanol (v/v) 0.0375% SDS (w/v)
Separating gel (SDS-PAGE)	375 mM Tris/HCl, pH 8.8 10%, 12%, 15% or 18% Acrylamide/Bisacrylamide mix (v/v) 0.1% SDS (w/v) 0.13% TEMED (v/v) 0.13% APS (w/v)
Stacking gel 4% (SDS-PAGE)	125 mM Tris/HCl, pH 6.8 4% Acrylamide/Biscrylamide mix (v/v) 0.1% SDS (w/v) 0.13% TEMED (v/v) 0.13% APS (w/v)
TAE buffer (50x)	0.1 M EDTA 2 M Tris pH 7.8 adjusted with acetic acid
Trypan blue solution	0.4% Trypan blue stain (Thermo Fisher Scientific)
Trypsin/EDTA	0.6 mM $CaCl_2$ 2 x H_2O 3 mM EDTA 2.6 mM KCl 1 mM KH_2PO_4 0.4 mM $MgSO_4$ 7 x H_2O 137 mM NaCl 6 mM Na_2HPO_4 2 x H_2O 0.125% Trypsin (w/v) pH 7.0 adjusted with NaOH

2.2 Cell biological methods

2.2.1 Cultivation and manipulation of human cells

2.2.1.1 Cultivation, passaging, freezing and thawing of cells

Adherent HeLa Kyoto (HK) cells were grown in Dulbecco's Modified Eagle's Medium (DMEM) supplemented with 10% heat inactivated fetal bovine serum (FBS) and 1% penicillin/streptomycin (P/S) in a humidified atmosphere at +37°C and 5% CO_2. U2OS 2-6-3 DSB reporter cells were cultured in DMEM with 10% Tet System Approved FBS, 1% P/S and 2 mM L-glutamine. Growth medium of cells was changed every second day unless cells reached 80-90% confluency. In this case, cells were usually passaged in a 1:10 or 1:5 ratio into 14.5 cm cell culture dishes (covered with 20 ml medium). The old medium was discarded and cells washed once with 10 ml phosphate-buffered saline (PBS) to remove apoptotic cells as well as remaining medium. After removal of PBS, cells were dissociated by the addition of 2 ml trypsin/EDTA for 5 min at +37°C. Complete detachment of cells was ensured by gently tapping of the plate. Unattached cells were resuspended in 8 ml of growth medium to stop the trypsin reaction and to fully separate the cells. For cultivation, cell suspension (according to splitting ratio) was added to a fresh cell culture plate containing full growth medium. If cells were needed for different experimental applications, cell viability and cell number were determined using the Countess cell counter (Invitrogen) and the respective amount of cells in suspension seeded into new tissue culture dishes (6-well, 10 cm or 14.5 cm plates). To store cells, trypsinized cells usually from a 14.5 cm tissue culture plate were pelleted by centrifugation for 5 min at 1.200 rpm and the supernatant removed. After one PBS wash, the cell pellet was dissolved in 1 ml freezing medium (90% FBS + 10% dimethylsulfoxide (DMSO)), transferred into cryotubes and stored in isopropanol-filled freezing containers at -80°C. For long-term storage, cryotubes were relocated and kept in liquid nitrogen tanks. Cells in culture were replaced every 2-3 month with freshly thawed cells and were routinely PCR tested for mycoplasma contaminations by an in-house service. To thaw cells, cryotubes were removed from liquid nitrogen containers and shortly incubated in a water bath at +37°C. For quickly removing toxic DMSO, thawed cells were resuspended in growth medium, spun down for 5 min at 1.200 rpm and supernatant discarded. After washing of cells once with PBS, full growth medium was added and cells plated to a fresh cell culture plate.

2.2.1.2 Transfection of plasmid DNA

To reach a confluence of 40-50%, 3×10^6 HK cells were seeded into 14.5 cm tissue culture plates containing growth medium (final volume 20 ml) 24 h prior to transfection. For transient transfections, a ratio of plasmid DNA to FuGENE HD transfection reagent (Promega) of 1:4 was applied. 20 µg of plasmid DNA was diluted in 100 µl of water (final volume) and 900 µl of Opti-MEM added to the reaction followed by the addition of 80 µl FuGENE HD transfection reagent. After incubation for 15 min at room temperature (RT), the transfection suspension was added dropwise onto the cells and dispensed by gently stirring the plate. Empty vector transfection and non-transfected cells acted as negative controls. In case of transfection of cells with plasmids coding for enhanced green fluorescent protein (GFP) or GFP-tagged proteins (listed in table 2.14), transfection efficiency was monitored 24-48 h after transfection by a combination of fluorescence microscopy and flow cytometry as described in section 2.2.3 and 2.2.4. Two days after transfection, cells were harvested for several experimental applications.

2.2.1.3 Transfection of small interfering RNAs (siRNAs)

One day prior to transfection, 2×10^5 HK or U2OS reporter cells were plated into 6-well tissue culture plates containing 2 ml of medium (final volume). 4 µl of the transfection reagent Oligofectamine (Thermo Fisher Scientific) was resuspended in 11 µl Opti-MEM and incubated for 5 min at RT. In the meantime, 2 µl of 100 µmol small interfering RNA (siRNA) stock solution (siRNAs and sequences are listed in table 2.13) was diluted in 8 µl of water (1:5 ratio) and subsequently mixed with 175 µl Opti-MEM. 15 µl of the Oligofectamine reagent mixture was added to the siRNA-containing suspension and incubated for 20 min at RT. Meanwhile, cells were washed twice with 2 ml of PBS to replace full growth medium with 800 µl of DMEM (without FBS or antibiotics). Transient gene silencing was achieved by adding the transfection suspension dropwise onto the cells and by briefly moving the plate to dispense all reagents. After incubating cells for 4 h at +37°C, 500 µl DMEM supplemented with 30% FBS was added. Two days after transfection, cells were collected and counted for several experimental applications. Knockdown efficiency of each experiment was controlled by a combination of immunoblotting (section 2.3.4) and/or reverse transcription quantitative PCR (RT-qPCR) (section 2.4.4 and 2.4.5).

2.2.2 Proliferation analysis of adherent HeLa Kyoto (HK) cells

Two days after siRNA transfection, cell proliferation of HK cells was monitored and quantified using the xCELLigence Real-Time Cell Analyzer (Agilent). Determining the baseline was achieved by measuring 100 µl of growth medium in each well of a 16-well E-plate (Agilent). Afterwards, 100 µl cell suspension at a density of 1×10^5 cells/ml was added. Each treatment was pipetted in triplicates, while the control well with medium only, were additionally filled with 100 µl of growth medium. The E-Plate was placed in the xCELLigence Real-Time Cell Analyzer that is located in a standard CO_2 cell culture incubator. Then, measurement was started over a period of 80 h. Every 10 min, the instrument was measuring, monitoring and recording the impedance in every well, providing information about cell proliferation or changes in cell morphology [312, 313]. At the end of each run, the data were depicted as graphs by the software and could be exported by the users.

2.2.3 Immunofluorescence (IF) Microscopy

2.2.3.1 IF staining

One day prior to transfection, 2×10^5 HK cells were seeded into 6-well cell culture plates containing coverslips as well as 2 ml of medium (final volume). 48 h after transfection of plasmid DNA or siRNAs, coverslips with adherent HK cells were transferred to 24-well plates and treated as follows. After three PBS washes (1 ml each), cells were fixed with 500 µl of 3% paraformaldehyde in PBS for 10 min at RT. Fixation solution was removed and replaced three times with PBS. At this point, coverslips could be stored in PBS at +4°C for several days or directly subjected to immunofluorescence (IF) staining. To this end, cells were permeabilized with 500 µl of PBS containing 0.5% Triton X-100 for 4.5 min on ice followed by three washing steps with PBS. Blocking of cells was performed with 500 µl of 1% bovine serum albumin (BSA) in PBS (blocking solution) for 15 min at RT. For target protein detection, coverslips were stepwise (with three washing steps in between) incubated with 50 µl of primary and then secondary Alexa Fluor-conjugated antibody dilutions (in blocking solution) at the desired concentrations (see table 2.8 and 2.9) for 1h at RT in a dark humidified chamber. After three PBS washes, DNA was counterstained with 200 µl of 10 µg/ml Hoechst H33342 (Sigma-Aldrich) in PBS for 5 min in the dark. Finally, coverslips were washed twice with PBS and mounted on slides with a small drop of Fluoromount-G mounting medium (VWR International). Slides were dried for

24 h at RT, subjected to IF microscopy (section 2.2.3.2) and/or kept at +4°C in the dark for long-term storage.

2.2.3.2 Microscopy

Images of treated HK cells on coverslips were acquired using an Axio Observer.Z1 inverted microscope (Carl Zeiss) equipped with the Zeiss Zen 3.1 (blue edition) software and the Axiocam 506 mono system (Carl Zeiss). Images were taken utilizing the EGFP ET and the DAPI Ultra Bandpass filter sets (AHF Analysentechnik) and accomplished by processing images with Fiji/ImageJ (version 1.51n).

2.2.3.3 Determination of nuclei and nucleoli sizes of HK cells

IF images of HK cells upon siRNA-mediated knockdowns were used to determine nuclei and nucleoli sizes in pixels. Data analysis was performed by Dr. Konstantin Kletenkov (a member of the Hake group) utilizing R language for statistical computing, RStudio and reshape2 package [314]. Cellular feature analysis was carried out using EBImage [315] and figures generated with ggplot2 and cowplot packages.

2.2.4 Flow cytometry analysis

Flow cytometry analysis was carried out using the BD Accuri C6 Plus Flow Cytometer (Becton Dickinson BD Biosciences), together with BD reagents and the BD Accuri C6 Plus v1.0 system software. The data were received as graphs by the software and could be exported by the users.

2.2.4.1 Transfection efficiency

In order to monitor GFP expression of HK cells transiently expressing GFP or GFP fusion proteins, cells were exposed to flow cytometry analysis two days after transfection. Manipulated cells were harvested and 200 µl of cell suspension saved for flow cytometry measurements, providing information about the transfection efficiency. GFP signal of 25.000 events was measured with the optical filter FL1 533/30 nm (formerly 530/30) and gate plotted to forward (FSC) and sideward (SSC) scatter into the viable cell population of non-transfected HK cells. The software

determines the percentage of GFP positive cells. If transfection efficiency was high enough, cells were used for several experimental applications.

2.2.4.2 Cell cycle analysis by propidium iodide (PI) staining

To analyse cell cycle progression of a HK cell population upon RNA interference (RNAi) treatment, cells were stained with the fluorescent, DNA intercalating dye propidium iodide (PI; Sigma-Aldrich) and subjected to flow cytometry analysis. The PI staining enables the measurement of the cell DNA content, which provides information about the current cell cycle phase of the population [316–319]. Two days after siRNA transfection, 1×10^6 cells were harvested and washed once with 1 ml PBS. After centrifugation for 5 min at 1.200 rpm, supernatant was discarded and cell pellet resuspended in 300 µl PBS. Carefully, 700 µl of 100% Methanol (MeOH) was added dropwise while vortexing the cell suspension. After this step, cells could be stored at -20°C for several days or for at least 1 h. After two washing steps with PBS, permeabilized cells were resuspended and incubated in 300 µl staining solution containing 100 µg/ml of DNase-free RNase A (Thermo Fisher Scientific) and 50 µg/ml of PI for 30 min at +37°C in the dark. Finally, cells were analysed by flow cytometry analysis using the optical filter FL2 585/40 nm. PI signal of 50.000 events was measured and gate set to forward (FSC) and sideward (SSC) scatter of PI positive cells for distinguishing healthy cells in G_1, S or G_2/M phase according to their DNA content. The software calculated the percentage of cells in every cell cycle phase.

2.2.5 Induction of DNA double-strand breaks (DSBs) in human cells

2.2.5.1 Ultraviolet (UV) irradiation of HK cells

Two days upon RNAi treatment, HK cells were subjected to Ultraviolet (UV) irradiation to induce DNA double-strand breaks (DSBs). Growth medium of cells was removed and 2 ml of PBS added. Afterwards, cells were treated with different doses of UVC light by placing the 6-well cell culture plate (without lid) into a UV crosslinker (UVP). PBS was replaced by 2 ml of growth medium and UV irradiated cells incubated for 3 h in a CO_2 cell culture incubator. After harvesting and lysing of cells (section 2.3.1), possible changes in the global phosphorylation level of the histone variant H2A.X at serine 139 (γH2A.X) were monitored by immunoblotting (section 2.3.4).

2.2.5.2 Generation of inducible DSBs in U2OS reporter cells

To induce DSBs at defined genomic locations and to analyse the occupancy of γH2A.X that occurs in close proximity to DSBs as a chromatin mediated damage response, the U2OS DSB reporter cell system was used (Figure 10). The U2OS 2-6-3 reporter cells are stably expressing a mCherry-LacI-FokI nuclease protein fused to a modified estradiol receptor (ER) unit and a destabilization domain (DD) to create inducible DSBs within a single genomic locus upon treatment [307, 308, 320, 321]. Under standard conditions, the fusion protein is usually degraded in the cytoplasm. Treatment of cells with Shield1 and 4-hydroxytamoxifen (4-OHT) leads to protein stabilization and consequently to a translocation of the fusion protein into the nucleus. The lac-repressor domain of the construct binds to 256 stable integrated Lac-operator (LacO) repeats approximately 5 kb upstream of a doxycycline-inducible YFP-MS2 reporter transgene. Accordingly, the FokI nuclease domain is targeted to these sites resulting in the generation of unspecific DSBs. As a DNA damage response, the histone variant H2A.X is phosphorylated at serine 139 downstream of DSBs.
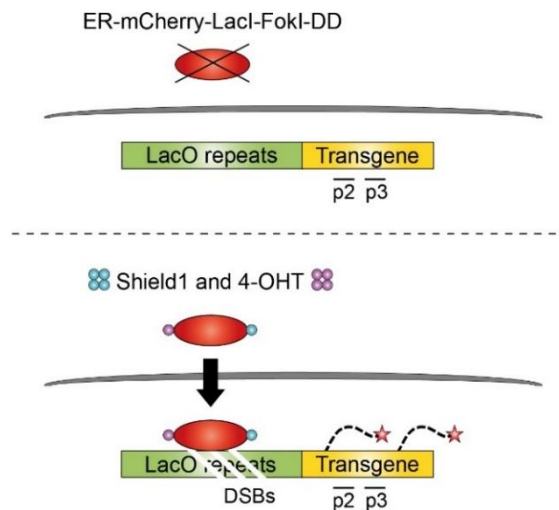
Figure 10: Schematic representation of the U2OS DSB reporter cell system. U2OS 2-6-3 reporter cells are stably expressing a fusion protein (red) consisting of an estradiol receptor (ER) unit, a mCherry protein, a lac-repressor domain (LacI) and a FokI nuclease fused to a destabilization domain (DD), which is usually degraded in the cytoplasm. After treatment of cells with Shield1 (blue dots) and 4-hydroxytamoxifen (4-OHT; magenta dots), the fusion protein is stabilized and translocates to the nucleus (black arrow). The LacI domain binds to stable integrated Lac-operator (LacO; green) repeats upstream of a doxycycline-inducible YFP-MS2 reporter transgene (yellow) followed by the induction of multiple nuclease-inducible DNA double-strand breaks (DSBs; white lines) by FokI. As a chromatin mediated damage response, the histone variant H2A.X is phosphorylated (red stars) at serine 139 (γH2A.X) and can be detected by ChIP-qPCR experiments using the primer sets p2 and p3. Additionally, the localization of the fusion protein can be further monitored and controlled by the mCherry unit using fluorescence microscopy [307, 308, 320, 321].

To monitor the level of γH2A.X at this specific genomic region upon RNAi treatment, cells were used for chromatin immunoprecipitation (ChIP) experiments followed by qPCR (ChIP-qPCR). Two days after siRNA transfection, creation of multiple nuclease-induced DSBs was achieved by treating reporter cells with 1 μM Shield1 as well as 4-hydroxytamoxifen (solved in 100% ethanol) followed by the incubation for 3 h in a CO_2 cell culture incubator. Negative control cells were treated with ethanol only. Afterwards, cells were harvested and collected for ChIP-qPCR experiments (section 2.3.7 and 2.4.6) to analyse the level of γH2A.X at target sites (p2 and p3 region) in knockdown and control as well as treated and untreated (ethanol) cells.

2.3   Biochemical methods

2.3.1 Preparation of cell lysates

To prepare whole cell lysates, 2×10^5 HK or U2OS reporter cells were freshly harvested and subsequently used to generate cell extracts by lysing cells in 48 μl of RIPA buffer for 5 min at +4°C followed by the addition of 12 μl Laemmli sample buffer (5x) and boiling of lysates for 5 min at +95°C. At this point, lysates could be stored at -20°C for several months or proteins directly separated by SDS polyacrylamide gel electrophoresis (SDS-PAGE, section 2.3.2).

RIPA buffer: 10 mM Tris/HCl, pH 7.5
                     150 mM NaCl
                     0.5 mM EDTA
                     0.1% SDS (v/v)
                     1% Triton X-100 (v/v)
                     1% Sodiumdeoxycholate (w/v)
                     add prior to use: protease inhibitor mix

2.3.2 SDS polyacrylamide gel electrophoresis (SDS-PAGE)

Protein separation was achieved by SDS polyacrylamide gel electrophoresis (SDS-PAGE). Gels were casted by hand using a Handcast System (Bio-Rad) and according to the molecular weight of proteins of interest, different percentages of acrylamide were used (usually 10-12%, see table 2.15). After gel polymerization, 20 μl of lysates and 8 μl of a protein marker (PageRuler Plus Prestained Protein Ladder, Thermo

Fisher Scientific) to determine protein molecular weights were loaded onto gels placed in an electrophoresis chamber (Bio-Rad) filled up with Laemmli buffer. Cell lid (Bio-Rad) was placed onto the buffer tank and power cables connected to the power supply unit (Bio-Rad). Finally, gels were run at 80 V until the marker started to separate, then run was continued at 150 V until the dye front was running out of the gel. Usually, gels were directly used for Coomassie staining (section 2.3.3) or immunoblotting (section 2.3.4).

2.3.3 Coomassie staining of SDS-PAGE gels

Coomassie staining of SDS-PAGE gels were mainly used for the visualization of acid extracted histone proteins (section 2.3.5) or to quantify and adjust the amount of proteins for subsequent immunoblotting analyses. SDS-PAGE gel separated proteins were detected by incubating the gels in Coomassie Brilliant Blue R-250 (Fluka) staining solution ON at +4°C. Next day, gels were destained in Coomassie destaining solution until protein bands become visible. Destained gels were recorded by scanning gels on a white light plate (Kaiser slimlite plano).

2.3.4 Immunoblotting

For antibody-based detection of proteins of interest, SDS-PAGE gels containing gel-separated proteins were blotted onto a nitrocellulose membrane (0.45 µl pore size, GE Healthcare Life Sciences) using a semi-dry blotting system (Bio-Rad) connected to a power supply unit (Bio-Rad). Blotting was achieved by shortly soaking the SDS-PAGE gel, a nitrocellulose membrane and four papers of Whatman cellulose (thickness 3 mm, GE Healthcare Life Sciences) in semi-dry transfer buffer and subsequently assembled to a so-called 'sandwich' in the following order (from bottom to top): two Whatman papers, membrane, gel and finally two papers of Whatman. Transfer of proteins from the gel to the membrane was carried out for 1 h at 200 mA. For specific protein detection, membrane was blocked in 10 ml PBS-T (PBS + 0.1% Tween20) containing 5% non-fat dry milk (blocking solution) for 1h at RT followed by the incubation of the membrane with 3 ml of primary antibody dilution (in blocking solution) at the desired concentration (see table 2.8) ON at +4°C. The following day, membrane was washed three times with PBS-T and incubated with 20 ml of HRP-conjugated secondary antibodies (see table 2.9) diluted in blocking solution (1:20.000) for 1 h at RT. After three PBS-T washes, membrane was developed by the

detection of HRP signals using the trident femto Western HRP substrate (GeneTex) and a developing machine (ChemoStar, INTAS).

2.3.5 Acid extraction of histones

To investigate possible changes in the global acetylation level of histone proteins after siRNA transfection, 1×10^7 HK cells were harvested and used for acid extraction of histones as described in [322] followed by immunoblotting analysis. After centrifugation of cells for 5 min at 1.200 rpm, cell pellet was resuspended in 1 ml PBS and the suspension transferred to a fresh 1.5 ml reaction tube. Cell lysis was achieved by adding 1 ml of ice-cold hypotonic lysis buffer followed by 30 min incubation while rotating (end-over-end rotation) at +4°C. Intact nuclei were pelleted by centrifugation for 10 min at 10.000 rpm in a pre-cooled centrifuge (+4°C). Next, nuclei pellet was resuspended in 400 µl of 0.4 N H_2SO_4 and incubated under rotation ON at +4°C. To remove cell debris, centrifugation was performed for 10 min at 13.000 rpm (+4°C) and the supernatant containing histone proteins transferred to a fresh tube. For histone precipitation, 132 µl of 100% trichloroacetic acid (TCA) was added dropwise to the suspension and the tube inverted several times. After incubation for 30 min at +4°C, extracted histones were spun down at 13.000 rpm for 10 min at +4°C. The supernatant was removed and the smear-like histone pellet carefully washed two times with 1 ml ice-cold acetone without disturbing the pellet. Afterwards, histones were air-dried for 10 min at RT and immediately dissolved in 50-100 µl sterile water without producing bubbles. Histone proteins were stored at +4°C or directly used for separation and detection by performing a combination of SDS-PAGE followed by Coomassie staining and immunoblotting. Histone lysates were prepared as follows: 2 µl of Laemmli sample buffer (5x) were added to 5 µl of histones, samples boiled for 5 min at +95°C and total volume loaded to a 15-18% SDS-PAGE gel.

Hypotonic lysis buffer: 10 mM Tris/HCl, pH 8.0
                                     1 mM KCl
                                     1.5 mM $MgCl_2$
                                     add prior to use: protease inhibitor mix

2.3.6 Immunoprecipitation (IP) of GFP-tagged proteins

HK cells transiently expressing GFP or GFP-tagged proteins were used for preparation of nuclear cell extracts. Non-transfected HK cells acted as negative control. For one immunoprecipitation (IP) reaction, 1×10^6 to 1×10^7 HK cells were harvested and resuspended in 200 µl ice-cold RIPA buffer supplemented with RNase-free DNase I (75 Kunitz U/ml, Thermo Fisher Scientific) and $MgCl_2$ (2.5 mM) followed by the incubation on ice for 30 min, while lysates were extensively pipetted up and down every 10 min. After centrifugation of cell extracts at 13.000 rpm for 10 min at +4°C to remove cell debris, the supernatant containing nuclear proteins was transferred into a fresh, pre-cooled tube and 300 µl of dilution buffer added. For immunoblotting analysis, 50 µl (10%) of diluted extracts were saved (input fraction). Next, for each IP 20 µl of GFP-Trap Dynabeads (Chromotek) were washed once with 500 µl ice-cold wash buffer for 10 min at +4°C, while rotating. Magnetic separation of beads was achieved by placing the tubes onto a magnetic rack (Diagenode) for 2 min until the lysates become clear. Carefully, the supernatant was discarded without disturbing the bead pellet. IPs were carried out by adding diluted lysates to the equilibrated beads and incubating the samples under rotation ON at +4°C. The following day, beads were magnetic separated and cleared lysates (supernatant) discarded. To remove unspecific bindings, beads were washed three times with 500 µl wash buffer for 5 min while rotating. Elution of immunoprecipitated proteins was realized by boiling beads in 10 µl Laemmli sample buffer (2x) for 5 min at +95°C. Finally, beads were magnetic separated and lysates containing dissociated immunocomplexes completely (100%) loaded to 12% SDS-PAGE gels. Separation as well as detection of proteins of interest and possible binding factors were performed by SDS-PAGE followed by immunoblotting.

Dilution buffer: 10 mM Tris/HCl, pH 7.5
150 mM NaCl
0.5 mM EDTA
add prior to use: protease inhibitor mix

Wash buffer: 10 mM Tris/HCl, pH 6.8
150 mM NaCl,
0.5 mM EDTA
0.05% Nonidet P-40 substitute (v/v)
add prior to use: protease inhibitor mix

2.3.7 Chromatin immunoprecipitation (ChIP) of U2OS reporter cells

In order to analyse the enrichment of γH2A.X at target sites in a DNA damage-dependent manner after RNAi treatment, ChIP experiments were performed as described in [176, 310] with a few adjustments. Two days after siRNA transfection, 2 x 10⁶ U2OS 2-6-3 reporter cells were harvested for each ChIP reaction and fixation of DNA-protein interactions were achieved by incubating cells in DMEM medium supplemented with 1% formaldehyde for 10 min at RT. Afterwards, cells were quenched with 125 mM glycine for 5 min at RT and subsequently washed three times with 10 ml of ice-cold PBS containing 10% FBS. After each washing step, cells were spun down for 5 min at 1.200 rpm followed by flash freezing of cells in liquid nitrogen. Fixed cells could be stored at -80°C or directly exposed to cell lysis and chromatin shearing. For cell lysis, reporter cells were resuspended in 5 ml ice-cold lysis buffer 1 and incubated for 10 min at +4°C under rotation followed by centrifugation of cells for 5 min at 1.500 rpm. Cell pellet was solved in 5 ml of lysis buffer 2 and incubated for 10 min at +4°C. After centrifugation for 5 min at 1.500 rpm, nuclei were resuspended in 1 ml of buffer B, transferred to 15 ml conical hard plastic tubes and subjected to Bioruptor (Diagenode) sonication with the following settings: 20 cycles high energy, 30 s on followed by 30 s off. To remove cell debris, sheared chromatin was centrifuged for 10 min at 13.000 rpm (+4°C) and supernatant separated into fresh pre-cooled 15 ml centrifuge tubes. Afterwards, 9 ml of ice-cold buffer A was added to the soluble chromatin fraction and 1 ml used for each ChIP reaction. For ChIP, 10 μl of Protein G coupled Dynabeads (Invitrogen) were washed two times with 500 μl PBS-T in 1.5 ml low binding tubes followed by the incubation of beads with primary antibody at the desired concentration (see table 2.8) in PBS-T for at least 2 h while rotating (+4°C). Next, antibody-coupled beads were washed two times with PBS-T by magnetically separating the beads and removing the supernatant. IPs were carried out by resuspending beads in 1 ml of diluted chromatin mixture followed by ON incubation at +4°C while rotating. Additionally, for each condition one mock sample (without the addition of antibody) was prepared as negative control. The following day, beads were collected and washed four times with 1 ml of ice-cold buffer A and one time with 1 ml of ice-cold buffer C. In addition, 50 μl (5%) of mock samples were saved as input fractions and 50 μl of elution buffer added. Beads were resuspended in 100 μl elution buffer and processed together with input samples. For reverse cross-linking, probes were incubated ON at +65°C while shaking. Next day, beads were magnetic separated and supernatant transferred to a fresh 1.5 ml reaction tube. After the addition of 100 μl Tris-EDTA (TE) and 4 μl of DNase-free RNase A (10 mg/ml),

samples were incubated for 1 h at +37°C. Finally, 2 µl of proteinase K (20 mg/ml) was added and the reaction incubated for 2 h at +56°C. ChIP DNA as well as input DNA were purified using the MinElute PCR Purification Kit following the manufacturer's instructions and eluted in 20 µl super clean water. Quantification of chromatins shearing degree (DNA sizes) was controlled by a 2% agarose gel (see 2.4.3) and purified DNA analysed by qPCR as described in section 2.4.6.

Lysis buffer 1:   50 mM HEPES, pH 7.5
140 mM NaCl
1 mM EDTA
10% Glycerol (v/v)
0.5% Nonidet P40 substitute (v/v)
0.25% Triton X-100 (v/v)
add prior to use: protease inhibitor mix

Lysis buffer 2:   10 mM Tris/HCl, pH 8.0
200 mM NaCl
1 mM EDTA
0.5 mM EGTA
add prior to use: protease inhibitor mix

Buffer B: 50 mM Tris/HCl, pH 8.0
10 mM EDTA
0.5% SDS (v/v)
add prior to use: protease inhibitor mix

Buffer A: 10 mM Tris/HCl, pH 7.5
1 mM EDTA
0.5 mM EGTA
140 mM NaCl
1% Triton X-100 (v/v)
0.1% SDS (v/v)
0.1% Sodiumdeoxycholate (w/v)
add prior to use: protease inhibitor mix

Buffer C: 10 mM Tris/HCl, pH 8.0
10 mM EDTA
add prior to use: protease inhibitor mix

Elution buffer: 50 mM Tris/HCl, pH 8.0

10 mM EDTA

1% SDS

add prior to use: protease inhibitor mix

TE: 10 mM Tris/HCl, pH 8.1

1 mM EDTA

2.3.8 Chromatin immunoprecipitation (ChIP) of HK cells followed by next generation sequencing (NGS): ChIP-seq

To investigate the occupancy as well as the acetylation level of the histone variant H2A.Z after RNAi treatment, ChIP experiments from siRNA treated human HK cells were performed and carried out in biological duplicates. Non-target siRNA (siNTC) treated cells served as negative control. Note that for this experiment, another ChIP protocol was used that has been proven to be much more efficient for HK cells. Since the above-mentioned protocol (section 2.3.7) differs from the new one in many aspects, it will be described in more detail below.

2.3.8.1 Chromatin immunoprecipitation (ChIP)

For each ChIP reaction, 1×10^7 HK cells were harvested two days after siRNA transfection and protein-DNA interactions cross-linked by fixation of cells in 10 ml DMEM medium containing 1% formaldehyde for 10 min at RT. The reaction was stopped by quenching cells with 125 mM glycine for 5 min at RT. Cells were then washed three times with 10 ml PBS, spun down for 5 min at 1.200 rpm and supernatant discarded. Fixed cells were resuspended in 1 ml SDS-lysis buffer and transferred to 15 ml conical hard plastic tubes for chromatin shearing. To generate chromatin fragments of 250 bp in average size, cell lysates were subjected to Bioruptor (Diagenode) sonication with the following settings: 15 cycles high energy, 30 s on followed by 30 s off. After shearing, cell extracts were centrifuged for 13.000 rpm for 10 min at +4°C and chromatin (supernatant) used for IPs. In addition, 10 µl (10%) of lysates were saved as input fractions. One day prior to ChIP, for each reaction 10 µl of magnetic Protein G coupled Dynabeads (Invitrogen) were washed once with dilution buffer mix for 10 min at +4°C under rotation. After magnetic separation of beads, clear supernatant was discarded and beads incubated with individual primary antibodies (see table 2.8) diluted in dilution buffer mix ON at +4°C

while rotating. The following day, antibody-coupled beads were washed three times with dilution buffer mix by magnetically separating beads and removing supernatant. ChIPs were carried out by resuspending the beads in 900 µl dilution buffer and by adding 100 µl of chromatin followed by ON incubation at +4°C under rotation. Next day, beads were collected and washed as follows (1 ml per washing step): 1x with low-salt buffer, 1x with high-salt buffer, 1x with LiCl buffer and 2x with TE. Afterwards, 100 µl of TE and 1 µl DNase-free RNase A (10 mg/ml) were added to the beads as well as to the input samples (processed together with ChIP samples) followed by 30 min incubation at +37°C. To each reaction 5 µl 10% SDS and 2.5 µl proteinase K (20 mg/ml) were added and incubated at +37°C for 4 h followed by ON incubation at +65°C (reverse cross-linking). Finally, beads were magnetic separated and immunoprecipitated DNA as well as input DNA purified as described in section 2.3.8.2.

SDS-lysis buffer: 50 mM Tris/HCl, pH 8.1
                                  10 mM EDTA
                                  1% SDS (v/v)
                                  add prior to use: protease inhibitor mix

Dilution buffer: 16.7 mM Tris/HCl, pH 8.1
                                  167 mM NaCl
                                  1.2 mM EDTA
                                  1% Triton X-100 (v/v)
                                  0.01% SDS (v/v)
                                  add prior to use: protease inhibitor mix

Dilution buffer mix: 90% dilution buffer
                                  10% SDS-lysis buffer
                                  add prior to use: protease inhibitor mix

Low-salt buffer: 20 mM Tris/HCl, pH 8.1
                                  150 mM NaCl
                                  2 mM EDTA
                                  1% Triton X-100 (v/v)
                                  0.1% SDS (v/v)
                                  add prior to use: protease inhibitor mix

High-salt buffer: 20 mM Tris/HCl, pH 8.1

500 mM NaCl

2 mM EDTA

1% Triton X-100 (v/v)

0.1% SDS (v/v)

add prior to use: protease inhibitor mix

LiCl buffer: 10 mM Tris/HCl, pH 8.1

1 mM EDTA

250 mM LiCl

1% Nonidet P40 substitute (v/v)

1% Sodiumdeoxycholate (w/v)

add prior to use: protease inhibitor mix

2.3.8.2 Purification of chromatin immunoprecipitated (ChIP) DNA

Purification of ChIP DNA and respective input DNA was reached by utilizing the Illustra GFX PCR DNA and Gel Band Purification Kit (GE Healthcare Life Sciences) according to the manufacturer's instructions. On-column purified DNA was eluted in 20 µl super clean water and concentrations determined with the Qubit 4 Fluorometer (Invitrogen) and the corresponding dsDNA HS Assay Kit (Invitrogen). Quantification of chromatins shearing degree (DNA sizes) was monitored by a combination of 2% agarose gel (see 2.4.3) and capillary electrophoresis (Fragment Analyzer, Agilent) using the HS Small Fragment Kit (Agilent). ChIP DNA was investigated by next generation sequencing (NGS).

2.3.8.3 Library preparation

For NGS, Illumina sequencing libraries were generated with the MicroPlex Library Preparation Kit (Diagenode) following the manufacturer's instructions with a few variations. Library amplification was performed by adjusting the number of amplification cycles to the amount of input material according to the manufacturer's amplification guide. Validation of library amplification was intermediately quantified by the determination of unpurified library concentrations using the Qubit 4 Fluorometer and the dsDNA HS Assay Kit. If required, in case library yield ($\sim$ 5 ng/µl) was not reached, samples were re-amplified for a few additional cycles. After purification, libraries were eluted in 20 µl of 0.1x TE buffer pH 8.0. Quality control of purified

libraries were assessed by checking DNA sizes with the Fragment Analyzer using the HS Small Fragment Kit. Finally, 10 µl of sequencing-ready libraries were send for NGS (75 bp read length, single-read) to the Laboratory of the Genomics Core Facility in Marburg (Philipps-University). Libraries were sequenced on an Illumina NextSeq550 platform. For bioinformatic data analysis see section 2.5.1. Validation of ChIP-seq results were performed by ChIP-qPCR experiments (section 2.4.6).

2.4 Molecular biological methods

2.4.1 RNA extraction of human cells

Two days after siRNA transfection, HK or U2OS reporter cells were harvested and total RNA isolated with the RNeasy Mini Kit (Qiagen) according to the manufacturer's instructions. During isolation, an on-column DNase digestion was performed using the RNase-free DNase set (Qiagen). Purified RNA was subsequently eluted in 30 µl elution buffer (Kit) and concentration of RNA immediately measured by the NanoPhotometer NP80 (Implen). For quality control, 1 µg of total RNA was analysed on a 1.5% agarose gel by electrophoresis (section 2.4.3). Afterwards, RNA was used for cDNA synthesis (section 2.4.4) followed by qPCR (section 2.4.5) or NGS (section 2.4.2). Storage of remaining RNA was accomplished at -80°C for up to a year without degradation.

2.4.2 RNA sequencing

In order to gain more insights into global changes in gene expression upon RNAi treatment, NGS of RNA (RNA-seq) was performed. Two days after siRNA exposure, HK cells were collected and total RNA isolated as described above in section 2.4.1. Quality of RNA was monitored by agarose gel electrophoresis. Additionally, assessment of RNA quality was achieved by capillary electrophoresis using the Fragment Analyzer and the RNA Kit (Agilent). By determining the 28S to 18S ribosomal RNA (rRNA) ratio, the RNA integrity number (RIN) was evaluated by the Fragment Analyzer software. The RIN ranges from 1 (fully degraded) to 10 (fully intact). If desired level of RNA integrity was obtained, RNA was used for NGS. Library preparation of total RNA using the QuantSeq 3' mRNA-Seq Library Prep Kit FWD (Lexogen) according to the manufacturer's protocol and sequencing (75 bp read length, single-read) on an Illumina NextSeq550 platform were carried out by the

Laboratory of the Genomics Core Facility in Marburg (Philipps-University). For bioinformatic analysis of RNA-seq data see section 2.5.2. Validation of RNA-seq was performed by quantification of mRNA levels with qPCR (section 2.4.4 and 2.4.5).

2.4.3 Agarose gel electrophoresis

Separation of nucleic acids was performed by agarose gel electrophoresis. Agarose gels were casted by hand using an electrophoresis system (VWR Peqlab) containing a comb, a gel tray and a lid. According to the size of nucleic acids, different amounts of agarose (Carl Roth; 1.5% agarose for RNA and 2% agarose for sheared DNA or qPCR products) were used. For casting a gel, agarose was weighed and the respective amount heated in 1x TAE buffer. The intercalating and fluorescent agent ethidium bromide (Carl Roth) was added to the hand-warm agarose mixture at a final concentration of 0.5 µg/ml. The solution was transferred to a gel tray containing a comb and after polymerization, electrophoresis chamber was filled up with 1x TAE buffer. 1 µg of RNA or DNA (diluted in 6x Orange G loading dye buffer) as well as 8 µl of a 1 kb or 100 bp Ladder (Thermo Fisher Scientific) to determine nucleic acid sizes were loaded onto the gel. Finally, lid was placed onto the chamber, power cables connected to the power supply and gels run at 90 V for about 30 min. Visualization of nucleic acids was achieved by UV light in an INTAS GelStick touch documentation system (Intas).

2.4.4 cDNA synthesis

For cDNA synthesis, 1 µg of total RNA was reverse transcribed utilizing the Transcriptor First Strand cDNA Synthesis Kit (Roche) following the manufacturer's protocol. Reverse transcription of poly(A) tail containing messenger RNAs (mRNA) was achieved using oligo(dT) primers. cDNA was stored at -20°C or directly used for qPCR analyses (section 2.4.5).

2.4.5 Quantification of mRNA levels with quantitative PCR (qPCR)

To investigate and to validate changes in gene expression upon RNAi treatment, qPCR of cDNA was performed in technical triplicates using SYBR Green master mix (Bio-Rad) and a CFX96 Real-Time System (Bio-Rad). Sequence-specific primer pairs for genes of interest were designed using the web-based Primer3 tool and were

BLASTed using the genome browser UCSC In-Silico PCR tool and the NCBI Basic Local Alignment Search Tool (BLAST) to ensure potential binding of primer pairs to one specific region (see table 2.11). Afterwards, PCR efficiency as well as specificity were examined by preparing a standard curve of serially diluted cDNA for each newly generated primer pair. Furthermore, at the end of each run a melting curve was generated for assessing qPCR product specificity. The primer efficiency of all primer sets used in this study ranged from 90-110% (amplification rate 1.9 to 2.1). Additionally, 10 µl of qPCR products were loaded to a 2% agarose gel and were subjected to gel electrophoresis to check the expected product size of amplified fragments. For qPCR assays, samples were analysed in a total reaction volume of 15 µl. Initially, a master mix containing 7.5 µl of 2x SYBR Green master mix (contains dNTPs, $MgCl_2$ and Sso7d fusion DNA polymerase), 1.5 µl of 4 µM primer mix (contains forward and reverse primer) and 1 µl of ddH_2O was prepared for each reaction. Total cDNA was diluted with ddH_2O in a 1:5 ratio and 5 µl of cDNA premix pipetted to a well of a 96-well plate. Then 10 µl of master mix was added to each well already containing the cDNA dilution. Water only (instead of cDNA premix) served as negative control to exclude master mix contaminations. Finally, the plate was sealed with an adhesive foil and loaded into the CFX96 Real-Time cycler with the following PCR program:

Table 2.16: qPCR program

Cycles	Step	Temperature	Duration	Other
1x	preincubation	+95°C	5 min	polymerase activation and DNA denaturation
40x	amplification	+95°C +60°C	3 sec 20 sec	denaturation and annealing/extension (plate read)
1x	melting curve	+65°C to +95°C	12°C/min	+1°C increments (plate read)

SYBR Green is a fluorescent DNA intercalating dye that allows detection of the DNA amplification progress in real-time [323, 324]. In each cycle, DNA was amplified that results in an increase in the level of fluorescence that is measured at the end of each extension step. The resulting cycle threshold (Ct) values were used for the calculation of fold change gene expression levels based on the 2−ΔΔCT method relative to the siLuci or siNTC negative control and normalized to the transcript level of the housekeeping gene Hypoxanthine phosphoribosyltransferase 1 (HPRT1). The

standard deviation (SD) of technical triplicates was calculated and presented as error bars.

2.4.6 Quantification of chromatin immunoprecipitated DNA with quantitative PCR (ChIP-qPCR)

To investigate and to validate the occupancy of specific histone proteins or histone modifications after RNAi treatment, ChIP experiments followed by quantitative PCR (ChIP-qPCR) were conducted. Primer pairs (listed in table 2.12) were designed and established as mentioned immediately before, in particular by using the Integrative Genomics Viewer (IGV). After ChIP, purified DNA was analysed in technical triplicates by qPCR as described above in section 2.4.5. Data analysis was performed according to the percent input method and standard deviation (SD) of technical triplicates calculated and presented as error bars.

2.5 Bioinformatics

2.5.1 ChIP-seq data analysis

Bioinformatics data analysis of ChIP-seq results were carried out by our collaborator Prof. Dr. Marek Bartkuhn (Biomedical Informatics and Systems Medicine Science Unit for Basic and Clinical Medicine, JLU, Giessen) as described in [257]. Read alignment of raw sequencing reads against the human genome (hg19) was performed using bowtie version 1.1.2. Duplicated reads were removed with Picard's MarkDuplicates and Samtools rmdup function. Reads per kilo base per million mapped reads (RPKM) normalized coverage vectors were created using the bamCoverage function of Deeptools [325]. Peak calling was performed using MACS2 [326]. For differential binding analysis, the resulting peak set was filtered against the ENCODE blacklisted regions and merged into reference peak sets. Detection of differentially bound sites was done using DESeq2 [327]. Binding sites were annotated to their corresponding genes, which were subsequently used for an analysis of overrepresented functional terms using Genomic Regions Enrichment of Annotations Tool (GREAT) [328]. Heatmaps were generated and plotted by collecting coverage vectors via Deeptools computeMatrix and Deeptools plotHeatmap function. Finally, comparison of differentially bound sites to chromatin states was performed as previously described

[310]. Both, raw and processed data are available in the NCBI Gene Expression Omnibus (GEO) under accession number GSE163318.

2.5.2 RNA-seq data analysis

Bioinformatics analysis of RNA-seq data were performed by Tobias Friedrich (Institute for Biochemistry, JLU, Giessen) and Prof. Dr. Marek Bartkuhn (Biomedical Informatics and Systems Medicine Science Unit for Basic and Clinical Medicine, JLU, Giessen) as described in [257] using a customized systemPipeR R/BioConductor package [329, 330] within R version 4.0.2 [331]. Random Unique Molecular Identifier (UMI) barcodes were extracted from raw sequencing reads with UMI-Tools [332] and these processed reads mapped to the human genome (hg19). Reads with identical UMIs (duplicates) were ommitted with UMI-Tools and gene annotation counts calculated using the summarizedOverlaps function of the GenomicAlignments R/BioConductor package [333]. Normalization as well as detection of differentially expressed genes upon knockdown were performed using DESeq2 v.1.28.1 [327]. Volcano-plots were created with EnhancedVolcano R/BioConductor package and Gene Set Enrichment Analysis (GSEA) performed using the clusterProfiler R/BioConductor package [334] with Gene Ontology (GO) and Kyoto Encyclopedia of Genes and Genomes (KEGG) databases. Sequencing data is available in the NCBI Gene Expression Omnibus (GEO) under accession number GSE16321.

3   RESULTS

3.1   JAZF1 associates with the histone acetyltransferase TIP60, a enzymatic subunit of the p400 complex

We identified JAZF1 as a novel member of an ANP32E-exluding p400 chaperone/remodelling sub-complex that contains MBTD1 [257] (Figure 7). As these findings received from the SILAC-MS approach were surprising in terms of potentially shedding new light on the biological functions of JAZF1, they need to be independently verified. To confirm the association of JAZF1 with the p400 complex, I performed pull-down experiments with GFP-TIP60, the specific histone acetyltransferase (HAT) subunit of the p400 complex, or, as negative control GFP alone, followed by immunoblot detection of JAZF1. For this purpose, I first transiently transfected HeLa Kyoto (HK) cells with constructs encoding GFP or GFP-TIP60 (Figure 11A) and two days after transfection, both the cellular localization and the expression of the recombinant proteins were assessed by a combination of immunofluorescence (IF) and flow cytometry analyses in comparison to non-transfected HK cells (-). Therefore, control and transfected cells were either fixed followed by IF microscopy or directly subjected to flow cytometry analysis. IF images revealed the solely nuclear localization of GFP-TIP60, while GFP is enriched in both the cytoplasm and the nucleus (Figure 11B). Moreover, flow cytometry analysis showed a rather mild GFP-TIP60 overexpression compared to GFP expressing cells (Figure 11C). However, since GFP and GFP-TIP60 could be expressed in adequate amounts in HK cells, I next carried out pull-down experiments. Nuclear extracts from transiently expressing GFP or GFP-TIP60 and non-transfected (-) HK cells were generated and used for pull-downs with GFP-Trap magnetic Dynabeads to precipitate TIP60 and its respective interaction partners (Figure 11D). Finally, verification of the binding of JAZF1 to TIP60 was analysed by immunoblots (Figure 11E). Indeed, GFP-TIP60 specifically pulled-down endogenous JAZF1, while no interaction between TIP60 and the negative control protein ZNHIT1, a SRCAP complex-specific component, could be observed (Figure 11E), thereby highlighting the specificity of the experimental approach. Utilizing an anti-GFP antibody served as control for successful GFP and GFP-TIP60 pull-downs, showing that both proteins were highly enriched after immunoprecipitations (IPs). Unfortunately, the reverse experiment pulling-down GFP-JAZF1 did not yield unambiguous results, as several TIP60 antibodies cross-reacted with GFP-JAZF1.
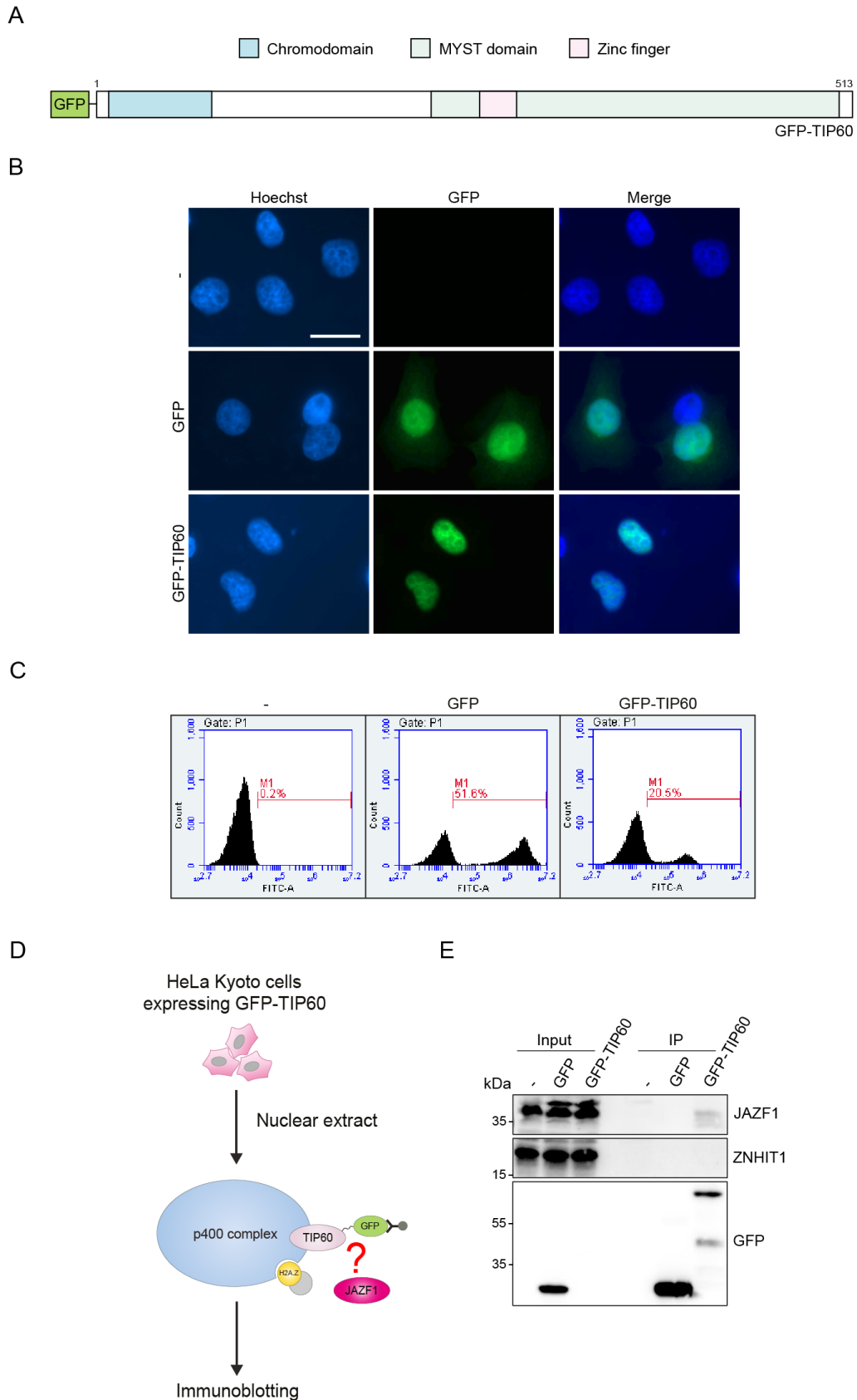
Figure 11: JAZF1 interacts with the p400-specific histone acetyltransferase TIP60.
(**A**) Schematic representation of the full-length GFP-TIP60 protein and its functional domains. The chromodomain, crucial for TIP60's binding to chromatin, is depicted in light blue and the MYST domain in light green, which contains an additional zinc finger (light pink) and the catalytic HAT domain (not shown).

(**B**) Immunofluorescence analysis of non-transfected (-) and transiently transfected HK cells with GFP or GFP-TIP60 for visualizing expression levels as well as protein localization of exogenous proteins. DNA was stained with Hoechst (blue). Scale bar (white) for all pictures = 20 μm. (**C**) Flow cytometry histogram of non-transfected (-), GFP or GFP-TIP60 transiently expressing HK cells described in (B) to determine transfection efficiency. The viable cell population was selected by applying the appropriate gate in the forward and sideward scatter Dot-plot of non-transfected HK cells (-) (see Figure A.1 in appendix for more information). (**D**) Schematic procedure of pull-down experiments performed in (E). The nuclear fraction of non-transfected (-) or transiently expressing GFP or GFP-TIP60 HK cells were isolated and used for precipitations with GFP-Trap magnetic Dynabeads (grey). Binding of JAZF1 (magenta) to the H2A.Z-specific p400 complex (blue) member TIP60 (pink-green) was analysed by immunoblot. (**E**) Immunoblotting of JAZF1, ZNHIT1 and GFP upon pull-down experiments of nuclear fractions of transient expressing GFP or GFP-TIP60 and non-transfected (-) HK cells. ZNHIT1, a SRCAP complex member, served as negative control. Representative immunoblot out of three biological replicates showing similar results is presented.

In summary, pull-down experiments demonstrated that JAZF1 associates with TIP60, the HAT member of the p400 complex, thereby reinforcing our previous MS findings, in which JAZF1 was identified as a new part of an H2A.Z-specific MBTD1-containing p400 sub-complex [257].

3.2 Dynamics of global γH2A.X are largely unimpeded by JAZF1

Since JAZF1 is functionally poorly characterized and it is still unclear in which cellular processes this factor is involved, I next aimed to decipher the role JAZF1 might play within the p400 chaperone/remodelling complex through knockdown studies. Interestingly, first preliminary data from our group uncovered a potential role of JAZF1 in DNA damage repair processes. In collaboration with Rebecca Smith and Gyula Timinszky (MPI Biochemistry, Munich), Martina Peritore (a former PhD student of our group) exposed HK cells transiently expressing GFP-tagged JAZF1 to laser irradiation and monitored the recruitment of JAZF1 to bleached sites of DNA damage, providing a first indication of whether JAZF1 participates in endogenous repair processes. Indeed, GFP-JAZF1 was rapidly recruited to DSBs, suggesting that the novel p400 complex member is somehow implicated in the DNA damage response, as these results were also obtained for GFP-MBTD1 and -TIP60 (unpublished data, not shown), which have already been linked to DNA damage repair [284]. Nevertheless, the underlying mechanisms by which JAZF1 could influence those processes is not

known yet. Therefore, JAZF1's involvement in DNA repair should first be analysed in more detail.

The phosphorylation of the histone variant H2A.X occurs as a first event in response to DSBs and act as a platform for several DNA repair-associated factors to facilitate chromatin opening and to initiate the repair of injured sites [206, 210, 213, 284]. Therefore, γH2A.X is an appropriate marker to examine the DNA damage generated and the subsequent repair of DNA lesions [335], while a prolonged persistence of γH2A.X foci mirrors not only an inability to destabilize them, but also an actual defect in DNA damage repair [284]. Interestingly, among other p400 chaperone complex factors, MBTD1 and TIP60 are essential in regulating DNA damage signalling cascades, and moreover, it has previously been shown that both influence the disappearance of γH2A.X foci after induction of DNA damage [284]. Hence, I wondered if JAZF1 also controls DNA damage repair processes since it is associated with the p400 chaperone complex, especially with MBTD1 and TIP60, as demonstrated by SILAC-MS and pull-down experiments [257] (Figure 7 and 11). To address this hypothesis, I investigated whether JAZF1 depletion does also affect the kinetics of γH2A.X formation in a DNA damage dependent manner, which might reflect a defect in DNA repair.

Firstly, I determined whether JAZF1 could be sufficiently downregulated in HK cells via RNAi. To do so, I transfected HK cells with two different siRNAs against JAZF1 mRNA (siJAZF1 #2 and #4) or, as negative control, with an siRNA targeting a Luciferase sequence (siLuci) that is not present in human cells. Afterwards, transient gene silencing of JAZF1 was ascertained by a combination of reverse transcription quantitative PCR (RT-qPCR) using two JAZF1-specific primer pairs and immunoblot analysis using an antibody against JAZF1. The analyses revealed that JAZF1 could be efficiently depleted, as transfection of HK cells with JAZF1-specific siRNAs (siJAZF1 #2 and #4) led to decreased JAZF1 mRNA (Figure 12A) and protein (Figure 12B) expression levels in comparison to the non-transfected (-) and/or siLuci control.
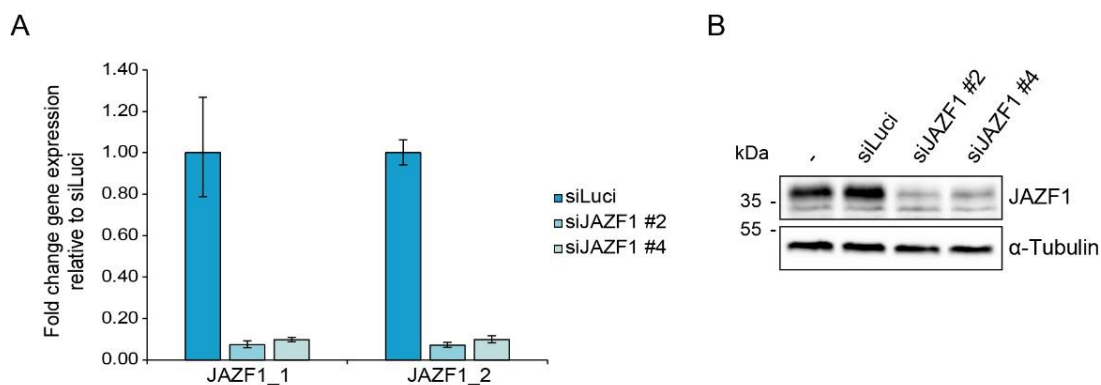
Figure 12: JAZF1 is efficiently depleted in HeLa Kyoto cells via RNAi. (**A**) JAZF1 mRNA expression analysis by RT-qPCR two days after control (siLuci, dark blue) or JAZF1 (siJAZF1 #2 (blue) and #4 (light blue)) siRNA-mediated knockdowns in HK cells using two JAZF1 primer pairs (JAZF1_1 and JAZF1_2). Shown is the fold change gene expression compared to control (siLuci) and normalized to HPRT1 expression levels. Error bars depict SD of three technical replicates. Illustrated is one out of three biological replicates with similar results. (**B**) Immunoblotting analysis of JAZF1 of non-transfected (-) or transfected HK cells with siRNAs against JAZF1 mRNA (siJAZF1 #2 and #4) or, as negative control, Luciferase-specific siRNA (siLuci). Antibody staining against α-Tubulin served as loading control. Shown is one out of three biological replicates with similar results.

As the two JAZF1-specific siRNAs were suitable for JAZF1 knockdown in HK cells, I next established the appropriate amount of UVC light required for initiation of cellular DNA damage signalling cascades. To this end, HK cells were treated with different doses of UVC light to induce DSBs. After three hours incubation, cells were used either for immunoblot analysis or IF staining with an antibody against γH2A.X, as a marker for the DNA damage produced. Immunoblot analysis detected an increase in global γH2A.X levels after exposing cells to UV irradiation (Figure 13A), a result that was successfully verified by IF (Figure 13B). This indicates that the UVC light induces DNA damage, which in turn activates cellular DNA damage repair processes. Moreover, the analyses revealed that the more intensive the UV radiation, the higher the level of γH2A.X (Figure 13A, B). However, the global level of γH2A.X appears to be already saturated after treating cells with 5.000 µJ/cm^2 UVC light (Figure 13A). I therefore decided to proceed with the 500 and 1.000 µJ/cm^2 energy modes in order to be able to capture whether JAZF1 affects global γH2A.X levels.
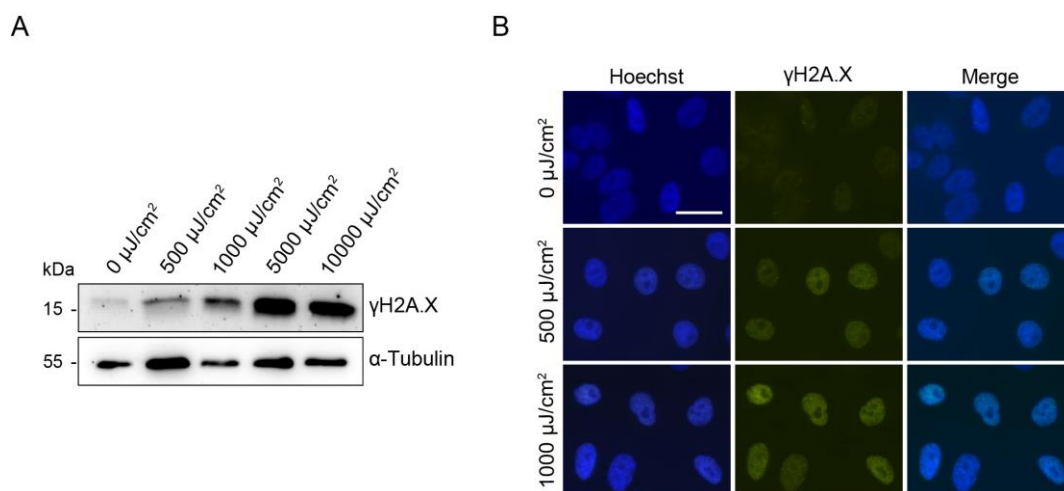
Figure 13: Exposure of HK cells to UV irradiation leads to increased phosphorylation of the histone variant H2A.X. (**A**) Immunoblot analysis with antibodies against γH2A.X or, as loading control, α-Tubulin of whole cell extracts after UVC irradiation (0, 500, 1000, 5000 and 10000 µJ/cm^2) of HK cells. Representative immunoblot of n = 2 showing similar results. (**B**) Representative immunofluorescence (IF) images from UV-irradiated (0, 500 and 1000 µJ/cm^2) HK cells stained with an antibody against γH2A.X (green). DNA was counterstained with Hoechst (blue). Scale bar (white) for all pictures = 20 µm.

Having determined an appropriate dose of UVC light exposure, I next set out to identify whether JAZF1 knockdown leads to global changes in the enrichment of γH2A.X after cell irradiation via immunoblotting (Figure 14A). Therefore, HK cells were first transfected with control siLuci or the two JAZF1-specific (siJAZF1 #2 and #4) siRNAs. Afterwards, JAZF1-depleted and control cells were subjected to the different doses of UVC light exposure (0, 500, 1000 µJ/cm^2) in order to induce DNA damage and the subsequent repair of DNA lesions. Finally, three hours after incubation possible alterations in the accumulation of γH2A.X were detected in a semi-quantitative manner by immunoblot analysis with antibodies against γH2A.X or, as proof for an adequate knockdown, JAZF1 (Figure 14B). Consistently with the previous IF and immunoblot results above (see Figure 13), the level of γH2A.X increases after exposing cells to UV irradiation (500 and 1000 µJ/cm^2) in comparison to the control (0 µJ/cm^2) condition (Figure 14B, upper blot), demonstrating the applicability of the experimental approach. However, downregulation of JAZF1 (Figure 14B, middle blot) did not significantly affect the global level of γH2A.X, as the controls (-, siLuci) showed similar phosphorylation levels of H2A.X (Figure 14B, upper blot).
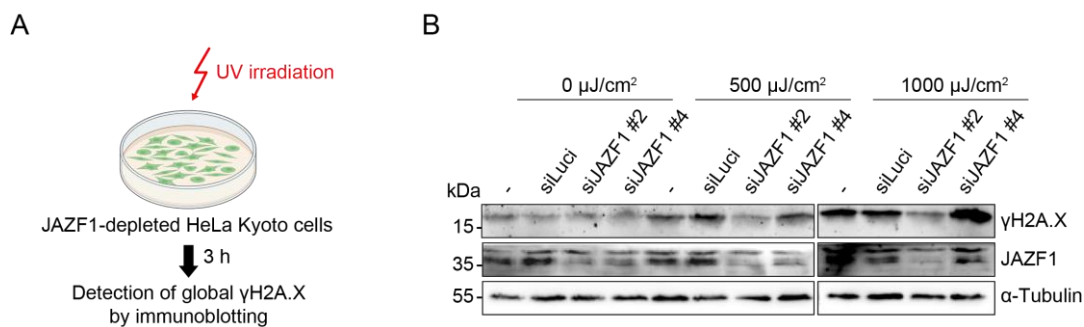
Figure 14: Loss of JAZF1 has no impact on the global level of γH2A.X. (A) Schematic depiction of the experimental approach performed in (B). Two days after siRNA-mediated knockdowns of control or JAZF1, HK cells were exposed to UV irradiation (red arrow) followed by immunoblot analysis of γH2A.X. Figure created with BioRender.com. **(B)** Immunoblotting of γH2A.X, JAZF1 and α-Tubulin of non-transfected (-) or transfected HK cells with siRNAs against JAZF1 mRNA (siJAZF1 #2 and #4) or, as negative control, Luciferase-specific siRNA (siLuci) followed by UVC light treatment (0, 500 and 1000 $\mu J/cm^2$). Antibody staining against α-Tubulin served as loading control. Representative immunoblot of n = 5 showing similar results.

The results obtained in the immunoblot analyses showed so far no evidence that depletion of JAZF1 affects global levels of γH2A.X. However, it could well be that slight changes occurring in the accumulation of γH2A.X after downregulation of JAZF1 are not ascertainable via immunoblotting. For this reason, the U2OS DSB reporter cell system [307, 320] was applied to quantitatively analyse the occupancy of γH2A.X at a specific DNA damage-inducible genomic region upon JAZF1 depletion (referred in section 2.2.5.2, Figure 10). In order to be able to implement this examination, I firstly determined whether JAZF1 could also be efficiently downregulated in the U2OS DSB reporter cells via RNAi. Therefore, I performed siRNA-mediated knockdowns of control or JAZF1 in U2OS reporter cells, followed by immunoblots with antibodies against JAZF1 or, as loading control, α-Tubulin. I could show that JAZF1 protein level was reduced after transient transfection of cells with the two JAZF1-specific siRNAs (siJAZF1 #2 and #4) in comparison to the non-transfected (-) and the Luciferase-specific (siLuci) control (Figure 15A). Afterwards, the reporter system had to be validated in our laboratory in order to confirm that the procedure employed for the appropriate examination is suitable for the intended purpose. To this end, the U2OS reporter cells were treated with Shield1 and 4-hydroxytamoxifen (4-OHT) to induce site-specific FokI-created DSBs (Figure 15B) followed by ChIP-qPCR analysis of γH2A.X at four selected sites to determine whether the chromatin-mediated damage response is activated in comparison to untreated (undamaged) cells. Indeed, ChIP-qPCR analysis revealed that after

treatment γH2A.X is significantly enriched at sites in close proximity to DSBs (p2 and p3) in comparison to the negative control regions (RPL11_2gb and PARS2+) (Figure 15C), indicating that a strong DNA damage response at the reporter locus is activated due to the FokI-mediated generation of DNA lesions and thus, confirming the feasibility of the experimental setup [307].
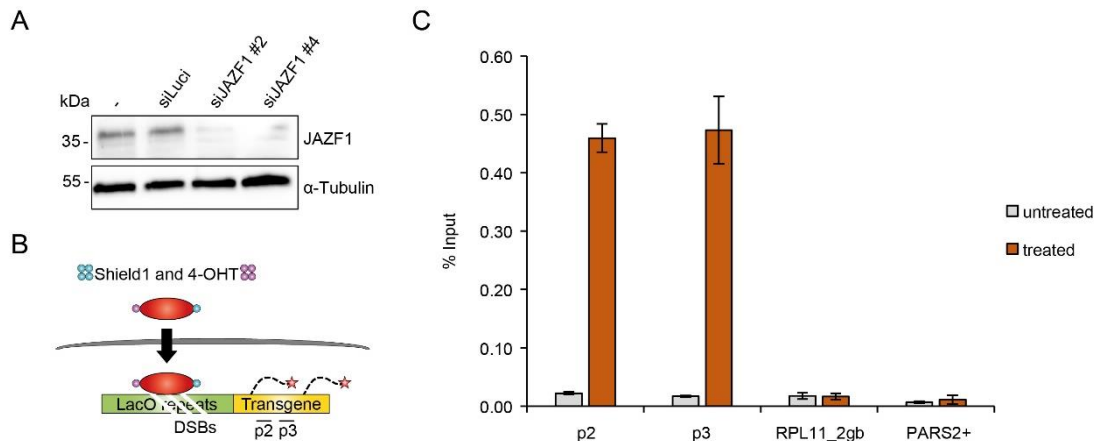
Figure 15: DSB induction by nuclease activity leads to a local accumulation of γH2A.X at the reporter locus transgene. (**A**) Immunoblotting analysis of JAZF1 of non-transfected (-) or transfected U2OS reporter cells with siRNAs against JAZF1 mRNA (siJAZF1 #2 and #4) or, as negative control, Luciferase-specific siRNA (siLuci). Antibody staining against α-Tubulin served as loading control. Shown is one out of two biological replicates with similar results. (**B**) Schematic overview of the U2OS DSB reporter cell system [307, 320]. After the addition of Shield1 (blue dots) and 4-hydroxytamoxifen (4-OHT; magenta dots), the fusion protein (red) is stabilized and translocates to the nucleus (black arrow). The LacI domain of the fusion protein binds to stable integrated Lac-operator (LacO; green) repeats upstream of a doxycycline-inducible YFP-MS2 reporter transgene (yellow) followed by the induction of multiple nuclease-inducible DNA double-strand breaks (DSBs; white lines) by FokI. As a chromatin mediated damage response, the histone variant H2A.X is phosphorylated (red stars) at serine 139 (γH2A.X) and could be detected by ChIP-qPCR experiments using primer sets p2 and p3. (**C**) ChIP-qPCR analysis of γH2A.X at different sites of U2OS reporter cells exposed to control (untreated, grey) or FokI-mediated DNA lesions (treated, dark red). p2 and p3 represent two H2A.X-occupied sites of the U2OS reporter cell locus, while RPL11_2gb (gb = gene body) and PARS2+ (H2A.Z-containing promoter site; + = +1 nucleosome relative to TSS) serve as negative controls, as both loci are devoid of γH2A.X. Respective enrichment of γH2A.X is depicted as percentage of input signals. Error bars indicate SD of three technical replicates. Shown is one out of two biological replicates with similar results.

Since JAZF1 could also be depleted by RNAi in the U2OS DSB reporter cells and the experimental set up seems to be suitable for the intended use, I next investigated whether JAZF1 depletion influences the level of γH2A.X at a subset of reporter locus sites via ChIP-qPCR. To this end, JAZF1 mRNA level was sufficiently knocked-down in the U2OS reporter cells as demonstrated by RT-qPCR (Figure 16A) using the two

JAZF1-specific siRNAs (siJAZF1 #2 and #4) or, as negative control, Luciferase (siLuci) siRNA followed by the FokI-mediated induction of site-specific breaks. Lastly, ChIP-qPCR experiments were executed to investigate the enrichment of γH2A.X at the reporter locus of JAZF1-depleted and control as well as treated (damaged) and untreated (undamaged) cells. Accordingly, as determined by previous ChIP-qPCR experiments (see Figure 15C), the level of γH2A.X is increased at sites surrounding DNA lesions (p2 and p3) compared to negative control regions (RPL11_2gb and PARS2+) (Figure 16B), suggesting initiation of a chromatin mediated damage response. Interestingly, upon JAZF1 depletion a subtle increase in the level of γH2A.X at the two γH2A.X-occupied loci could be observed. This finding might not only reflect a defect in DNA repair, but could also constitute a first indication that JAZF1 mediates repair of injured DNA as it has already been proved for other p400 chaperone complex components such as MBTD1 and TIP60 [284, 336–338].
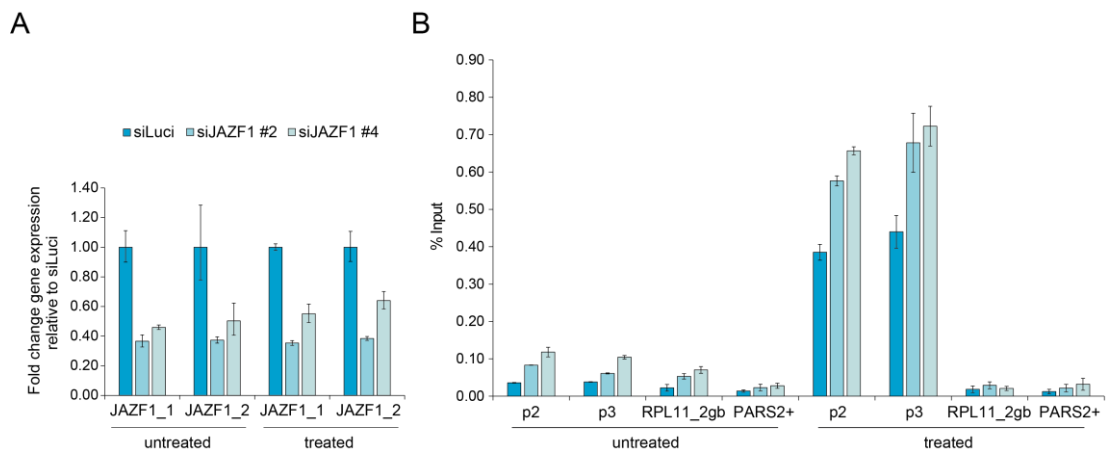
Figure 16: JAZF1 depletion results in a slight increase of γH2A.X at two selected reporter locus sites. (**A**) Expression analysis of JAZF1 by RT-qPCR two days after control (siLuci, dark blue) or JAZF1 (siJAZF1 #2 (blue) and #4 (light blue)) siRNA-mediated knockdowns in untreated (undamaged) and treated (damaged) U2OS reporter cells using two JAZF1 primer pairs (JAZF1_1 and JAZF1_2). Shown is the fold change gene expression compared to control (siLuci) and normalized to HPRT1 expression levels. Error bars depict SD of two technical replicates. Shown is one out of two biological replicates with similar results. (**B**) ChIP-qPCR analysis of γH2A.X at two H2A.X-enriched (p2 and p3) reporter loci and two H2A.X-lacking (RPL11_2gb and PARS2+) sites of U2OS reporter cells treated as described in (A). Respective enrichment of γH2A.X is depicted as percentage of input signals. Error bars indicate SD of three technical replicates.

Taken together, the results suggest that JAZF1 does not influence the global level of γH2A.X in context of DNA damage. Nevertheless, at certain sites we observed an increased persistence of γH2A.X in close proximity to DSBs, which may indicate a

defect in DNA repair due to the absence of JAZF1. However, the underlying molecular mechanism by which JAZF1 could influence DNA damage repair processes remains so far unclear and will be the focus of future research.

3.3 Loss of JAZF1 impairs expression of genes involved in ribosome biogenesis

Since JAZF1 is described as a transcriptional repressor of the nuclear orphan receptor TAK1/TR4 [295], and because of its association with the p400 chaperone complex [257], which is involved in the regulation of transcription [276], we next speculated whether JAZF1 is also implicated in gene expression control. To examine this presumption more closely, I made use of RNA-seq to investigate the role of JAZF1 in regulating gene expression and to uncover putative JAZF1-regulated genes. For this purpose, JAZF1 was depleted in HK cells via RNAi using a new siRNA pool containing four chemically modified JAZF1-specific siRNAs in order to enhance knockdown efficiency and minimize off-target effects, thereby offering advantages in both efficacy and specificity [339]. I therefore initially transfected HK cells with JAZF1-specific (siJAZF1) or, as negative control, non-target (siNTC) siRNA pools and two days after transfection, I determined JAZF1 transcript and protein levels by RT-qPCR, immunoblotting and IF analyses in order to determine how efficient those siRNAs actually are. Indeed, RT-qPCR and immunoblotting analyses clearly demonstrated that, when using the JAZF1-targeted siRNA pool (siJAZF1), JAZF1 mRNA (Figure 17A) and protein (Figure 17B) levels were significantly reduced in comparison to the control (siNTC) knockdown. Interestingly, I also observed bright JAZF1 speckles in the nucleus of control HK cells that were absent in JAZF1-depleted cells, as IF microscopy pictures of endogenous JAZF1 demonstrated (Figure 17C). Therefore, IF analysis not only confirmed the proper knockdown of the JAZF1 protein in HK cells, but also indicated that JAZF1 is localized in the nucleus and possibly enriched in specific nuclear sub-compartments, as those bright JAZF1 dots seem to appear in nucleoli.
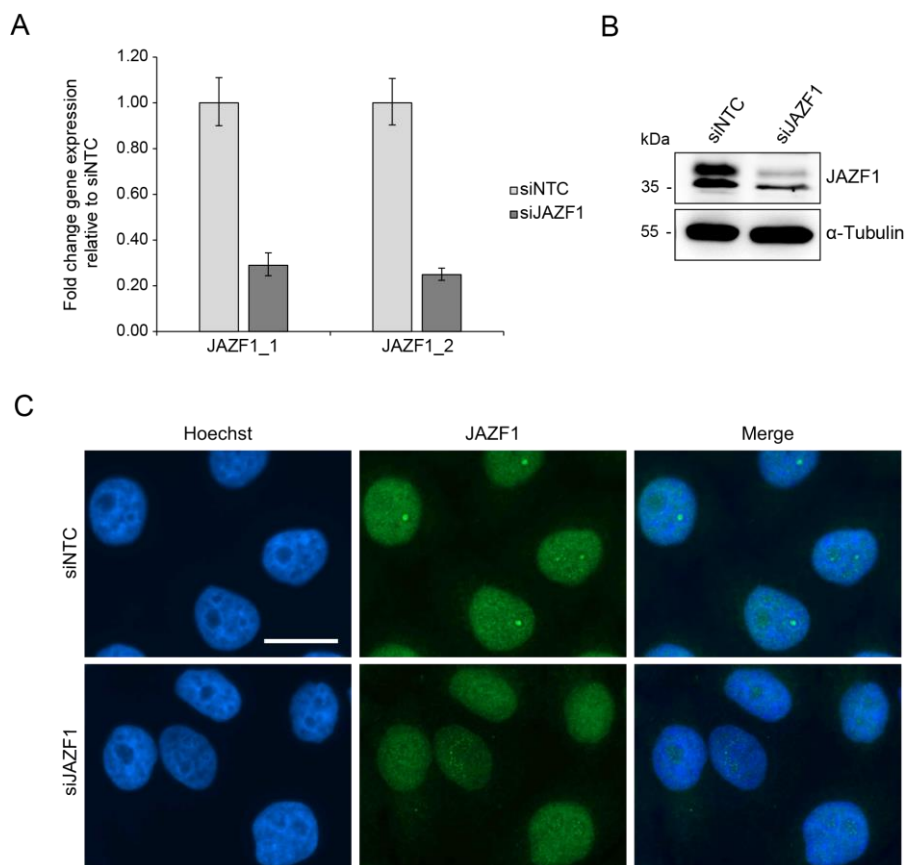
Figure 17: Utilizing a JAZF1-specific siRNA pool leads to significantly reduction of nuclear JAZF1. (**A**) Expression analysis of JAZF1 by RT-qPCR two days after control (siNTC, light grey) or JAZF1 (siJAZF1, dark grey) siRNA pool-mediated knockdowns in HK cells using two JAZF1 primer pairs (JAZF1_1 and JAZF1_2). Shown is the fold change JAZF1 mRNA expression compared to control (siNTC) and normalized to HPRT1 expression levels. Error bars depict SD of three technical replicates. Illustrated is one of more than three biological replicates showing similar results. (**B**) Immunoblot analysis of JAZF1 of whole cell extracts from control (siNTC) or JAZF1-depleted (siJAZF1) HK cells described in (A). Antibody staining against α-Tubulin served as loading control. Shown is one of more than three biological replicates showing similar results. (**C**) IF images from control (siNTC) or JAZF1-depleted (siJAZF1) HK cells stained with an antibody against JAZF1 (green). DNA was counterstained with Hoechst (blue). Scale bar (white) for all pictures = 20 µm.

As the JAZF1-targeted siRNA pool has shown to be efficient, it was used for depleting JAZF1 in HK cells followed by RNA-seq experiments. To this end, I isolated RNA from control (siNTC) and JAZF1-depleted (siJAZF1) HK cells of two time-distinct batch experiments with two (Figure 18A) and three (Figure 18B) biological replicates, respectively. Afterwards, I first verified knockdown efficiency by RT-qPCR analyses and showed that JAZF1 mRNA expression was highly decreased in all JAZF1 siRNA pool-transfected samples compared to the control transfection (Figure 18).
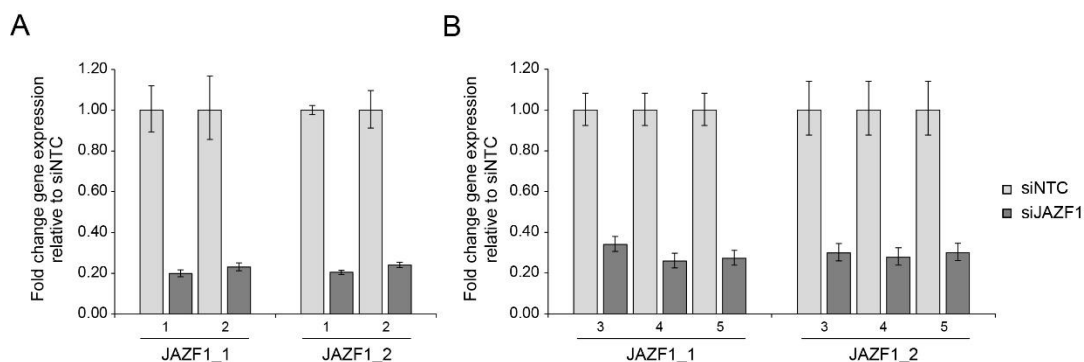
Figure 18: Assessment of JAZF1 mRNA level revealed successful downregulation of JAZF1 in HK cells via RNAi for RNA-seq experiments. (**A, B**) Expression analysis of JAZF1 by RT-qPCR two days after control (siNTC, light grey) or JAZF1 (siJAZF1, dark grey) siRNA-mediated knockdowns in HK cells using two JAZF1 primer pairs (JAZF1_1 and JAZF1_2) of two independent batch experiments (batch one (A) and batch two (B)). Numbers (1-5) represent the respective biological replicate. Shown is the fold change gene expression compared to control (siNTC) and normalized to HPRT1 expression levels. Error bars depict SD of three technical replicates.

Having determined proper knockdown of JAZF1, next libraries of quantified RNA samples were prepared and sequenced by Dr. Andrea Nist (Genomics Core Facility, Marburg). The subsequent RNA-seq data analysis was done by Tobias Friedrich (Institute for Biochemistry, JLU, Giessen) and Prof. Dr. Marek Bartkuhn (Biomedical Informatics and Systems Medicine Science Unit for Basic and Clinical Medicine, JLU, Giessen). Quality assessment of the RNA-seq dataset was achieved by a classical principle component analysis (PCA), providing information about the variance of RNA-seq samples between the different conditions within the two batch experiments, thereby helping identifying outlying samples. Although the PCA of RNA-seq data revealed strong variations between the two independent batch experiments, it has to be noted that the transcriptional consequences upon loss of JAZF1 compared to the controls are highly similar among batches and replicates (Figure 19A), pointing out that the biological effects resemble each other within one condition. Overall, the RNA-seq experiment identified in total 162 genes that were statistically significant (FDR < 0.1 & $\log_2$FC > 0.5 or < -0.5) deregulated (130 down- and 32 upregulated) upon JAZF1 depletion (Figure 19B).

A

B
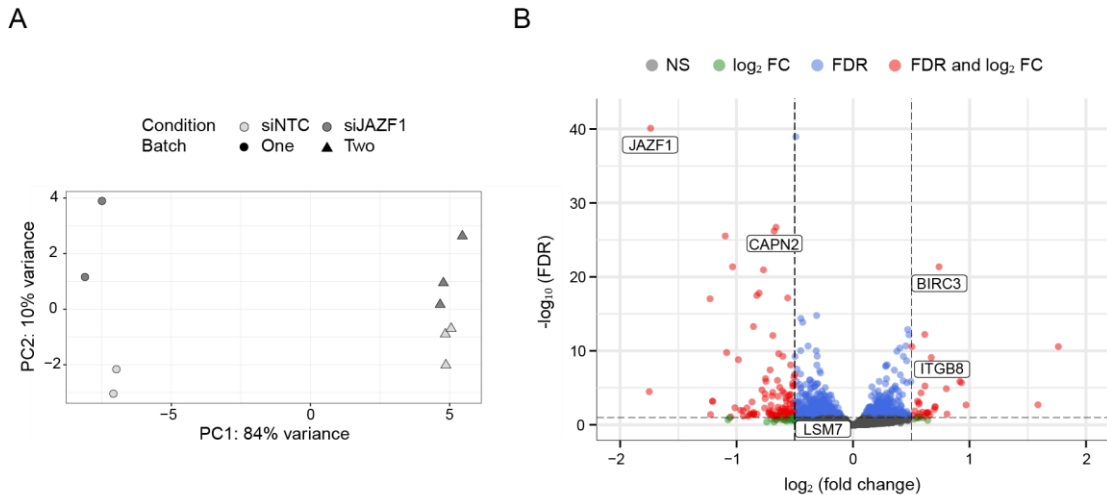
Figure 19: Loss of JAZF1 impairs expression of a large number of genes. (**A**) Principle component analysis (PCA) of gene expression data received from RNA-seq experiments showing variation of control (siNTC, two and three biological replicates shown in light grey) and JAZF1 (siJAZF1, two and three biological replicates shown in dark grey) knockdowns of two time-independent experiments (circles: batch one, squares: batch two). (**B**) Volcano-plot visualization of deregulated genes of HK cells upon JAZF1 depletion (siJAZF1) in comparison to control (siNTC) knockdown. Red dots depict statistically significant differentially expressed genes (log2FC > 0.5 or < -0.5 and false discovery rate (FDR) < 0.1), blue dots depict deregulated genes with only statistically significant values (FDR < 0.1), green dots depict genes with only significant expression changes (log2FC > 0.5 or < -0.5) and grey dots depict genes without any statistical or fold-change significance. Genes highlighted with boxes were validated via RT-qPCR (see Figure 20A).

In order to confirm the obtained results from the RNA-seq experiment, these needed to be validated in a next step by RT-qPCR. For this purpose, qPCR primers for a subset of JAZF1-deregulated genes (CAPN2, BIRC3, ITGB8) or, as control, one in its expression largely unchanged gene (LSM7) from generated RNA-seq data were established followed by qPCR analysis of cDNA derived from control (siNTC) or JAZF1-depleted HK cells. Accordingly, as previously determined by RNA-seq (see Figure 19B), expression levels of the three JAZF1-dependent genes (that are highlighted with boxes in Figure 19B) were deregulated upon JAZF1 knockdown, while LSM7 remained to a large extent unaffected (Figure 20A).

Since RNA-seq data could be successfully verified, we next aimed to gain greater biological insights on the differentially expressed genes obtained from the RNA-seq datatset. Therefore, Tobias Friedrich performed Gene Set Enrichment Analyses (GSEA) for the sub-ontology (GO database) biological pathway (BP) or cellular compartment (CC) and showed that JAZF1-deregulated genes were notably associated with ribosomes (Figure 20B, C). More precisely, the GSEA-plot deciphered a statistically robust and concordant transcriptional change of genes

related to the GO pathway "Ribosome biogenesis", among other pathways (Figure 20D). Interestingly, GSEA also revealed that loss of JAZF1 affects expression of genes related to DNA repair (Figure 20B), supporting our speculation of JAZF1 as being somehow implicated in DNA damage repair processes, possibly on a transcriptional level.
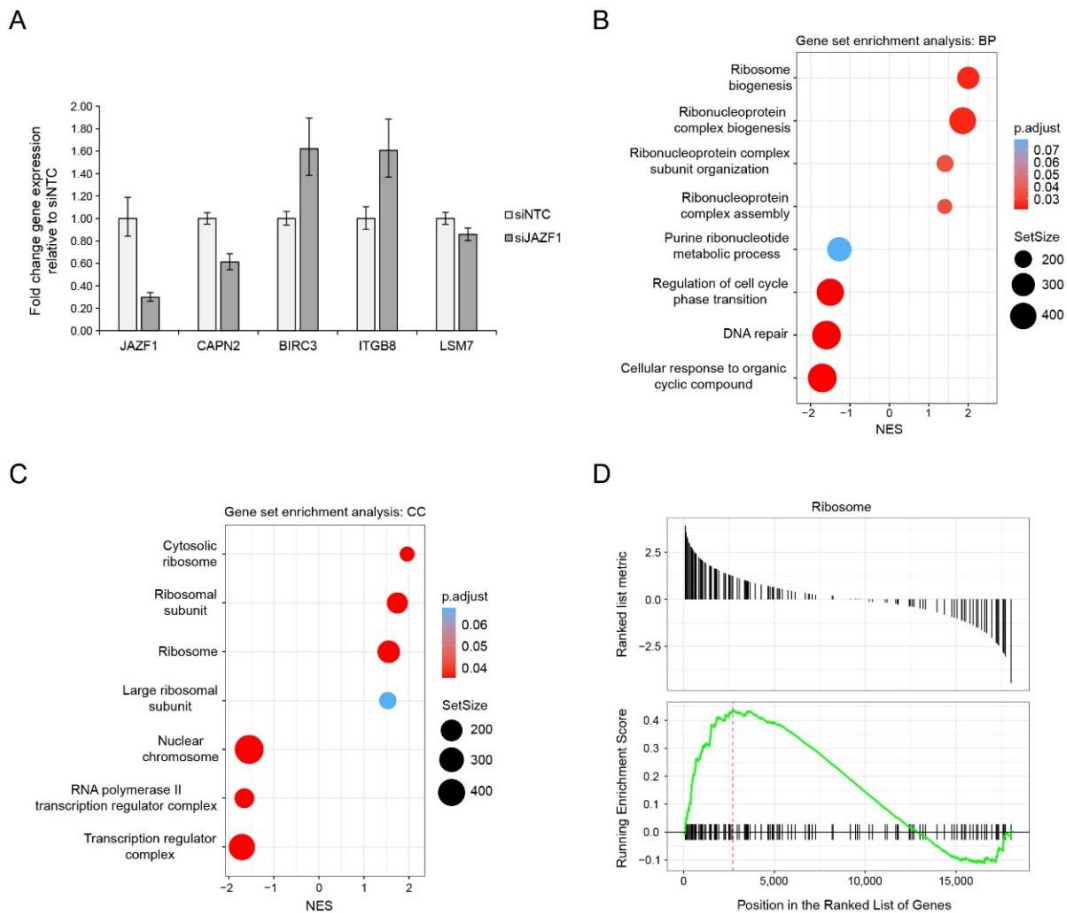
Figure 20: JAZF1 depletion leads to deregulation of several genes, with some of them involved in ribosome biogenesis. (**A**) Verification of RNA-seq data by RT-qPCR of a subset of JAZF1-deregulated (CAPN2, BIRC3, ITGB8) and one in its expression unaffected (LSM7) genes (that were highlighted with boxes in Figure 19B) upon JAZF1 depletion (siJAZF1, dark grey) in comparison to control (siNTC, light grey) knockdown in HK cells. Shown is the fold change gene expression compared to control (siNTC) and normalized to HPRT1 expression levels. Error bars represent SD of three technical replicates. Presented is one out of three biological replicates with similar results. (**B, C**) Dot-plots visualizing Gene Set Enrichment Analysis (GSEA) of RNA-seq data (as described in Figure 19) for the sub-ontology (GO database) biological pathway (BP; (B)) and cellular compartment (CC; (C)), representing the three pathways with the greatest statistical significance as well as all significant pathways related to 'Ribosome/Ribosome Biogenesis'. Scales in the right center show adjusted p-values (color) for each set or the number of genes belonging to each pathway (SetSize, black), respectively. Position of dots on the x-axis displays Normalized Enrichment Score (NES). (**D**) Gene Set Enrichment Analysis (GSEA) comparing expression changes upon loss of JAZF1 (siJAZF1) in comparison to control (siNTC) knockdown, demonstrated that several deregulated genes are associated with the Kyoto Encyclopedia of Genes and Genomes (KEGG) pathway "Ribosome".

Overall, JAZF1 is a nuclear protein that is involved in the regulation of, among others, ribosomal protein gene expression [257].

3.4 JAZF1 is a nucleoli- and Cajal Body-associated nuclear protein

Interestingly, a study by Halkidou et al. demonstrated that TIP60 is partially localized in the nucleolus, the center of ribosome biogenesis [340], where it is actively involved in the transcription of rDNA and ribosomal genes in prostate cancer cell lines [341]. Since JAZF1 associates with TIP60 (see Figure 11) and the results received from the RNA-seq experiment indicate that JAZF1 could be involved in regulating expression of some ribosomal protein genes as well (see Figure 20) [257], it is conceivable that JAZF1 is also located in the cellular sub-compartment of the nucleus to perform its functions as a putative transcription factor involved in the regulation of ribosome biogenesis. Support for this assumption also comes from our previous IF analysis of endogenous JAZF1 (see Figure 17C), in which we observed bright JAZF1 speckles that may occur in nucleoli. To test this hypothesis, IF analyses of non-transfected HK cells (-) or cells transiently expressing GFP (as negative control), GFP-TIP60 (as positive control) or GFP-JAZF1 were carried out. I therefore first transiently transfected HK cells with constructs encoding GFP, GFP-TIP60 or GFP-JAZF1 (see Figure 21A, top) and two days after transfection, cells were stained with a Fibrillarin-specific antibody and IF images taken. Since Fibrillarin is an exclusively nucleolar protein [342], it was used as a marker for the visualization of nucleoli. Interestingly, besides JAZF1's nuclear localization, it is also highly enriched in the nucleolus as conspicuous bright JAZF1-occupied areas overlap with the nucleoli-associated protein Fibrillarin (Figure 21B), thereby reinforcing our prior observations implicating JAZF1 in ribosomal protein gene transcription. A result that could be partly confirmed for TIP60 as well (Figure 21B). These findings suggest that JAZF1 contains at least one nucleolar localization sequence (NoLS) accountable for its localization to the nucleolus. To evaluate which domain of JAZF1 is potentially responsible for its cellular distribution, three different truncations of the full-length GFP-JAZF1 construct (see Figure 21A), were used for further IF analyses that were performed as described above. Hence, HK cells were transiently transfected with plasmids encoding GFP or three GFP-JAZF1 domain deletions, in which a short (ΔN101) or a long (ΔN163) part of the N-term or a portion of the C-term (ΔC164) is missing (Figure 21A). After two days incubation, cells were subjected to IF staining with an antibody against Fibrillarin followed by IF microscopy. Strikingly, only the two mutants, which lack the N-terminal

part of JAZF1 were still localized in nucleoli (Figure 21C), indicating that the NoLS resides in the C-term portion of JAZF1.
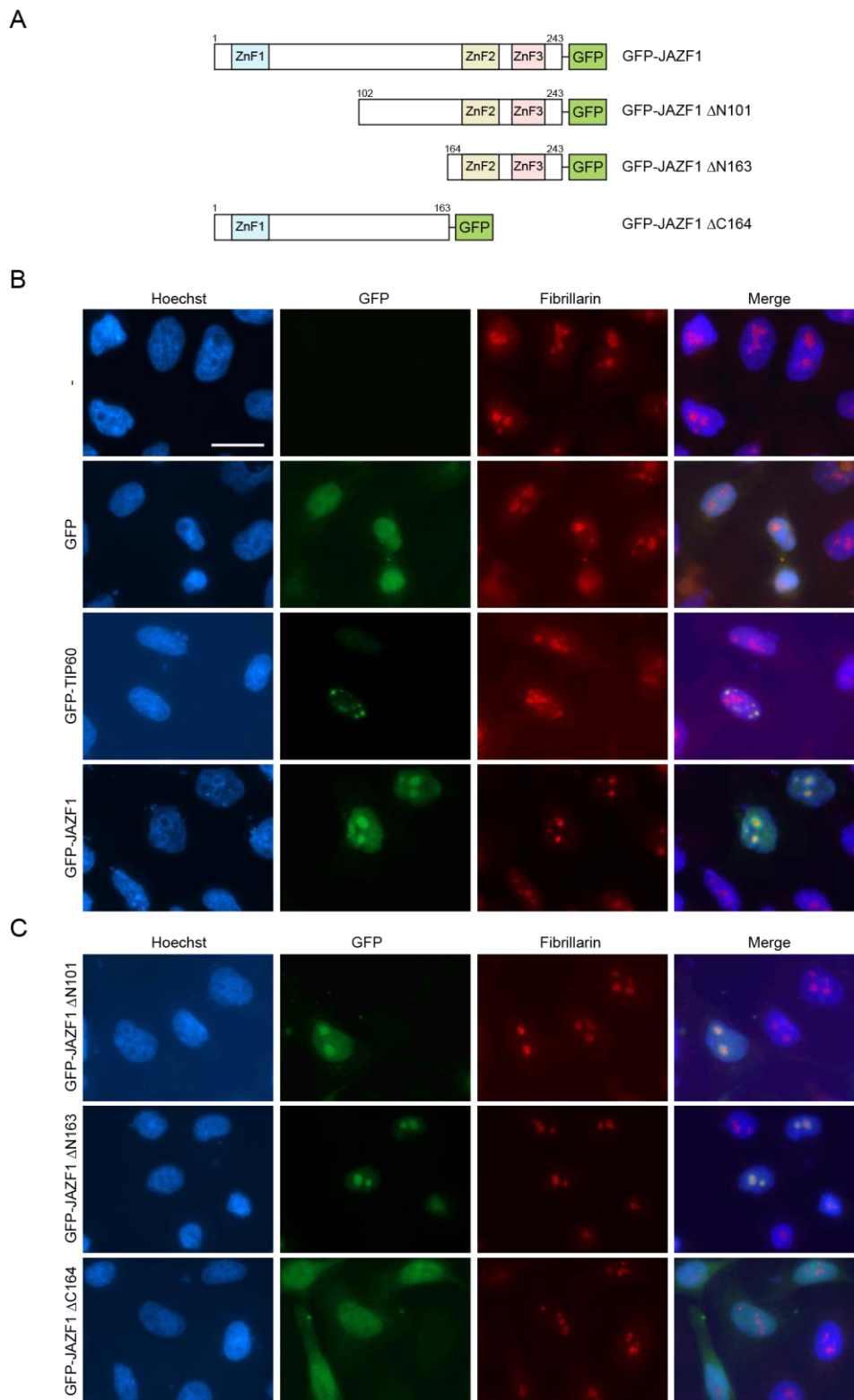
Figure 21: JAZF1 is a nucleoli-enriched protein. (**A**) Schematic representation of full-length GFP-JAZF1 and three GFP-JAZF1 domain delection proteins that were expressed in HK cells for IF analyses shown in (B) and (C).

(**B, C**) Representative IF images from (B) non-transfected (-) or HK cells transiently expressing GFP, GFP-TIP60 and GFP-JAZF1 or (C) from HK cells transiently expressing different GFP-JAZF1 truncations as illustrated in (A). Transfected cells were stained with an antibody against Fibrillarin (red). DNA was counterstained with Hoechst (blue). Scale bar (white) for all pictures = 20 µm. Shown is one out of two biological replicates with similar results.

So far, we identified JAZF1 as a transcriptional regulator of many genes, with several of them belonging to ribosomal protein genes [257]. This is in accordance with the result that JAZF1 localizes not only to the nucleus, but also accumulates to high levels in nucleoli. These findings indicate a possible role for JAZF1 in ribosome biogenesis.

Remarkably, alterations in ribosome biogenesis are frequently linked with changes in nucleolar morphology [343]. Since RNA-seq experiments demonstrated that several genes associated with ribosome synthesis were deregulated upon JAZF1 depletion, I analysed whether this transcriptional interference is reflected in morphologically abnormal nucleoli by deploying another IF approach. Therefore, HK cells were transfected with control (siNTC) or JAZF1-specific (siJAZF1) siRNA pools and subsequently used for co-staining with antibodies against JAZF1 or Fibrillarin to verify knockdown efficiency on the protein level of JAZF1 and, on the other hand, to capture nucleoli structures. As expected, endogenous JAZF1 (red) also co-localized with Fibrillarin (green) (Figure 22A, white arrow head), thereby supporting our previous findings on JAZF1 as being enriched in nucleoli (see Figure 21B, C). Moreover, I perceived that depletion of JAZF1 resulted in an increase in nucleoli sizes (Figure 22A). An observation I was also able to succuessfully quantify with the help of Dr. Konstantin Kletenkov (member of the Hake group) by determining the nuclei and nucleoli sizes in pixels of IF pictures and evidenced that JAZF1-depleted (siJAZF1) HK cells exhibit larger nuclei and nucleoli in comparison to control (siNTC) transfected cells (Figure 22B). This finding indicates a defect in ribosome biogenesis due to the loss of JAZF1.

Our results are in line with a recent study, which already identified JAZF1 as a nucleolar protein with numerous functions in ribosome-related processes and larger nucleoli in pancreatic β-cells upon JAZF1 depletion [344], thereby not only strengthen our results, but also highlighting JAZF1's implication in ribosome biogenesis. However, we noticed that some bright JAZF1 speckles were also located in the immediate proximity of nucleoli (Figure 22A, magenta arrow head).
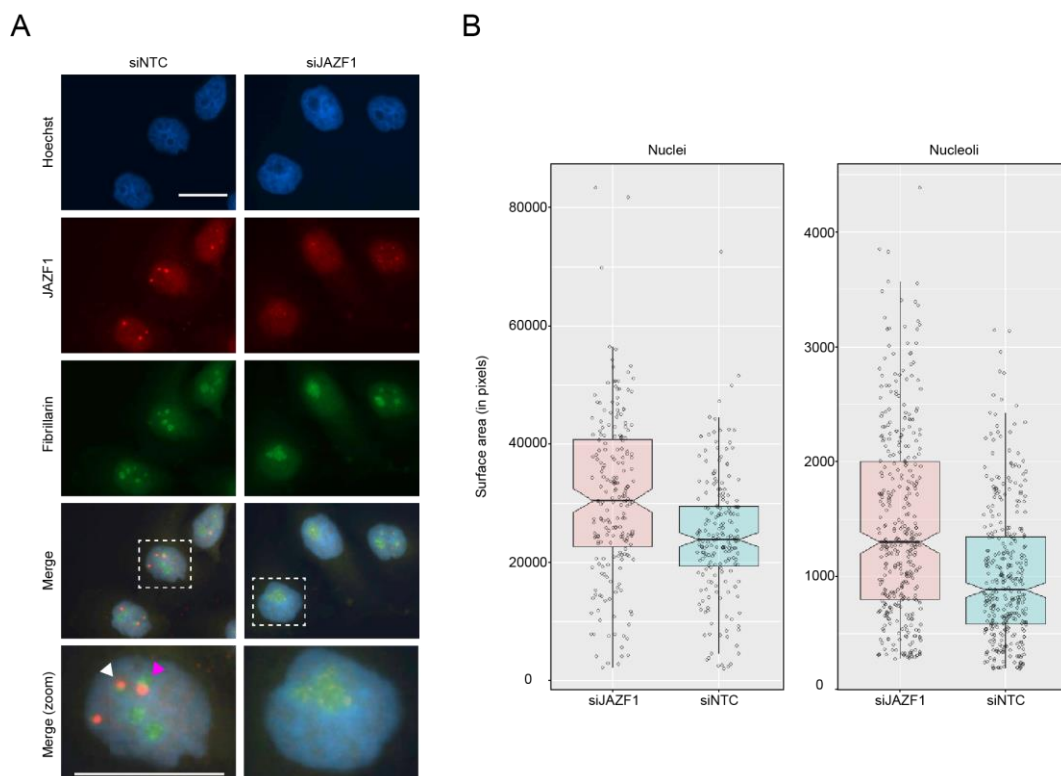
Figure 22: Deficit in JAZF1 protein affects morphology of nucleoli. (**A**) Representative IF images from HK cells co-stained with antibodies against JAZF1 (red) and Fibrillarin (green) upon control (siNTC) or JAZF1 (siJAZF1) knockdowns. DNA was counterstained with Hoechst (blue). Highlighted cells with boxes (white dashed lines) have been magnified by a factor of two, which are shown below (zoom). White arrow head indicates colocalization between JAZF1 and Fibrillarin, whereas the magenta arrow head depicts only a partial overlap of JAZF1 and Fibrillarin. Scale bar (white) for all pictures = 20 µm. (**B**) Box-plots showing distribution of nuclei (left) and nucleoli (right) surface areas (in pixels) from IF images of JAZF1-depleted (siJAZF1, red) or control (siNTC, blue) HK cells described in (A). Dots represent individual observations. The upper and lower whiskers extend to the largest or smallest value, while dots beyond the end of the whiskers are called 'outlying' points.

Since JAZF1 obviously did not only overlap with Fibrillarin, as IF images of co-staining of endogenous JAZF1 with Fibrillarin demonstrated [257] (see Figure 22A), it could well be that JAZF1 is also present in other nuclear sub-compartments. Interestingly, nuclear Cajal Bodies (CBs) have been found in the vicinity of nucleoli and have been associated with the biogenesis of ribosomes and spliceosomes [345–348]. As some observed JAZF1 speckles reside in close proximity to nucleoli (see Figure 22A), we next speculated whether JAZF1 also accumulates in CBs. In order to uncover whether an association of JAZF1 with CBs exist, IF analyses with antibodies against JAZF1 or Coilin, a signature marker for CBs [343], of control (siNTC) and JAZF1-depleted (siJAZF1) HK cells were conducted. Indeed, IF images revealed that many JAZF1 dots (green) also co-localize with Coilin (red) (Figure 23). Additionally, it seems that

the number of Coilin spots per cell increases upon loss of JAZF1, suggesting a putative defect in the biogenesis of not only ribosomes, but also spliceosomes.
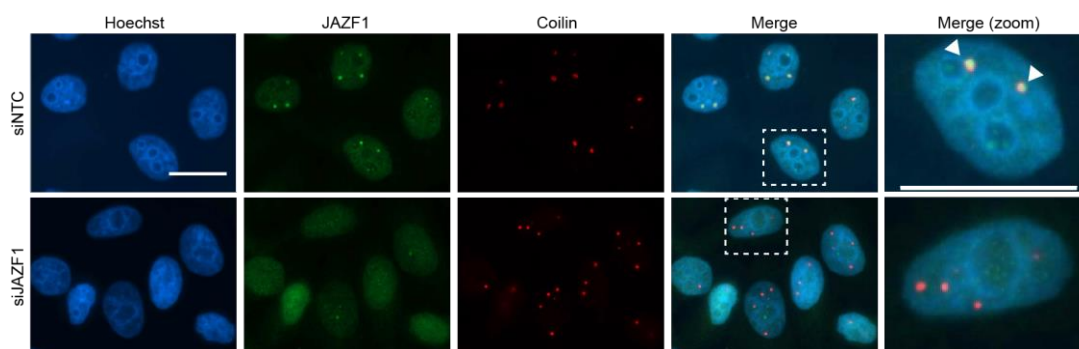
Figure 23: JAZF1 associates with Cajal Bodies. Representative IF images from HK cells co-stained with antibodies against JAZF1 (green) and Coilin (red) upon control (siNTC) or JAZF1 (siJAZF1) knockdowns. DNA was counterstained with Hoechst (blue). Scale bar (white) for all pictures = 20 μm. Highlighted cells with boxes (white dashed lines) have been magnified by a factor of two, which are shown on the right side (zoom). White arrow heads indicate colocalization between JAZF1 and Coilin.

In conclusion, JAZF1 is a nucleoli- and CB-associated nuclear protein with functions in regulating expression of various genes, including those related to ribosome biogenesis [257].

3.5 Loss of JAZF1 impairs cell proliferation, but does not influence cell cycle progressen

Since depletion of JAZF1 results in the deregulation of expression of many ribosomal protein genes and my data hint towards a defect in ribosome biogenesis, the question arose: What will be the cellular outcome of this interference? As proliferating cells exhibit an increased demand for protein synthesis that is accomplished by changes in the rate of ribosome biogenesis [349], it might be conceivable that loss of JAZF1 leads to changes in cell growth and cell proliferation. Interestingly, mere counting of JAZF1-depleted (siJAZF1) HK cells indicated a decrease in cell number compared to control (siNTC) transfected cells. Therefore, I next conducted functional analyses of JAZF1-depleted cells to analyse the cellular consequences in greater detail. First, growth curves of control or JAZF1-depleted HK cells were generated over a period of 80 h with the xCELLigence Real-Time Cell Analyzer, providing information about cell proliferation. To this end, HK cells were transfected with either JAZF1-specific

(siJAZF1) or control (siNTC) siRNA pools and after two days incubation, cells were transferred into the xCELLigence E-plate and measurements started. Meanwhile, I additionally performed RT-qPCR analysis of control (siNTC) and JAZF1-depleted (siJAZF1) HK cells in order to ensure proper knockdown of the JAZF1 transcript and showed an adequate reduction of JAZF1 mRNA level (Figure 24A). Indeed, the observed growth defect determined by sole cell counting could be reproduced, as the growth curve of JAZF1-depleted (siJAZF1) cells showed decreased cell proliferation rates compared to control-transfected (siNTC) cells (Figure 24B). In order to identify whether the proliferation defect of JAZF1-depleted HK cells is caused by a deregulation of the cell cycle, I next carried out flow cytometry analyses of PI-stained control (siNTC) or JAZF1-depleted (siJAZF1) HK cells, but was not able to identify significant changes in cell cycle progression, as the percentage of cells in respective cell cycle phases did not alter upon JAZF1 depletion (Figure 24C).
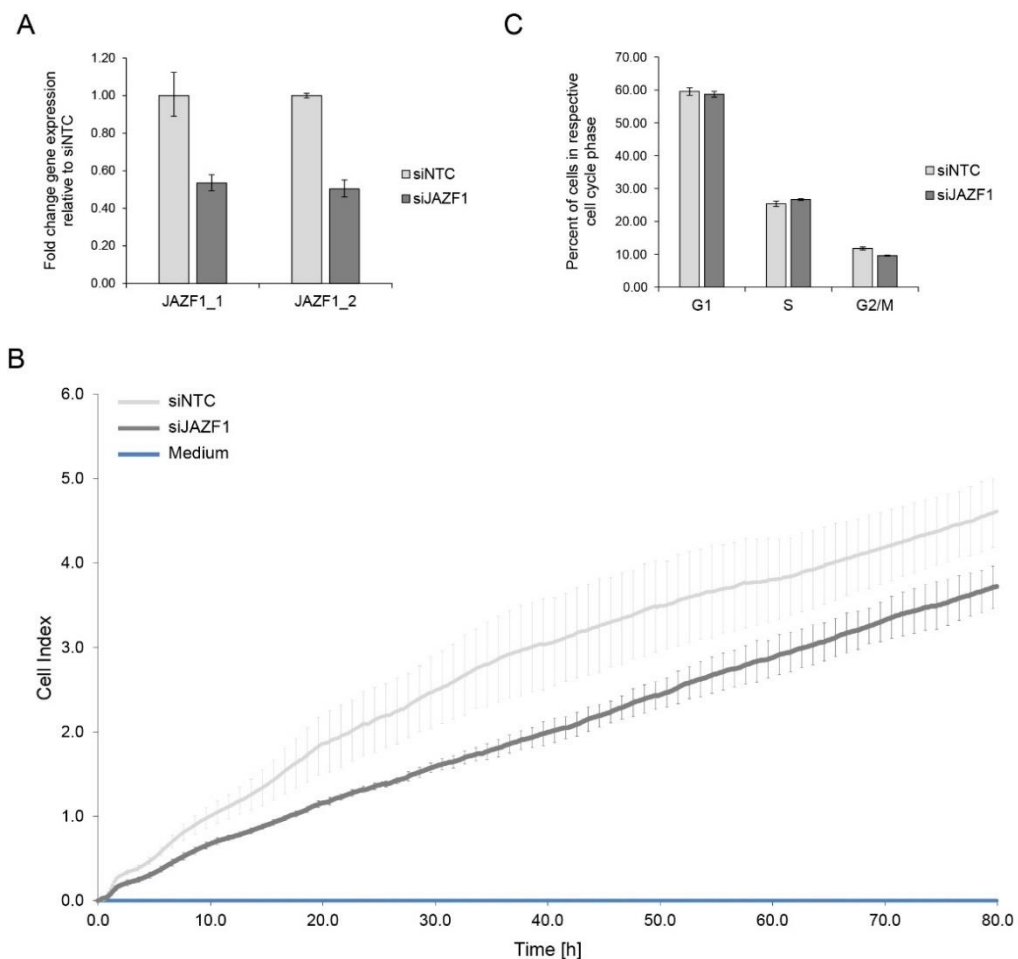
Figure 24: Depletion of JAZF1 leads to cellular proliferation defects. (**A**) Expression analysis of JAZF1 by RT-qPCR two days after control (siNTC, light grey) or JAZF1 (siJAZF1, dark grey) siRNA pool-mediated knockdowns of HK cells using two JAZF1 primer pairs (JAZF1_1 and JAZF1_2).

Shown is the fold change gene expression compared to control (siNTC), normalized to HPRT1 expression levels. Error bars depict SD of three technical replicates. (**B**) Proliferation profiles of control transfected (siNTC, light grey) or JAZF1-depleted (siJAZF1, dark grey) HK cells as described in (A). Cell proliferation was monitored for 80 hours. Medium without cells is depicted in blue and served as control. Error bars represent SD of three technical replicates. Shown is one out of three biological replicates with similar results. (**C**) Quantification of three flow cytometry experiments of control (siNTC) or JAZF1-depleted (siJAZF1) HK cells stained with propidium iodide (PI) followed by the determination of the number of cells in G_1, S and G_2/M phase according to their DNA content by flow cytometry analysis two days after siRNA-mediated knockdowns. Error bars represent SD of three independent experiments. For detailed flow cytometry profiles see Figure A.2 in appendix.

In summary, loss of JAZF1 results in a proliferation defect of HK cells, possibly due to an impaired rate of ribosome biogenesis. However, cell cycle progression remained largely unaffected upon JAZF1 depletion and leads to the question what actually causes the proliferation defect? An exciting issue that could be the focus of future research.

3.6 JAZF1 depletion leads to reduced H2A.Zac levels at regulatory regions, while H2A.Z remains untainted

After the identification of JAZF1 as a transcriptional regulator of several genes, one important question emerges: How does JAZF1 exercise its functions in controlling gene regulation? As a novel TIP60-associated member of the H2A.Z-specific p400 chaperone/remodelling complex, it is imaginable that JAZF1 influences gene expression via recruiting the TIP60-containing p400 complex to certain regions in the genome, where it might perform its versatile functions such as deposition/removal of H2A.Z and/or acetylation of various histone proteins, thereby leading to distinct JAZF1-coordinated transcriptional outcomes.

In order to gain a first impression whether JAZF1 complies some of its functions via the enzymatically active p400 complex, I evaluated global H2A.Z and histone modification levels of TIP60-targets upon loss of JAZF1. For this objective, histones of JAZF1-depleted and control HK cells were isolated and possible changes assessed via immunoblotting. Therefore, I first performed control (siNTC) and JAZF1 (siJAZF1) siRNA-mediated knockdowns in HK cells and two days after transfection, proper knockdown of the JAZF1 transcript and protein was controlled by a combination of RT-qPCR and immunoblotting. The qPCR analysis confirmed the actual knockdown of the JAZF1 transcript in HK cells (Figure 25A), a result also verified on protein level,

as demonstrated by immunoblotting of JAZF1 (Figure 25B). Afterwards, nuclei of JAZF1-depleted and control cells were isolated, histone proteins acid-extracted and subjected to SDS-PAGE separation (Figure 25C). In order to quantify and adjust the amount of acid-extracted histone proteins for subsequent immunoblotting analyses, Coomassie Brilliant Blue staining of SDS-PAGE gels were executed first. The Coomassie Brilliant Blue-stained SDS gel not only revealed the successful extraction of linker histone H1 and the core histone proteins H3, H2B, H2A and H4, but also demonstrated a comparable amount of extracted histone proteins between the two samples derived from control (siNTC) or JAZF1-depleted (siJAZF1) HK cells (Figure 25D). Finally, histones of control and JAZF1-depleted HK cells were subjected to SDS-PAGE gel separation followed by immunoblotting with antibodies against H2A.Z or diverse histone modifications. However, after JAZF1 knockdown (siJAZF1), no global changes in the level of H2A.Z or other histone acetylation sites could be noticed in comparison to the control (siNTC) knockdown (Figure 25E).
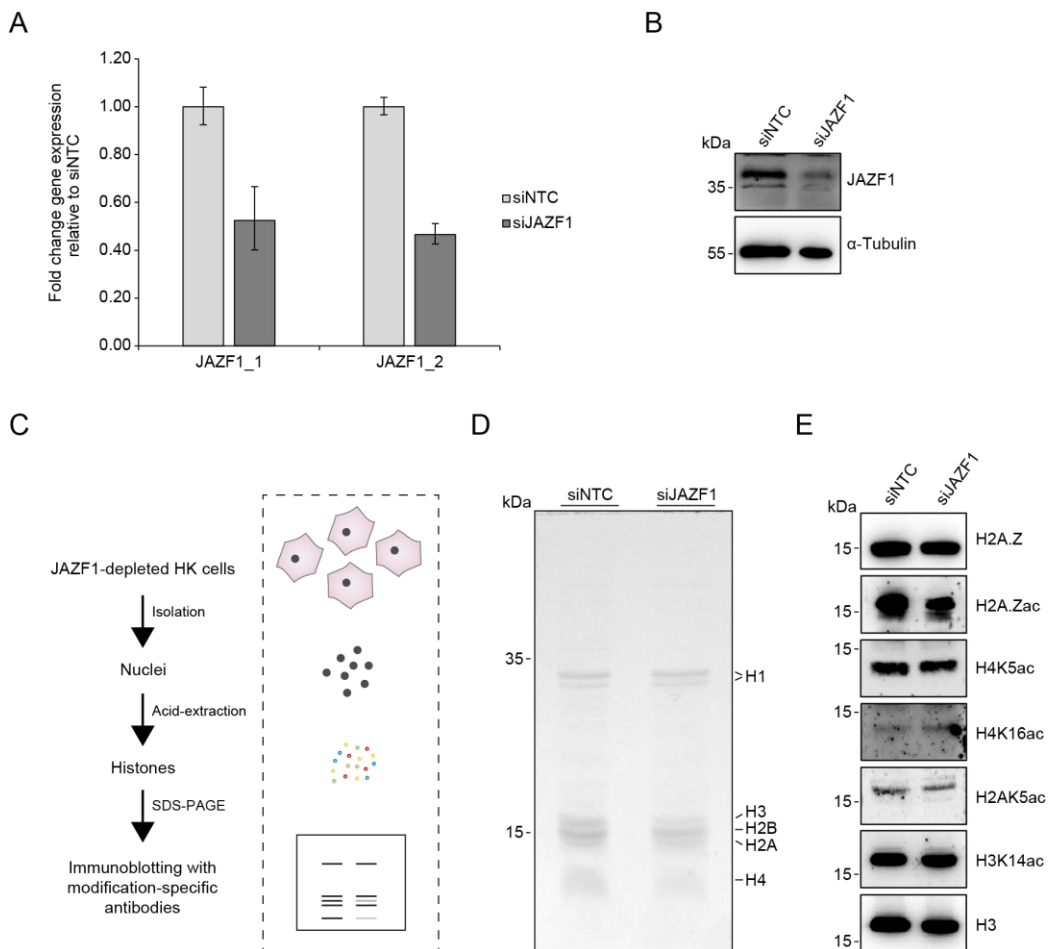
Figure 25: Global acetylation levels of TIP60-targets and H2A.Z remained largely unchanged after JAZF1 depletion. (**A**) Expression analysis of JAZF1 by RT-qPCR two days after control (siNTC, light grey) or JAZF1 (siJAZF1, dark grey) siRNA pool-mediated knockdowns of HK cells using two JAZF1 primer pairs (JAZF1_1 and JAZF1_2).

Shown is the fold change gene expression compared to control (siNTC) and normalized to HPRT1 expression levels. Error bars depict SD of three technical replicates. (**B**) Immunoblotting analysis of JAZF1 of whole cell extracts from control (siNTC) or JAZF1-depleted (siJAZF1) HK cells described in (A). Antibody staining against α-Tubulin served as loading control. (**C**) Schematic flowchart of acid-extraction and analysis of histone proteins. Nuclei (black dots) of control and JAZF1-depleted HK cells were isolated, histone proteins (colored dots) acid-extracted and separated by SDS-PAGE gel electrophoresis. Analysis of histone protein levels was achieved by a combination of Coomassie Brilliant Blue staining of SDS-PAGE gels and immunoblotting with modification-specific antibodies. (**D**) Coomassie Blue-stained SDS-PAGE gel with acid-extracted histone proteins received from control (siNTC) or JAZF1-depleted (siJAZF1) HK cells as described in (A). Detection of the linker histone H1 and the core histones H3, H2B, H2A and H4 are highlighted. (**E**) Representative immunoblots of acid-extracted histones from HK cells two days after control (siNTC) or JAZF1 (siJAZF1) knockdowns as described in (A) using antibodies against indicated histone proteins. H3 served as loading control. Shown is one out of three biological replicates with similar results.

So far, I ascertained no global changes in H2A.Z or other histone modification levels of TIP60-targets upon loss of JAZF1. To examine in greater detail whether JAZF1 is involved in the chromatin deposition/eviction of H2A.Z or in its acetylation at specific genomic regions, thereby potentially influencing gene expression of some target genes, I took advantage of ChIP-seq. Therefore, I first tested commercial H2A.Z and H2A.Zac antibodies for their suitability in ChIP assays. For this purpose, HK cells were fixed and subjected to chromatin shearing followed by ChIP with antibodies against H2A.Z, H2A.Zac or, as positive control, H3K4me3 – as this antibody has already been successfully tested in ChIP assays [310] – or, as negative control, without the addition of antibody (mock). Then, precipitated DNA was purified and analysed by qPCR with primers for specific loci (Figure 26A). The histone variant H2A.Z is predominately positioned at the -1 and +1 nucleosomes that flank the nucleosome-depleted region (NDR) of transcription start sites (TSSs) of promoters [257, 264]. The PARS2+ (+1 nucleosome relative to the TSS) and PARS2- (-1 nucleosome relative to the TSS) primer pairs used, bind downstream or upstream of the TSS of the PARS2 gene, serving thus as positive controls for a H2A.Z-occupied promoter region, while the negative control primer pair RPL11_2gb recognizes an H2A.Z-depleted gene body (gb) site within the RPL11 gene (Figure 26A). ChIP-qPCR analysis not only confirmed an enrichment for H2A.Z at the -1 and +1 nucleosomes flanking the NDR of the TSS of the PARS2 gene, but also demonstrated that H2A.Zac is most notably enriched at the +1 nucleosome position (PARS2+) (Figure 26B). A result that could also be observed for H3K4me3, a histone mark predominately found at the TSS of active genes [350]. These findings are in line with other reports showing consistently

incorporation of H2A.Z or trimethylation of histone H3 (H3K4me3) primarily into/at the +1 nucleosome of actively transcribed genes [53, 351]. Accordingly, based on the data received from the ChIP-qPCR, I thus clearly demonstrated that the employed experimental set up is applicable for the intended use.
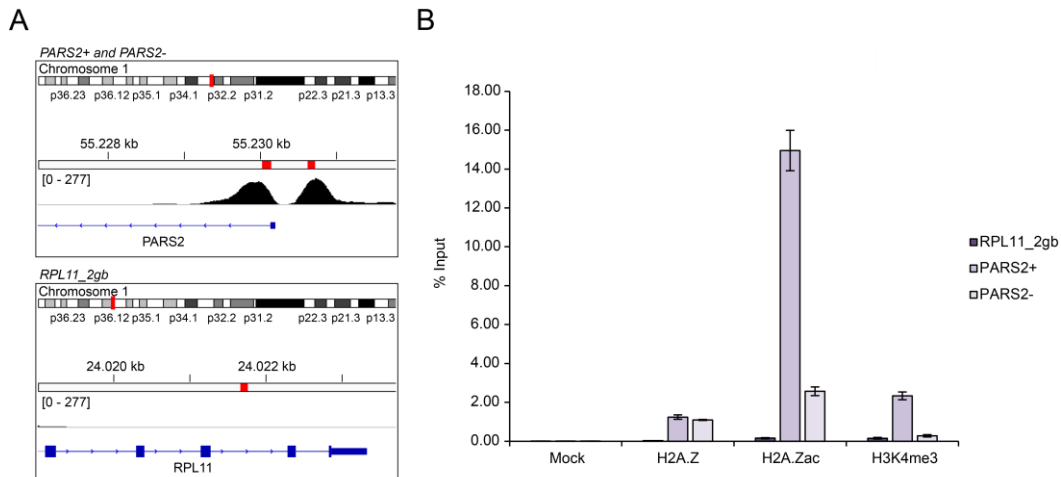
Figure 26: Acetylation of H2A.Z primarily occurs at the +1 nucleosome of the TSS of the PARS2 gene. (**A**) IGV snap shots of the chromosome 1 locus showing H2A.Z ChIP-seq signals of HK cells (ENCODE). The TSS of the PARS2 gene is depicted above, visualizing broadly enriched H2A.Z ChIP-seq signals up- and downstream of the NDR of the TSS, according to the +1 and -1 nucleosome positions. Binding sites of PARS2+ (+ = +1 nucleosome relative to the TSS, left black peak) and PARS2- (- = -1 nucleosome relative to the TSS, right black peak) primer pairs are represented as red bars. The H2A.Z-depleted region of the RPL11 gene is illustrated below. Binding site of the RPL11_2gb primer is depicted as red bar. (**B**) ChIP-qPCR analysis of H2A.Z, H2A.Zac and H3K4me3 levels at the PARS2+ (purple), PARS2- (light purple) and RPL11 (dark purple) loci described in (A) using antibodies against H2A.Z, H2A.Zac, H3K4me3 or, as negative control, no antibody (mock). Respective enrichment of H2A.Z, H2A.Zac or H3K4me3 is depicted as percentage of input signals. Error bars indicate SD of three technical replicates. Shown is one out of two biological replicates that showed similar results.

Having determined suitable antibodies for ChIP assays, I next set out to identify via ChIP-seq whether JAZF1 depletion affects deposition/eviction mechanisms of H2A.Z and/or its acetylation. Therefore, I performed siRNA-mediated knockdowns of control (siNTC) or JAZF1 (siJAZF1) in HK cells. In order to ensure proper depletion of JAZF1 for ChIP experiments, I first carried out RT-qPCR and immunoblotting analyses and confirmed that JAZF1 mRNA (Figure 27A) and protein (Figure 27B) levels were adequately reduced in both replicates via RNAi.
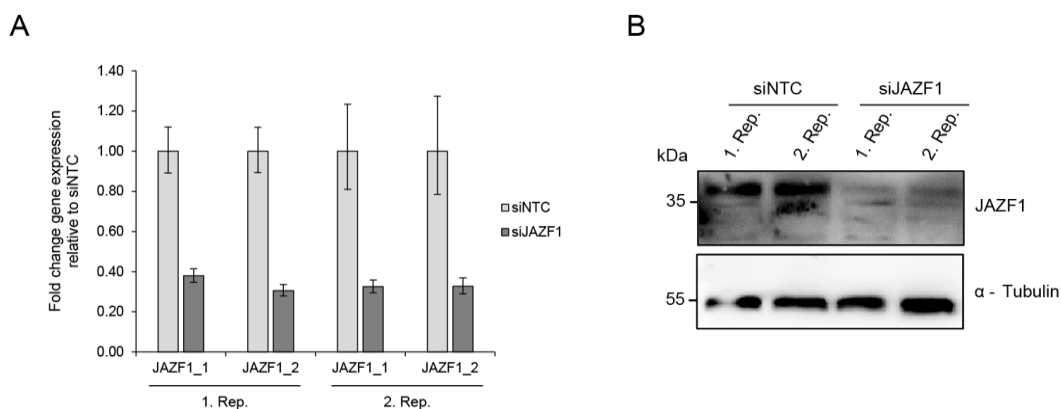
Figure 27: Assessment of JAZF1 transcript and protein levels showing successful downregulation of JAZF1 in HK cells via RNAi for ChIP-seq experiments. (**A**) Expression analysis of JAZF1 by RT-qPCR two days after control (siNTC, light grey, two replicates) or JAZF1 (siJAZF1, dark grey, two replicates) siRNA-mediated knockdowns in HK cells using two JAZF1 primer pairs (JAZF1_1, JAZF1_2). Shown is the fold change gene expression compared to control (siNTC) and normalized to HPRT1 expression levels. Error bars indicate SD of three technical replicates. (**B**) Representative immunoblot analysis of whole cell extracts of control (siNTC, two replicates) and JAZF1-depleted (siJAZF1, two replicates) HK cells two days after RNAi treatment as described in (A). Antibody against α-Tubulin served as loading control.

Afterwards, lysates of fixed control and JAZF1-depleted HK cells were prepared and subjected to chromatin shearing. As the length of DNA fragments should not exceed 500 bp for optimal sequencing accuracy, I first determined the degree of sheared chromatin by agarose gel electrophoresis to guarantee precise DNA sizes for sequencing. Visualization of fragmented DNA on a 2% agarose gel revealed the generation of appropriate chromatin fragments with an average size of 300 bp for all samples (Figure 28A), a result that was also successfully quantified by capillary electrophoresis (data not shown).

Finally, to evaluate whether JAZF1 depletion leads to changes in H2A.Z and/or H2A.Zac levels within chromatin, generated cell extracts of control or JAZF1-depleted HK cells were subjected to ChIP assays with antibodies against H2A.Z, H2A.Zac or, as negative control, IgG followed by reverse cross-linking and subsequent purification of ChIP DNA. Purified DNA was then used for qPCR analyses to control success of H2A.Z and H2A.Zac IPs. Accordingly, as already determined above (see Figure 26), ChIP-qPCR demonstrated an enrichment for H2A.Z and H2A.Zac at the TSS of the PARS2 gene, while no occupancy of H2A.Z and H2A.Zac at the negative control gene body region of RPL11 could be detected (Figure 28B), thereby confirming sufficient and specific pull-downs of H2A.Z and H2A.Zac.
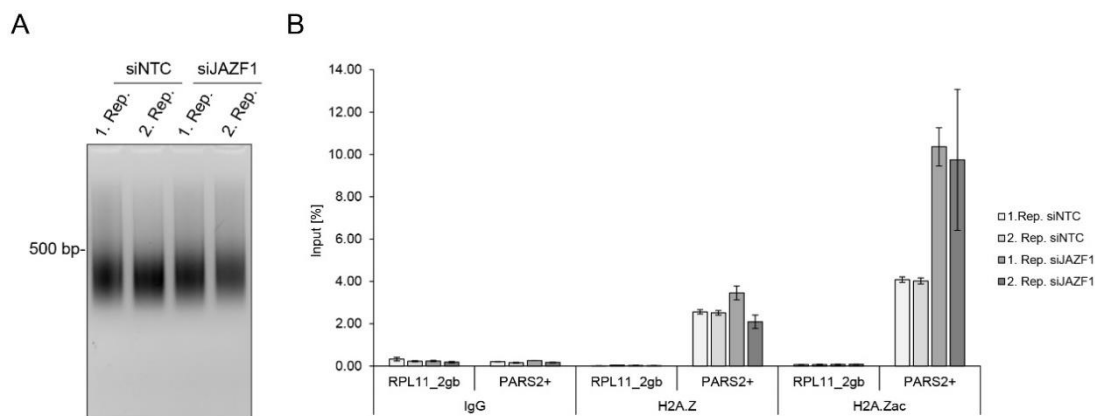
Figure 28: Evaluation of H2A.Z and H2A.Zac pull-downs for subsequent sequencing of associated genomic DNA. (**A**) Cell lysates of cross-linked control (siNTC) or JAZF1-depleted (siJAZF1) HK cells were subjected to chromatin shearing followed by DNA extraction and subsequent agarose gel electrophoresis, revealing generation of chromatin fragments with an average size of 300 bp. (**B**) Cell extracts of control (siNTC, two replicates, both light grey) or JAZF1-depleted (siJAZF1, two replicates, both dark grey) HK cells described in (A) were subjected to ChIP experiments with antibodies against H2A.Z, H2A.Zac or, as negative control, IgG followed by purification of ChIP DNA and subsequent qPCR analysis using primer pairs for the PARS2 and the RPL11 region as described in Figure 26. Respective enrichment of H2A.Z or H2A.Zac is depicted as percentage of input signals. Error bars indicate SD of three technical replicates.

Afterwards, libraries of ChIP DNA were prepared, sequenced by Dr. Andrea Nist (Genomics Core Facility, Marburg) and bioinformatically evaluated by Prof. Dr. Marek Bartkuhn (Biomedical Informatics and Systems Medicine Science Unit for Basic and Clinical Medicine, JLU, Giessen). First, focusing on the genome-wide distribution patterns of H2A.Z (green) and H2A.Zac (blue) ChIP-seq peaks from control (siNTC) and JAZF1-depleted (siJAZF1) HK cells not only confirmed the predominately incorporation of H2A.Z into the +1 and -1 nucleosomes, which flank the NDR of TSSs of genes, but also revealed that H2A.Z is strongly acetylated at those sites (Figure 29A). However, comparing H2A.Z ChIP-seq signals from control with those of JAZF1-depleted HK cells, we ascertained no changes in the level and localization of H2A.Z [257] (Figure 29A, B). To test whether JAZF1 actually does not influence H2A.Z chromatin deposition/eviction mechanisms, I conducted ChIP-qPCR experiments to validate ChIP-seq results for a subset of genomic regions. Therefore, I established ChIP-qPCR primers for selected loci from generated ChIP-seq data. Afterwards, ChIP experiments with an antibody against H2A.Z of control (siNTC) or JAZF1-depleted (siJAZF1) HK cells were performed followed by qPCR analysis of purified ChIP-DNA. Consistently, no differential levels of H2A.Z could be observed upon JAZF1 depletion in comparison to the control (Figure 29C), indicating that JAZF1 is not involved in H2A.Z deposition/eviction pathways [257].

A
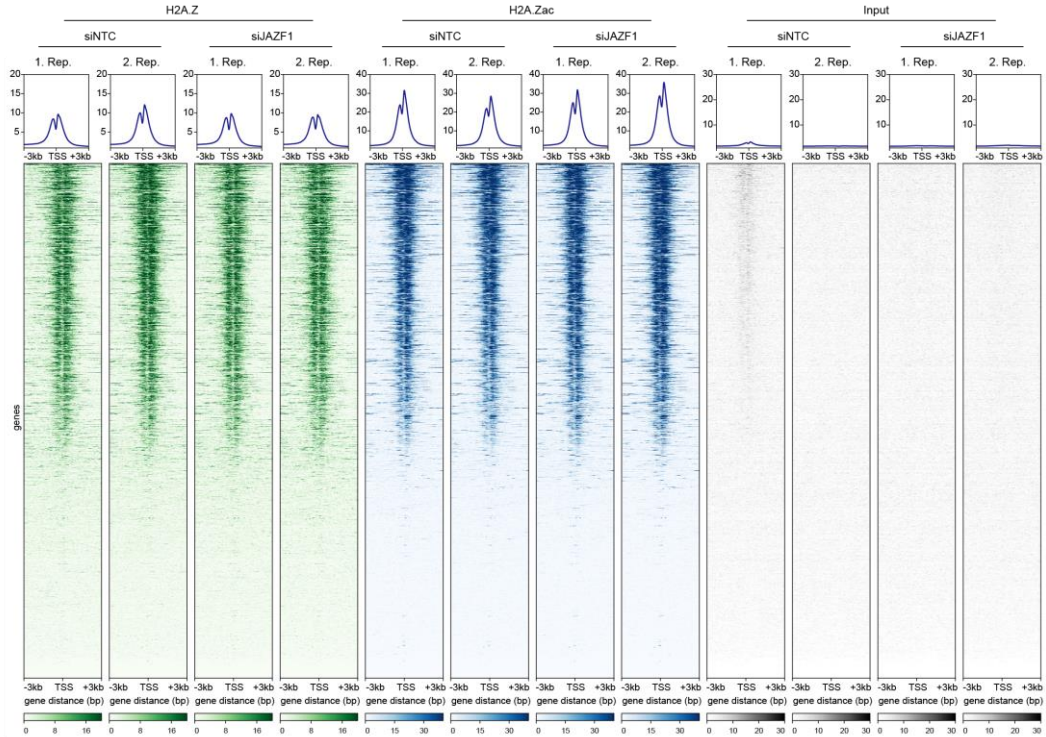
B
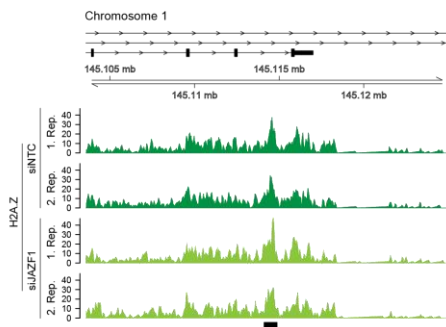
C
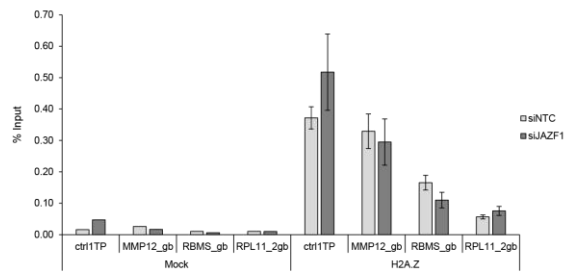
Figure 29: H2A.Z levels and positions remained unaffected upon loss of JAZF1. (**A**) Density heatmaps showing ChIP-seq signals of global H2A.Z (green), H2A.Zac (blue) and Input (grey) of control (siNTC, two replicates) or JAZF1-depleted (siJAZF1, two replicates) HK cells. Color intensities represent normalized and globally scaled tag counts. (**B**) Representative genome browser snap shot of human chromosome 1 locus showing H2A.Z ChIP-seq signals of control (siNTC, dark green, two replicates) or JAZF1-depleted (siJAZF1, light green, two replicates) HK cells. Note that upon JAZF1 depletion no change in the level of H2A.Z is detectable (black bar). (**C**) ChIP-qPCR analysis of H2A.Z levels at three different in its occupancy unchanged sites (ctrl1TP, MMP12_gb, RBMS1_gb; gb: gene body) and one control site that devoid of H2A.Z (RPL11_2gb) upon control (siNTC, light grey) and JAZF1 (siJAZF1, dark grey) knockdowns in HK cells using antibodies against H2A.Z or no antibody (mock). Respective enrichment of H2A.Z is depicted as percentage of input signals. Error bars indicate SD of three technical replicates. Shown is one out of three biological replicates showing similar results.

However, we identified an overwhelming number of deregulated H2A.Zac sites showing diminished acetylation upon JAZF1 depletion compared to control knockdowns (Figure 30A, B). Interestingly, comparing density heatmaps of differentially acetylated H2A.Z ChIP-seq signals with ENCODE data for two enhancer marks (H3K27ac and H3K4me1), we observed similar intensities for H3K27ac (blue) and partly for H3K4me1 (red) at those sites (Figure 30B), indicating that JAZF1-affected H2A.Zac sites are particular enriched at regulatory enhancer regions. Overall, JAZF1 depletion resulted in a significant reduction in the acetylation level of H2A.Z at >1.000 sites, while H2A.Z levels remained unaffected [257] (Figure 30C).
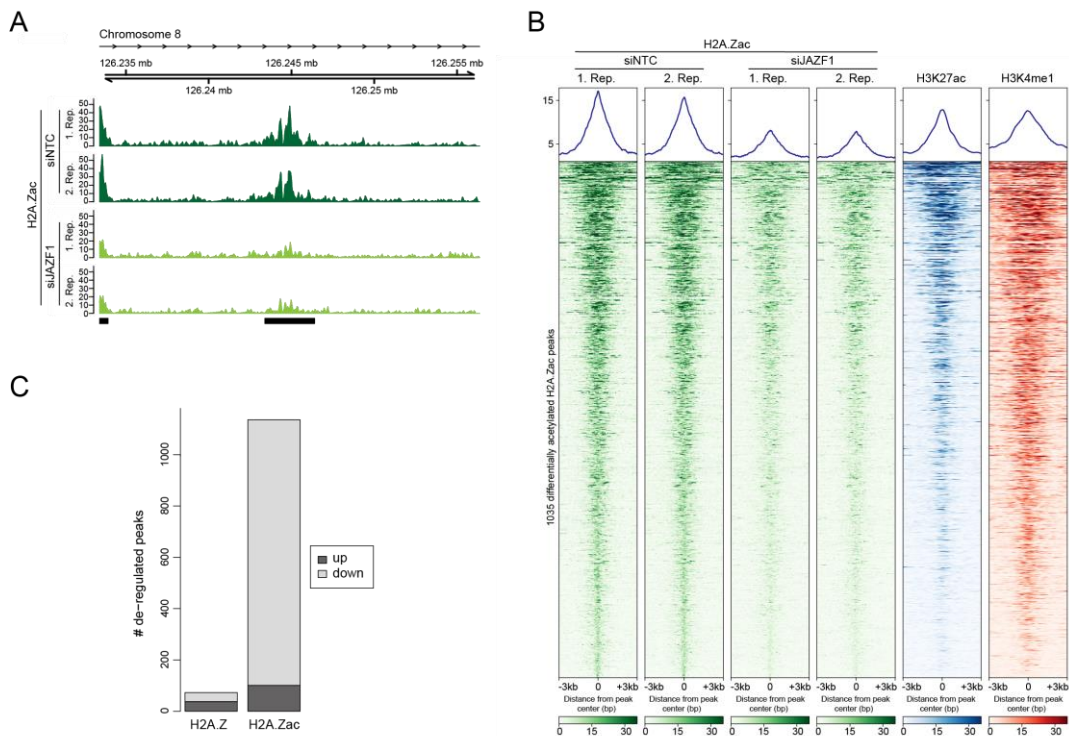
Figure 30: JAZF1 depletion leads to decreased acetylation of H2A.Z at >1.000 regulatory sites. (**A**) Representative genome browser snap shot of human chromosome 8 locus showing H2A.Zac ChIP-seq signals of control (siNTC, dark green, two replicates) and JAZF1-depleted (siJAZF1, light green, two replicates) HK cells. Differentially acetylated sites are highlighted with black bars. (**B**) Density heatmaps displaying differentially acetylated H2A.Z ChIP-seq peaks after control (siNTC) and JAZF1 (siJAZF1) knockdowns in HK cells (green, two replicates) in comparison to density heatmaps of H3K27ac (blue, ENCODE) and H3K4me1 (red, ENCODE) at those particular regions. Color intensities depict normalized and globally scaled tag counts. (**C**) Bar-plots illustrating statistically significant upregulated (dark grey) and downregulated (light grey) H2A.Z and H2A.Zac ChIP-seq peaks upon JAZF1 knockdown in HK cells.

In order to characterize the distinct functional properties of JAZF1-regulated H2A.Zac sites even more, we compared our ChIP-seq data of differentially acetylated H2A.Z sites (diffH2A.Zac) with chromatin states defined by a 10-state model trained on ENCODE data for H3K4me3, H3K4me1, H3K27ac, H3K36me3 and H3K27me3, using ChromHMM [352, 353]. Surprisingly, comparing global H2A.Zac with those of diffH2A.Zac sites, we observed no changes at active promoters harbouring high levels of H3K4me3 (states 1 and 3), but we noticed an increased enrichment at the chromatin states 2 and 6, which are marked by H3K36me3, H3K4me1 and H3K27ac, indicating that JAZF1-dependent sites with a significant decrease of H2A.Zac signal were highly enriched at the functional class of active enhancers within gene bodies [257] (Figure 31A, B).
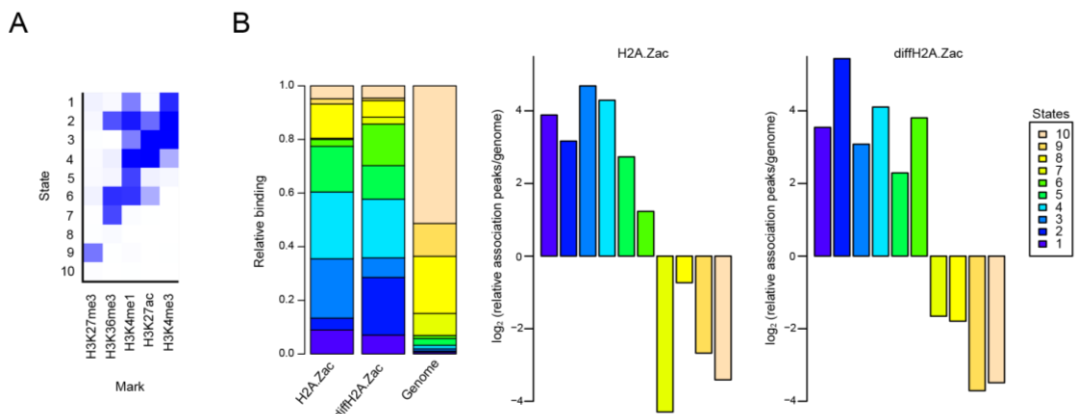
Figure 31: JAZF1-dependent differentially acetylated H2A.Z sites are located at regulatory enhancer regions within gene bodies. (**A**) Heatmap visualizing different functional chromatin states (1-10) that are characterized by the occurrence of individual histone modifications (marks) according to ChromHMM. (**B**) Enrichment of global H2A.Zac or differentially acetylated H2A.Z ChIP-seq sites (diffH2A.Zac) upon JAZF1 depletion in different functional chromatin states (1-10) compared to the human genome (left) and $\log_2$-fold enrichment of global H2A.Zac and diffH2A.Zac sites in specific chromatin states based to frequency in complete genome (right).

Generally, H2A.Zac has been primarily found at promoter regions [246, 247], however, at those sites we ascertained no changes in the acetylation level of H2A.Z upon JAZF1 depletion (Figure 31, 32A). More precisely, sites showing decreased acetylation of H2A.Z upon loss of JAZF1 were predominantly apparent at introns of genes, as determined by relative annotating genomic regions to diffH2A.Zac ChIP-seq sites (Figure 32B), suggesting that the changes in H2A.Z acetylation occur at defined genomic locations.
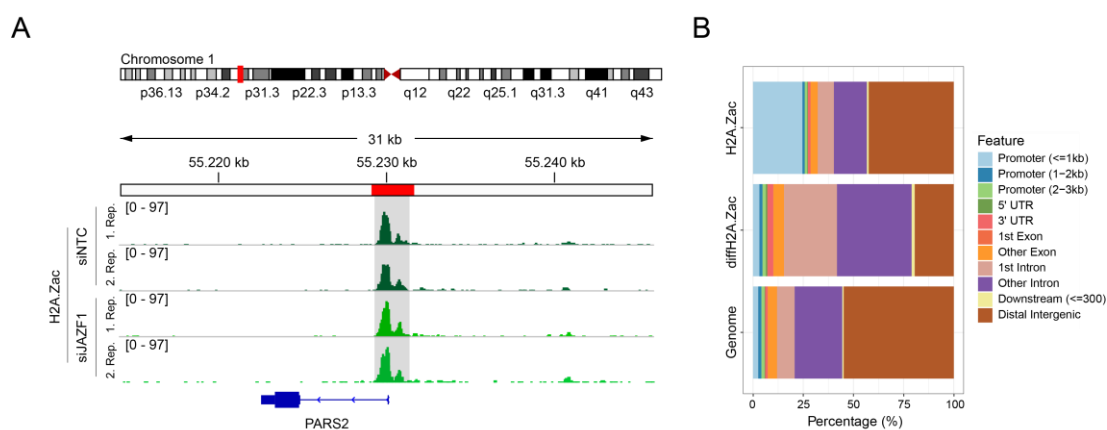
Figure 32: Differentially acetylated H2A.Z sites are enriched at regulatory chromatin regions within introns. (**A**) Representative genome browser snap shot of human chromosome 1 locus showing H2A.Zac ChIP-seq signals at the promoter region of the PARS2 gene of control (siNTC, dark green, two replicates) and JAZF1-depleted (siJAZF1, light green, two replicates) HK cells. Note that we observed no changes in H2A.Z acetylation at promoter regions (highlighted in gray). (**B**) Bar-chart showing genomic feature distribution of global H2A.Zac and JAZF1-dependent differential acetylated H2A.Z ChIP-seq peaks (diffH2A.Zac) in comparison to the human genome.

So far, JAZF1 depletion resulted in a decreased acetylation of H2A.Z at >1.000 regulatory sites within introns, while global H2A.Z levels remained unchanged [257], implying that JAZF1 does not affect chromatin deposition or ejection machanisms of H2A.Z, but influences its acetylation. These results raise the question of how JAZF1 can manipulate acetylation of H2A.Z, since it does not exhibit any enzymatic activity. At least one scenario can be envisioned, in which JAZF1 fulfils its functional role in controlling acetylation levels of H2A.Z via recruiting TIP60's enzymatic activity responsible for H2A.Z's acetylation at those particular regulatory sites, since we found JAZF1 bound to the KAT (see Figure 11). To test this hypothesis, I set out to evaluate TIP60's possible role in affecting acetylation levels of H2A.Z at some JAZF1-targeted sites via ChIP-qPCR. Therefore, I first performed siRNA-mediated knockdowns of control (siNTC), JAZF1 (siJAZF1) and TIP60 (siTIP60 #1 and #2) in HK cells and checked proper depletion of JAZF1 and TIP60 transcripts via RT-qPCR using two JAZF1- or TIP60-specific primer pairs, respectively. RT-qPCR analyses confirmed an appropriate reduction in JAZF1 (Figure 33A) and TIP60 (Figure 33B) mRNA levels.

A

B
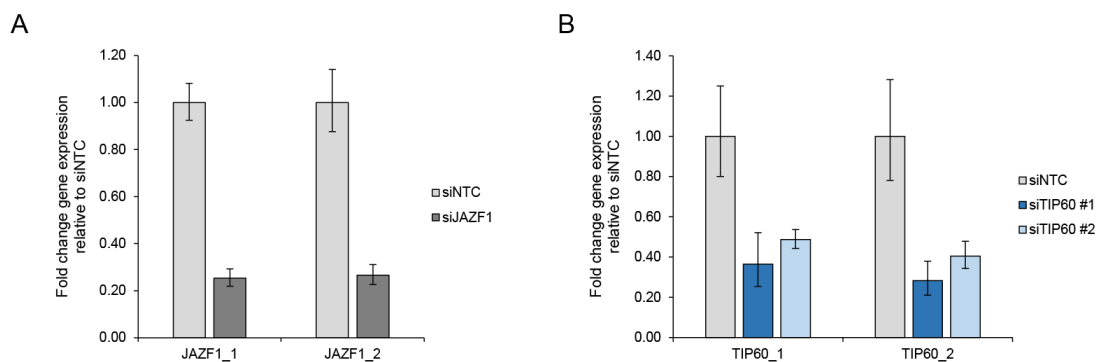
Figure 33: TIP60 transcript level was sufficiently downregulated via RNAi. (**A**) Expression analysis of JAZF1 by RT-qPCR two days after control (siNTC, light grey) or JAZF1 (siJAZF1, dark grey) siRNA-mediated knockdowns in HK cells using two JAZF1 primer pairs (JAZF1_1, JAZF1_2). Shown is the fold change gene expression compared to control (siNTC) and normalized to HPRT1 expression levels. Error bars indicate SD of three technical replicates. (**B**) Expression analysis of TIP60 by RT-qPCR analysis two days after control (siNTC, light grey) or TIP60 (siTIP60 #1 and #2, dark and light blue) siRNA-mediated knockdowns in HK cells using two TIP60 primer pairs (TIP60_1, TIP60_2). Shown is the fold change gene expression compared to control (siNTC) and normalized to HPRT1 expression levels. Error bars indicate SD of three technical replicates. Illustrated is one of three biological replicates showing similar results.

Afterwards, I established ChIP-qPCR primers (ctrl1TP, MMP12_gb, RBMS1_gb) for selected loci from previously generated ChIP-seq data showing reduced acetylation level of H2A.Z upon loss of JAZF1 (Figure 34A), but no change in H2A.Z occupancy (see Figure 29C). Finally, ChIP experiments of control (siNTC), JAZF1- (siJAZF1) or TIP60-depleted (siTIP60 #1 and #2) HK cells with an antibody against H2A.Zac were carried out followed by qPCR analyses of purified ChIP-DNA. In line with our previous ChIP-seq findings, JAZF1 depletion led to reduced acetylation of H2A.Z at the selected sites (Figure 34B), thereby verifying our obtained ChIP-seq results. Interestingly, TIP60 knockdown also resulted in an decrease in H2A.Zac at those JAZF1-targeted sites (Figure 34B), indicating that TIP60 is the histone acetyltransferase responsible for the acetylation of H2A.Z at least at some JAZF1-dependent chromatin regulatory enhancer regions [257].
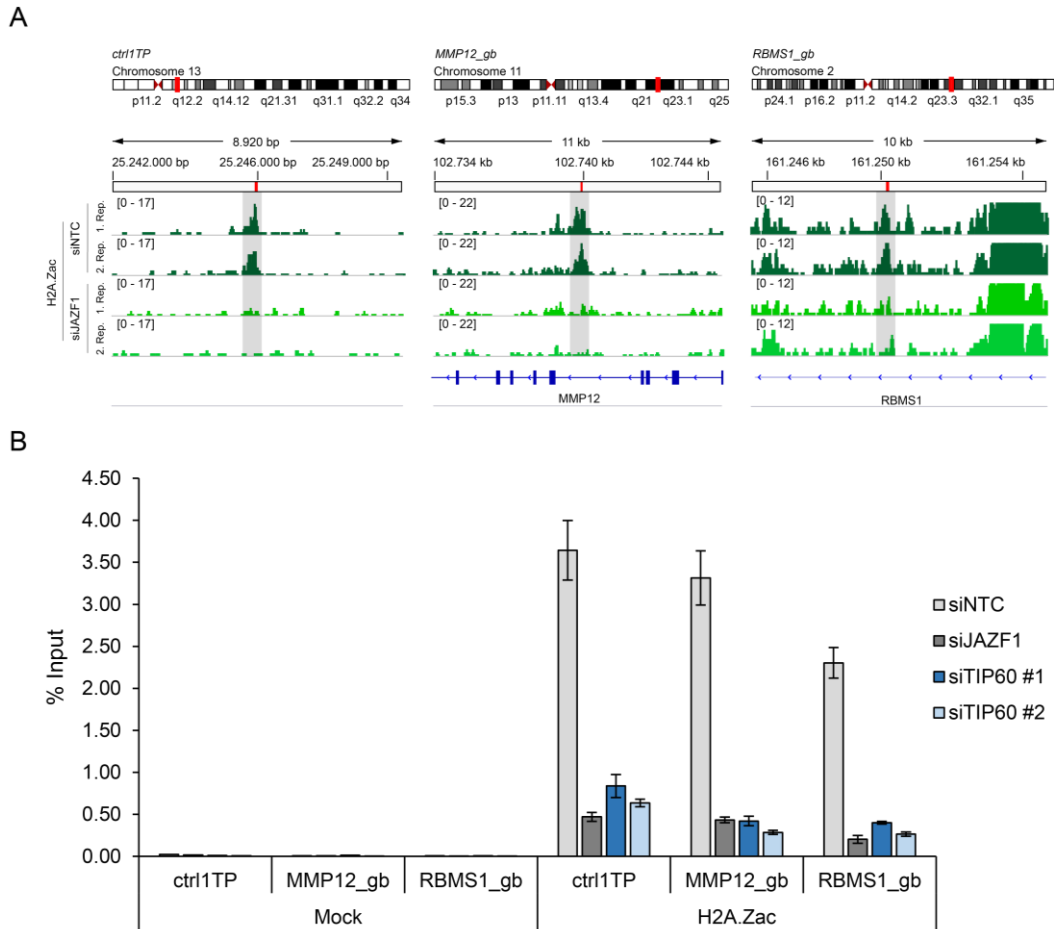
Figure 34: TIP60 depletion leads to reduction in H2A.Zac levels at some JAZF1-dependent differentially acetylated H2A.Z sites. (**A**) Three representative IGV snap shots of human chromosome 13 (left), 11 (middle), 2 (right) loci showing H2A.Zac ChIP-seq signals of control (siNTC, two replicates, dark green) or JAZF1-depleted (siJAZF1, two replicates, light green) HK cells. Binding sites of the ctrlTP1 (left), MMP12_gb (middle) and RBMS1_gb (right) ChIP-qPCR primer pairs used in (B) are depicted as red bars. Differentially acetylated H2A.Z sites are highlighted in grey. (**B**) ChIP-qPCR analysis of H2A.Zac levels at three JAZF1-dependent differentially modified sites (ctrl1TP, MMP12_gb, RBMS1_gb; gb: gene body) upon control (siNTC, light grey), JAZF1 (siJAZF1, dark grey) or TIP60 (siTIP60 #1 and #2, dark and light blue) knockdowns in HK cells using an antibody against H2A.Zac or no antibody (mock). Respective enrichment of H2A.Zac is depicted as percentage of input signals. Error bars indicate SD of three technical replicates.

All in all, we discovered JAZF1 as a crucial factor for regulating acetylation of H2A.Z at specific regulatory sites, possibly via targeting the histone acetyltransferase TIP60 of the p400 complex to such regions [257].

Note that the major part of this section has already been published in the following manuscript [257].

4 DISCUSSION AND FUTURE PERSPECTIVES

4.1 JAZF1 as a novel member of the p400 complex

Among several other proteins, we identified the proposed transcriptional regulator JAZF1 as a novel chromatin-free H2A.Z-binding protein of an MBTD1- and TIP60-containing p400 chaperone/remodelling sub-complex that excludes ANP32E in HeLa Kyoto (HK) cells as demonstrated by SILAC-MS and pull-down experiments [257] (see Figure 6, 7, 11). This suggests that such a complex can exist in different mammalian cell types, as JAZF1's association with the p400 complex has already been shown in human endometrial stromal cells [306]. However, the biological consequences have not been further characterized [306]. On the other hand, a p400 complex that contains both JAZF1 and MBTD1 but precludes ANP32E had so far not been reported and is an exciting finding that raises several questions, which can be elucidated by future research: How do JAZF1 and MBTD1 bind to the p400 complex? Do they recognize specific factors such as TIP60, since we found JAZF1 bound to the KAT (see Figure 11)? Do they compete with ANP32E for binding to the p400 complex? In this way, our discovery can provide a basis for further studies. Moreover, it opens up completely new and interesting functions for JAZF1. Apart from its already known transcriptional properties and metabolic features [295, 354], nothing is known about the putative role JAZF1 might play within the multifunctional p400 complex. Since JAZF1 has been linked to cancer development [355, 356] and is overexpressed in many cancer types (see Figure 35 [357–359]), highlighting the importance of this factor, it will be of particular interest to evaluate JAZF1's functional implication in p400-mediated biological processes to obtain access to the poorly understood molecular mechanisms of JAZF1 in health and disease. Therefore, I aimed in the present study to unravel the yet unexplored p400-associated chromatin functions of JAZF1.
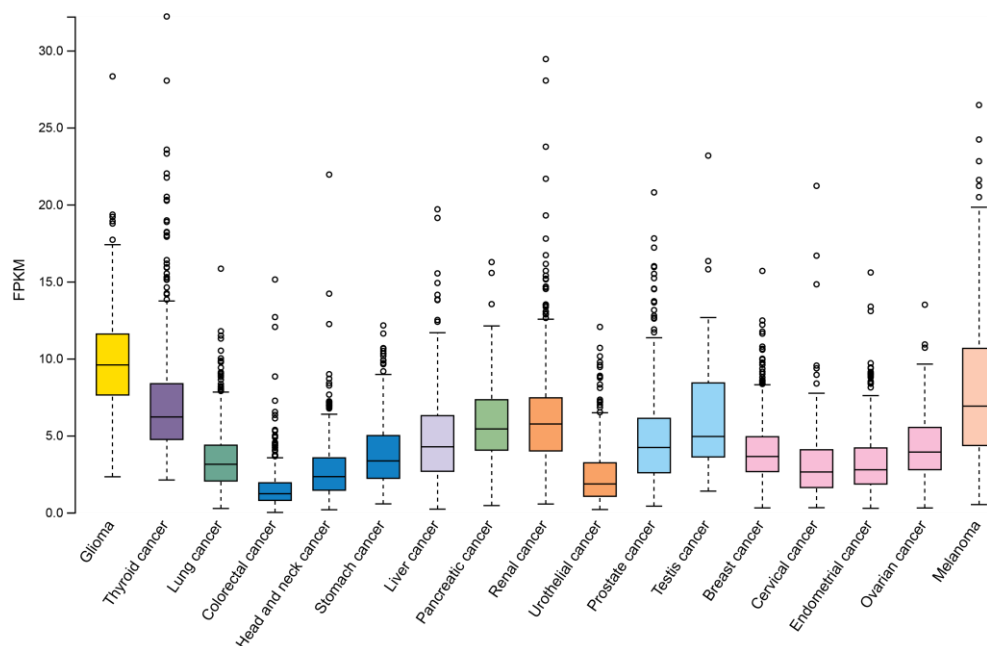
Figure 35: JAZF1 mRNA expression levels are increased in several cancer types.
Box-plots showing JAZF1 mRNA expression in 17 cancer types depicted as median
number Fragments per Kilobase of exon per Million reads (FPKM) obtained from RNA-seq
data by the Cancer Genome Atlas (TCGA). Image (RNA Expression Overview) received
from the Human Protein Atlas (http://www.proteinatlas.org) [357–359]. Available from
v20.1.proteinatlas.org (Expression of JAZF1 in cancer – Summary – The Human Protein
Atlas: https://www.proteinatlas.org/ENSG00000153814-JAZF1/pathology). Copyright © by
Human Protein Atlas.

4.2 Towards understanding the functions of JAZF1 beyond its metabolic roles

JAZF1 – an underrated transcription factor involved in DNA damage repair processes?

Interestingly, first preliminary data from our group and collaboration partners
demonstrated that GFP-JAZF1 is rapidly recruited to DSBs after laser irradiation (data
not shown), suggesting that JAZF1 could be involved in the DNA damage response
as it has already been demonstrated for other p400 complex components such as
MBTD1, TIP60 or ANP32E [210, 275, 281, 284, 338, 360]. The study by Jacquet et
al. revealed that MBTD1 and TIP60 participate in DNA repair by influencing the
disappearance of γH2A.X foci, which is indispensable for the final repair of DSBs
through homologous recombination (HR) [284]. It has been shown that depletion of
MBTD1 or TIP60 leads to a prolonged persistence of those foci, which appears about
150 min after cell irradiation and persists for up to 12 hours, whereas control cells

reach basal levels of γH2A.X already after 6 hours [284, 336–338]. This phenomenon could reflect a defect in DNA repair due to the loss of MBTD1 or TIP60 [284]. Surprisingly, 180 min after induction of DSBs, we also observed higher levels of γH2A.X upon loss of JAZF1, as demonstrated by ChIP-qPCR experiments (see Figure 16), while global levels remained unaffected (see Figure 14). This finding provide a first indication that JAZF1 might be required for the repair of DSBs at certain sites, raising the question of what role JAZF1 does play in DNA repair processes. The function of MBTD1 and TIP60 in DNA damage repair has been partly uncovered, while the influence of JAZF1 on this cellular process is still unknown.

In response to DSBs a large number of proteins is phosphorylated by the ATM kinase, thereby mediating initiation of an early signalling cascade that in turn leads to the regulation of chromatin structure as well as transcriptional activity and facilitates the binding of downstream effectors for efficient repair of injured DNA [361, 362]. These coordinated mechanisms are primarily regulated by nucleic acid binding as well as PTM recognition and protein-protein interactions at DNA lesions [363]. Among several other DNA damage-related proteins, MBTD1 and TIP60 contain structural and functional features allowing them to recognize specific histone modification patterns and/or acetylate target proteins in the temporal and spatial orchestration of DSB repair [284, 364]. However, based on homology searches (BLAST) it is highly unlikely that JAZF1 possesses histone reader domains or any enzymatic activity, but JAZF1 comprises three C2H2-type zinc finger (ZnF) motifs (see Figure 9) commonly found in transcription factors (TFs) and has been originally described as an putative transcriptional regulator [296, 354]. Interestingly, beyond the classical functions of TFs involving gene regulatory roles through DNA, RNA or protein binding, a large number of these factors also participate in the DNA damage response [363]. At least two different scenarios can be envisioned how TFs regulate DNA repair [365]. Firstly, they can indirectly promote repair by controlling the expression of genes encoding key determinants of the DNA repair system and on the other hand, they can regulate DNA recovery directly through acting as an integral component of the DNA repair machinery itself [365]. A recent study by Izhar et al. identified several TFs as being DNA damage localized after laser microirradiation, where they are presumably able to facilitate repair of DNA lesions [363, 366]. Interestingly, JAZF1 is also promptly recruited to DSBs (data not shown) and, in addition, we showed that JAZF1 regulates the transcription of several DNA repair-associated factors, since loss of JAZF1 impaired expression of genes related to DNA repair as demonstrated by RNA-seq experiments (Figure 20B). Gene Set Enrichment Analysis (GSEA) of our RNA-seq dataset of JAZF1-depleted (siJAZF1) HK cells in comparison to control (siNTC)

knockdown, deciphered a statistically consistent transcriptional change of genes related to the GO pathway "DNA repair" (Figure 36). These findings corroborates the belief of JAZF1 being implicated in DNA damage repair processes as a putative transcriptional regulator.
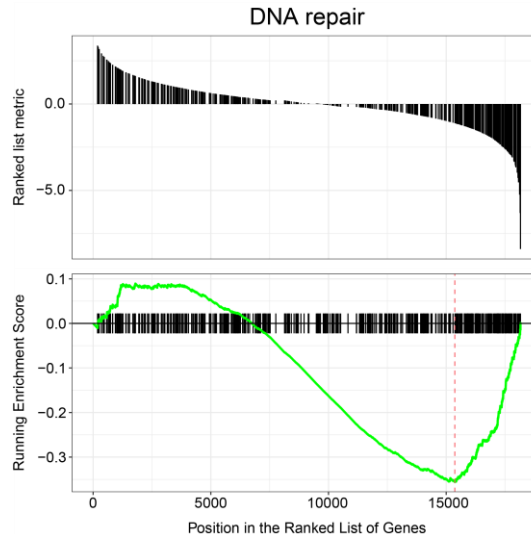
Figure 36: JAZF1 depletion leads to the deregulation of several genes, with some of them involved in DNA repair processes. Gene Set Enrichment Analysis (GSEA) of expression changes upon loss of JAZF1 (siJAZF1) in comparison to control (siNTC) knockdown in HK cells received from the RNA-seq dataset as described in Figure 19 and 20, demonstrated that several deregulated genes are associated with the Kyoto Encyclopedia of Genes and Genomes (KEGG) pathway "DNA repair".

Given these results, it can be considered that JAZF1 may function as a DNA-binding factor in a spatio-temporal fashion to control the activity of key mediators involved in DNA repair processes by modulating their expression. Likewise, it might also be possible that JAZF1 as a member of the p400 complex rapidly translocates to DNA breaks, thereby allowing access of the p400 complex to sites of action in order to facilitate efficient repair of injured DNA. These interesting proposals could be the focus of future research.

Moreover, TFs are often posttranslationally phosphorylated in order to regulate their activity [367]. Interestingly, MS data in the literature (PhosphoSitePlus database) revealed that JAZF1 exhibits many putative phosphorylation sites: Y55, S85, T99, T109, T113, T117, S119, S120 and Y216, which can possibly modulate both the DNA-binding and the transcriptional activity of JAZF1 upon phosphorylation. Therefore, it could be of particular interest to investigate whether JAZF1 indeed gets phosphorylated, also in context of DNA damage and which kinase(s) is/are

responsible for modifying JAZF1, thereby potentially contributing not only to the fundamental understanding of JAZF1's molecular functioning, but also to its putative role in DNA damage repair processes. This proposal could be realized by protein dephosphorylation assays (for instance using the Lambda phosphatase enzyme) followed by immunoblotting analysis of JAZF1. In order to determine the kinase(s) responsible for the phosphorylation of JAZF1, *in vitro* kinase assays using specific kinase inhibitors could be performed followed by immunoblot detection of JAZF1. However, it should be noted that in response to DNA damage, it is highly unlikely that JAZF1 becomes phosphorylated by the ATM, ATR or the DNA-PK, as these kinases preferentially phosphorylate SQ/TQ motifs of target substrates [368–370], which are missing in putative JAZF1 phosphorylation sites.

Furthermore, in response to DNA damage the transcription of genes flanking DSBs is suppressed and only restored after completion of DNA repair [308]. Dieter Werner, a former master student of our group I supervised, investigated whether JAZF1 might be even required for DSB-induced transcriptional silencing, since it is described as an potential transcriptional repressor [295]. Using the here described U2OS reporter cell system [307, 320], Dieter determined nascent transcript levels of the doxycycline-inducible YFP-MS2 reporter transgene upon JAZF1 depletion in an DSB-occuring environment. First indications received from its RT-qPCR experiments provided that downregulation of JAZF1 did not lead to changes in the reporter transcript level at various time points (data not shown, Master Thesis of Dieter Werner). It can therefore be assumed that the duration of the DSBs-induced transcription arrest of the transgene remains largely unaffected upon loss of JAZF1, arguing against an actual defect in DNA damage repair and a role of JAZF1 in the regulation of DSB-dependent transcriptional repression events. Nevertheless, due to a lack of time this experiment was only performed once and should therefore be repeated in order to clarify whether JAZF1 attends in transcriptional silencing in response to DNA damage.

Overall, our results provide a first evidence that JAZF1 is somehow implicated in DNA repair, but the mechanism by which JAZF1 potentially influences this cellular essential process remains unknown. Therefore, future research is required to decipher the exact role JAZF1 might have in DNA damage repair processes. Continuative experiments such as ChIP-seq of JAZF1 after induction of DSBs at precise loci can be employed to gain further knowledge regarding JAZF1's genomic localization, thereby contributing to a clearer understanding whether JAZF1 may actually act as a transcriptional regulator of putative DNA repair-associated genes. Likewise, other p400 complex members such as TIP60 and MBTD1 could also be traced via ChIP-seq in order to analyse whether a genomic colocalization with JAZF1 exist at those

sites, thereby taking the p400 complex into account. Performing immunofluorescence (IF) analyses after inducing DNA damage can also deliver insights into JAZF1's cellular distribution and whether a colocalization with the DNA damage marker γH2A.X exist. Last but not least, since we only identified by SILAC-MS JAZF1's and MBTD1's chromatin-free binding partners, it could also be interesting to evaluate whether MBTD1, JAZF1 and ANP32E act in concert on chromatin in a spatio-temporal dynamic to facilitate DNA repair, since both MBTD1 and ANP32E have already been linked to DNA damage repair [281, 284]. In the future, it will be of particular interest to investigate the precise molecular functions of JAZF1 in this biological essential pathway.

JAZF1, a transcriptional regulator of ribosome biogenesis

Interestingly, RNA-seq experiments of control (siNTC) and JAZF1-depleted (siJAZF1) HK cells revealed that JAZF1 not only regulates the transcription of DNA repair-associated factors, but also controls expression of several genes involved in ribosome biogenesis (Figure 20). Support for this observation comes from a recent study by Kobiita et al., showing that JAZF1 is a key transcriptional regulator of ribosome biogenesis in pancreatic ß-cells [344], thereby indicating that the regulatory functions of JAZF1 are not restricted to a specific cell type [257]. Moreover, Kobiita and colleagues also identified JAZF1 as nucleoli-enriched protein, whose depletion led to enlarged nucleoli sizes, reflecting a defect in ribosome biogenesis [344]. Additional IF analyses of our group demonstrated that nuclear JAZF1 also associates with Coilin, a signature protein of Cajal Bodies (CB) [371] (Figure 23). Several studies have implicated CBs in modifying non-coding RNAs, which include those forming the core of small nucleolar ribonucleoproteins (snoRNPs) involved in ribosomal RNA (rRNA) processing [257, 348], thereby playing a crucial role in the regulation of ribosome and spliceosome kinetics [345–347]. Interestingly, we also noted that some deregulated genes upon loss of JAZF1 were significantly associated with the KEGG pathway 'Spliceosomal complex' (Figure 37), indicating that JAZF1 is a transcriptional regulator not only of ribosome biogenesis-associated genes, but also of some spliceosomal-related genes. This is supported by the mere observation of an increased number of CBs upon downregulation of JAZF1 (Figure 23), possibly in response to an impaired splicing rate [372].
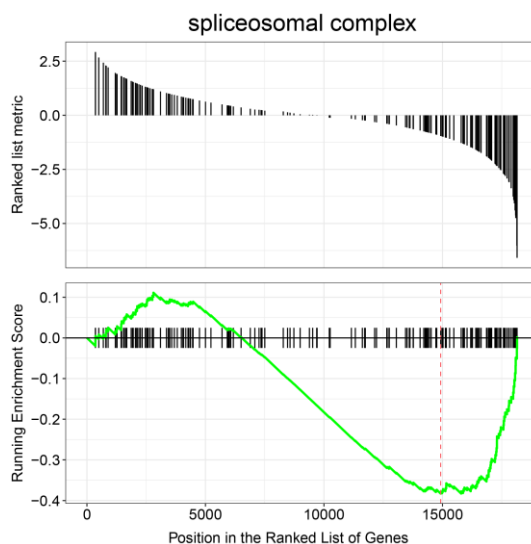
Figure 37: JAZF1 depletion leads to deregulation of many spliceosomal complex-associated genes. Gene Set Enrichment Analysis (GSEA) of expression changes upon loss of JAZF1 (siJAZF1) in comparison to control (siNTC) knockdown in HK cells received from the RNA-seq dataset as described in Figure 19 and 20, demonstrated that several deregulated genes are associated with the Kyoto Encyclopedia of Genes and Genomes (KEGG) pathway "spliceosomal complex".

Moreover, proliferation analyses of control (siNTC) and JAZF1-depleted (siJAZF1) HK cells demonstrated that loss of JAZF1 resulted in proliferation defects (Figure 24B), possibly due to a deregulated rate of ribosome biogenesis, while I was not able to detect changes in cell cycle progression upon JAZF1 knockdown (Figure 24C). However, this type of analysis utilized is not useable for detecting slight changes in cell cycle progression, as growing cell cultures are generally asynchronous and thus exhibiting cells in different stages of the cell cycle [373]. This fact makes it difficult to ascertain minor changes in cell cycle progression of heterogeneous cell populations. Therefore, it is best to synchronize cells to create a homogeneous population of cells at a single cell cycle stage by inhibiting cells from cycling [373]. The use of chemical agents such as the rapidly-reversible inhibitor Nocodazole causes cell arrest in G_2/M phase [373]. After cell synchronization, cells reentry into the cell cycle and continue cycling at the same stage, thereby allowing detection of subtle changes in cell cycle events [373]. Therefore, it cannot be excluded whether depletion of JAZF1 leads to a slight defect in a cell cycle phase, which need to be elucidated by future research. Moreover, it could also well be that depletion of JAZF1 leads to increased cell death, as deregulation of ribosome biogenesis and larger nucleoli sizes have frequently been linked to an increased cellular propensity to undergo apoptosis and/or senescence [344, 374, 375]. Therefore, it might be very interesting to analyse the cellular

relevance of the observed proliferation defect by further research. Performing apoptosis and senescence assays of control (siNTC) and JAZF1-depleted (siJAZF1) HK cells could provide insights into the resulting cellular consequences upon JAZF1 depletion, thereby potentially contributing to the fundamental understanding of JAZF1's cellular role in health and disease. For instance, flow cytometry analyses of fluorescently labeled Annexin V (a marker for apoptosis)-stained cells could be conducted to detect and quantify apoptotic cells [376]. Since Annexin V not only stains apoptotic, but also necrotic cells, co-staining with propidium iodide (PI) should be performed to distinguish apoptotic from nectrotic cells, as PI only enters necrotic cells [376]. In contrast, determination of cellular senescence could be realized by measuring senescence-associated (SA) ß-galactosidase activity using the artificial substrate X-gal, as only senescent cells are able to convert X-gal into a blue product, which can be easily detected by microscopy [377, 378].

JAZF1 has been identified as a TAK1/TR4-interacting protein with functions as a co-repressor of TAK1-mediated direct repeat DNA-element (DR1)-dependent transcriptional activation [295]. It is suggested that the TAK1-associated transcriptional regulation involves the recruitment of various transcription intermediary factors, which in turn allow binding of complexes to induce changes in chromatin structure through their histone deactelyase or acetylase activities [295, 379]. Interestingly, a study by O'Geen et al. demonstrated that TAK1 target genes were enriched in fundamental biological processes such as ribosome and RNA processing [380], indicating that TAK1 might be an important regulator of ribosome biogenesis. Taking our insights and those of the study by O'Geen et al. into account one exciting question emerges: Does TAK1 concomitant bind with the transcriptional regulator JAZF1 to some target sites, which might lead to the recruitment of the p400 complex to control transcription of ribosomal genes via the histone acetyltransferase TIP60? It would thus be very interesting to re-analyse our RNA-seq dataset received from JAZF1-depleted HK cells with respect to TAK1-dependent target genes to unravel whether JAZF1 and TAK1 regulate common genes. Astonishingly, support for our assumption also comes from another publication by Halkidou et al. revealing that TIP60 plays a role in rDNA and ribosomal gene transcription in prostate cancer cell lines [341]. Moreover, in yeast, the catalytic component Esa1 of the NuA4 histone acetyltransferase complex is involved in the transcriptional regulation of ribosomal protein genes by the acetylation of target histone proteins [381], indicating that histone acetylation by the NuA4 complex could constitute a conserved mechanism of regulating transcription of ribosomal genes.

Overall, JAZF1 supposedly affect ribosome biogenesis on a transcriptional level, however, it remains still unclear how JAZF1 mechanistically exercises its transcriptional functions. Hypothetically, JAZF1 may act as a chromatin modulator via recruiting the TIP60-containing p400 complex to respective target sites.

Unmasking of JAZF1 as chromatin modulator

Using ChIP-seq analyses, we discovered JAZF1 as a crucial factor for regulating acetylation of the histone variant H2A.Z at more than 1.000 regulatory sites within intronic enhancers [257] (Figure 30, 31, 32). This is in line with our RNA-seq experiment demonstrating that more genes were down- than upregulated upon JAZF1 depletion, as acetylation of H2A.Z has generally been linked to transcriptional activation [247]. Since JAZF1 does not seem to exhibit any enzymatic activity, it is thus tempting to speculate that the acetylation of H2A.Z at these JAZF1-targeted sites is catalyzed by the histone acetyltransferase TIP60, as we found JAZF1 bound to the KAT (Figure 11), and both belong to the same H2A.Z-specific p400 chaperone/remodelling sub-complex [257] (Figure 6, 7). Moreover, depletion of TIP60 resulted in decreased H2A.Zac levels at some JAZF1-regulated sites (Figure 34), supporting our hypothesis of TIP60 being the driving force for modifying H2A.Z at these specific JAZF1-orchestrated regulatory regions. Thus, it seems likely that JAZF1 recruits the enzymatically active KAT TIP60 to some regulatory sites to orchestrate acetylation of H2A.Z, thereby controlling expression of many genes, with several of them involved in ribosome biogenesis [257]. As already mentioned, the publication from Halkidou et al. corroborates this theory by demonstrating a putative role of TIP60 in ribosomal gene transcription [341]. To provide more detailed information on whether the observed changes in H2A.Zac correlate with the deregulation of target genes upon JAZF1 knockdown, we compared our datasets derived from the ChIP-seq and RNA-seq experiments with each other. Unfortunately, comparison of these two types of data did not reveal a statistically significant overlap of genes that were differentially expressed in close proximity to the deregulated H2A.Zac sites upon JAZF1 depletion (Figure 38).
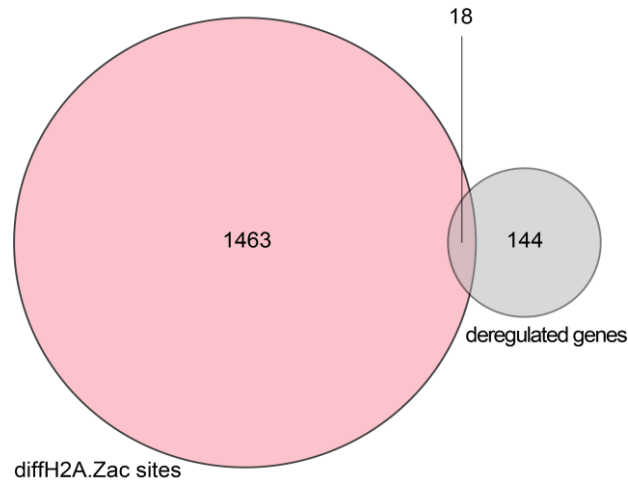
Figure 38: Correlation between JAZF1-dependent diffH2A.Zac sites and target genes. Venn diagram showing overlap of differentially acetylated H2A.Z (diffH2A.Zac) ChIP-seq peaks (red) and differentially expressed genes (grey) obtained from the RNA-seq dataset upon JAZF1 depletion. Note that there is no statistically significant overlap of genes that were differentially expressed in close proximity to the deregulated H2A.Zac sites upon JAZF1 depletion (number of overlapped genes: 18).

However, it can be quite challenging to establish direct links between histone acetylation and changes in gene expression, as JAZF1-affected H2A.Zac sites were mainly found within intronic enhancers. Therefore, it might be possible that the alterations of H2A.Zac affect expression of distant genes through a long regulatory path that depends on the combinatorial action of multiple factors. Accordingly, it will be interesting to determine whether JAZF1 act in concert with other regulatory determinants on chromatin, since we only looked at the chromatin-free interaction partners of JAZF1 [257], thereby contributing to the understanding of how JAZF1 actually performs its chromatin-associated functions.

Moreover, it would be crucial to map the genomic binding sites of JAZF1 and TIP60 on a genome-wide level via ChIP-seq to confirm our previous results and to identify additional target genes of JAZF1, since we only evaluated the impact of JAZF1 on chromatin. To determine putative biological processes for JAZF1 targets, GO and KEGG analyses could be conducted. Regrettably, I was not able to identify where in the genome JAZF1 and TIP60 actually bind, neither of endogenous nor of GFP-tagged proteins, as countless antibodies were not applicable for ChIP-seq assays and/or did not yield evaluable results. In the meanwhile, Kobiita and colleagues succeeded in the genome-wide identification of JAZF1 targets in pancreatic ß-cells by ChIP-seq [344]. Interestingly, they identified numerous JAZF1 target genes that were related to biological processes such as translation, ribosome, mRNA splicing,

chromatin remodelling, and regulation of translation fidelity [344]. While the discovered JAZF1 target sites were enriched mainly at proximal promoter regions [344], we only found changes in H2A.Zac in enhancers regions [257]. However, it should be noted that JAZF1 binding sites have also been found within the first and other intron regions [344], which often contain functional elements such as enhancers important for regulating expression of genes that can be located over as much as a million base pairs away [382–384]. In addition, JAZF1-associated binding sites within transcriptional start sites corresponded to E26 transformation-specific (ETS) and direct repeat DNA-element (DR1) transcription factor motifs [344]. Interestingly, TAK1 also binds strongly to DNA elements containing a DR1 motif [295, 344]. Since JAZF1 associates with TAK1 and both are involved in the regulation of ribosomal gene expression [295, 344, 380], it could well be that JAZF1 is part of a second complex including TAK1, which controls the expression of target genes directly via binding to respective transcriptional start sites. Another possible explanation for this controversial finding might be that depending on the cell type and/or differentiation state, different JAZF1-dependent transcriptional regulatory mechanisms exist, including the p400 or the TAK1/TR4 complex. Therefore, it will be also very interesting to compare published TIP60 and TAK1 ChIP-seq data with those of JAZF1 to resolve this discrepancy.

However, several questions remain open for future research that need to be further explored to expand our knowledge of how JAZF1 orchestrate chromatin/DNA transcriptional regulation events, especially in regard to its impact in ribosome biogenesis. Since two different putative mechanism how JAZF1 could control transcriptional outputs of target genes has been published [257, 344], it would be crucial to analyse whether JAZF1 might be actually a member of several different complexes and whether these JAZF1-mediated transcriptional processes are rather general principles to regulate expression of various gene sets or whether these are cell type- or differentiation-dependent mechanisms.

Based on our data, at least one hypothetical model can be imagined (Figure 39), in which JAZF1 might function as a recruiter of the TIP60-containing p400 complex to some intronic regulatory enhancer regions, where TIP60 catalyzes the acetylation of the histone variant H2A.Z, thereby controlling expression of target genes, with many of them involved in ribosome biogenesis.
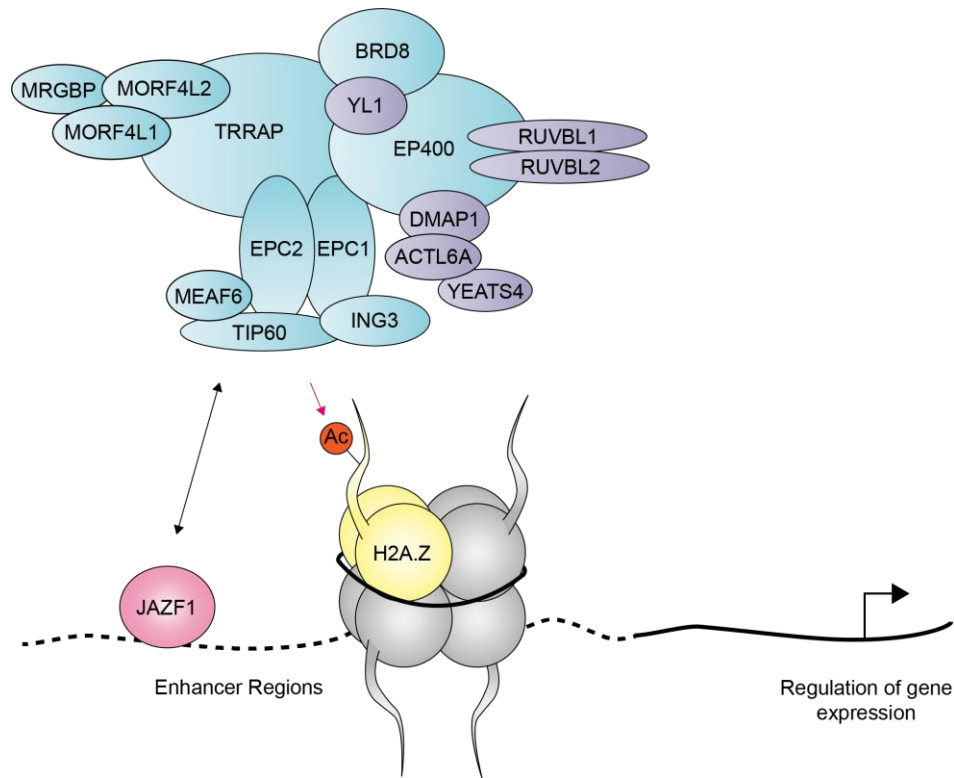
Figure 39: Proposed model of JAZF1-mediated transcriptional regulation of target genes. We identified JAZF1 (pink) as a novel member of an TIP60-containing p400 sub-complex (members of the p400 complex are depicted in blue and shared members of the p400 and SRCAP complexes are shown in purple), which recruits TIP60's enzymatic activity to regulatory enhancer regions within introns (black arrow), where it acetylates (red circle) the histone variant H2A.Z (yellow), thereby regulating transcription of many target genes.

4.3   Yeast SFP1 a putative counterpart of human JAZF1

Inferring functional and evolutionary relationships of JAZF1 by homology searches using the web browser-based NCBI Basic Local Alignment Search Tool (BLAST) revealed that the yeast transcription factor Split finger protein 1 (SFP1) is a putative ortholog of human JAZF1. This is consistent with the study from Kobiita et al. [344] and a study by Loewith and Virgilio, which uncovered several human orthologues of *S. cerevisiae* TOR signalling network components with the web-based YOGY resource [385]. Both, JAZF1 and SFP1 contain three putative C2H2-type zinc finger (Znf) motifs [292, 386] (Figure 40A), which resemble not only in their distribution, but also in their amino acid sequences, as demonstrated by alignment of human JAZF1 and yeast SFP1 protein sequences using the web browser-based Clustal Omega [387] (Figure 40B).

Figure 40: Human JAZF1 shares sequence homologies to yeast SFP1. (**A**) Schematic domain organization of the human JAZF1 (upper) and yeast SFP1 (below) proteins. JAZF1 and SFP1 contain three putative C2H2-type zinc finger (ZnF) domains. (**B**) Clustal Omega-based alignment [387] of human JAZF1 and yeast SFP1 amino acid sequences. The three putative zinc finger motifs (ZnF1-3) are highlighted with the respective color as shown in (A). Asterisk (*) represents fully conserved residues, colon (:) represents conserved strongly similar residues and period (.) represents conserved weakly similar residues.

Among other functions, yeast SFP1 acts as a transcriptional regulator of genes required for ribosome biogenesis, similar to JAZF1 in human [344, 385, 386, 388, 389], indicating that in addition to their structural accordance, JAZF1 and SFP1 might share functional similarities. It is suggested that SFP1 affects ribosome biogenesis on a transcriptional level by regulating expression of ribosomal genes [386, 390], however, SFP1 has not been detected directly on corresponding promoter elements, suggesting that SFP1 might regulate gene expression through an indirect mechanism [386]. Interestingly, SFP1 was found to interact with yeast Transcription-associated protein 1 (Tra1) (homolog of human TRRAP), a subunit of the NuA4 histone acetyltransferase complex [391–393]. In a previous study, depletion of SFP1 or Tra1 in yeast strains resulted in a deregulation of ribosomal protein gene expression, indicating that both proteins function in the same pathway [391]. In addition, deletion of Tra1 displayed decreased recruitment of the catalytic subunit Esa1 of the NuA4 complex to target sites [391]. In yeast, Esa1 has already been found to play a crucial role in the coordinated regulation of ribosomal gene expression by the acetylation of chromatin substrates [381] and moreover, Esa1 is highly similar to human TIP60 [394]. With regard to our data, at least one hypothetical scenario can be envisioned, in which JAZF1 and SFP1 might function as transcriptional regulators via recruiting the Esa1- or TIP60-containing NuA4/p400 complex to respective target sites for the regulation of target gene expression, implying that eukaryotes have evolved a common/conserved transcriptional regulatory mechanism of ribosomal genes.

Furthermore, like for JAZF1, SFP1 has been proposed to regulate expression of genes involved in the DNA-damage response, while loss of SFP1 impairs DNA repair in yeast [386, 395]. Since expression of SFP1 is increased after DNA damage [386], it would thus be very interesting to evaluate whether JAZF1 expression is also upregulated in response to DNA damage, thereby contributing to the assumption of JAZF1 being a crucial regulator in DNA repair processes. Moreover, SFP1 has been proposed as a key element in controlling cell growth and cell cycle progression by regulating expression of genes required for many growth-promoting processes [388, 390]. However, as previously mentioned I was not able to detect changes in cell cycle progression upon JAZF1 depletion, possibly due to a lack of cell synchronization. In summary, our results are consistent with those of Kobiita et al. revealing that JAZF1 is a putative functional ortholog of SFP1, a key determinant in regulating transcription of ribosomal genes [344]. Moreover, Clustal Omega-based alignment [387] of the human JAZF1 protein sequence revealed not only amino acid similiarities to yeast SFP1, but also a high conservation across other species, indicating that JAZF1 is highly conserved (see Figure A.3 in appendix).

4.4 JAZF1 and its association with human endometrial stromal sarcomas

Since JAZF1's discovery as a transcriptional TAK1-interacting coregulator in 2004 [295, 356], it has frequently been found to be associated with various cellular metabolic energy processes such as gluconeogenesis, lipid metabolism, and insulin sensitivity [292, 293]. It is therefore not surprising that genetic variations of the JAZF1 gene has been reportedly closely linked to metabolic disorders like type 2 diabetes mellitus (T2DM) [354, 396, 397]. However, human diseases associated with deregulation of JAZF1 also include cancer, in particular prostate cancer and endometrial stromal sarcomas (ESS) [300, 355, 398], while the underlying mechanisms of how JAZF1 contributes to the occurrence of these neoplasms are largely unknown. Due to a great interest and an important biological as well as clinical relevance, I will focus in the following section on JAZF1's putative involvement in human ESS.

Over the past years, genetic investigations have revealed that human sarcomas are frequently characterized by the appearance of specific chromosomal translocations, thereby leading to the generation of chimeric proteins, which contain combined properties of the original proteins [399]. Since genes encoding transcription factors are often affected by these nonrandom genetic rearrangement events, it might be conceivable that the novel proteins function as deregulated transcription and signalling factors, resulting in the disruption of tightly regulated biological processes [399]. Human ESSs are extremely rare mesenchymal malignant tumors of the uterine [400]. One of the most common cytogenetic abnormalities found in ESSs is the t(7;17)(p15:q21) chromosomal translocation, involving genes encoding the two zinc-finger proteins JAZF1 and SUZ12 [300, 401]. The resulting fusion protein contains the N-terminal fragment of JAZF1 and a large portion of the C-terminal part of SUZ12 [300] (Figure 41). SUZ12 is a member of the Polycomb repressive complex 2 (PRC2) that controls chromatin compaction and transcriptional repression through trimethylation of histone H3 on lysine 27 [402]. Interestingly, a recent study demonstrated that the JAZF1-SUZ12 fusion mediates an spatial interaction between the transcriptional active p400 and the repressive PRC2 complexes [306], while the biological consequences remain still unknown.
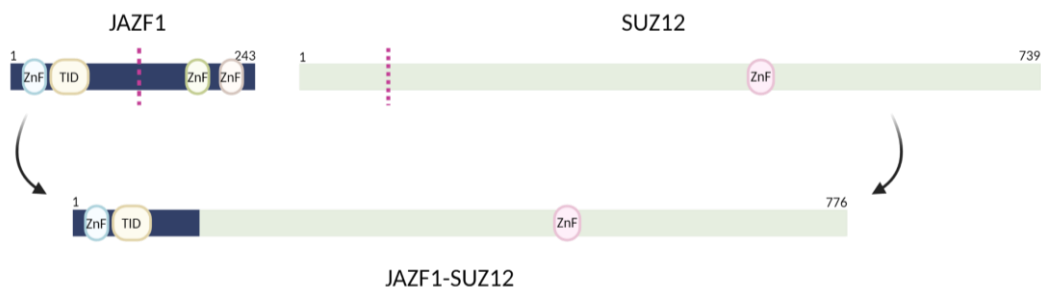
Figure 41: Schematic domain structure of the JAZF1-SUZ12 sarcoma-specific fusion protein. JAZF1 (black) consists of a nuclear orphan receptor TAK1/TR4 interacting domain (TID, yellow) required for the interaction with TAK1/TR4 and three putative zinc finger motifs (ZnF) shown in blue, green and brown. SUZ12 (green) contains one zinc finger domain (ZnF, pink) crucial for the interaction with PRC2 complex members. The aberrant sarcoma-specific fusion protein JAZF1-SUZ12 contains the N-terminal part of JAZF1 and a large portion of the C-terminal part of the SUZ12 protein. Magenta dashed lines indicate breakpoints. Figure created with BioRender.com.

Besides JAZF1-SUZ12, other chimeric proteins have been detected in ESS including JAZF1-PHF1, EPC1-PHF1, MEAF6-PHF1, MBTD1-CXorf67, MBTD1-PHF1 [304, 306, 403]. Conspicuously, all of these fusions potentially have the capability to physical linkage the p400 and PRC2 complexes, as they harbor at the N-terminus components of the p400 complex and at the C-terminus members or recruitment factors of the PRC2 complex. However, some of these fusions do not arise exclusively in ESS, but have also been observed in other human sarcomas such as ossifying sarcoma of the heart or ossifying fibromyxoid tumor (OFMT) [303, 404]. This suggests that despite the molecular diversity of the individual sarcoma types, the malign degeneration of these cells might occur due to a possible common epigenetic pathway, involving the p400 and PRC2 complexes. There are various possibilities of how sarcoma-specific fusion proteins can contribute to the development of human sarcomas. Firstly, acetylation of H2A.Z and/or methylation of H3K27 at target sites can be disrupted or promoted in the presence of fusion proteins. Secondly, acetylation of H2A.Z may arise at H3K27me3-targeted PRC2 sites or methylation of H3K27 at genomic H2A.Z-targeted p400 sites. Finally, not only acetylation of H2A.Z, but also its chromatin deposition/evicition can be affected. Altogether, sarcoma-specific fusion proteins could deregulate expression of specific target genes during mesenchymal differentiation processes via epigenetic mechanisms, thereby changing the transcriptional program of these cells that could significantly contribute to cancer pathology.

In consideration of our results, it is conceivable that JAZF1-containing fusion proteins lead to changes in ribosomal gene expression and thus, promoting cell proliferation and inhibition of apoptosis as indicated by the study of Li et al. [405]. From a structural point of view, fusion proteins with JAZF1 should have the continuing ability to interact with TAK1, as the TAK1 interaction domain is still present in the fusions [295] (see Figure 41). However, the C-terminal part of JAZF1 is missing in the fusion proteins, which might be important for JAZF1's localization into nucleoli as demonstrated by IF analyses (Figure 21). Thus, it would be also very interesting to evaluate whether JAZF1-containing fusion proteins are still able to localize to the nucleolus. Moreover, it would be also necessary to investigate which domain of JAZF1 is important for its binding to TIP60. Unfortunately, all attempts to identify JAZF1's domain responsible for its interaction with TIP60 failed. Nevertheless, the recent study by Piunti et al. has been shown that the JAZF1-SUZ12 fusion is still able to associate with TIP60 [306], thereby corroborating the theory of JAZF1-containing fusion proteins might lead to a deregulation of the acetylation of H2A.Z at specific sites. However, these conclusions are currently only speculations, hence further research is required to unravel the biological relevance and consequence of sarcoma-specific fusion proteins. But how can future research contribute to the fundamental understanding of the molecular mechanism of sarcoma-specific fusion proteins to develop appropriate treatments for better outcomes for people with this disease? First of all, basic research and pre-clinical studies are quite challenging due to not readily available sarcoma cell lines [406]. Therefore, common human cell lines could be used to generate cells stably expressing fusion proteins of interest. These cells can serve for both immunoprecipitation (IP) and MS experiments to verify whether fusion proteins actually act as spatial bridging factors between the p400 and PRC2 complexes. To evaluate the influence of fusion proteins on chromatin, ChIP-seq experiments can be performed. On the one hand, the precise genomic localization of the fusion proteins can be determined and on the other hand, H2A.Z, H2A.Zac and H3K27me3 levels can be traced by another ChIP-seq approach that allows the determination of whether fusion proteins lead to changes in epigenetic profiles. Moreover, resulting alterations in global gene expression levels can be analysed by RNA-seq. Together, comparing MS-IP, ChIP-seq and RNA-seq datasets can uncover the underlying epigenetic mechanism by which sarcoma-specific fusion proteins might contribute to the development of human sarcomas. As an interesting therapeutic approach, cells showing high levels of H3K27me3 could be treated with the pharmacological reagent 3-Deazaneplanocin A (DZNep), an inhibitor of EZH2 protein expression [407], to block an aberrant methylation of PRC2 targets. EZH2 is the enzymatic active component of

the PRC2 complex [408], therefore, treating cells with DZNep should lead to reduced trimethylation of lysine 27 on histone H3. Furthermore, if cells exhibit increased H2A.Zac levels, they could be treated with a specific TIP60 inhibitor such as NU9056 to repress its enzymatic activity. After treatment, expression of certain genes could be validated by RT-qPCR experiments. These initial tests could provide a basis for larger studies with respect to develop potential therapeutics for fusion-based human sarcomas as well as acute leukemia, since several studies have identified similar chromosomal translocations in acute leukemia patients [409, 410], indicating that fusion proteins might lead to a common epigenetic mechanism frequently found in cancer.

4.5 Summary

Since we identified JAZF1 as a novel member of an MBTD1-containing, but ANP32E-excluding p400 sub-complex that associates with the histoneacetyltransferase TIP60 (Figure 42), I aimed in the present study to unravel the yet unexplored chromatin functions of JAZF1, especially with regard to the role JAZF1 might play within the H2A.Z-specific p400 chaperone/remodelling complex. First data hint towards a role of JAZF1 in the regulation of DSB repair (Figure 42), as it has already been shown for other p400 complex components, but the underlying molecular mechanism by which JAZF1 could influence DNA damage repair processes remains so far unclear. Overall, we identified JAZF1 as a proposed chromatin modulator that orchestrates acetylation of the histone variant H2A.Z via recruiting the enzymatic active TIP60-containing p400 complex to regulatory enhancer regions within introns, thereby controlling expression of target genes with several of them involved not only in DNA damage repair, but also in ribosome biogenesis (Figure 42). Altogether, this study contributes to a better understanding of the largely unknown functions of JAZF1 and may thus provide a starting point for future research to clarify its putative role in the development of diseases such as cancer (Figure 42).
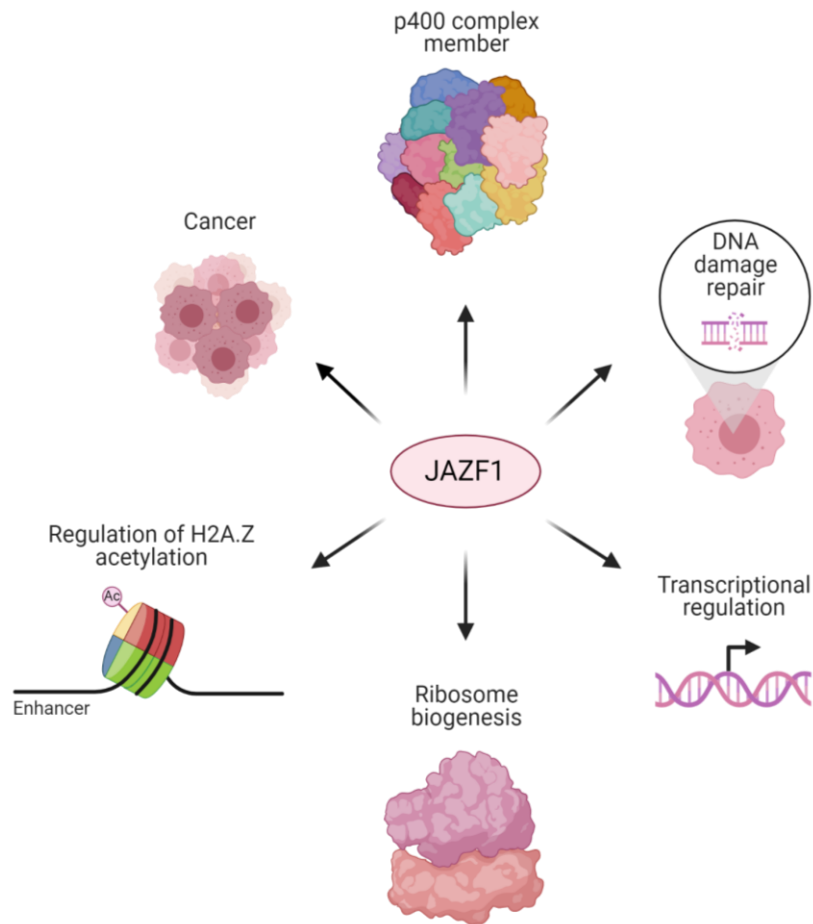
Figure 42: Summary of JAZF1's partially known and novel chromatin-associated functions. JAZF1, as a new member of an H2A.Z-specific p400 chaperone/remodelling sub-complex, is involved in several chromatin-related processes including DNA damage repair, transcriptional regulation of many genes with several of them involved in ribosome biogenesis, regulation of H2A.Z acetylation at regulatory regions and cancer such as human sarcomas. Figure created with BioRender.com.

ABBREVIATIONS

ac	Acetyl
ACTL6A	Actin-like protein 6A
ANP32E	Acidic leucine-rich nuclear phosphoprotein 32 family member E
APS	Ammonium persulfate
ATM	Ataxia telangiectasia mutated
ATP	Adenosine triphosphate
ATR	Ataxia telangiectasia and rad3 related
ATRX	Alpha-thalassemia/mental retardation syndrome X-linked protein
Bbd	Barr body deficient
BER	Base excision repair
BET	Bromo- and extra-terminal
BIR	Baculovirus inhibitor of apoptosis protein repeat
BLAST	Basic Local Alignment Search Tool
bp	Base pair
BP	Biological pathway
BRCA1	Breast cancer type 1 susceptibility protein
BRCT	BRCA1 C-terminus
BRD	Bromodomain
BRD8	Bromodomain-containing protein 8
BSA	Bovine serum albumin
CAF-1	Chromatin assembly complex 1
CB	Cajal body
CC	Cellular compartment
cDNA	Complementary DNA
CHD	Chromodomain helicase DNA-binding protein
ChIP	Chromatin immunoprecipitation
CpG	Cytosine-phosphate-guanine
Ct	Cycle treshold
DAPI	4',6-diamidino-2-phenylindole
DAXX	Death domain-associated protein
DD	Destabilization domain
ddH$_2$O	Double-distilled water
DDR	DNA damage response
diffH2A.Zac	Differentially acetylated H2A.Z ChIP-seq sites
DNA	Deoxyribonucleic acid
DNA-PK	DNA-dependent protein kinase
dNTP	Deoxynucleotide
DMAP1	DNA methyltransferase 1-associated protein 1

DMEM	Dulbecco's modified eagle medium
DMSO	Dimethylsulfoxide
DR1	Direct repeat DNA-element
DSB	DNA double-strand break
DZNep	3-Deazaneplanocin A
EDTA	Ethylenediaminetetraacetic acid
eGFP	Enhanced green fluorescent protein
EPC1	Enhancer of polycomb homolog 1
EP400	E1A binding protein p400
ER	Estradiol receptor
ESS	Endometrial stromal sarcoma
ETS	E26 transformation-specific
EZH2	Enhancer of zeste homolog 2
FACT	Facilitates chromatin transcription
FBS	Fetal bovine serum
FDR	False discovery rate
FSC	Forward scatter
gb	Gene body
GEO	NCBI Gene Expression Omnibus
GO	Gene Ontology
GREAT	Genomic Regions Enrichment of Annotations Tool
GSEA	Gene Set Enrichment Analysis
G1	Gap 1
G2	Gap 2
HAT	Histone acetyltransferase
HDAC	Histone deacetylase
hEnSC	Human endometrial stromal cell
HEPES	2-[4-(2-hydroxyethyl)piperazin-1-yl]ethanesulfonic acid
HFD	Histone fold domain
hg19	Human genome assembly GRCh37
HIRA	Histone regulatory homolog A
HK	HeLa Kyoto
HP1	Heterochromatin protein 1
HPRT1	Hypoxanthine Phosphoribosyltransferase 1
HR	Homologous recombination
HRP	Horseradish peroxidase
IB	Immunoblotting
IF	Immunofluorescence
IGV	Integrative Genomics Viewer
INO80	Inositol-requiring 80
IP	Immunoprecipitation
ISWI	Imitation switch

JAZF1	Juxtaposed with another zinc finger 1
JMJD2	Jumonji domain-containing 2
KAT	Lysine acetyltransferase
kb	Kilo base
kDa	Kilo dalton
KDAC	Lysine deacetylase
KDM	Lysine demethylase
KEGG	Kyoto Encyclopedia of Genes and Genomes
KMT	Lysine methyltransferase
LacI	Lac-repressor
LacO	Lac-operator
LB	Lysogeny broth
lncRNA	Long noncoding RNA
LSM7	U6 snRNA-associated Sm-like protein LSm7
M	Mitosis
mAb	Monoclonal antibody
MBT	Malignant brain tumor
MBTD1	MBT domain protein 1
me	Methyl
MEAF6	MYST/Esa1 associated factor 6
MeCP2	Methyl-CpG-binding protein 2
MeOH	Methanol
MIER1	Mesoderm induction early response 1
MMP12	Matrix metallopeptidase 12
Morf	Monocytic leukemia zinc-finger protein-related factor
mRNA	Messenger RNA
MS	Mass spectrometry
N	Normality or equivalent concentration
NCBI	National Center for Biotechnology Information
NCP	Nucleosome core particle
ncRNA	Non-coding RNA
NDR	Nucleosome-depleted region
NES	Normalized enrichment score
NGS	Next generation sequencing
NHEJ	Non-homologous end joining
NoLS	Nucleolar localization signal
NuA4	Nucleosome acetyltransferase of histone H4
OFMT	Ossifying fibromyxoid tumor
ON	Over night
pAb	Polyclonal antibody
PAGE	Polyacrylamide gel electrophoresis
PARS2	Prolyl-tRNA synthetase

ABBREVIATIONS

PBS	Phosphate buffered saline
PCA	Principle Component Analysis
PCR	Polymerase chain reaction
PHD	Plant homeodomain
PI	Propidium iodide
PRC2	Polycomb repressive complex 2
PWWP	Pro-trp-trp-pro
PWWP2A	PWWP domain-containing protein 2A
PTM	Posttranslational modification
P/S	Penicillin/streptomycin
p400	p400/NuA4/Tip60
q	Quantitative
RBMS1	RNA binding motif single stranded interacting protein 1
RIN	RNA integrity number
RNA	Ribonucleic acid
RNAi	RNA interference
RPL11	Ribosomal protein L11
rpm	Rounds per minute
rRNA	Ribosomal RNA
RT	Room temperature
RTCA	Real-Time Cell Analyzer
RT-qPCR	Reverse transcription quantitative PCR
RUVBL1	RuvB-like 1
RUVBL2	RuvB-like 2
S	Synthesis phase
Sas2	Something about silencing protein 2
SD	Standard deviation
SDS	Sodium dodecyl sulfate
seq	Sequencing
SILAC	Stable isotope labeling by amino acids in cell culture
siNTC	Non-target control siRNA
siJAZF1	JAZF1-specific siRNA
siLuci	Luciferase-specific siRNA
siTIP60	TIP60-specific siRNA
siRNA	Small interfering RNA
snoRNA	Small nucleolar ribonucleic acid
snoRNP	Small nucleolar ribonuclear protein
SNP	Single nucleotide polymorphism
SRCAP	Snf2 related CREBBP activator protein
SSC	Sideward scatter
SWI/SNF	Switch/sucrose non-fermentable
T	Tween20

TAE	Tris-acetate-EDTA
TCA	Trichloroacetic acid
TE	Tris-EDTA
TF	Transcription factor
TID	TR4 interacting domain
TIP60	TAT-interactive protein 60 kDa
TRRAP	Transformation/transcription domain-associated protein
TSS	Transcription start site
T2DM	Type 2 diabetes mellitus
UCSC	University of California Santa Cruz
UV	Ultraviolet
wt	Wild type
Ybf2/Sas3	Something about silencing protein 3
YEATS4	YEATS domain-containing protein 4
YL1/VPS72	Vacuolar protein sorting-associated protein 72 homolog
ZnF	Zinc finger
α	Alpha
-	Non-transfected
4-OHT	4-hydroxytamoxifen
5mC	5-methylcytosine
53BP1	p53-binding protein

REFERENCES

[1] Avery, O.T., Macleod, C.M., McCarty, M. (1944). Studies on the chemical nature of the substance inducing transformation of pneumococcal types Induction of transformation by a desoxyribonucleic acid fraction isolated from pneumococcus type iii, *The Journal of experimental medicine*, Vol. 79, No. 2, 137–158, doi: 10.1084/jem.79.2.137.

[2] Cartenì, F., Bonanomi, G., Giannino, F., Incerti, G., Vincenot, C.E., Chiusano, M.L., Mazzoleni, S. (2016). Self-dna inhibitory effects: Underlying mechanisms and ecological implications, *Plant signaling & behavior*, Vol. 11, No. 4, e1158381, doi: 10.1080/15592324.2016.1158381.

[3] Travers, A., Muskhelishvili, G. (2015). Dna structure and function, *The FEBS journal*, Vol. 282, No. 12, 2279–2295, doi: 10.1111/febs.13307.

[4] WATSON, J.D., CRICK, F.H. (1953). Molecular structure of nucleic acids; a structure for deoxyribose nucleic acid, *Nature*, Vol. 171, No. 4356, 737–738, doi: 10.1038/171737a0.

[5] Campbell, N.A., Reece, J.B., Urry, L.A., Cain, M.L., Wasserman, S.A., Minorsky, P.V., Jackson, R.B. (2016). *Campbell Biologie*, Pearson, Hallbergmoos/Germany.

[6] Saenger, W. (1984). *Principles of nucleic acid structure*, Springer, New York.

[7] Bodmer, W. (2013). Human Genome Project, *Brenner's Encyclopedia of Genetics*, Elsevier, 552–554, doi: 10.1016/B978-0-12-374984-0.00746-4.

[8] Venter, J.C., Adams, M.D., Myers, E.W., Li, P.W., Mural, R.J., Sutton, G.G., Smith, H.O., Yandell, M., Evans, C.A., Holt, R.A., Gocayne, J.D., Amanatides, P., Ballew, R.M., Huson, D.H., Wortman, J.R., Zhang, Q., Kodira, C.D., Zheng, X.H., Chen, L., Skupski, M., Subramanian, G., Thomas, P.D., Zhang, J., Gabor Miklos, G.L., Nelson, C., Broder, S., Clark, A.G., Nadeau, J., McKusick, V.A., Zinder, N., Levine, A.J., Roberts, R.J., Simon, M., Slayman, C., Hunkapiller, M., Bolanos, R., Delcher, A., Dew, I., Fasulo, D., Flanigan, M., Florea, L., Halpern, A., Hannenhalli, S., Kravitz, S., Levy, S., Mobarry, C., Reinert, K., Remington, K., Abu-Threideh, J., Beasley, E., Biddick, K., Bonazzi, V., Brandon, R., Cargill, M., Chandramouliswaran, I., Charlab, R., Chaturvedi, K., Deng, Z., Di Francesco, V., Dunn, P., Eilbeck, K., Evangelista, C., Gabrielian, A.E., Gan, W., Ge, W., Gong, F., Gu, Z., Guan, P., Heiman, T.J., Higgins, M.E., Ji, R.R., Ke, Z., Ketchum, K.A., Lai, Z., Lei, Y., Li, Z., Li, J., Liang, Y., Lin, X., Lu, F., Merkulov, G.V., Milshina, N., Moore, H.M., Naik, A.K., Narayan, V.A., Neelam, B., Nusskern, D., Rusch, D.B., Salzberg, S., Shao, W., Shue, B., Sun, J., Wang, Z., Wang, A., Wang, X., Wang, J., Wei, M., Wides, R., Xiao, C., Yan, C., Yao, A., Ye, J., Zhan, M., Zhang, W., Zhang, H., Zhao, Q., Zheng, L., Zhong, F., Zhong, W., Zhu, S., Zhao, S., Gilbert, D., Baumhueter, S., Spier, G., Carter, C., Cravchik, A., Woodage, T., Ali, F., An, H., Awe, A., Baldwin, D., Baden, H., Barnstead, M., Barrow, I., Beeson, K., Busam, D., Carver, A., Center, A., Cheng, M.L., Curry, L., Danaher, S., Davenport, L., Desilets, R., Dietz, S.,

Dodson, K., Doup, L., Ferriera, S., Garg, N., Gluecksmann, A., Hart, B., Haynes, J., Haynes, C., Heiner, C., Hladun, S., Hostin, D., Houck, J., Howland, T., Ibegwam, C., Johnson, J., Kalush, F., Kline, L., Koduru, S., Love, A., Mann, F., May, D., McCawley, S., McIntosh, T., McMullen, I., Moy, M., Moy, L., Murphy, B., Nelson, K., Pfannkoch, C., Pratts, E., Puri, V., Qureshi, H., Reardon, M., Rodriguez, R., Rogers, Y.H., Romblad, D., Ruhfel, B., Scott, R., Sitter, C., Smallwood, M., Stewart, E., Strong, R., Suh, E., Thomas, R., Tint, N.N., Tse, S., Vech, C., Wang, G., Wetter, J., Williams, S., Williams, M., Windsor, S., Winn-Deen, E., Wolfe, K., Zaveri, J., Zaveri, K., Abril, J.F., Guigó, R., Campbell, M.J., Sjolander, K.V., Karlak, B., Kejariwal, A., Mi, H., Lazareva, B., Hatton, T., Narechania, A., Diemer, K., Muruganujan, A., Guo, N., Sato, S., Bafna, V., Istrail, S., Lippert, R., Schwartz, R., Walenz, B., Yooseph, S., Allen, D., Basu, A., Baxendale, J., Blick, L., Caminha, M., Carnes-Stine, J., Caulk, P., Chiang, Y.H., Coyne, M., Dahlke, C., Mays, A., Dombroski, M., Donnelly, M., Ely, D., Esparham, S., Fosler, C., Gire, H., Glanowski, S., Glasser, K., Glodek, A., Gorokhov, M., Graham, K., Gropman, B., Harris, M., Heil, J., Henderson, S., Hoover, J., Jennings, D., Jordan, C., Jordan, J., Kasha, J., Kagan, L., Kraft, C., Levitsky, A., Lewis, M., Liu, X., Lopez, J., Ma, D., Majoros, W., McDaniel, J., Murphy, S., Newman, M., Nguyen, T., Nguyen, N., Nodell, M., Pan, S., Peck, J., Peterson, M., Rowe, W., Sanders, R., Scott, J., Simpson, M., Smith, T., Sprague, A., Stockwell, T., Turner, R., Venter, E., Wang, M., Wen, M., Wu, D., Wu, M., Xia, A., Zandieh, A., Zhu, X. (2001). The sequence of the human genome, *Science (New York, N.Y.)*, Vol. 291, No. 5507, 1304–1351, doi: 10.1126/science.1058040.

[9] Lander, E.S., Linton, L.M., Birren, B., Nusbaum, C., Zody, M.C., Baldwin, J., Devon, K., Dewar, K., Doyle, M., FitzHugh, W., Funke, R., Gage, D., Harris, K., Heaford, A., Howland, J., Kann, L., Lehoczky, J., LeVine, R., McEwan, P., McKernan, K., Meldrim, J., Mesirov, J.P., Miranda, C., Morris, W., Naylor, J., Raymond, C., Rosetti, M., Santos, R., Sheridan, A., Sougnez, C., Stange-Thomann, Y., Stojanovic, N., Subramanian, A., Wyman, D., Rogers, J., Sulston, J., Ainscough, R., Beck, S., Bentley, D., Burton, J., Clee, C., Carter, N., Coulson, A., Deadman, R., Deloukas, P., Dunham, A., Dunham, I., Durbin, R., French, L., Grafham, D., Gregory, S., Hubbard, T., Humphray, S., Hunt, A., Jones, M., Lloyd, C., McMurray, A., Matthews, L., Mercer, S., Milne, S., Mullikin, J.C., Mungall, A., Plumb, R., Ross, M., Shownkeen, R., Sims, S., Waterston, R.H., Wilson, R.K., Hillier, L.W., McPherson, J.D., Marra, M.A., Mardis, E.R., Fulton, L.A., Chinwalla, A.T., Pepin, K.H., Gish, W.R., Chissoe, S.L., Wendl, M.C., Delehaunty, K.D., Miner, T.L., Delehaunty, A., Kramer, J.B., Cook, L.L., Fulton, R.S., Johnson, D.L., Minx, P.J., Clifton, S.W., Hawkins, T., Branscomb, E., Predki, P., Richardson, P., Wenning, S., Slezak, T., Doggett, N., Cheng, J.F., Olsen, A., Lucas, S., Elkin, C., Uberbacher, E., Frazier, M., Gibbs, R.A., Muzny, D.M., Scherer, S.E., Bouck, J.B., Sodergren, E.J., Worley, K.C., Rives, C.M., Gorrell, J.H., Metzker, M.L., Naylor, S.L., Kucherlapati, R.S., Nelson, D.L., Weinstock, G.M., Sakaki, Y., Fujiyama, A., Hattori, M., Yada, T., Toyoda, A., Itoh, T., Kawagoe, C., Watanabe, H., Totoki, Y., Taylor, T., Weissenbach, J., Heilig, R., Saurin, W., Artiguenave, F., Brottier, P., Bruls, T., Pelletier, E., Robert, C., Wincker, P., Smith, D.R., Doucette-Stamm, L., Rubenfield, M., Weinstock, K., Lee, H.M., Dubois, J., Rosenthal, A., Platzer, M., Nyakatura, G., Taudien, S., Rump, A., Yang, H., Yu, J., Wang, J., Huang, G., Gu, J., Hood, L., Rowen, L., Madan, A., Qin, S., Davis, R.W., Federspiel, N.A.,

REFERENCES

Abola, A.P., Proctor, M.J., Myers, R.M., Schmutz, J., Dickson, M., Grimwood, J., Cox, D.R., Olson, M.V., Kaul, R., Shimizu, N., Kawasaki, K., Minoshima, S., Evans, G.A., Athanasiou, M., Schultz, R., Roe, B.A., Chen, F., Pan, H., Ramser, J., Lehrach, H., Reinhardt, R., McCombie, W.R., La Bastide, M. de, Dedhia, N., Blöcker, H., Hornischer, K., Nordsiek, G., Agarwala, R., Aravind, L., Bailey, J.A., Bateman, A., Batzoglou, S., Birney, E., Bork, P., Brown, D.G., Burge, C.B., Cerutti, L., Chen, H.C., Church, D., Clamp, M., Copley, R.R., Doerks, T., Eddy, S.R., Eichler, E.E., Furey, T.S., Galagan, J., Gilbert, J.G., Harmon, C., Hayashizaki, Y., Haussler, D., Hermjakob, H., Hokamp, K., Jang, W., Johnson, L.S., Jones, T.A., Kasif, S., Kaspryzk, A., Kennedy, S., Kent, W.J., Kitts, P., Koonin, E.V., Korf, I., Kulp, D., Lancet, D., Lowe, T.M., McLysaght, A., Mikkelsen, T., Moran, J.V., Mulder, N., Pollara, V.J., Ponting, C.P., Schuler, G., Schultz, J., Slater, G., Smit, A.F., Stupka, E., Szustakowski, J., Thierry-Mieg, D., Thierry-Mieg, J., Wagner, L., Wallis, J., Wheeler, R., Williams, A., Wolf, Y.I., Wolfe, K.H., Yang, S.P., Yeh, R.F., Collins, F., Guyer, M.S., Peterson, J., Felsenfeld, A., Wetterstrand, K.A., Patrinos, A., Morgan, M.J., Jong, P. de, Catanese, J.J., Osoegawa, K., Shizuya, H., Choi, S., Chen, Y.J. (2001). Initial sequencing and analysis of the human genome, *Nature*, Vol. 409, No. 6822, 860–921, doi: 10.1038/35057062.

[10] Blanco, A., Blanco, G. (2017). Nucleic Acids, *Medical Biochemistry*, Elsevier, 121–140, doi: 10.1016/B978-0-12-803550-4.00006-9.

[11] *Mcgraw-hill encyclopedia of science & technology: An international reference work in twenty volumes including an index* (2007), McGraw-Hill, New York, NY.

[12] Conklin, E.G. (1912). Cell size and nuclear size, *Journal of Experimental Zoology*, Vol. 12, No. 1, 1–98, doi: 10.1002/jez.1400120102.

[13] Alberts, B., Johnson, A., Lewis, J., Raff, M., Roberts, K., Walter, P. (2002). *Molecular biology of the cell*, Garland Science Taylor & Francis Group, New York, NY.

[14] Flemming, W. (1882). *Zellsubstanz, Kern und Zelltheilung*, F.C.W. Vogel, Leipzig, doi: 10.5962/bhl.title.168645.

[15] Paweletz, N. (2001). Walther flemming: Pioneer of mitosis research, *Nature reviews. Molecular cell biology*, Vol. 2, No. 1, 72–75, doi: 10.1038/35048077.

[16] Olins, A.L., Olins, D.E. (1974). Spheroid Chromatin Units (ngr Bodies), *Science (New York, N.Y.)*, Vol. 183, No. 4122, 330–332, doi: 10.1126/science.183.4122.330.

[17] Woodcock, C., Safer, J.P., Stanchfield, J.E. (1976). Structural repeating units in chromatin, *Experimental Cell Research*, Vol. 97, No. 1, 101–110, doi: 10.1016/0014-4827(76)90659-5.

[18] Albrecht Kossel. Über die chemische Beschaffenheit des Zellkerns, *Munchen Med Wochenschrift*, Vol. 1911.

[19] Gross, D.S., Chowdhary, S., Anandhakumar, J., Kainth, A.S. (2015). Chromatin, *Current biology CB*, Vol. 25, No. 24, R1158-63, doi: 10.1016/j.cub.2015.10.059.

[20] Kornberg, R.D. (1974). Chromatin structure: A repeating unit of histones and dna, *Science (New York, N.Y.)*, Vol. 184, No. 4139, 868–871, doi: 10.1126/science.184.4139.868.

[21] Oudet, P., Gross-Bellard, M., Chambon, P. (1975). Electron microscopic and biochemical evidence that chromatin structure is a repeating unit, *Cell*, Vol. 4, No. 4, 281–300, doi: 10.1016/0092-8674(75)90149-x.

[22] Luger, K., Mäder, A.W., Richmond, R.K., Sargent, D.F., Richmond, T.J. (1997). Crystal structure of the nucleosome core particle at 2.8 a resolution, *Nature*, Vol. 389, No. 6648, 251–260, doi: 10.1038/38444.

[23] Richmond, T.J., Davey, C.A. (2003). The structure of dna in the nucleosome core, *Nature*, Vol. 423, No. 6936, 145–150, doi: 10.1038/nature01595.

[24] Hjelm, R.P., Kneale, G.G., Suau, P., Baldwin, J.P., Bradbury, E.M., Ibel, K. (1977). Small angle neutron scattering studies of chromatin subunits in solution, *Cell*, Vol. 10, No. 1, 139–151, doi: 10.1016/0092-8674(77)90148-9.

[25] Richmond, T.J., Finch, J.T., Rushton, B., Rhodes, D., Klug, A. (1984). Structure of the nucleosome core particle at 7 a resolution, *Nature*, Vol. 311, No. 5986, 532–537, doi: 10.1038/311532a0.

[26] Wakamori, M., Fujii, Y., Suka, N., Shirouzu, M., Sakamoto, K., Umehara, T., Yokoyama, S. (2015). Intra- and inter-nucleosomal interactions of the histone H4 tail revealed with a human nucleosome core particle with genetically-incorporated H4 tetra-acetylation, *Scientific reports*, Vol. 5, No. 1, doi: 10.1038/srep17204.

[27] van Holde, K.E., Sahasrabuddhe, C.G., Shaw, B.R. (1974). A model for particulate structure in chromatin, *Nucleic acids research*, Vol. 1, No. 11, 1579–1586, doi: 10.1093/nar/1.11.1579.

[28] Davey, C.A., Sargent, D.F., Luger, K., Maeder, A.W., Richmond, T.J. (2002). Solvent Mediated Interactions in the Structure of the Nucleosome Core Particle at 1.9Å Resolution, *Journal of Molecular Biology*, Vol. 319, No. 5, 1097–1113, doi: 10.1016/S0022-2836(02)00386-8.

[29] Andrews, A.J., Luger, K. (2011). Nucleosome structure(s) and stability: Variations on a theme, *Annual review of biophysics*, Vol. 40, 99–117, doi: 10.1146/annurev-biophys-042910-155329.

[30] Ramaswamy, A., Ioshikhes, I. (2013). Dynamics of modeled oligonucleosomes and the role of histone variant proteins in nucleosome organization, *Advances in protein chemistry and structural biology*, Vol. 90, 119–149, doi: 10.1016/B978-0-12-410523-2.00004-3.

REFERENCES

[31] Bendandi, A., Patelli, A.S., Diaspro, A., Rocchia, W. (2020). The role of histone tails in nucleosome stability: An electrostatic perspective, *Computational and structural biotechnology journal*, Vol. 18, 2799–2809, doi: 10.1016/j.csbj.2020.09.034.

[32] Bowman, G.D., Poirier, M.G. (2015). Post-translational modifications of histones that influence nucleosome dynamics, *Chemical reviews*, Vol. 115, No. 6, 2274–2295, doi: 10.1021/cr500350x.

[33] Muthurajan, U.M., Bao, Y., Forsberg, L.J., Edayathumangalam, R.S., Dyer, P.N., White, C.L., Luger, K. (2004). Crystal structures of histone sin mutant nucleosomes reveal altered protein-dna interactions, *The EMBO journal*, Vol. 23, No. 2, 260–271, doi: 10.1038/sj.emboj.7600046.

[34] Erler, J., Zhang, R., Petridis, L., Cheng, X., Smith, J.C., Langowski, J. (2014). The role of histone tails in the nucleosome: A computational study, *Biophysical journal*, Vol. 107, No. 12, 2911–2922, doi: 10.1016/j.bpj.2014.10.065.

[35] Biswas, M., Voltz, K., Smith, J.C., Langowski, J. (2011). Role of histone tails in structural stability of the nucleosome, *PLoS computational biology*, Vol. 7, No. 12, e1002279, doi: 10.1371/journal.pcbi.1002279.

[36] Luger, K., Dechassa, M.L., Tremethick, D.J. (2012). New insights into nucleosome and chromatin structure: An ordered state or a disordered affair?, *Nature reviews. Molecular cell biology*, Vol. 13, No. 7, 436–447, doi: 10.1038/nrm3382.

[37] Kalashnikova, A.A., Porter-Goff, M.E., Muthurajan, U.M., Luger, K., Hansen, J.C. (2013). The role of the nucleosome acidic patch in modulating higher order chromatin structure, *Journal of the Royal Society, Interface*, Vol. 10, No. 82, 20121022, doi: 10.1098/rsif.2012.1022.

[38] Pepenella, S., Murphy, K.J., Hayes, J.J. (2014). Intra- and inter-nucleosome interactions of the core histone tail domains in higher-order chromatin structure, *Chromosoma*, Vol. 123, 1-2, 3–13, doi: 10.1007/s00412-013-0435-8.

[39] Zhu, P., Li, G. (2016). Structural insights of nucleosome and the 30-nm chromatin fiber, *Current opinion in structural biology*, Vol. 36, 106–115, doi: 10.1016/j.sbi.2016.01.013.

[40] Allan, J., Harborne, N., Rau, D.C., Gould, H. (1982). Participation of core histone "tails" in the stabilization of the chromatin solenoid, *The Journal of cell biology*, Vol. 93, No. 2, 285–297, doi: 10.1083/jcb.93.2.285.

[41] Thoma, F., Koller, T., Klug, A. (1979). Involvement of histone h1 in the organization of the nucleosome and of the salt-dependent superstructures of chromatin, *The Journal of cell biology*, Vol. 83, 2 Pt 1, 403–427, doi: 10.1083/jcb.83.2.403.

[42] Bednar, J., Dimitrov, S. (2011). Chromatin under mechanical stress: From single 30 nm fibers to single nucleosomes, *The FEBS journal*, Vol. 278, No. 13, 2231–2243, doi: 10.1111/j.1742-4658.2011.08153.x.

REFERENCES

[43] Rippe, K., Mazurkiewicz, J., Kepper, N. (2008). Interactions of Histones with DNA: Nucleosome Assembly, Stability, Dynamics, and Higher Order Structure, In: Dias, R., Lindman, B. (eds.), *DNA Interactions with Polymers and Surfactants*, John Wiley & Sons, Inc, Hoboken, NJ, USA, 135–172, doi: 10.1002/9780470286364.ch6.

[44] McBryant, S.J., Adams, V.H., Hansen, J.C. (2006). Chromatin architectural proteins, *Chromosome research an international journal on the molecular, supramolecular and evolutionary aspects of chromosome biology*, Vol. 14, No. 1, 39–51, doi: 10.1007/s10577-006-1025-x.

[45] Hansen, J.C., Ausio, J., Stanik, V.H., van Holde, K.E. (1989). Homogeneous reconstituted oligonucleosomes, evidence for salt-dependent folding in the absence of histone h1, *Biochemistry*, Vol. 28, No. 23, 9129–9136, doi: 10.1021/bi00449a026.

[46] Hansen, J.C. (2002). Conformational dynamics of the chromatin fiber in solution: Determinants, mechanisms, and functions, *Annual review of biophysics and biomolecular structure*, Vol. 31, 361–392, doi: 10.1146/annurev.biophys.31.101101.140858.

[47] Szerlong, H.J., Hansen, J.C. (2011). Nucleosome distribution and linker dna: Connecting nuclear function to dynamic chromatin structure, *Biochemistry and cell biology = Biochimie et biologie cellulaire*, Vol. 89, No. 1, 24–34, doi: 10.1139/o10-139.

[48] Tremethick, D.J. (2007). Higher-order structures of chromatin: The elusive 30 nm fiber, *Cell*, Vol. 128, No. 4, 651–654, doi: 10.1016/j.cell.2007.02.008.

[49] Robinson, P.J.J., Rhodes, D. (2006). Structure of the '30 nm' chromatin fibre: A key role for the linker histone, *Current opinion in structural biology*, Vol. 16, No. 3, 336–343, doi: 10.1016/j.sbi.2006.05.007.

[50] McGhee, J.D., Rau, D.C., Charney, E., Felsenfeld, G. (1980). Orientation of the nucleosome within the higher order structure of chromatin, *Cell*, Vol. 22, No. 1, 87–96, doi: 10.1016/0092-8674(80)90157-9.

[51] Finch, J.T., Klug, A. (1976). Solenoidal model for superstructure in chromatin, *Proceedings of the National Academy of Sciences of the United States of America*, Vol. 73, No. 6, 1897–1901, doi: 10.1073/pnas.73.6.1897.

[52] Schalch, T., Duda, S., Sargent, D.F., Richmond, T.J. (2005). X-ray structure of a tetranucleosome and its implications for the chromatin fibre, *Nature*, Vol. 436, No. 7047, 138–141, doi: 10.1038/nature03686.

[53] Venkatesh, S., Workman, J.L. (2015). Histone exchange, chromatin structure and the regulation of transcription, *Nature reviews. Molecular cell biology*, Vol. 16, No. 3, 178–189, doi: 10.1038/nrm3941.

[54] Dillon, N. (2004). Heterochromatin structure and function, *Biology of the cell*, Vol. 96, No. 8, 631–637, doi: 10.1016/j.biolcel.2004.06.003.

REFERENCES

[55] Allis, C.D., Jenuwein, T. (2016). The molecular hallmarks of epigenetic control, *Nature reviews. Genetics*, Vol. 17, No. 8, 487–500, doi: 10.1038/nrg.2016.59.

[56] Trojer, P., Reinberg, D. (2007). Facultative heterochromatin: Is there a distinctive molecular signature?, *Molecular cell*, Vol. 28, No. 1, 1–13, doi: 10.1016/j.molcel.2007.09.011.

[57] Waddington, C.H. (2012). The epigenotype. 1942, *International journal of epidemiology*, Vol. 41, No. 1, 10–13, doi: 10.1093/ije/dyr184.

[58] Weinhold, B. (2006). Epigenetics: The science of change, *Environmental health perspectives*, Vol. 114, No. 3, A160-7, doi: 10.1289/ehp.114-a160.

[59] Bönisch, C., Nieratschker, S.M., Orfanos, N.K., Hake, S.B. (2008). Chromatin proteomics and epigenetic regulatory circuits, *Expert review of proteomics*, Vol. 5, No. 1, 105–119, doi: 10.1586/14789450.5.1.105.

[60] Bird, A.P. (1986). Cpg-rich islands and the function of dna methylation, *Nature*, Vol. 321, No. 6067, 209–213, doi: 10.1038/321209a0.

[61] Choy, M.-K., Movassagh, M., Goh, H.-G., Bennett, M.R., Down, T.A., Foo, R.S.Y. (2010). Genome-wide conserved consensus transcription factor binding motifs are hyper-methylated, *BMC genomics*, Vol. 11, 519, doi: 10.1186/1471-2164-11-519.

[62] Fuks, F. (2005). Dna methylation and histone modifications: Teaming up to silence genes, *Current opinion in genetics & development*, Vol. 15, No. 5, 490–495, doi: 10.1016/j.gde.2005.08.002.

[63] Handy, D.E., Castro, R., Loscalzo, J. (2011). Epigenetic modifications: Basic mechanisms and role in cardiovascular disease, *Circulation*, Vol. 123, No. 19, 2145–2156, doi: 10.1161/CIRCULATIONAHA.110.956839.

[64] Denis, H., Ndlovu, M.N., Fuks, F. (2011). Regulation of mammalian dna methyltransferases: A route to new mechanisms, *EMBO reports*, Vol. 12, No. 7, 647–656, doi: 10.1038/embor.2011.110.

[65] Okano, M., Bell, D.W., Haber, D.A., Li, E. (1999). DNA Methyltransferases Dnmt3a and Dnmt3b Are Essential for De Novo Methylation and Mammalian Development, *Cell*, Vol. 99, No. 3, 247–257, doi: 10.1016/s0092-8674(00)81656-6.

[66] Bestor, T.H., Ingram, V.M. (1983). Two dna methyltransferases from murine erythroleukemia cells: Purification, sequence specificity, and mode of interaction with dna, *Proceedings of the National Academy of Sciences of the United States of America*, Vol. 80, No. 18, 5559–5563, doi: 10.1073/pnas.80.18.5559.

[67] Bommarito, P.A., Fry, R.C. (2019). The Role of DNA Methylation in Gene Regulation, *Toxicoepigenetics*, Elsevier, 127–151, doi: 10.1016/B978-0-12-812433-8.00005-8.

[68] Neidhart, M. (2016). DNA Methylation – Introduction, *DNA Methylation and Complex Human Disease*, Elsevier, 1–8, doi: 10.1016/B978-0-12-420194-1.00001-4.

[69] Moore, L.D., Le, T., Fan, G. (2013). Dna methylation and its basic function, *Neuropsychopharmacology official publication of the American College of Neuropsychopharmacology*, Vol. 38, No. 1, 23–38, doi: 10.1038/npp.2012.112.

[70] Bochtler, M., Kolano, A., Xu, G.-L. (2017). Dna demethylation pathways: Additional players and regulators, *BioEssays news and reviews in molecular, cellular and developmental biology*, Vol. 39, No. 1, 1–13, doi: 10.1002/bies.201600178.

[71] L. Alcaraz-Estrada, S., Leija-Montoya, G., Serafín-Higuera, N., García, S., E. Millán-Testa, C., Sierra-Martínez, M., Blanco-Morales, M., Sandoval-Basilio, J. (2020). DNA Hydroxymethylation in the Regulation of Gene Expression in Human Solid Cancer, In: Budak, M., Yıldız, M. (eds.), *DNA Methylation Mechanism*, IntechOpen, doi: 10.5772/intechopen.92016.

[72] Godderis, L., Schouteden, C., Tabish, A., Poels, K., Hoet, P., Baccarelli, A.A., van Landuyt, K. (2015). Global methylation and hydroxymethylation in dna from blood and saliva in healthy volunteers, *BioMed research international*, Vol. 2015, 845041, doi: 10.1155/2015/845041.

[73] Shukla, A., Sehgal, M., Singh, T.R. (2015). Hydroxymethylation and its potential implication in dna repair system: A review and future perspectives, *Gene*, Vol. 564, No. 2, 109–118, doi: 10.1016/j.gene.2015.03.075.

[74] Valinluck, V., Tsai, H.-H., Rogstad, D.K., Burdzy, A., Bird, A., Sowers, L.C. (2004). Oxidative damage to methyl-cpg sequences inhibits the binding of the methyl-cpg binding domain (mbd) of methyl-cpg binding protein 2 (mecp2), *Nucleic acids research*, Vol. 32, No. 14, 4100–4108, doi: 10.1093/nar/gkh739.

[75] Robertson, K.D. (2005). Dna methylation and human disease, *Nature reviews. Genetics*, Vol. 6, No. 8, 597–610, doi: 10.1038/nrg1655.

[76] Frías-Lasserre, D., Villagra, C.A. (2017). The importance of ncrnas as epigenetic mechanisms in phenotypic variation and organic evolution, *Frontiers in microbiology*, Vol. 8, 2483, doi: 10.3389/fmicb.2017.02483.

[77] Cao, J. (2014). The functional role of long non-coding rnas and epigenetics, *Biological procedures online*, Vol. 16, 11, doi: 10.1186/1480-9222-16-11.

[78] Böhmdorfer, G., Wierzbicki, A.T. (2015). Control of chromatin structure by long noncoding rna, *Trends in cell biology*, Vol. 25, No. 10, 623–632, doi: 10.1016/j.tcb.2015.07.002.

[79] Teppan, J., Barth, D.A., Prinz, F., Jonas, K., Pichler, M., Klec, C. (2020). Involvement of long non-coding rnas (lncrnas) in tumor angiogenesis, *Non-coding RNA*, Vol. 6, No. 4, doi: 10.3390/ncrna6040042.

[80] Castel, S.E., Martienssen, R.A. (2013). Rna interference in the nucleus: Roles for small rnas in transcription, epigenetics and beyond, *Nature reviews. Genetics*, Vol. 14, No. 2, 100–112, doi: 10.1038/nrg3355.

[81] Mercer, T.R., Dinger, M.E., Mattick, J.S. (2009). Long non-coding rnas: Insights into functions, *Nature reviews. Genetics*, Vol. 10, No. 3, 155–159, doi: 10.1038/nrg2521.

[82] Becker, P.B., Workman, J.L. (2013). Nucleosome remodeling and epigenetics, *Cold Spring Harbor perspectives in biology*, Vol. 5, No. 9, doi: 10.1101/cshperspect.a017905.

[83] Clapier, C.R., Iwasa, J., Cairns, B.R., Peterson, C.L. (2017). Mechanisms of action and regulation of atp-dependent chromatin-remodelling complexes, *Nature reviews. Molecular cell biology*, Vol. 18, No. 7, 407–422, doi: 10.1038/nrm.2017.26.

[84] Längst, G., Manelyte, L. (2015). Chromatin remodelers: From function to dysfunction, *Genes*, Vol. 6, No. 2, 299–324, doi: 10.3390/genes6020299.

[85] Clapier, C.R., Cairns, B.R. (2009). The biology of chromatin remodeling complexes, *Annual review of biochemistry*, Vol. 78, 273–304, doi: 10.1146/annurev.biochem.77.062706.153223.

[86] Eberharter, A., Becker, P.B. (2004). Atp-dependent nucleosome remodelling: Factors and functions, *Journal of cell science*, Vol. 117, Pt 17, 3707–3711, doi: 10.1242/jcs.01175.

[87] Wu, J.I. (2012). Diverse functions of atp-dependent chromatin remodeling complexes in development and cancer, *Acta biochimica et biophysica Sinica*, Vol. 44, No. 1, 54–69, doi: 10.1093/abbs/gmr099.

[88] Mayes, K., Qiu, Z., Alhazmi, A., Landry, J.W. (2014). Atp-dependent chromatin remodeling complexes as novel targets for cancer therapy, *Advances in cancer research*, Vol. 121, 183–233, doi: 10.1016/B978-0-12-800249-0.00005-6.

[89] Willhoft, O., Wigley, D.B. (2020). Ino80 and swr1 complexes: The non-identical twins of chromatin remodelling, *Current opinion in structural biology*, Vol. 61, 50–58, doi: 10.1016/j.sbi.2019.09.002.

[90] Bannister, A.J., Kouzarides, T. (2011). Regulation of chromatin by histone modifications, *Cell research*, Vol. 21, No. 3, 381–395, doi: 10.1038/cr.2011.22.

[91] Ng, M.K., Cheung, P. (2016). A brief histone in time: Understanding the combinatorial functions of histone ptms in the nucleosome context, *Biochemistry and cell biology = Biochimie et biologie cellulaire*, Vol. 94, No. 1, 33–42, doi: 10.1139/bcb-2015-0031.

[92] Xu, Y.-M., Du, J.-Y., Lau, A.T.Y. (2014). Posttranslational modifications of human histone h3: An update, *Proteomics*, Vol. 14, 17-18, 2047–2060, doi: 10.1002/pmic.201300435.

REFERENCES

[93] Di Zhang, Tang, Z., Huang, H., Zhou, G., Cui, C., Weng, Y., Liu, W., Kim, S., Lee, S., Perez-Neut, M., Ding, J., Czyz, D., Hu, R., Ye, Z., He, M., Zheng, Y.G., Shuman, H.A., Dai, L., Ren, B., Roeder, R.G., Becker, L., Zhao, Y. (2019). Metabolic regulation of gene expression by histone lactylation, *Nature*, Vol. 574, No. 7779, 575–580, doi: 10.1038/s41586-019-1678-1.

[94] Olsen, C.A. (2012). Expansion of the lysine acylation landscape, *Angewandte Chemie (International ed. in English)*, Vol. 51, No. 16, 3755–3756, doi: 10.1002/anie.201200316.

[95] Wang, M., Mok, M.W., Harper, H., Lee, W.H., Min, J., Knapp, S., Oppermann, U., Marsden, B., Schapira, M. (2010). Structural genomics of histone tail recognition, *Bioinformatics (Oxford, England)*, Vol. 26, No. 20, 2629–2630, doi: 10.1093/bioinformatics/btq491.

[96] Zhang, T., Cooper, S., Brockdorff, N. (2015). The interplay of histone modifications - writers that read, *EMBO reports*, Vol. 16, No. 11, 1467–1481, doi: 10.15252/embr.201540945.

[97] Strahl, B.D., Allis, C.D. (2000). The language of covalent histone modifications, *Nature*, Vol. 403, No. 6765, 41–45, doi: 10.1038/47412.

[98] Orlandi, K., McKnight, J. (2020). Bulky histone modifications may have an oversized role in nucleosome dynamics, *BioEssays news and reviews in molecular, cellular and developmental biology*, Vol. 42, No. 1, e1900217, doi: 10.1002/bies.201900217.

[99] Avvakumov, N., Nourani, A., Côté, J. (2011). Histone chaperones: Modulators of chromatin marks, *Molecular cell*, Vol. 41, No. 5, 502–514, doi: 10.1016/j.molcel.2011.02.013.

[100] Murawska, M., Brehm, A. (2011). Chd chromatin remodelers and the transcription cycle, *Transcription*, Vol. 2, No. 6, 244–253, doi: 10.4161/trns.2.6.17840.

[101] Petty, E., Pillus, L. (2013). Balancing chromatin remodeling and histone modifications in transcription, *Trends in genetics TIG*, Vol. 29, No. 11, 621–629, doi: 10.1016/j.tig.2013.06.006.

[102] Krajewski, W.A. (2020). "Direct" and "indirect" effects of histone modifications: Modulation of sterical bulk as a novel source of functionality, *BioEssays news and reviews in molecular, cellular and developmental biology*, Vol. 42, No. 1, e1900136, doi: 10.1002/bies.201900136.

[103] Simon, M., North, J.A., Shimko, J.C., Forties, R.A., Ferdinand, M.B., Manohar, M., Zhang, M., Fishel, R., Ottesen, J.J., Poirier, M.G. (2011). Histone fold modifications control nucleosome unwrapping and disassembly, *Proceedings of the National Academy of Sciences of the United States of America*, Vol. 108, No. 31, 12711–12716, doi: 10.1073/pnas.1106264108.

REFERENCES

[104]   Jack, A.P.M., Hake, S.B. (2014). Getting down to the core of histone modifications, *Chromosoma*, Vol. 123, No. 4, 355–371, doi: 10.1007/s00412-014-0465-x.

[105]   Tessarz, P., Kouzarides, T. (2014). Histone core modifications regulating nucleosome structure and dynamics, *Nature reviews. Molecular cell biology*, Vol. 15, No. 11, 703–708, doi: 10.1038/nrm3890.

[106]   Mersfelder, E.L., Parthun, M.R. (2006). The tale beyond the tail: Histone core domain modifications and the regulation of chromatin structure, *Nucleic acids research*, Vol. 34, No. 9, 2653–2662, doi: 10.1093/nar/gkl338.

[107]   Khorasanizadeh, S. (2004). The Nucleosome, *Cell*, Vol. 116, No. 2, 259–272, doi: 10.1016/S0092-8674(04)00044-3.

[108]   Jambhekar, A., Dhall, A., Shi, Y. (2019). Roles and regulation of histone methylation in animal development, *Nature reviews. Molecular cell biology*, Vol. 20, No. 10, 625–641, doi: 10.1038/s41580-019-0151-1.

[109]   Barski, A., Cuddapah, S., Cui, K., Roh, T.-Y., Schones, D.E., Wang, Z., Wei, G., Chepelev, I., Zhao, K. (2007). High-resolution profiling of histone methylations in the human genome, *Cell*, Vol. 129, No. 4, 823–837, doi: 10.1016/j.cell.2007.05.009.

[110]   Bannister, A.J., Schneider, R., Myers, F.A., Thorne, A.W., Crane-Robinson, C., Kouzarides, T. (2005). Spatial distribution of di- and tri-methyl lysine 36 of histone h3 at active genes, *The Journal of biological chemistry*, Vol. 280, No. 18, 17732–17736, doi: 10.1074/jbc.M500796200.

[111]   Heintzman, N.D., Stuart, R.K., Hon, G., Fu, Y., Ching, C.W., Hawkins, R.D., Barrera, L.O., van Calcar, S., Qu, C., Ching, K.A., Wang, W., Weng, Z., Green, R.D., Crawford, G.E., Ren, B. (2007). Distinct and predictive chromatin signatures of transcriptional promoters and enhancers in the human genome, *Nature genetics*, Vol. 39, No. 3, 311–318, doi: 10.1038/ng1966.

[112]   Bernstein, B.E., Kamal, M., Lindblad-Toh, K., Bekiranov, S., Bailey, D.K., Huebert, D.J., McMahon, S., Karlsson, E.K., Kulbokas, E.J., Gingeras, T.R., Schreiber, S.L., Lander, E.S. (2005). Genomic maps and comparative analysis of histone modifications in human and mouse, *Cell*, Vol. 120, No. 2, 169–181, doi: 10.1016/j.cell.2005.01.001.

[113]   Becker, J.S., Nicetto, D., Zaret, K.S. (2016). H3k9me3-dependent heterochromatin: Barrier to cell fate changes, *Trends in genetics TIG*, Vol. 32, No. 1, 29–41, doi: 10.1016/j.tig.2015.11.001.

[114]   Gong, F., Miller, K.M. (2019). Histone methylation and the dna damage response, *Mutation research*, Vol. 780, 37–47, doi: 10.1016/j.mrrev.2017.09.003.

[115]   Simon, J.A., Lange, C.A. (2008). Roles of the ezh2 histone methyltransferase in cancer epigenetics, *Mutation research*, Vol. 647, 1-2, 21–29, doi: 10.1016/j.mrfmmm.2008.07.010.

[116]   Lu, R., Wang, G.G. (2013). Tudor: A versatile family of histone methylation 'readers', *Trends in biochemical sciences*, Vol. 38, No. 11, 546–555, doi: 10.1016/j.tibs.2013.08.002.

[117]   Rossetto, D., Avvakumov, N., Côté, J. (2012). Histone phosphorylation: A chromatin modification involved in diverse nuclear events, *Epigenetics*, Vol. 7, No. 10, 1098–1108, doi: 10.4161/epi.21975.

[118]   Ellenbroek, B., Youn, J. (2016). Environment Challenges and the Brain, *Gene-Environment Interactions in Psychiatry*, Elsevier, 107–139, doi: 10.1016/B978-0-12-801657-2.00005-7.

[119]   Musselman, C.A., Lalonde, M.-E., Côté, J., Kutateladze, T.G. (2012). Perceiving the epigenetic landscape through histone readers, *Nature structural & molecular biology*, Vol. 19, No. 12, 1218–1227, doi: 10.1038/nsmb.2436.

[120]   Sawicka, A., Seiser, C. (2014). Sensing core histone phosphorylation - a matter of perfect timing, *Biochimica et biophysica acta*, Vol. 1839, No. 8, 711–718, doi: 10.1016/j.bbagrm.2014.04.013.

[121]   Yu, X., Chini, C.C.S., He, M., Mer, G., Chen, J. (2003). The brct domain is a phospho-protein binding domain, *Science (New York, N.Y.)*, Vol. 302, No. 5645, 639–642, doi: 10.1126/science.1088753.

[122]   Cao, X., Dang, W. (2018). Histone Modification Changes During Aging, *Epigenetics of Aging and Longevity*, Elsevier, 309–328, doi: 10.1016/B978-0-12-811060-7.00015-2.

[123]   Grant, P.A. (2001). A tale of histone modifications, *Genome biology*, Vol. 2, No. 4, REVIEWS0003, doi: 10.1186/gb-2001-2-4-reviews0003.

[124]   Wolffe, A.P., Kurumizaka, H. (1998). The Nucleosome: A Powerful Regulator of Transcription, Elsevier, 379–422, doi: 10.1016/s0079-6603(08)60832-6.

[125]   ALLFREY, V.G., FAULKNER, R., MIRSKY, A.E. (1964). Acetylation and methylation of histones and their possible role in the regulation of rna synthesis, *Proceedings of the National Academy of Sciences of the United States of America*, Vol. 51, 786–794, doi: 10.1073/pnas.51.5.786.

[126]   Muddassir, M., Soni, K., Sangani, C.B., Alarifi, A., Afzal, M., Abduh, N.A.Y., Duan, Y., Bhadja, P. (2021). Bromodomain and BET family proteins as epigenetic targets in cancer therapy: their degradation, present drugs, and possible PROTACs, *RSC Advances*, Vol. 11, No. 2, 612–636, doi: 10.1039/D0RA07971E.

[127]   Allis, C.D., Berger, S.L., Cote, J., Dent, S., Jenuwien, T., Kouzarides, T., Pillus, L., Reinberg, D., Shi, Y., Shiekhattar, R., Shilatifard, A., Workman, J., Zhang, Y. (2007). New nomenclature for chromatin-modifying enzymes, *Cell*, Vol. 131, No. 4, 633–636, doi: 10.1016/j.cell.2007.10.039.

REFERENCES

[128]   Lee, K.K., Workman, J.L. (2007). Histone acetyltransferase complexes: One size doesn't fit all, *Nature reviews. Molecular cell biology*, Vol. 8, No. 4, 284–295, doi: 10.1038/nrm2145.

[129]   Zhang, X., Wu, J., Luan, Y. (2017). Tip60: Main functions and its inhibitors, *Mini reviews in medicinal chemistry*, Vol. 17, No. 8, 675–682, doi: 10.2174/1389557516666160923125031.

[130]   Friedmann, D.R., Marmorstein, R. (2013). Structure and mechanism of non-histone protein acetyltransferase enzymes, *The FEBS journal*, Vol. 280, No. 22, 5570–5581, doi: 10.1111/febs.12373.

[131]   Watanabe, S., Peterson, C.L. (2010). The ino80 family of chromatin-remodeling enzymes: Regulators of histone variant dynamics, *Cold Spring Harbor symposia on quantitative biology*, Vol. 75, 35–42, doi: 10.1101/sqb.2010.75.063.

[132]   Colino-Sanguino, Y., Cornett, E.M., Moulder, D., Smith, G.C., Hrit, J., Cordeiro-Spinetti, E., Vaughan, R.M., Krajewski, K., Rothbart, S.B., Clark, S.J., Valdés-Mora, F. (2019). A read/write mechanism connects p300 bromodomain function to h2a.Z acetylation, *iScience*, Vol. 21, 773–788, doi: 10.1016/j.isci.2019.10.053.

[133]   Ikura, M., Furuya, K., Matsuda, S., Matsuda, R., Shima, H., Adachi, J., Matsuda, T., Shiraki, T., Ikura, T. (2015). Acetylation of histone h2ax at lys 5 by the tip60 histone acetyltransferase complex is essential for the dynamic binding of nbs1 to damaged chromatin, *Molecular and cellular biology*, Vol. 35, No. 24, 4147–4157, doi: 10.1128/MCB.00757-15.

[134]   Choi, J., Heo, K., An, W. (2009). Cooperative action of tip48 and tip49 in h2a.Z exchange catalyzed by acetylation of nucleosomal h2a, *Nucleic acids research*, Vol. 37, No. 18, 5993–6007, doi: 10.1093/nar/gkp660.

[135]   Long, M., Sun, X., Shi, W., an Yanru, Leung, S.T.C., Ding, D., Cheema, M.S., MacPherson, N., Nelson, C.J., Ausio, J., Yan, Y., Ishibashi, T. (2019). A novel histone h4 variant h4g regulates rdna transcription in breast cancer, *Nucleic acids research*, Vol. 47, No. 16, 8399–8409, doi: 10.1093/nar/gkz547.

[136]   Buschbeck, M., Hake, S.B. (2017). Variants of core histones and their roles in cell fate decisions, development and cancer, *Nature reviews. Molecular cell biology*, Vol. 18, No. 5, 299–314, doi: 10.1038/nrm.2016.166.

[137]   Maze, I., Noh, K.-M., Soshnev, A.A., Allis, C.D. (2014). Every amino acid matters: Essential contributions of histone variants to mammalian development and disease, *Nature reviews. Genetics*, Vol. 15, No. 4, 259–271, doi: 10.1038/nrg3673.

[138]   Talbert, P.B., Henikoff, S. (2010). Histone variants--ancient wrap artists of the epigenome, *Nature reviews. Molecular cell biology*, Vol. 11, No. 4, 264–275, doi: 10.1038/nrm2861.

[139]   Ausió, J. (2006). Histone variants--the structure behind the function, *Briefings in functional genomics & proteomics*, Vol. 5, No. 3, 228–243, doi: 10.1093/bfgp/ell020.

[140]   Vardabasso, C., Hasson, D., Ratnakumar, K., Chung, C.-Y., Duarte, L.F., Bernstein, E. (2014). Histone variants: Emerging players in cancer biology, *Cellular and molecular life sciences CMLS*, Vol. 71, No. 3, 379–404, doi: 10.1007/s00018-013-1343-z.

[141]   Zink, L.-M., Hake, S.B. (2016). Histone variants: Nuclear function and disease, *Current opinion in genetics & development*, Vol. 37, 82–89, doi: 10.1016/j.gde.2015.12.002.

[142]   Probst, A.V., Desvoyes, B., Gutierrez, C. (2020). Similar yet critically different: The distribution, dynamics and function of histone variants, *Journal of experimental botany*, Vol. 71, No. 17, 5191–5204, doi: 10.1093/jxb/eraa230.

[143]   Ausió, J., Abbott, D.W., Wang, X., Moore, S.C. (2001). Histone variants and histone modifications: A structural perspective, *Biochemistry and Cell Biology*, Vol. 79, No. 6, 693–708, doi: 10.1139/bcb-79-6-693.

[144]   West, M.H., Bonner, W.M. (1980). Histone 2a, a heteromorphous family of eight protein species, *Biochemistry*, Vol. 19, No. 14, 3238–3245, doi: 10.1021/bi00555a022.

[145]   Talbert, P.B., Henikoff, S. (2017). Histone variants on the move: Substrates for chromatin dynamics, *Nature reviews. Molecular cell biology*, Vol. 18, No. 2, 115–126, doi: 10.1038/nrm.2016.148.

[146]   Marzluff, W.F., Wagner, E.J., Duronio, R.J. (2008). Metabolism and regulation of canonical histone mrnas: Life without a poly(a) tail, *Nature reviews. Genetics*, Vol. 9, No. 11, 843–854, doi: 10.1038/nrg2438.

[147]   Skene, P.J., Henikoff, S. (2013). Histone variants in pluripotency and disease, *Development (Cambridge, England)*, Vol. 140, No. 12, 2513–2524, doi: 10.1242/dev.091439.

[148]   Kamakaka, R.T., Biggins, S. (2005). Histone variants: Deviants?, *Genes & development*, Vol. 19, No. 3, 295–310, doi: 10.1101/gad.1272805.

[149]   Marzluff, W.F. (2005). Metazoan replication-dependent histone mrnas: A distinct set of rna polymerase ii transcripts, *Current opinion in cell biology*, Vol. 17, No. 3, 274–280, doi: 10.1016/j.ceb.2005.04.010.

[150]   Bustin, M., Catez, F., Lim, J.-H. (2005). The dynamics of histone h1 function in chromatin, *Molecular cell*, Vol. 17, No. 5, 617–620, doi: 10.1016/j.molcel.2005.02.019.

[151]   Starkova, T.Y., Polyanichko, A.M., Artamonova, T.O., Khodorkovskii, M.A., Kostyleva, E.I., Chikhirzhina, E.V., Tomilin, A.N. (2017). Post-translational modifications of linker histone h1 variants in mammals, *Physical biology*, Vol. 14, No. 1, 16005, doi: 10.1088/1478-3975/aa551a.

REFERENCES

[152]   Parseghian, M.H., Henschen, A.H., Krieglstein, K.G., Hamkalo, B.A. (1994). A proposal for a coherent mammalian histone h1 nomenclature correlated with amino acid sequences, *Protein science a publication of the Protein Society*, Vol. 3, No. 4, 575–587, doi: 10.1002/pro.5560030406.

[153]   Seyedin, S.M., Kistler, W.S. (1980). Isolation and characterization of rat testis H1t. An H1 histone variant associated with spermatogenesis, *The Journal of biological chemistry*, Vol. 255, No. 12, 5949–5954, doi: 10.1016/S0021-9258(19)70722-4.

[154]   Martianov, I., Brancorsini, S., Catena, R., Gansmuller, A., Kotaja, N., Parvinen, M., Sassone-Corsi, P., Davidson, I. (2005). Polar nuclear localization of h1t2, a histone h1 variant, required for spermatid elongation and dna condensation during spermiogenesis, *Proceedings of the National Academy of Sciences of the United States of America*, Vol. 102, No. 8, 2808–2813, doi: 10.1073/pnas.0406060102.

[155]   Yan, W., Ma, L., Burns, K.H., Matzuk, M.M. (2003). Hils1 is a spermatid-specific linker histone h1-like protein implicated in chromatin remodeling during mammalian spermiogenesis, *Proceedings of the National Academy of Sciences of the United States of America*, Vol. 100, No. 18, 10546–10551, doi: 10.1073/pnas.1837812100.

[156]   Tanaka, M., Kihara, M., Meczekalski, B., King, G.J., Adashi, E.Y. (2003). H1oo: a pre-embryonic H1 linker histone in search of a function, *Molecular and Cellular Endocrinology*, Vol. 202, 1-2, 5–9, doi: 10.1016/s0303-7207(03)00054-6.

[157]   Alami, R., Fan, Y., Pack, S., Sonbuchner, T.M., Besse, A., Lin, Q., Greally, J.M., Skoultchi, A.I., Bouhassira, E.E. (2003). Mammalian linker-histone subtypes differentially affect gene expression in vivo, *Proceedings of the National Academy of Sciences of the United States of America*, Vol. 100, No. 10, 5920–5925, doi: 10.1073/pnas.0736105100.

[158]   Urahama, T., Harada, A., Maehara, K., Horikoshi, N., Sato, K., Sato, Y., Shiraishi, K., Sugino, N., Osakabe, A., Tachiwana, H., Kagawa, W., Kimura, H., Ohkawa, Y., Kurumizaka, H. (2016). Histone h3.5 forms an unstable nucleosome and accumulates around transcription start sites in human testis, *Epigenetics & chromatin*, Vol. 9, 2, doi: 10.1186/s13072-016-0051-y.

[159]   Tachiwana, H., Osakabe, A., Kimura, H., Kurumizaka, H. (2008). Nucleosome formation with the testis-specific histone h3 variant, h3t, by human nucleosome assembly proteins in vitro, *Nucleic acids research*, Vol. 36, No. 7, 2208–2218, doi: 10.1093/nar/gkn060.

[160]   Wen, H., Shi, X. (2020). H3.3s31 phosphorylation: Linking transcription elongation to stimulation responses, *Signal transduction and targeted therapy*, Vol. 5, No. 1, 176, doi: 10.1038/s41392-020-00293-6.

[161]   Goldberg, A.D., Banaszynski, L.A., Noh, K.-M., Lewis, P.W., Elsaesser, S.J., Stadler, S., Dewell, S., Law, M., Guo, X., Li, X., Wen, D., Chapgier, A., DeKelver, R.C., Miller, J.C., Lee, Y.-L., Boydston, E.A., Holmes, M.C., Gregory,

P.D., Greally, J.M., Rafii, S., Yang, C., Scambler, P.J., Garrick, D., Gibbons, R.J., Higgs, D.R., Cristea, I.M., Urnov, F.D., Zheng, D., Allis, C.D. (2010). Distinct factors control histone variant h3.3 localization at specific genomic regions, *Cell*, Vol. 140, No. 5, 678–691, doi: 10.1016/j.cell.2010.01.003.

[162]   Ahmad, K., Henikoff, S. (2002). The Histone Variant H3.3 Marks Active Chromatin by Replication-Independent Nucleosome Assembly, *Molecular cell*, Vol. 9, No. 6, 1191–1200, doi: 10.1016/S1097-2765(02)00542-7.

[163]   Sauer, P.V., Timm, J., Liu, D., Sitbon, D., Boeri-Erba, E., Velours, C., Mücke, N., Langowski, J., Ochsenbein, F., Almouzni, G., Panne, D. (2017). Insights into the molecular architecture and histone h3-h4 deposition mechanism of yeast chromatin assembly factor 1, *eLife*, Vol. 6, doi: 10.7554/eLife.23474.

[164]   Udugama, M., M Chang, F.T., Chan, F.L., Tang, M.C., Pickett, H.A., R McGhie, J.D., Mayne, L., Collas, P., Mann, J.R., Wong, L.H. (2015). Histone variant h3.3 provides the heterochromatic h3 lysine 9 tri-methylation mark at telomeres, *Nucleic acids research*, Vol. 43, No. 21, 10227–10237, doi: 10.1093/nar/gkv847.

[165]   Tagami, H., Ray-Gallet, D., Almouzni, G., Nakatani, Y. (2004). Histone H3.1 and H3.3 Complexes Mediate Nucleosome Assembly Pathways Dependent or Independent of DNA Synthesis, *Cell*, Vol. 116, No. 1, 51–61, doi: 10.1016/S0092-8674(03)01064-X.

[166]   Loppin, B., Bonnefoy, E., Anselme, C., Laurençon, A., Karr, T.L., Couble, P. (2005). The histone h3.3 chaperone hira is essential for chromatin assembly in the male pronucleus, *Nature*, Vol. 437, No. 7063, 1386–1390, doi: 10.1038/nature04059.

[167]   Lewis, J.D., Abbott, D.W., Ausió, J. (2003). A haploid affair: Core histone transitions during spermatogenesis, *Biochemistry and Cell Biology*, Vol. 81, No. 3, 131–140, doi: 10.1139/o03-045.

[168]   Hake, S.B., Garcia, B.A., Kauer, M., Baker, S.P., Shabanowitz, J., Hunt, D.F., Allis, C.D. (2005). Serine 31 phosphorylation of histone variant h3.3 is specific to regions bordering centromeres in metaphase chromosomes, *Proceedings of the National Academy of Sciences of the United States of America*, Vol. 102, No. 18, 6344–6349, doi: 10.1073/pnas.0502413102.

[169]   Armache, A., Yang, S., Martínez de Paz, A., Robbins, L.E., Durmaz, C., Cheong, J.Q., Ravishankar, A., Daman, A.W., Ahimovic, D.J., Klevorn, T., Yue, Y., Arslan, T., Lin, S., Panchenko, T., Hrit, J., Wang, M., Thudium, S., Garcia, B.A., Korb, E., Armache, K.-J., Rothbart, S.B., Hake, S.B., Allis, C.D., Li, H., Josefowicz, S.Z. (2020). Histone h3.3 phosphorylation amplifies stimulation-induced transcription, *Nature*, Vol. 583, No. 7818, 852–857, doi: 10.1038/s41586-020-2533-0.

[170]   Hake, S.B., Garcia, B.A., Duncan, E.M., Kauer, M., Dellaire, G., Shabanowitz, J., Bazett-Jones, D.P., Allis, C.D., Hunt, D.F. (2006). Expression patterns and post-translational modifications associated with mammalian

histone h3 variants, *The Journal of biological chemistry*, Vol. 281, No. 1, 559–568, doi: 10.1074/jbc.M509266200.

[171]   Wiedemann, S.M., Mildner, S.N., Bönisch, C., Israel, L., Maiser, A., Matheisl, S., Straub, T., Merkl, R., Leonhardt, H., Kremmer, E., Schermelleh, L., Hake, S.B. (2010). Identification and characterization of two novel primate-specific histone h3 variants, h3.X and h3.Y, *The Journal of cell biology*, Vol. 190, No. 5, 777–791, doi: 10.1083/jcb.201002043.

[172]   Hake, S.B., Allis, C.D. (2006). Histone h3 variants and their potential role in indexing mammalian genomes: The "h3 barcode hypothesis", *Proceedings of the National Academy of Sciences of the United States of America*, Vol. 103, No. 17, 6428–6435, doi: 10.1073/pnas.0600803103.

[173]   Sullivan, K.F., Hechenberger, M., Masri, K. (1994). Human cenp-a contains a histone h3 related histone fold domain that is required for targeting to the centromere, *The Journal of cell biology*, Vol. 127, No. 3, 581–592, doi: 10.1083/jcb.127.3.581.

[174]   Howman, E.V., Fowler, K.J., Newson, A.J., Redward, S., MacDonald, A.C., Kalitsis, P., Choo, K.H. (2000). Early disruption of centromeric chromatin organization in centromere protein a (cenpa) null mice, *Proceedings of the National Academy of Sciences of the United States of America*, Vol. 97, No. 3, 1148–1153, doi: 10.1073/pnas.97.3.1148.

[175]   Abendroth, C., Hofmeister, A., Hake, S.B., Kamweru, P.K., Miess, E., Dornblut, C., Küffner, I., Deng, W., Leonhardt, H., Orthaus, S., Hoischen, C., Diekmann, S. (2015). The cenp-t c-terminus is exclusively proximal to h3.1 and not to h3.2 or h3.3, *International journal of molecular sciences*, Vol. 16, No. 3, 5839–5863, doi: 10.3390/ijms16035839.

[176]   Zink, L.-M., Delbarre, E., Eberl, H.C., Keilhauer, E.C., Bönisch, C., Pünzeler, S., Bartkuhn, M., Collas, P., Mann, M., Hake, S.B. (2017). H3.Y discriminates between hira and daxx chaperone complexes and reveals unexpected insights into human daxx-h3.3-h4 binding and deposition requirements, *Nucleic acids research*, Vol. 45, No. 10, 5691–5706, doi: 10.1093/nar/gkx131.

[177]   Resnick, R., Wong, C.-J., Hamm, D.C., Bennett, S.R., Skene, P.J., Hake, S.B., Henikoff, S., van der Maarel, S.M., Tapscott, S.J. (2019). Dux4-induced histone variants h3.X and h3.Y mark dux4 target genes for expression, *Cell reports*, Vol. 29, No. 7, 1812-1820.e5, doi: 10.1016/j.celrep.2019.10.025.

[178]   Kujirai, T., Horikoshi, N., Sato, K., Maehara, K., Machida, S., Osakabe, A., Kimura, H., Ohkawa, Y., Kurumizaka, H. (2016). Structure and function of human histone h3.Y nucleosome, *Nucleic acids research*, Vol. 44, No. 13, 6127–6141, doi: 10.1093/nar/gkw202.

[179]   Pang, M.Y.H., Sun, X., Ausió, J., Ishibashi, T. (2020). Histone h4 variant, h4g, drives ribosomal rna transcription and breast cancer cell proliferation by loosening nucleolar chromatin structure, *Journal of cellular physiology*, Vol. 235, No. 12, 9601–9608, doi: 10.1002/jcp.29770.

[180] Bernstein, E., Hake, S.B. (2006). The nucleosome: A little variation goes a long way, *Biochemistry and Cell Biology*, Vol. 84, No. 4, 505–517, doi: 10.1139/o06-085.

[181] Li, A., Maffey, A.H., Abbott, W.D., Conde e Silva, N., Prunell, A., Siino, J., Churikov, D., Zalensky, A.O., Ausió, J. (2005). Characterization of nucleosomes consisting of the human testis/sperm-specific histone h2b variant (htsh2b), *Biochemistry*, Vol. 44, No. 7, 2529–2535, doi: 10.1021/bi048061n.

[182] Urahama, T., Horikoshi, N., Osakabe, A., Tachiwana, H., Kurumizaka, H. (2014). Structure of human nucleosome containing the testis-specific histone variant tsh2b, *Acta crystallographica. Section F, Structural biology communications*, Vol. 70, Pt 4, 444–449, doi: 10.1107/S2053230X14004695.

[183] Boulard, M., Gautier, T., Mbele, G.O., Gerson, V., Hamiche, A., Angelov, D., Bouvet, P., Dimitrov, S. (2006). The nh2 tail of the novel histone variant h2bfwt exhibits properties distinct from conventional h2b with respect to the assembly of mitotic chromosomes, *Molecular and cellular biology*, Vol. 26, No. 4, 1518–1526, doi: 10.1128/MCB.26.4.1518-1526.2006.

[184] Churikov, D., Siino, J., Svetlova, M., Zhang, K., Gineitis, A., Morton Bradbury, E., Zalensky, A. (2004). Novel human testis-specific histone h2b encoded by the interrupted gene on the x chromosome, *Genomics*, Vol. 84, No. 4, 745–756, doi: 10.1016/j.ygeno.2004.06.001.

[185] Santoro, S.W., Dulac, C. (2012). The activity-dependent histone variant h2be modulates the life span of olfactory neurons, *eLife*, Vol. 1, e00070, doi: 10.7554/eLife.00070.

[186] Pusarla, R.-H., Bhargava, P. (2005). Histones in functional diversification. Core histone variants, *The FEBS journal*, Vol. 272, No. 20, 5149–5168, doi: 10.1111/j.1742-4658.2005.04930.x.

[187] Corujo, D., Buschbeck, M. (2018). Post-translational modifications of h2a histone variants and their role in cancer, *Cancers*, Vol. 10, No. 3, doi: 10.3390/cancers10030059.

[188] Bönisch, C., Hake, S.B. (2012). Histone h2a variants in nucleosomes and chromatin: More or less stable?, *Nucleic acids research*, Vol. 40, No. 21, 10719–10741, doi: 10.1093/nar/gks865.

[189] Ausió, J., Abbott, D.W. (2002). The many tales of a tail: Carboxyl-terminal tail heterogeneity specializes histone h2a variants for defined chromatin function, *Biochemistry*, Vol. 41, No. 19, 5945–5949, doi: 10.1021/bi020059d.

[190] Shukla, M.S., Syed, S.H., Goutte-Gattat, D., Richard, J.L.C., Montel, F., Hamiche, A., Travers, A., Faivre-Moskalenko, C., Bednar, J., Hayes, J.J., Angelov, D., Dimitrov, S. (2011). The docking domain of histone h2a is required for h1 binding and rsc-mediated nucleosome remodeling, *Nucleic acids research*, Vol. 39, No. 7, 2559–2570, doi: 10.1093/nar/gkq1174.

REFERENCES

[191]   Chadwick, B.P., Willard, H.F. (2001). A novel chromatin protein, distantly related to histone h2a, is largely excluded from the inactive x chromosome, *The Journal of cell biology*, Vol. 152, No. 2, 375–384, doi: 10.1083/jcb.152.2.375.

[192]   Sansoni, V., Casas-Delucchi, C.S., Rajan, M., Schmidt, A., Bönisch, C., Thomae, A.W., Staege, M.S., Hake, S.B., Cardoso, M.C., Imhof, A. (2014). The histone variant h2a.Bbd is enriched at sites of dna synthesis, *Nucleic acids research*, Vol. 42, No. 10, 6405–6420, doi: 10.1093/nar/gku303.

[193]   Bao, Y., Konesky, K., Park, Y.-J., Rosu, S., Dyer, P.N., Rangasamy, D., Tremethick, D.J., Laybourn, P.J., Luger, K. (2004). Nucleosomes containing the histone variant h2a.Bbd organize only 118 base pairs of dna, *The EMBO journal*, Vol. 23, No. 16, 3314–3324, doi: 10.1038/sj.emboj.7600316.

[194]   Doyen, C.-M., Montel, F., Gautier, T., Menoni, H., Claudet, C., Delacour-Larose, M., Angelov, D., Hamiche, A., Bednar, J., Faivre-Moskalenko, C., Bouvet, P., Dimitrov, S. (2006). Dissection of the unusual structural and functional properties of the variant h2a.Bbd nucleosome, *The EMBO journal*, Vol. 25, No. 18, 4234–4244, doi: 10.1038/sj.emboj.7601310.

[195]   Tolstorukov, M.Y., Goldman, J.A., Gilbert, C., Ogryzko, V., Kingston, R.E., Park, P.J. (2012). Histone variant h2a.Bbd is associated with active transcription and mrna processing in human cells, *Molecular cell*, Vol. 47, No. 4, 596–607, doi: 10.1016/j.molcel.2012.06.011.

[196]   Soboleva, T.A., Nekrasov, M., Pahwa, A., Williams, R., Huttley, G.A., Tremethick, D.J. (2011). A unique h2a histone variant occupies the transcriptional start site of active genes, *Nature structural & molecular biology*, Vol. 19, No. 1, 25–30, doi: 10.1038/nsmb.2161.

[197]   Ishibashi, T., Li, A., Eirín-López, J.M., Zhao, M., Missiaen, K., Abbott, D.W., Meistrich, M., Hendzel, M.J., Ausió, J. (2010). H2a.Bbd: An x-chromosome-encoded histone involved in mammalian spermiogenesis, *Nucleic acids research*, Vol. 38, No. 6, 1780–1789, doi: 10.1093/nar/gkp1129.

[198]   Pehrson, J.R., Fried, V.A. (1992). Macroh2a, a core histone containing a large nonhistone region, *Science (New York, N.Y.)*, Vol. 257, No. 5075, 1398–1400, doi: 10.1126/science.1529340.

[199]   Rasmussen, T.P., Huang, T., Mastrangelo, M.A., Loring, J., Panning, B., Jaenisch, R. (1999). Messenger rnas encoding mouse histone macroh2a1 isoforms are expressed at similar levels in male and female cells and result from alternative splicing, *Nucleic acids research*, Vol. 27, No. 18, 3685–3689, doi: 10.1093/nar/27.18.3685.

[200]   Doyen, C.-M., An, W., Angelov, D., Bondarenko, V., Mietton, F., Studitsky, V.M., Hamiche, A., Roeder, R.G., Bouvet, P., Dimitrov, S. (2006). Mechanism of polymerase ii transcription repression by the histone variant macroh2a, *Molecular and cellular biology*, Vol. 26, No. 3, 1156–1164, doi: 10.1128/MCB.26.3.1156-1164.2006.

REFERENCES

[201]   Buschbeck, M., Uribesalgo, I., Wibowo, I., Rué, P., Martin, D., Gutierrez, A., Morey, L., Guigó, R., López-Schier, H., Di Croce, L. (2009). The histone variant macroh2a is an epigenetic regulator of key developmental genes, *Nature structural & molecular biology*, Vol. 16, No. 10, 1074–1079, doi: 10.1038/nsmb.1665.

[202]   Kozlowski, M., Corujo, D., Hothorn, M., Guberovic, I., Mandemaker, I.K., Blessing, C., Sporn, J., Gutierrez-Triana, A., Smith, R., Portmann, T., Treier, M., Scheffzek, K., Huet, S., Timinszky, G., Buschbeck, M., Ladurner, A.G. (2018). Macroh2a histone variants limit chromatin plasticity through two distinct mechanisms, *EMBO reports*, Vol. 19, No. 10, doi: 10.15252/embr.201744445.

[203]   Costanzi, C., Pehrson, J.R. (1998). Histone macroh2a1 is concentrated in the inactive x chromosome of female mammals, *Nature*, Vol. 393, No. 6685, 599–601, doi: 10.1038/31275.

[204]   Angelov, D., Molla, A., Perche, P.-Y., Hans, F., Côté, J., Khochbin, S., Bouvet, P., Dimitrov, S. (2003). The Histone Variant MacroH2A Interferes with Transcription Factor Binding and SWI/SNF Nucleosome Remodeling, *Molecular cell*, Vol. 11, No. 4, 1033–1041, doi: 10.1016/S1097-2765(03)00100-X.

[205]   Gamble, M.J., Frizzell, K.M., Yang, C., Krishnakumar, R., Kraus, W.L. (2010). The histone variant macroh2a1 marks repressed autosomal chromatin, but protects a subset of its target genes from silencing, *Genes & development*, Vol. 24, No. 1, 21–32, doi: 10.1101/gad.1876110.

[206]   Fernandez-Capetillo, O., Lee, A., Nussenzweig, M., Nussenzweig, A. (2004). H2ax: The histone guardian of the genome, *DNA repair*, Vol. 3, 8-9, 959–967, doi: 10.1016/j.dnarep.2004.03.024.

[207]   Aleksandrov, R., Hristova, R., Stoynov, S., Gospodinov, A. (2020). The chromatin response to double-strand dna breaks and their repair, *Cells*, Vol. 9, No. 8, doi: 10.3390/cells9081853.

[208]   Rogakou, E.P., Pilch, D.R., Orr, A.H., Ivanova, V.S., Bonner, W.M. (1998). Dna double-stranded breaks induce histone h2ax phosphorylation on serine 139, *The Journal of biological chemistry*, Vol. 273, No. 10, 5858–5868, doi: 10.1074/jbc.273.10.5858.

[209]   Shroff, R., Arbel-Eden, A., Pilch, D., Ira, G., Bonner, W.M., Petrini, J.H., Haber, J.E., Lichten, M. (2004). Distribution and dynamics of chromatin modification induced by a defined dna double-strand break, *Current biology CB*, Vol. 14, No. 19, 1703–1711, doi: 10.1016/j.cub.2004.09.047.

[210]   Rossetto, D., Truman, A.W., Kron, S.J., Côté, J. (2010). Epigenetic modifications in double-strand break dna damage signaling and repair, *Clinical cancer research an official journal of the American Association for Cancer Research*, Vol. 16, No. 18, 4543–4552, doi: 10.1158/1078-0432.CCR-10-0513.

[211]   Dudás, A., Chovanec, M. (2004). Dna double-strand break repair by homologous recombination, *Mutation research*, Vol. 566, No. 2, 131–167, doi: 10.1016/j.mrrev.2003.07.001.

[212]   Burma, S., Chen, B.P., Murphy, M., Kurimasa, A., Chen, D.J. (2001). Atm phosphorylates histone h2ax in response to dna double-strand breaks, *The Journal of biological chemistry*, Vol. 276, No. 45, 42462–42467, doi: 10.1074/jbc.C100466200.

[213]   Xu, Y., Price, B.D. (2011). Chromatin dynamics and the repair of dna double strand breaks, *Cell cycle (Georgetown, Tex.)*, Vol. 10, No. 2, 261–267, doi: 10.4161/cc.10.2.14543.

[214]   Murr, R., Loizou, J.I., Yang, Y.-G., Cuenin, C., Li, H., Wang, Z.-Q., Herceg, Z. (2006). Histone acetylation by trrap-tip60 modulates loading of repair proteins and repair of dna double-strand breaks, *Nature cell biology*, Vol. 8, No. 1, 91–99, doi: 10.1038/ncb1343.

[215]   Turinetto, V., Giachino, C. (2015). Multiple facets of histone variant h2ax: A dna double-strand-break marker with several biological functions, *Nucleic acids research*, Vol. 43, No. 5, 2489–2498, doi: 10.1093/nar/gkv061.

[216]   Dobersch, S., Rubio, K., Singh, I., Günther, S., Graumann, J., Cordero, J., Castillo-Negrete, R., Huynh, M.B., Mehta, A., Braubach, P., Cabrera-Fuentes, H., Bernhagen, J., Chao, C.-M., Bellusci, S., Günther, A., Preissner, K.T., Kugel, S., Dobreva, G., Wygrecka, M., Braun, T., Papy-Garcia, D., Barreto, G. (2021). Positioning of nucleosomes containing γ-h2ax precedes active dna demethylation and transcription initiation, *Nature communications*, Vol. 12, No. 1, 1072, doi: 10.1038/s41467-021-21227-y.

[217]   Zlatanova, J., Thakar, A. (2008). H2a.Z: View from the top, *Structure (London, England 1993)*, Vol. 16, No. 2, 166–179, doi: 10.1016/j.str.2007.12.008.

[218]   Cheema, M.S., Good, K.V., Kim, B., Soufari, H., O'Sullivan, C., Freeman, M.E., Stefanelli, G., Casas, C.R., Zengeler, K.E., Kennedy, A.J., Eirin Lopez, J.M., Howard, P.L., Zovkic, I.B., Shabanowitz, J., Dryhurst, D.D., Hunt, D.F., Mackereth, C.D., Ausió, J. (2020). Deciphering the enigma of the histone h2a.Z-1/h2a.Z-2 isoforms: Novel insights and remaining questions, *Cells*, Vol. 9, No. 5, doi: 10.3390/cells9051167.

[219]   van Daal, A., Elgin, S.C. (1992). A histone variant, h2avd, is essential in drosophila melanogaster, *Molecular biology of the cell*, Vol. 3, No. 6, 593–602, doi: 10.1091/mbc.3.6.593.

[220]   Clarkson, M.J., Wells, J.R., Gibson, F., Saint, R., Tremethick, D.J. (1999). Regions of variant histone his2avd required for drosophila development, *Nature*, Vol. 399, No. 6737, 694–697, doi: 10.1038/21436.

[221]   Liu, X., Li, B., GorovskyMA (1996). Essential and nonessential histone h2a variants in tetrahymena thermophila, *Molecular and cellular biology*, Vol. 16, No. 8, 4305–4311, doi: 10.1128/mcb.16.8.4305.

[222]   Iouzalen, N., Moreau, J., Méchali, M. (1996). H2a.Zi, a new variant histone expressed during xenopus early development exhibits several distinct features

from the core histone h2a, *Nucleic acids research*, Vol. 24, No. 20, 3947–3952, doi: 10.1093/nar/24.20.3947.

[223]   Ridgway, P., Brown, K.D., Rangasamy, D., Svensson, U., Tremethick, D.J. (2004). Unique residues on the h2a.Z containing nucleosome surface are important for xenopus laevis development, *The Journal of biological chemistry*, Vol. 279, No. 42, 43815–43820, doi: 10.1074/jbc.M408409200.

[224]   Faast, R., Thonglairoam, V., Schulz, T.C., Beall, J., Wells, J.R., Taylor, H., Matthaei, K., Rathjen, P.D., Tremethick, D.J., Lyons, I. (2001). Histone variant H2A.Z is required for early mammalian development, *Current biology CB*, Vol. 11, No. 15, 1183–1187, doi: 10.1016/S0960-9822(01)00329-3.

[225]   Dunn, C.J., Sarkar, P., Bailey, E.R., Farris, S., Zhao, M., Ward, J.M., Dudek, S.M., Saha, R.N. (2017). Histone hypervariants h2a.Z.1 and h2a.Z.2 play independent and context-specific roles in neuronal activity-induced transcription of arc/arg3.1 and other immediate early genes, *eNeuro*, Vol. 4, No. 4, doi: 10.1523/ENEURO.0040-17.2017.

[226]   Kim, K., Punj, V., Choi, J., Heo, K., Kim, J.-M., Laird, P.W., An, W. (2013). Gene dysregulation by histone variant h2a.Z in bladder cancer, *Epigenetics & chromatin*, Vol. 6, No. 1, 34, doi: 10.1186/1756-8935-6-34.

[227]   Vardabasso, C., Gaspar-Maia, A., Hasson, D., Pünzeler, S., Valle-Garcia, D., Straub, T., Keilhauer, E.C., Strub, T., Dong, J., Panda, T., Chung, C.-Y., Yao, J.L., Singh, R., Segura, M.F., Fontanals-Cirera, B., Verma, A., Mann, M., Hernando, E., Hake, S.B., Bernstein, E. (2015). Histone variant h2a.Z.2 mediates proliferation and drug sensitivity of malignant melanoma, *Molecular cell*, Vol. 59, No. 1, 75–88, doi: 10.1016/j.molcel.2015.05.009.

[228]   Svotelis, A., Gévry, N., Grondin, G., Gaudreau, L. (2010). H2a.Z overexpression promotes cellular proliferation of breast cancer cells, *Cell cycle (Georgetown, Tex.)*, Vol. 9, No. 2, 364–370, doi: 10.4161/cc.9.2.10465.

[229]   Dryhurst, D., Ishibashi, T., Rose, K.L., Eirín-López, J.M., McDonald, D., Silva-Moreno, B., Veldhoen, N., Helbing, C.C., Hendzel, M.J., Shabanowitz, J., Hunt, D.F., Ausió, J. (2009). Characterization of the histone h2a.Z-1 and h2a.Z-2 isoforms in vertebrates, *BMC biology*, Vol. 7, 86, doi: 10.1186/1741-7007-7-86.

[230]   Bönisch, C., Schneider, K., Pünzeler, S., Wiedemann, S.M., Bielmeier, C., Bocola, M., Eberl, H.C., Kuegel, W., Neumann, J., Kremmer, E., Leonhardt, H., Mann, M., Michaelis, J., Schermelleh, L., Hake, S.B. (2012). H2a.Z.2.2 is an alternatively spliced histone h2a.Z variant that causes severe nucleosome destabilization, *Nucleic acids research*, Vol. 40, No. 13, 5951–5964, doi: 10.1093/nar/gks267.

[231]   Wratting, D., Thistlethwaite, A., Harris, M., Zeef, L.A.H., Millar, C.B. (2012). A conserved function for the h2a.Z c terminus, *The Journal of biological chemistry*, Vol. 287, No. 23, 19148–19157, doi: 10.1074/jbc.M111.317990.

REFERENCES

[232]   Suto, R.K., Clarkson, M.J., Tremethick, D.J., Luger, K. (2000). Crystal structure of a nucleosome core particle containing the variant histone h2a.Z, *Nature structural biology*, Vol. 7, No. 12, 1121–1124, doi: 10.1038/81971.

[233]   Thambirajah, A.A., Dryhurst, D., Ishibashi, T., Li, A., Maffey, A.H., Ausió, J. (2006). H2a.Z stabilizes chromatin in a way that is dependent on core histone acetylation, *The Journal of biological chemistry*, Vol. 281, No. 29, 20036–20044, doi: 10.1074/jbc.M601975200.

[234]   Park, Y.-J., Dyer, P.N., Tremethick, D.J., Luger, K. (2004). A new fluorescence resonance energy transfer approach demonstrates that the histone variant h2az stabilizes the histone octamer within the nucleosome, *The Journal of biological chemistry*, Vol. 279, No. 23, 24274–24282, doi: 10.1074/jbc.M313152200.

[235]   Abbott, D.W., Ivanova, V.S., Wang, X., Bonner, W.M., Ausió, J. (2001). Characterization of the stability and folding of h2a.Z chromatin particles: Implications for transcriptional activation, *The Journal of biological chemistry*, Vol. 276, No. 45, 41945–41949, doi: 10.1074/jbc.M108217200.

[236]   Jin, C., Felsenfeld, G. (2007). Nucleosome stability mediated by histone variants h3.3 and h2a.Z, *Genes & development*, Vol. 21, No. 12, 1519–1529, doi: 10.1101/gad.1547707.

[237]   Weber, C.M., Henikoff, J.G., Henikoff, S. (2010). H2a.Z nucleosomes enriched over active genes are homotypic, *Nature structural & molecular biology*, Vol. 17, No. 12, 1500–1507, doi: 10.1038/nsmb.1926.

[238]   Chen, P., Zhao, J., Wang, Y., Wang, M., Long, H., Liang, D., Huang, L., Wen, Z., Li, W., Li, X., Feng, H., Zhao, H., Zhu, P., Li, M., Wang, Q., Li, G. (2013). H3.3 actively marks enhancers and primes gene transcription via opening higher-ordered chromatin, *Genes & development*, Vol. 27, No. 19, 2109–2124, doi: 10.1101/gad.222174.113.

[239]   Fan, J.Y., Rangasamy, D., Luger, K., Tremethick, D.J. (2004). H2a.Z alters the nucleosome surface to promote hp1alpha-mediated chromatin fiber folding, *Molecular cell*, Vol. 16, No. 4, 655–661, doi: 10.1016/j.molcel.2004.10.023.

[240]   Thambirajah, A.A., Li, A., Ishibashi, T., Ausió, J. (2009). New developments in post-translational modifications and functions of histone h2a variants, *Biochemistry and Cell Biology*, Vol. 87, No. 1, 7–17, doi: 10.1139/o08-103.

[241]   Kalocsay, M., Hiller, N.J., Jentsch, S. (2009). Chromosome-wide rad51 spreading and sumo-h2a.Z-dependent chromosome fixation in response to a persistent dna double-strand break, *Molecular cell*, Vol. 33, No. 3, 335–343, doi: 10.1016/j.molcel.2009.01.016.

[242]   Sarcinella, E., Zuzarte, P.C., Lau, P.N.I., Draker, R., Cheung, P. (2007). Monoubiquitylation of h2a.Z distinguishes its association with euchromatin or facultative heterochromatin, *Molecular and cellular biology*, Vol. 27, No. 18, 6457–6468, doi: 10.1128/MCB.00241-07.

[243]   Billon, P., Côté, J. (2013). Precise deposition of histone h2a.Z in chromatin for genome expression and maintenance, *Biochimica et biophysica acta*, Vol. 1819, 3-4, 290–302, doi: 10.1016/j.bbagrm.2011.10.004.

[244]   Bruce, K., Myers, F.A., Mantouvalou, E., Lefevre, P., Greaves, I., Bonifer, C., Tremethick, D.J., Thorne, A.W., Crane-Robinson, C. (2005). The replacement histone h2a.Z in a hyperacetylated form is a feature of active genes in the chicken, *Nucleic acids research*, Vol. 33, No. 17, 5633–5639, doi: 10.1093/nar/gki874.

[245]   Ren, Q., Gorovsky, M.A. (2001). Histone H2A.Z Acetylation Modulates an Essential Charge Patch, *Molecular cell*, Vol. 7, No. 6, 1329–1335, doi: 10.1016/S1097-2765(01)00269-6.

[246]   Valdés-Mora, F., Song, J.Z., Statham, A.L., Strbenac, D., Robinson, M.D., Nair, S.S., Patterson, K.I., Tremethick, D.J., Stirzaker, C., Clark, S.J. (2012). Acetylation of h2a.Z is a key epigenetic modification associated with gene deregulation and epigenetic remodeling in cancer, *Genome research*, Vol. 22, No. 2, 307–321, doi: 10.1101/gr.118919.110.

[247]   Valdés-Mora, F., Gould, C.M., Colino-Sanguino, Y., Qu, W., Song, J.Z., Taylor, K.M., Buske, F.A., Statham, A.L., Nair, S.S., Armstrong, N.J., Kench, J.G., Lee, K.M.L., Horvath, L.G., Qiu, M., Ilinykh, A., Yeo-Teh, N.S., Gallego-Ortega, D., Stirzaker, C., Clark, S.J. (2017). Acetylated histone variant h2a.Z is involved in the activation of neo-enhancers in prostate cancer, *Nature communications*, Vol. 8, No. 1, 1346, doi: 10.1038/s41467-017-01393-8.

[248]   Colino-Sanguino, Y., Clark, S.J., Valdes-Mora, F. (2016). H2a.Z acetylation and transcription: Ready, steady, go!, *Epigenomics*, Vol. 8, No. 5, 583–586, doi: 10.2217/epi-2016-0016.

[249]   Keogh, M.-C., Mennella, T.A., Sawa, C., Berthelet, S., Krogan, N.J., Wolek, A., Podolny, V., Carpenter, L.R., Greenblatt, J.F., Baetz, K., Buratowski, S. (2006). The saccharomyces cerevisiae histone h2a variant htz1 is acetylated by nua4, *Genes & development*, Vol. 20, No. 6, 660–665, doi: 10.1101/gad.1388106.

[250]   Millar, C.B., Xu, F., Zhang, K., Grunstein, M. (2006). Acetylation of h2az lys 14 is associated with genome-wide gene activity in yeast, *Genes & development*, Vol. 20, No. 6, 711–722, doi: 10.1101/gad.1395506.

[251]   Giaimo, B.D., Ferrante, F., Vallejo, D.M., Hein, K., Gutierrez-Perez, I., Nist, A., Stiewe, T., Mittler, G., Herold, S., Zimmermann, T., Bartkuhn, M., Schwarz, P., Oswald, F., Dominguez, M., Borggrefe, T. (2018). Histone variant h2a.Z deposition and acetylation directs the canonical notch signaling response, *Nucleic acids research*, Vol. 46, No. 16, 8197–8215, doi: 10.1093/nar/gky551.

[252]   Guillemette, B., Gaudreau, L. (2006). Reuniting the contrasting functions of h2a.Z, *Biochemistry and Cell Biology*, Vol. 84, No. 4, 528–535, doi: 10.1139/o06-077.

REFERENCES

[253]   Marques, M., Laflamme, L., Gervais, A.L., Gaudreau, L. (2010). Reconciling
        the positive and negative roles of histone h2a.Z in gene transcription,
        Epigenetics, Vol. 5, No. 4, 267–272, doi: 10.4161/epi.5.4.11520.

[254]   Hardy, S., Jacques, P.-E., Gévry, N., Forest, A., Fortin, M.-E., Laflamme, L.,
        Gaudreau, L., Robert, F. (2009). The euchromatic and heterochromatic
        landscapes are shaped by antagonizing effects of transcription on h2a.Z
        deposition, *PLoS genetics*, Vol. 5, No. 10, e1000687, doi:
        10.1371/journal.pgen.1000687.

[255]   Greaves, I.K., Rangasamy, D., Ridgway, P., Tremethick, D.J. (2007). H2a.Z
        contributes to the unique 3d structure of the centromere, *Proceedings of the
        National Academy of Sciences of the United States of America*, Vol. 104, No. 2,
        525–530, doi: 10.1073/pnas.0607870104.

[256]   Rangasamy, D., Berven, L., Ridgway, P., Tremethick, D.J. (2003).
        Pericentric heterochromatin becomes enriched with h2a.Z during early
        mammalian development, *The EMBO journal*, Vol. 22, No. 7, 1599–1607, doi:
        10.1093/emboj/cdg160.

[257]   Procida, T., Friedrich, T., Jack, A.P.M., Peritore, M., Bönisch, C., Eberl, H.C.,
        Daus, N., Kletenkov, K., Nist, A., Stiewe, T., Borggrefe, T., Mann, M., Bartkuhn,
        M., Hake, S.B. (2021). Jazf1, a novel p400/tip60/nua4 complex member,
        regulates h2a.Z acetylation at regulatory regions, *International journal of
        molecular sciences*, Vol. 22, No. 2, doi: 10.3390/ijms22020678.

[258]   Pünzeler, S., Link, S., Wagner, G., Keilhauer, E.C., Kronbeck, N., Spitzer,
        R.M., Leidescher, S., Markaki, Y., Mentele, E., Regnard, C., Schneider, K.,
        Takahashi, D., Kusakabe, M., Vardabasso, C., Zink, L.M., Straub, T., Bernstein,
        E., Harata, M., Leonhardt, H., Mann, M., Rupp, R.A., Hake, S.B. (2017).
        Multivalent binding of pwwp2a to h2a.Z regulates mitosis and neural crest
        differentiation, *The EMBO journal*, Vol. 36, No. 15, 2263–2279, doi:
        10.15252/embj.201695757.

[259]   Giaimo, B.D., Ferrante, F., Herchenröther, A., Hake, S.B., Borggrefe, T.
        (2019). The histone variant h2a.Z in gene regulation, *Epigenetics & chromatin*,
        Vol. 12, No. 1, 37, doi: 10.1186/s13072-019-0274-9.

[260]   Brahma, S., Udugama, M.I., Kim, J., Hada, A., Bhardwaj, S.K., Hailu, S.G.,
        Lee, T.-H., Bartholomew, B. (2017). Ino80 exchanges h2a.Z for h2a by
        translocating on dna proximal to histone dimers, *Nature communications*, Vol.
        8, 15616, doi: 10.1038/ncomms15616.

[261]   Obri, A., Ouararhni, K., Papin, C., Diebold, M.-L., Padmanabhan, K., Marek,
        M., Stoll, I., Roy, L., Reilly, P.T., Mak, T.W., Dimitrov, S., Romier, C., Hamiche,
        A. (2014). Anp32e is a histone chaperone that removes h2a.Z from chromatin,
        Nature, Vol. 505, No. 7485, 648–653, doi: 10.1038/nature12922.

[262]   Latrick, C.M., Marek, M., Ouararhni, K., Papin, C., Stoll, I., Ignatyeva, M.,
        Obri, A., Ennifar, E., Dimitrov, S., Romier, C., Hamiche, A. (2016). Molecular
        basis and specificity of h2a.Z-h2b recognition and deposition by the histone

chaperone yl1, *Nature structural & molecular biology*, Vol. 23, No. 4, 309–316, doi: 10.1038/nsmb.3189.

[263]   Liang, X., Shan, S., Pan, L., Zhao, J., Ranjan, A., Wang, F., Zhang, Z., Huang, Y., Feng, H., Wei, D., Huang, L., Liu, X., Zhong, Q., Lou, J., Li, G., Wu, C., Zhou, Z. (2016). Structural basis of h2a.Z recognition by srcap chromatin-remodeling subunit yl1, *Nature structural & molecular biology*, Vol. 23, No. 4, 317–323, doi: 10.1038/nsmb.3190.

[264]   Bargaje, R., Alam, M.P., Patowary, A., Sarkar, M., Ali, T., Gupta, S., Garg, M., Singh, M., Purkanti, R., Scaria, V., Sivasubbu, S., Brahmachari, V., Pillai, B. (2012). Proximity of h2a.Z containing nucleosome to the transcription start site influences gene expression levels in the mammalian liver and brain, *Nucleic acids research*, Vol. 40, No. 18, 8965–8978, doi: 10.1093/nar/gks665.

[265]   Jin, C., Zang, C., Wei, G., Cui, K., Peng, W., Zhao, K., Felsenfeld, G. (2009). H3.3/h2a.Z double variant-containing nucleosomes mark 'nucleosome-free regions' of active promoters and other regulatory regions, *Nature genetics*, Vol. 41, No. 8, 941–945, doi: 10.1038/ng.409.

[266]   Heisel, S., Habel, N.C., Schuetz, N., Ruggieri, A., Meese, E. (2010). The yeats family member gas41 interacts with the general transcription factor tfiif, *BMC molecular biology*, Vol. 11, 53, doi: 10.1186/1471-2199-11-53.

[267]   Altaf, M., Auger, A., Monnet-Saksouk, J., Brodeur, J., Piquet, S., Cramet, M., Bouchard, N., Lacoste, N., Utley, R.T., Gaudreau, L., Côté, J. (2010). Nua4-dependent acetylation of nucleosomal histones h4 and h2a directly stimulates incorporation of h2a.Z by the swr1 complex, *The Journal of biological chemistry*, Vol. 285, No. 21, 15966–15977, doi: 10.1074/jbc.M110.117069.

[268]   Ikura, T., Ogryzko, V.V., Grigoriev, M., Groisman, R., Wang, J., Horikoshi, M., Scully, R., Qin, J., Nakatani, Y. (2000). Involvement of the TIP60 Histone Acetylase Complex in DNA Repair and Apoptosis, *Cell*, Vol. 102, No. 4, 463–473, doi: 10.1016/S0092-8674(00)00051-9.

[269]   Fuchs, M., Gerber, J., Drapkin, R., Sif, S., Ikura, T., Ogryzko, V., Lane, W.S., Nakatani, Y., Livingston, D.M. (2001). The p400 Complex Is an Essential E1A Transformation Target, *Cell*, Vol. 106, No. 3, 297–307, doi: 10.1016/s0092-8674(01)00450-0.

[270]   Jha, S., Shibata, E., Dutta, A. (2008). Human rvb1/tip49 is required for the histone acetyltransferase activity of tip60/nua4 and for the downregulation of phosphorylation on h2ax after dna damage, *Molecular and cellular biology*, Vol. 28, No. 8, 2690–2700, doi: 10.1128/MCB.01983-07.

[271]   Gévry, N., Chan, H.M., Laflamme, L., Livingston, D.M., Gaudreau, L. (2007). P21 transcription is regulated by differential localization of histone h2a.Z, *Genes & development*, Vol. 21, No. 15, 1869–1881, doi: 10.1101/gad.1545707.

[272]   Workman, J.L., Abmayr, S.M. (eds.) (2014). *Fundamentals of Chromatin*, Springer New York, New York, NY, doi: 10.1007/978-1-4614-8624-4.

REFERENCES

[273]   Lashgari, A., Fauteux, M., Maréchal, A., Gaudreau, L. (2018). Cellular depletion of brd8 causes p53-dependent apoptosis and induces a dna damage response in non-stressed cells, *Scientific reports*, Vol. 8, No. 1, 14089, doi: 10.1038/s41598-018-32323-3.

[274]   Samuelson, A.V., Narita, M., Chan, H.-M., Jin, J., Stanchina, E. de, McCurrach, M.E., Narita, M., Fuchs, M., Livingston, D.M., Lowe, S.W. (2005). P400 is required for e1a to promote apoptosis, *The Journal of biological chemistry*, Vol. 280, No. 23, 21915–21923, doi: 10.1074/jbc.M414564200.

[275]   Courilleau, C., Chailleux, C., Jauneau, A., Grimal, F., Briois, S., Boutet-Robinet, E., Boudsocq, F., Trouche, D., Canitrot, Y. (2012). The chromatin remodeler p400 atpase facilitates rad51-mediated repair of dna double-strand breaks, *The Journal of cell biology*, Vol. 199, No. 7, 1067–1081, doi: 10.1083/jcb.201205059.

[276]   Fujii, T., Ueda, T., Nagata, S., Fukunaga, R. (2010). Essential role of p400/mdomino chromatin-remodeling atpase in bone marrow hematopoiesis and cell-cycle progression, *The Journal of biological chemistry*, Vol. 285, No. 39, 30214–30223, doi: 10.1074/jbc.M110.104513.

[277]   Frank, S.R., Parisi, T., Taubert, S., Fernandez, P., Fuchs, M., Chan, H.-M., Livingston, D.M., Amati, B. (2003). Myc recruits the tip60 histone acetyltransferase complex to chromatin, *EMBO reports*, Vol. 4, No. 6, 575–580, doi: 10.1038/sj.embor.embor861.

[278]   Sun, Y., Jiang, X., Chen, S., Fernandes, N., Price, B.D. (2005). A role for the tip60 histone acetyltransferase in the acetylation and activation of atm, *Proceedings of the National Academy of Sciences of the United States of America*, Vol. 102, No. 37, 13182–13187, doi: 10.1073/pnas.0504211102.

[279]   Chen, D., Li, N., Wang, Y., Wu, X., Wang, B. (2018). A mini review about Tip60 functional mechanism: A potential therapeutic target in Cardiovascular Disease, *Journal of Integrative Cardiology*, Vol. 4, No. 6, doi: 10.15761/JIC.1000262.

[280]   Mao, Z., Pan, L., Wang, W., Sun, J., Shan, S., Dong, Q., Liang, X., Dai, L., Ding, X., Chen, S., Zhang, Z., Zhu, B., Zhou, Z. (2014). Anp32e, a higher eukaryotic histone chaperone directs preferential recognition for h2a.Z, *Cell research*, Vol. 24, No. 4, 389–399, doi: 10.1038/cr.2014.30.

[281]   Gursoy-Yuzugullu, O., Ayrapetov, M.K., Price, B.D. (2015). Histone chaperone anp32e removes h2a.Z from dna double-strand breaks and promotes nucleosome reorganization and dna repair, *Proceedings of the National Academy of Sciences of the United States of America*, Vol. 112, No. 24, 7507–7512, doi: 10.1073/pnas.1504868112.

[282]   Piquet, S., Le Parc, F., Bai, S.-K., Chevallier, O., Adam, S., Polo, S.E. (2018). The histone chaperone fact coordinates h2a.X-dependent signaling and repair of dna damage, *Molecular cell*, Vol. 72, No. 5, 888-901.e7, doi: 10.1016/j.molcel.2018.09.010.

REFERENCES

[283]   Fell, V.L., Schild-Poulter, C. (2015). The ku heterodimer: Function in dna repair and beyond, *Mutation research. Reviews in mutation research*, Vol. 763, 15–29, doi: 10.1016/j.mrrev.2014.06.002.

[284]   Jacquet, K., Fradet-Turcotte, A., Avvakumov, N., Lambert, J.-P., Roques, C., Pandita, R.K., Paquet, E., Herst, P., Gingras, A.-C., Pandita, T.K., Legube, G., Doyon, Y., Durocher, D., Côté, J. (2016). The tip60 complex regulates bivalent chromatin recognition by 53bp1 through direct h4k20me binding and h2ak15 acetylation, *Molecular cell*, Vol. 62, No. 3, 409–421, doi: 10.1016/j.molcel.2016.03.031.

[285]   Wu, W., Bai, S., Zhu, D., Li, K., Dong, W., He, W., Peng, S., Lai, Y., Wang, Q., Guo, Z., Liu, L., Huang, H. (2019). Overexpression of malignant brain tumor domain containing protein 1 predicts a poor prognosis of prostate cancer, *Oncology letters*, Vol. 17, No. 5, 4640–4646, doi: 10.3892/ol.2019.10109.

[286]   Zhang, H., Devoucoux, M., Song, X., Li, L., Ayaz, G., Cheng, H., Tempel, W., Dong, C., Loppnau, P., Côté, J., Min, J. (2020). Structural basis for epc1-mediated recruitment of mbtd1 into the nua4/tip60 acetyltransferase complex, *Cell reports*, Vol. 30, No. 12, 3996-4002.e4, doi: 10.1016/j.celrep.2020.03.003.

[287]   Lechtenberg, B.C., Allen, M.D., Rutherford, T.J., Freund, S.M.V., Bycroft, M. (2009). Solution structure of the fcs zinc finger domain of the human polycomb group protein l(3)mbt-like 2, *Protein science a publication of the Protein Society*, Vol. 18, No. 3, 657–661, doi: 10.1002/pro.51.

[288]   Eryilmaz, J., Pan, P., Amaya, M.F., Allali-Hassani, A., Dong, A., Adams-Cioaba, M.A., Mackenzie, F., Vedadi, M., Min, J. (2009). Structural studies of a four-mbt repeat protein mbtd1, *PloS one*, Vol. 4, No. 10, e7274, doi: 10.1371/journal.pone.0007274.

[289]   Alfieri, C., Gambetta, M.C., Matos, R., Glatt, S., Sehr, P., Fraterman, S., Wilm, M., Müller, J., Müller, C.W. (2013). Structural basis for targeting the chromatin repressor sfmbt to polycomb response elements, *Genes & development*, Vol. 27, No. 21, 2367–2379, doi: 10.1101/gad.226621.113.

[290]   Rooij, J.D.E. de, van den Heuvel-Eibrink, M.M., Kollen, W.J.W., Sonneveld, E., Kaspers, G.J.L., Beverloo, H.B., Fornerod, M., Pieters, R., Zwaan, C.M. (2016). Recurrent translocation t(10;17)(p15;q21) in minimally differentiated acute myeloid leukemia results in zmynd11/mbtd1 fusion, *Genes, chromosomes & cancer*, Vol. 55, No. 3, 237–241, doi: 10.1002/gcc.22326.

[291]   Dewaele, B., Przybyl, J., Quattrone, A., Finalet Ferreiro, J., Vanspauwen, V., Geerdens, E., Gianfelici, V., Kalender, Z., Wozniak, A., Moerman, P., Sciot, R., Croce, S., Amant, F., Vandenberghe, P., Cools, J., Debiec-Rychter, M. (2014). Identification of a novel, recurrent mbtd1-cxorf67 fusion in low-grade endometrial stromal sarcoma, *International journal of cancer*, Vol. 134, No. 5, 1112–1122, doi: 10.1002/ijc.28440.

[292]   Liao, Z.-Z., Wang, Y.-D., Qi, X.-Y., Xiao, X.-H. (2019). Jazf1, a relevant metabolic regulator in type 2 diabetes, *Diabetes/metabolism research and reviews*, Vol. 35, No. 5, e3148, doi: 10.1002/dmrr.3148.

REFERENCES

[293]   Yang, M., Dai, J., Jia, Y., Suo, L., Li, S., Guo, Y., Liu, H., Li, L., Yang, G. (2014). Overexpression of juxtaposed with another zinc finger gene 1 reduces proinflammatory cytokine release via inhibition of stress-activated protein kinases and nuclear factor-κb, *The FEBS journal*, Vol. 281, No. 14, 3193–3205, doi: 10.1111/febs.12853.

[294]   Zhou, M., Xu, X., Wang, H., Yang, G., Yang, M., Zhao, X., Guo, H., Song, J., Zheng, H., Zhu, Z., Li, L. (2020). Effect of central jazf1 on glucose production is regulated by the pi3k-akt-ampk pathway, *FASEB journal official publication of the Federation of American Societies for Experimental Biology*, Vol. 34, No. 5, 7058–7074, doi: 10.1096/fj.201901836RR.

[295]   Nakajima, T., Fujino, S., Nakanishi, G., Kim, Y.-S., Jetten, A.M. (2004). Tip27: A novel repressor of the nuclear orphan receptor tak1/tr4, *Nucleic acids research*, Vol. 32, No. 14, 4194–4204, doi: 10.1093/nar/gkh741.

[296]   Yuan, L., Luo, X., Zeng, M., Zhang, Y., Yang, M., Zhang, L., Liu, R., Boden, G., Liu, H., Ma, Z.A., Li, L., Yang, G. (2015). Transcription factor tip27 regulates glucose homeostasis and insulin sensitivity in a pi3-kinase/akt-dependent manner in mice, *International journal of obesity (2005)*, Vol. 39, No. 6, 949–958, doi: 10.1038/ijo.2015.5.

[297]   Ming, G., Li, X., Yin, J., Ai, Y., Xu, D., Ma, X., Liu, Z., Liu, H., Zhou, H., Liu, Z. (2014). Jazf1 regulates visfatin expression in adipocytes via pparα and pparβ/δ signaling, *Metabolism: clinical and experimental*, Vol. 63, No. 8, 1012–1021, doi: 10.1016/j.metabol.2014.05.006.

[298]   Ming, G., Di Xiao, Gong, W., Liu, H., Liu, J., Zhou, H., Liu, Z. (2014). Jazf1 can regulate the expression of lipid metabolic genes and inhibit lipid accumulation in adipocytes, *Biochemical and biophysical research communications*, Vol. 445, No. 3, 673–680, doi: 10.1016/j.bbrc.2014.02.088.

[299]   Park, S.J., Kwon, W., Park, S., Jeong, J., Kim, D., Jang, S., Kim, S.-Y., Sung, Y., Kim, M.O., Choi, S.-K., Ryoo, Z.Y. (2021). Jazf1 acts as a regulator of insulin-producing β-cell differentiation in induced pluripotent stem cells and glucose homeostasis in mice, *The FEBS journal*, doi: 10.1111/febs.15751.

[300]   Hrzenjak, A. (2016). Jazf1/suz12 gene fusion in endometrial stromal sarcomas, *Orphanet journal of rare diseases*, Vol. 11, 15, doi: 10.1186/s13023-016-0400-8.

[301]   Panagopoulos, I., Mertens, F., Griffin, C.A. (2008). An endometrial stromal sarcoma cell line with the jazf1/phf1 chimera, *Cancer genetics and cytogenetics*, Vol. 185, No. 2, 74–77, doi: 10.1016/j.cancergencyto.2008.04.020.

[302]   Chiang, S., Ali, R., Melnyk, N., McAlpine, J.N., Huntsman, D.G., Gilks, C.B., Lee, C.-H., Oliva, E. (2011). Frequency of known gene rearrangements in endometrial stromal tumors, *The American journal of surgical pathology*, Vol. 35, No. 9, 1364–1372, doi: 10.1097/PAS.0b013e3182262743.

REFERENCES

[303]   Schneider, N., Fisher, C., Thway, K. (2016). Ossifying fibromyxoid tumor:
        Morphology, genetics, and differential diagnosis, *Annals of diagnostic
        pathology*, Vol. 20, 52–58, doi: 10.1016/j.anndiagpath.2015.11.002.

[304]   Dickson, B.C., Lum, A., Swanson, D., Bernardini, M.Q., Colgan, T.J., Shaw,
        P.A., Yip, S., Lee, C.-H. (2018). Novel epc1 gene fusions in endometrial stromal
        sarcoma, *Genes, chromosomes & cancer*, Vol. 57, No. 11, 598–603, doi:
        10.1002/gcc.22649.

[305]   Makise, N., Sekimizu, M., Kobayashi, E., Yoshida, H., Fukayama, M., Kato,
        T., Kawai, A., Ichikawa, H., Yoshida, A. (2019). Low-grade endometrial stromal
        sarcoma with a novel meaf6-suz12 fusion, *Virchows Archiv an international
        journal of pathology*, Vol. 475, No. 4, 527–531, doi: 10.1007/s00428-019-
        02588-8.

[306]   Piunti, A., Smith, E.R., Morgan, M.A.J., Ugarenko, M., Khaltyan, N., Helmin,
        K.A., Ryan, C.A., Murray, D.C., Rickels, R.A., Yilmaz, B.D., Rendleman, E.J.,
        Savas, J.N., Singer, B.D., Bulun, S.E., Shilatifard, A. (2019). Catacomb: An
        endogenous inducible gene that antagonizes h3k27 methylation activity of
        polycomb repressive complex 2 via an h3k27m-like mechanism, *Science
        advances*, Vol. 5, No. 7, eaax2887, doi: 10.1126/sciadv.aax2887.

[307]   Tang, J., Cho, N.W., Cui, G., Manion, E.M., Shanbhag, N.M., Botuyan, M.V.,
        Mer, G., Greenberg, R.A. (2013). Acetylation limits 53bp1 association with
        damaged chromatin to promote homologous recombination, *Nature structural &
        molecular biology*, Vol. 20, No. 3, 317–325, doi: 10.1038/nsmb.2499.

[308]   Kakarougkas, A., Ismail, A., Chambers, A.L., Riballo, E., Herbert, A.D.,
        Künzel, J., Löbrich, M., Jeggo, P.A., Downs, J.A. (2014). Requirement for pbaf
        in transcriptional repression and repair at dna breaks in actively transcribed
        regions of chromatin, *Molecular cell*, Vol. 55, No. 5, 723–732, doi:
        10.1016/j.molcel.2014.06.028.

[309]   Meisenberg, C., Pinder, S.I., Hopkins, S.R., Wooller, S.K., Benstead-Hume,
        G., Pearl, F.M.G., Jeggo, P.A., Downs, J.A. (2019). Repression of transcription
        at dna breaks requires cohesin throughout interphase and prevents genome
        instability, *Molecular cell*, Vol. 73, No. 2, 212-223.e7, doi:
        10.1016/j.molcel.2018.11.001.

[310]   Link, S., Spitzer, R.M.M., Sana, M., Torrado, M., Völker-Albert, M.C.,
        Keilhauer, E.C., Burgold, T., Pünzeler, S., Low, J.K.K., Lindström, I., Nist, A.,
        Regnard, C., Stiewe, T., Hendrich, B., Imhof, A., Mann, M., Mackay, J.P.,
        Bartkuhn, M., Hake, S.B. (2018). Pwwp2a binds distinct chromatin moieties and
        interacts with an mta1-specific core nurd complex, *Nature communications*, Vol.
        9, No. 1, 4300, doi: 10.1038/s41467-018-06665-5.

[311]   Hattori, T., Coustry, F., Stephens, S., Eberspaecher, H., Takigawa, M.,
        Yasuda, H., Crombrugghe, B. de (2008). Transcriptional regulation of
        chondrogenesis by coactivator tip60 via chromatin association with sox9 and
        sox5, *Nucleic acids research*, Vol. 36, No. 9, 3011–3024, doi:
        10.1093/nar/gkn150.

[312]   Hamidi, H., Lilja, J., Ivaska, J. (2017). Using xcelligence rtca instrument to measure cell adhesion, *Bio-protocol*, Vol. 7, No. 24, doi: 10.21769/BioProtoc.2646.

[313]   Ke, N., Wang, X., Xu, X., Abassi, Y.A. (2011). The xcelligence system for real-time and label-free monitoring of cell viability, *Methods in molecular biology (Clifton, N.J.)*, Vol. 740, 33–43, doi: 10.1007/978-1-61779-108-6_6.

[314]   Wickham, H. (2007). Reshaping Data with the reshape Package, *Journal of Statistical Software*, Vol. 21, No. 12, doi: 10.18637/jss.v021.i12.

[315]   Pau, G., Fuchs, F., Sklyar, O., Boutros, M., Huber, W. (2010). Ebimage--an r package for image processing with applications to cellular phenotypes, *Bioinformatics (Oxford, England)*, Vol. 26, No. 7, 979–981, doi: 10.1093/bioinformatics/btq046.

[316]   Riccardi, C., Nicoletti, I. (2006). Analysis of apoptosis by propidium iodide staining and flow cytometry, *Nature protocols*, Vol. 1, No. 3, 1458–1461, doi: 10.1038/nprot.2006.238.

[317]   Crowley, L.C., Chojnowski, G., Waterhouse, N.J. (2016). Measuring the dna content of cells in apoptosis and at different cell-cycle stages by propidium iodide staining and flow cytometry, *Cold Spring Harbor protocols*, Vol. 2016, No. 10, doi: 10.1101/pdb.prot087247.

[318]   Pozarowski, P., Darzynkiewicz, Z. (2004). Analysis of cell cycle by flow cytometry, *Methods in molecular biology (Clifton, N.J.)*, Vol. 281, 301–311, doi: 10.1385/1-59259-811-0:301.

[319]   Darzynkiewicz, Z., Huang, X., Zhao, H. (2017). Analysis of cellular dna content by flow cytometry, *Current protocols in immunology*, Vol. 119, 5.7.1-5.7.20, doi: 10.1002/cpim.36.

[320]   Shanbhag, N.M., Greenberg, R.A. (2013). The dynamics of dna damage repair and transcription, *Methods in molecular biology (Clifton, N.J.)*, Vol. 1042, 227–235, doi: 10.1007/978-1-62703-526-2_16.

[321]   Shanbhag, N.M., Rafalska-Metcalf, I.U., Balane-Bolivar, C., Janicki, S.M., Greenberg, R.A. (2010). Atm-dependent chromatin changes silence transcription in cis to dna double-strand breaks, *Cell*, Vol. 141, No. 6, 970–981, doi: 10.1016/j.cell.2010.04.038.

[322]   Shechter, D., Dormann, H.L., Allis, C.D., Hake, S.B. (2007). Extraction, purification and analysis of histones, *Nature protocols*, Vol. 2, No. 6, 1445–1457, doi: 10.1038/nprot.2007.202.

[323]   Schneeberger, C., Speiser, P., Kury, F., Zeillinger, R. (1995). Quantitative detection of reverse transcriptase-pcr products by means of a novel and sensitive dna stain, *PCR methods and applications*, Vol. 4, No. 4, 234–238, doi: 10.1101/gr.4.4.234.

[324] Dragan, A.I., Pavlovic, R., McGivney, J.B., Casas-Finet, J.R., Bishop, E.S., Strouse, R.J., Schenerman, M.A., Geddes, C.D. (2012). Sybr green i: Fluorescence properties and interaction with dna, *Journal of fluorescence*, Vol. 22, No. 4, 1189–1199, doi: 10.1007/s10895-012-1059-8.

[325] Ramírez, F., Dündar, F., Diehl, S., Grüning, B.A., Manke, T. (2014). Deeptools: A flexible platform for exploring deep-sequencing data, *Nucleic acids research*, Vol. 42, Web Server issue, W187-91, doi: 10.1093/nar/gku365.

[326] Zhang, Y., Liu, T., Meyer, C.A., Eeckhoute, J., Johnson, D.S., Bernstein, B.E., Nusbaum, C., Myers, R.M., Brown, M., Li, W., Liu, X.S. (2008). Model-based analysis of chip-seq (macs), *Genome biology*, Vol. 9, No. 9, R137, doi: 10.1186/gb-2008-9-9-r137.

[327] Love, M.I., Huber, W., Anders, S. (2014). Moderated estimation of fold change and dispersion for rna-seq data with deseq2, *Genome biology*, Vol. 15, No. 12, 550, doi: 10.1186/s13059-014-0550-8.

[328] McLean, C.Y., Bristor, D., Hiller, M., Clarke, S.L., Schaar, B.T., Lowe, C.B., Wenger, A.M., Bejerano, G. (2010). Great improves functional interpretation of cis-regulatory regions, *Nature biotechnology*, Vol. 28, No. 5, 495–501, doi: 10.1038/nbt.1630.

[329] H Backman, T.W., Girke, T. (2016). Systempiper: Ngs workflow and report generation environment, *BMC bioinformatics*, Vol. 17, 388, doi: 10.1186/s12859-016-1241-0.

[330] Reimers, M., Carey, V.J. (2006). [8] Bioconductor: An Open Source Framework for Bioinformatics and Computational Biology, *DNA Microarrays, Part B: Databases and Statistics*, Elsevier, 119–134, doi: 10.1016/S0076-6879(06)11008-3.

[331] The R Core Team (2020). R: A language and environment for statistical computing, *R Foundation for Statistical Computing*.

[332] Smith, T., Heger, A., Sudbery, I. (2017). Umi-tools: Modeling sequencing errors in unique molecular identifiers to improve quantification accuracy, *Genome research*, Vol. 27, No. 3, 491–499, doi: 10.1101/gr.209601.116.

[333] Lawrence, M., Huber, W., Pagès, H., Aboyoun, P., Carlson, M., Gentleman, R., Morgan, M.T., Carey, V.J. (2013). Software for computing and annotating genomic ranges, *PLoS computational biology*, Vol. 9, No. 8, e1003118, doi: 10.1371/journal.pcbi.1003118.

[334] Yu, G., Wang, L.-G., Han, Y., He, Q.-Y. (2012). Clusterprofiler: An r package for comparing biological themes among gene clusters, *Omics a journal of integrative biology*, Vol. 16, No. 5, 284–287, doi: 10.1089/omi.2011.0118.

[335] Sharma, A., Singh, K., Almasan, A. (2012). Histone h2ax phosphorylation: A marker for dna damage, *Methods in molecular biology (Clifton, N.J.)*, Vol. 920, 613–626, doi: 10.1007/978-1-61779-998-3_40.

[336]   Sharma, G.G., So, S., Gupta, A., Kumar, R., Cayrou, C., Avvakumov, N., Bhadra, U., Pandita, R.K., Porteus, M.H., Chen, D.J., Cote, J., Pandita, T.K. (2010). Mof and histone h4 acetylation at lysine 16 are critical for dna damage response and double-strand break repair, *Molecular and cellular biology*, Vol. 30, No. 14, 3582–3595, doi: 10.1128/MCB.01476-09.

[337]   Luo, Y.-B., Ma, J.-Y., Zhang, Q.-H., Lin, F., Wang, Z.-W., Huang, L., Schatten, H., Sun, Q.-Y. (2013). Mbtd1 is associated with pr-set7 to stabilize h4k20me1 in mouse oocyte meiotic maturation, *Cell cycle (Georgetown, Tex.)*, Vol. 12, No. 7, 1142–1150, doi: 10.4161/cc.24216.

[338]   Soria, G., Polo, S.E., Almouzni, G. (2012). Prime, repair, restore: The active role of chromatin in the dna damage response, *Molecular cell*, Vol. 46, No. 6, 722–734, doi: 10.1016/j.molcel.2012.06.002.

[339]   Jackson, A.L., Burchard, J., Leake, D., Reynolds, A., Schelter, J., Guo, J., Johnson, J.M., Lim, L., Karpilow, J., Nichols, K., Marshall, W., Khvorova, A., Linsley, P.S. (2006). Position-specific chemical modification of sirnas reduces "off-target" transcript silencing, *RNA (New York, N.Y.)*, Vol. 12, No. 7, 1197–1205, doi: 10.1261/rna.30706.

[340]   Chen, D., Huang, S. (2001). Nucleolar components involved in ribosome biogenesis cycle between the nucleolus and nucleoplasm in interphase cells, *The Journal of cell biology*, Vol. 153, No. 1, 169–176, doi: 10.1083/jcb.153.1.169.

[341]   Halkidou, K., Logan, I.R., Cook, S., Neal, D.E., Robson, C.N. (2004). Putative involvement of the histone acetyltransferase tip60 in ribosomal gene transcription, *Nucleic acids research*, Vol. 32, No. 5, 1654–1665, doi: 10.1093/nar/gkh296.

[342]   Shubina, M.Y., Musinova, Y.R., Sheval, E.V. (2016). Nucleolar methyltransferase fibrillarin: Evolution of structure and functions, *Biochemistry. Biokhimiia*, Vol. 81, No. 9, 941–950, doi: 10.1134/S0006297916090030.

[343]   Boulon, S., Westman, B.J., Hutten, S., Boisvert, F.-M., Lamond, A.I. (2010). The nucleolus under stress, *Molecular cell*, Vol. 40, No. 2, 216–227, doi: 10.1016/j.molcel.2010.09.024.

[344]   Kobiita, A., Godbersen, S., Araldi, E., Ghoshdastider, U., Schmid, M.W., Spinas, G., Moch, H., Stoffel, M. (2020). The diabetes gene jazf1 is essential for the homeostatic control of ribosome biogenesis and function in metabolic stress, *Cell reports*, Vol. 32, No. 1, 107846, doi: 10.1016/j.celrep.2020.107846.

[345]   Stanek, D., Pridalova-Hnilicová, J., Novotný, I., Huranová, M., Blazíková, M., Wen, X., Sapra, A.K., Neugebauer, K.M. (2008). Spliceosomal small nuclear ribonucleoprotein particles repeatedly cycle through cajal bodies, *Molecular biology of the cell*, Vol. 19, No. 6, 2534–2543, doi: 10.1091/mbc.E07-12-1259.

[346]   Matera, A.G., Wang, Z. (2014). A day in the life of the spliceosome, *Nature reviews. Molecular cell biology*, Vol. 15, No. 2, 108–121, doi: 10.1038/nrm3742.

REFERENCES

[347]   Sawyer, I.A., Sturgill, D., Sung, M.-H., Hager, G.L., Dundr, M. (2016). Cajal body function in genome organization and transcriptome diversity, *BioEssays news and reviews in molecular, cellular and developmental biology*, Vol. 38, No. 12, 1197–1208, doi: 10.1002/bies.201600144.

[348]   Trinkle-Mulcahy, L., Sleeman, J.E. (2017). The cajal body and the nucleolus: "in a relationship" or "it's complicated"?, *RNA biology*, Vol. 14, No. 6, 739–751, doi: 10.1080/15476286.2016.1236169.

[349]   Donati, G., Montanaro, L., Derenzini, M. (2012). Ribosome biogenesis and control of cell proliferation: P53 is not alone, *Cancer research*, Vol. 72, No. 7, 1602–1607, doi: 10.1158/0008-5472.CAN-11-3992.

[350]   Lloret-Llinares, M., Pérez-Lluch, S., Rossell, D., Morán, T., Ponsa-Cobas, J., Auer, H., Corominas, M., Azorín, F. (2012). Dkdm5/lid regulates h3k4me3 dynamics at the transcription-start site (tss) of actively transcribed developmental genes, *Nucleic acids research*, Vol. 40, No. 19, 9493–9505, doi: 10.1093/nar/gks773.

[351]   Mchaourab, Z.F., Perreault, A.A., Venters, B.J. (2018). Chip-seq and chip-exo profiling of pol ii, h2a.Z, and h3k4me3 in human k562 cells, *Scientific data*, Vol. 5, 180030, doi: 10.1038/sdata.2018.30.

[352]   Ernst, J., Kellis, M. (2012). Chromhmm: Automating chromatin-state discovery and characterization, *Nature methods*, Vol. 9, No. 3, 215–216, doi: 10.1038/nmeth.1906.

[353]   Ernst, J., Kellis, M. (2017). Chromatin-state discovery and genome annotation with chromhmm, *Nature protocols*, Vol. 12, No. 12, 2478–2492, doi: 10.1038/nprot.2017.124.

[354]   Jang, W.Y., Bae, K.B., Kim, S.H., Yu, D.H., Kim, H.J., Ji, Y.R., Park, S.J., Park, S.J., Kang, M.-C., Jeong, J. in, Park, S.-J., Lee, S.G., Lee, I., Kim, M.O., Yoon, D., Ryoo, Z.Y. (2014). Overexpression of jazf1 reduces body weight gain and regulates lipid metabolism in high fat diet, *Biochemical and biophysical research communications*, Vol. 444, No. 3, 296–301, doi: 10.1016/j.bbrc.2013.12.094.

[355]   Sung, Y., Park, S., Park, S.J., Jeong, J., Choi, M., Lee, J., Kwon, W., Jang, S., Lee, M.-H., Kim, D.J., Liu, K., Kim, S.-H., Lee, J.-H., Ha, Y.-S., Kwon, T.G., Lee, S., Dong, Z., Ryoo, Z.Y., Kim, M.O. (2018). Jazf1 promotes prostate cancer progression by activating jnk/slug, *Oncotarget*, Vol. 9, No. 1, 755–765, doi: 10.18632/oncotarget.23146.

[356]   Huang, L., Cai, Y., Luo, Y., Xiong, D., Hou, Z., Lv, J., Zeng, F., Yang, Y., Cheng, X. (2019). Jazf1 suppresses papillary thyroid carcinoma cell proliferation and facilitates apoptosis via regulating tak1/nf-κb pathways, *OncoTargets and therapy*, Vol. 12, 10501–10514, doi: 10.2147/OTT.S230597.

[357]   Uhlén, M., Fagerberg, L., Hallström, B.M., Lindskog, C., Oksvold, P., Mardinoglu, A., Sivertsson, Å., Kampf, C., Sjöstedt, E., Asplund, A., Olsson, I., Edlund, K., Lundberg, E., Navani, S., Szigyarto, C.A.-K., Odeberg, J.,

Djureinovic, D., Takanen, J.O., Hober, S., Alm, T., Edqvist, P.-H., Berling, H., Tegel, H., Mulder, J., Rockberg, J., Nilsson, P., Schwenk, J.M., Hamsten, M., Feilitzen, K. von, Forsberg, M., Persson, L., Johansson, F., Zwahlen, M., Heijne, G. von, Nielsen, J., Pontén, F. (2015). Proteomics. Tissue-based map of the human proteome, *Science (New York, N.Y.)*, Vol. 347, No. 6220, 1260419, doi: 10.1126/science.1260419.

[358]   Thul, P.J., Åkesson, L., Wiking, M., Mahdessian, D., Geladaki, A., Ait Blal, H., Alm, T., Asplund, A., Björk, L., Breckels, L.M., Bäckström, A., Danielsson, F., Fagerberg, L., Fall, J., Gatto, L., Gnann, C., Hober, S., Hjelmare, M., Johansson, F., Lee, S., Lindskog, C., Mulder, J., Mulvey, C.M., Nilsson, P., Oksvold, P., Rockberg, J., Schutten, R., Schwenk, J.M., Sivertsson, Å., Sjöstedt, E., Skogs, M., Stadler, C., Sullivan, D.P., Tegel, H., Winsnes, C., Zhang, C., Zwahlen, M., Mardinoglu, A., Pontén, F., Feilitzen, K. von, Lilley, K.S., Uhlén, M., Lundberg, E. (2017). A subcellular map of the human proteome, *Science (New York, N.Y.)*, Vol. 356, No. 6340, doi: 10.1126/science.aal3321.

[359]   Uhlen, M., Zhang, C., Lee, S., Sjöstedt, E., Fagerberg, L., Bidkhori, G., Benfeitas, R., Arif, M., Liu, Z., Edfors, F., Sanli, K., Feilitzen, K. von, Oksvold, P., Lundberg, E., Hober, S., Nilsson, P., Mattsson, J., Schwenk, J.M., Brunnström, H., Glimelius, B., Sjöblom, T., Edqvist, P.-H., Djureinovic, D., Micke, P., Lindskog, C., Mardinoglu, A., Ponten, F. (2017). A pathology atlas of the human cancer transcriptome, *Science (New York, N.Y.)*, Vol. 357, No. 6352, doi: 10.1126/science.aan2507.

[360]   Xu, Y., Sun, Y., Jiang, X., Ayrapetov, M.K., Moskwa, P., Yang, S., Weinstock, D.M., Price, B.D. (2010). The p400 atpase regulates nucleosome stability and chromatin ubiquitination during dna repair, *The Journal of cell biology*, Vol. 191, No. 1, 31–43, doi: 10.1083/jcb.201001160.

[361]   Rai, R., Dai, H., Multani, A.S., Li, K., Chin, K., Gray, J., Lahad, J.P., Liang, J., Mills, G.B., Meric-Bernstam, F., Lin, S.-Y. (2006). Brit1 regulates early dna damage response, chromosomal integrity, and cancer, *Cancer cell*, Vol. 10, No. 2, 145–157, doi: 10.1016/j.ccr.2006.07.002.

[362]   Maréchal, A., Zou, L. (2013). Dna damage sensing by the atm and atr kinases, *Cold Spring Harbor perspectives in biology*, Vol. 5, No. 9, doi: 10.1101/cshperspect.a012716.

[363]   Vilas, C.K., Emery, L.E., Denchi, E.L., Miller, K.M. (2018). Caught with one's zinc fingers in the genome integrity cookie jar, *Trends in genetics TIG*, Vol. 34, No. 4, 313–325, doi: 10.1016/j.tig.2017.12.011.

[364]   Sun, Y., Jiang, X., Price, B.D. (2010). Tip60: Connecting chromatin to dna damage signaling, *Cell cycle (Georgetown, Tex.)*, Vol. 9, No. 5, 930–936, doi: 10.4161/cc.9.5.10931.

[365]   Malewicz, M., Perlmann, T. (2014). Function of transcription factors at dna lesions in dna repair, *Experimental Cell Research*, Vol. 329, No. 1, 94–100, doi: 10.1016/j.yexcr.2014.08.032.

REFERENCES

[366]   Izhar, L., Adamson, B., Ciccia, A., Lewis, J., Pontano-Vaites, L., Leng, Y.,
        Liang, A.C., Westbrook, T.F., Harper, J.W., Elledge, S.J. (2015). A systematic
        analysis of factors localized to damaged chromatin reveals parp-dependent
        recruitment of transcription factors, *Cell reports*, Vol. 11, No. 9, 1486–1500, doi:
        10.1016/j.celrep.2015.04.053.

[367]   Franklin, C.C., Adler, V., Kraft, A.S. (1995). [37] Phosphorylation of
        transcription factors, *Oncogene techniques*, Elsevier, 550–564, doi:
        10.1016/0076-6879(95)54039-3.

[368]   Matsuoka, S., Ballif, B.A., Smogorzewska, A., McDonald, E.R., Hurov, K.E.,
        Luo, J., Bakalarski, C.E., Zhao, Z., Solimini, N., Lerenthal, Y., Shiloh, Y., Gygi,
        S.P., Elledge, S.J. (2007). Atm and atr substrate analysis reveals extensive
        protein networks responsive to dna damage, *Science (New York, N.Y.)*, Vol.
        316, No. 5828, 1160–1166, doi: 10.1126/science.1140321.

[369]   Blackford, A.N., Jackson, S.P. (2017). Atm, atr, and dna-pk: The trinity at the
        heart of the dna damage response, *Molecular cell*, Vol. 66, No. 6, 801–817, doi:
        10.1016/j.molcel.2017.05.015.

[370]   Traven, A., Heierhorst, J. (2005). Sq/tq cluster domains: Concentrated
        atm/atr kinase phosphorylation site regions in dna-damage-response proteins,
        BioEssays news and reviews in molecular, cellular and developmental biology,
        Vol. 27, No. 4, 397–407, doi: 10.1002/bies.20204.

[371]   Stanek, D., Neugebauer, K.M. (2006). The cajal body: A meeting place for
        spliceosomal snrnps in the nuclear maze, *Chromosoma*, Vol. 115, No. 5, 343–
        354, doi: 10.1007/s00412-006-0056-6.

[372]   Mahmoudi, S., Henriksson, S., Weibrecht, I., Smith, S., Söderberg, O.,
        Strömblad, S., Wiman, K.G., Farnebo, M. (2010). Wrap53 is essential for cajal
        body formation and for targeting the survival of motor neuron complex to cajal
        bodies, *PLoS biology*, Vol. 8, No. 11, e1000521, doi:
        10.1371/journal.pbio.1000521.

[373]   Jackman, J., O'Connor, P.M. (2001). Methods for synchronizing cells at
        specific stages of the cell cycle, *Current protocols in cell biology*, Chapter 8,
        Unit 8.3, doi: 10.1002/0471143030.cb0803s00.

[374]   Zentner, G.E., Saiakhova, A., Manaenkov, P., Adams, M.D., Scacheri, P.C.
        (2011). Integrative genomic analysis of human ribosomal dna, *Nucleic acids
        research*, Vol. 39, No. 12, 4949–4960, doi: 10.1093/nar/gkq1326.

[375]   Bowman, P.D., Meek, R.L., Daniel, C.W. (1976). Decreased synthesis of
        nucleolar RNA in aging human cells in vitro, *Experimental Cell Research*, Vol.
        101, No. 2, 434–437, doi: 10.1016/0014-4827(76)90399-2.

[376]   Crowley, L.C., Marfell, B.J., Scott, A.P., Waterhouse, N.J. (2016).
        Quantitation of apoptosis and necrosis by annexin v binding, propidium iodide
        uptake, and flow cytometry, *Cold Spring Harbor protocols*, Vol. 2016, No. 11,
        doi: 10.1101/pdb.prot087288.

REFERENCES

[377]   Noren Hooten, N., Evans, M.K. (2017). Techniques to induce and quantify cellular senescence, *Journal of visualized experiments JoVE, No.* 123, doi: 10.3791/55533.

[378]   Itahana, K., Campisi, J., Dimri, G.P. (2007). Methods to detect biomarkers of cellular senescence: The senescence-associated beta-galactosidase assay, *Methods in molecular biology (Clifton, N.J.)*, Vol. 371, 21–31, doi: 10.1007/978-1-59745-361-5_3.

[379]   Xu, L., Glass, C.K., Rosenfeld, M.G. (1999). Coactivator and corepressor complexes in nuclear receptor function, *Current opinion in genetics & development*, Vol. 9, No. 2, 140–147, doi: 10.1016/S0959-437X(99)80021-5.

[380]   O'Geen, H., Lin, Y.-H., Xu, X., Echipare, L., Komashko, V.M., He, D., Frietze, S., Tanabe, O., Shi, L., Sartor, M.A., Engel, J.D., Farnham, P.J. (2010). Genome-wide binding of the orphan nuclear receptor tr4 suggests its general role in fundamental biological processes, *BMC genomics*, Vol. 11, 689, doi: 10.1186/1471-2164-11-689.

[381]   Reid, J.L., Iyer, V.R., Brown, P.O., Struhl, K. (2000). Coordinate Regulation of Yeast Ribosomal Protein Genes Is Associated with Targeted Recruitment of Esa1 Histone Acetylase, *Molecular cell*, Vol. 6, No. 6, 1297–1307, doi: 10.1016/s1097-2765(00)00128-3.

[382]   Panigrahi, A., O'Malley, B.W. (2021). Mechanisms of enhancer action: the known and the unknown, *Genome biology*, Vol. 22, No. 1, doi: 10.1186/s13059-021-02322-1.

[383]   Nizovtseva, E.V., Studitsky, V.M. (2001). Mechanisms of Enhancer Action, In: John Wiley & Sons, L. (ed.), *eLS*, Wiley, 1–7, doi: 10.1002/9780470015902.a0028532.

[384]   Meng, F., Zhao, H., Zhu, B., Zhang, T., Yang, M., Li, Y., Han, Y., Jiang, J. (2021). Genomic editing of intronic enhancers unveils their role in fine-tuning tissue-specific gene expression in arabidopsis thaliana, *The Plant cell*, doi: 10.1093/plcell/koab093.

[385]   Virgilio, C. de, Loewith, R. (2006). Cell growth control: Little eukaryotes make big contributions, *Oncogene*, Vol. 25, No. 48, 6392–6415, doi: 10.1038/sj.onc.1209884.

[386]   Fingerman, I., Nagaraj, V., Norris, D., Vershon, A.K. (2003). Sfp1 plays a key role in yeast ribosome biogenesis, *Eukaryotic cell*, Vol. 2, No. 5, 1061–1068, doi: 10.1128/EC.2.5.1061-1068.2003.

[387]   Madeira, F., Park, Y.M., Lee, J., Buso, N., Gur, T., Madhusoodanan, N., Basutkar, P., Tivey, A.R.N., Potter, S.C., Finn, R.D., Lopez, R. (2019). The embl-ebi search and sequence analysis tools apis in 2019, *Nucleic acids research*, Vol. 47, W1, W636-W641, doi: 10.1093/nar/gkz268.

[388]   Cipollina, C., van den Brink, J., Daran-Lapujade, P., Pronk, J.T., Vai, M., Winde, J.H. de (2008). Revisiting the role of yeast sfp1 in ribosome biogenesis

and cell size control: A chemostat study, *Microbiology (Reading, England)*, Vol. 154, Pt 1, 337–346, doi: 10.1099/mic.0.2007/011767-0.

[389]   Marion, R.M., Regev, A., Segal, E., Barash, Y., Koller, D., Friedman, N., O'Shea, E.K. (2004). Sfp1 is a stress- and nutrient-sensitive regulator of ribosomal protein gene expression, *Proceedings of the National Academy of Sciences of the United States of America*, Vol. 101, No. 40, 14315–14322, doi: 10.1073/pnas.0405353101.

[390]   Albert, B., Tomassetti, S., Gloor, Y., Dilg, D., Mattarocci, S., Kubik, S., Hafner, L., Shore, D. (2019). Sfp1 regulates transcriptional networks driving cell growth and division through multiple promoter-binding modes, *Genes & development*, Vol. 33, 5-6, 288–293, doi: 10.1101/gad.322040.118.

[391]   Jiang, Y., Berg, M.D., Genereaux, J., Ahmed, K., Duennwald, M.L., Brandl, C.J., Lajoie, P. (2019). Sfp1 links torc1 and cell growth regulation to the yeast saga-complex component tra1 in response to polyq proteotoxicity, *Traffic (Copenhagen, Denmark)*, Vol. 20, No. 4, 267–283, doi: 10.1111/tra.12637.

[392]   Lempiäinen, H., Uotila, A., Urban, J., Dohnal, I., Ammerer, G., Loewith, R., Shore, D. (2009). Sfp1 interaction with torc1 and mrs6 reveals feedback regulation on tor signaling, *Molecular cell*, Vol. 33, No. 6, 704–716, doi: 10.1016/j.molcel.2009.01.034.

[393]   Grant, P.A., Schieltz, D., Pray-Grant, M.G., Yates, J.R., Workman, J.L. (1998). The ATM-Related Cofactor Tra1 Is a Component of the Purified SAGA Complex, *Molecular cell*, Vol. 2, No. 6, 863–867, doi: 10.1016/S1097-2765(00)80300-7.

[394]   Boudreault, A.A., Cronier, D., Selleck, W., Lacoste, N., Utley, R.T., Allard, S., Savard, J., Lane, W.S., Tan, S., Côté, J. (2003). Yeast enhancer of polycomb defines global esa1-dependent acetylation of chromatin, *Genes & development*, Vol. 17, No. 11, 1415–1428, doi: 10.1101/gad.1056603.

[395]   Xu, Z., Norris, D. (1998). The sfp1 gene product of saccharomyces cerevisiae regulates g2/m transitions during the mitotic cell cycle and dna-damage response, *Genetics*, Vol. 150, No. 4, 1419–1428.

[396]   Meng, F., Lin, Y., Yang, M., Li, M., Yang, G., Hao, P., Li, L. (2018). Jazf1 inhibits adipose tissue macrophages and adipose tissue inflammation in diet-induced diabetic mice, *BioMed research international*, Vol. 2018, 4507659, doi: 10.1155/2018/4507659.

[397]   Li, L., Yang, Y., Yang, G., Lu, C., Yang, M., Liu, H., Zong, H. (2011). The role of jazf1 on lipid metabolism and related genes in vitro, *Metabolism: clinical and experimental*, Vol. 60, No. 4, 523–530, doi: 10.1016/j.metabol.2010.04.021.

[398]   Yuasa, K., Aoki, N., Hijikata, T. (2015). Jazf1 promotes proliferation of c2c12 cells, but retards their myogenic differentiation through transcriptional repression of mef2c and mrf4-implications for the role of jazf1 variants in oncogenesis and type 2 diabetes, *Experimental Cell Research*, Vol. 336, No. 2, 287–297, doi: 10.1016/j.yexcr.2015.06.009.

[399]   Tomescu, O., Barr, F.G. (2001). Chromosomal translocations in sarcomas: prospects for therapy, *Trends in Molecular Medicine*, Vol. 7, No. 12, 554–559, doi: 10.1016/S1471-4914(01)02244-4.

[400]   Capozzi, V.A., Monfardini, L., Ceni, V., Cianciolo, A., Butera, D., Gaiano, M., Berretta, R. (2020). Endometrial stromal sarcoma: A review of rare mesenchymal uterine neoplasm, *The journal of obstetrics and gynaecology research*, Vol. 46, No. 11, 2221–2236, doi: 10.1111/jog.14436.

[401]   Koontz, J.I., Soreng, A.L., Nucci, M., Kuo, F.C., Pauwels, P., van den Berghe, H., Dal Cin, P., Fletcher, J.A., Sklar, J. (2001). Frequent fusion of the jazf1 and jjaz1 genes in endometrial stromal tumors, *Proceedings of the National Academy of Sciences of the United States of America*, Vol. 98, No. 11, 6348–6353, doi: 10.1073/pnas.101132598.

[402]   Ma, X., Wang, J., Wang, J., Ma, C.X., Gao, X., Patriub, V., Sklar, J.L. (2017). The jazf1-suz12 fusion protein disrupts prc2 complexes and impairs chromatin repression during human endometrial stromal tumorogenesis, *Oncotarget*, Vol. 8, No. 3, 4062–4078, doi: 10.18632/oncotarget.13270.

[403]   Han, L., Liu, Y.J., Ricciotti, R.W., Mantilla, J.G. (2020). A novel mbtd1-phf1 gene fusion in endometrial stromal sarcoma: A case report and literature review, *Genes, chromosomes & cancer*, Vol. 59, No. 7, 428–432, doi: 10.1002/gcc.22845.

[404]   Schoolmeester, J.K., Sukov, W.R., Maleszewski, J.J., Bedroske, P.P., Folpe, A.L., Hodge, J.C. (2013). Jazf1 rearrangement in a mesenchymal tumor of nonendometrial stromal origin: Report of an unusual ossifying sarcoma of the heart demonstrating jazf1/phf1 fusion, *The American journal of surgical pathology*, Vol. 37, No. 6, 938–942, doi: 10.1097/PAS.0b013e318282da9d.

[405]   Li, H., Ma, X., Wang, J., Koontz, J., Nucci, M., Sklar, J. (2007). Effects of rearrangement and allelic exclusion of jjaz1/suz12 on cell proliferation and survival, *Proceedings of the National Academy of Sciences of the United States of America*, Vol. 104, No. 50, 20001–20006, doi: 10.1073/pnas.0709986104.

[406]   Hattori, E., Oyama, R., Kondo, T. (2019). Systematic review of the current status of human sarcoma cell lines, *Cells*, Vol. 8, No. 2, doi: 10.3390/cells8020157.

[407]   Girard, N., Bazille, C., Lhuissier, E., Benateau, H., Llombart-Bosch, A., Boumediene, K., Bauge, C. (2014). 3-deazaneplanocin a (dznep), an inhibitor of the histone methyltransferase ezh2, induces apoptosis and reduces cell migration in chondrosarcoma cells, *PloS one*, Vol. 9, No. 5, e98176, doi: 10.1371/journal.pone.0098176.

[408]   Pereira, J.D., Sansom, S.N., Smith, J., Dobenecker, M.-W., Tarakhovsky, A., Livesey, F.J. (2010). Ezh2, the histone methyltransferase of prc2, regulates the balance between self-renewal and differentiation in the cerebral cortex, *Proceedings of the National Academy of Sciences of the United States of America*, Vol. 107, No. 36, 15957–15962, doi: 10.1073/pnas.1002530107.

REFERENCES

[409]   Look, A.T. (1997). Oncogenic transcription factors in the human acute leukemias, *Science (New York, N.Y.)*, Vol. 278, No. 5340, 1059–1064, doi: 10.1126/science.278.5340.1059.

[410]   Tempescul, A., Guillerm, G., Douet-Guilbert, N., Morel, F., Le Bris, M.-J., Braekeleer, M. de (2007). Translocation (10;17)(p15;q21) is a recurrent anomaly in acute myeloblastic leukemia, *Cancer genetics and cytogenetics*, Vol. 172, No. 1, 74–76, doi: 10.1016/j.cancergencyto.2006.08.001.

APPENDIX
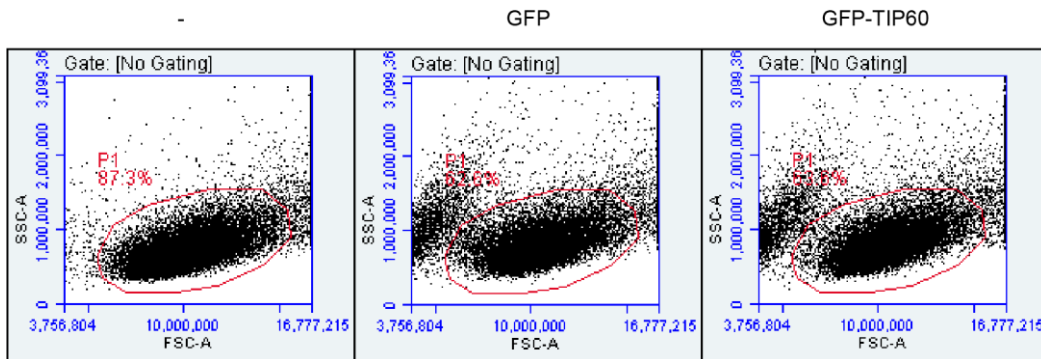
Figure A.1: Density-plot of transiently expressing GFP, GFP-TIP60 or non-transfected HK cell populations. Flow cytometry analysis of non-transfected (-) HK cells or transiently expressing GFP or GFP-TIP60 to determine transfection efficiency. GFP signal of 25.000 events was measured and gate plotted to forward and sideward scatter into the viable cell population of non-transfected HK cells (P1). For more information see Figure 11.
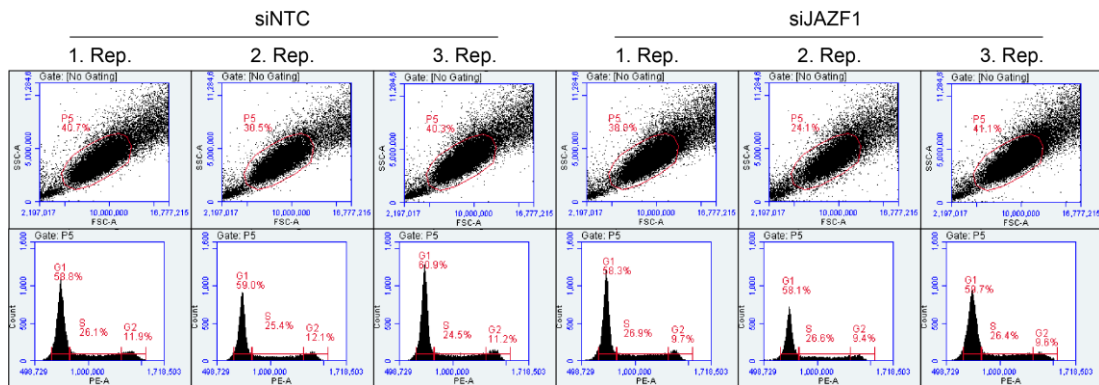
Figure A.2: JAZF1 knockdown does not lead to changes in cell cycle progression. Flow cytometry analyses of control (siNTC, three replicates) and JAZF1-depleted (siJAZF1, three replicates) HK cells stained with PI followed by the determination of the number of cells in G_1, S and G_2/M phase according to their DNA content, as shown by flow cytometry histograms (lower). Gate was plotted to forward and sideward scatter into the viable cell population of control transfected HK cells, as demonstrated by density-plots (upper). For more information see Figure 24.

<div align="center">ZnF1</div>

```
Danio rerio      -MTGIAAASFFSNICQFGGCGLHFESLAELIVHIEDNHIDTDPRVLEKQELQQPTYVALS  59
Xenopus laevis   MMTGIAAASFFSNACRFGGCGLHFTSLAELIEHIEDNHIDTDPRVLEKQELQQPTYVALS  60
Gallus gallus    -MTGIAAASFFSNACRFGGCGLHFPTLAELIEHIEDNHIDTDPRVLEKQELQQPTYVALS  59
Homo sapiens     -MTGIAAASFFSNTCRFGGCGLHFPTLADLIEHIEDNHIDTDPRVLEKQELQQPTYVALS  59
Pongo abelii     -MTGIAAASFFSNTCRFGGCGLHFPTLADLIEHIEDNHIDTDPRVLEKQELQQPTYVALS  59
Mus musculus     -MTGIAAASFFSNTCRFGGCGLHFPTLADLIEHIEDNHIDTDPRVLEKQELQQPTYVALS  59
                  *********** *.******** .**.** **************************

Danio rerio      YINRFMTDAARREHESLKKKVQPKLSLSLMGSLSRSSVATPPRHNSGNLTPPVTPPITPS  119
Xenopus laevis   YINRFMTDAARREQETLKKKIQPKLSLTLSSSVSRGNVSTPPRHGSGSLTPPVTPPITPS  120
Gallus gallus    YINRFMTDAARREQESLKKKIQPKLSLTLSSTVSRGNVSTPPRHSSGSLTPPVTPPITPS  119
Homo sapiens     YINRFMTDAARREQESLKKKIQPKLSLTLSSSVSRGNVSTPPRHSSGSLTPPVTPPITPS  119
Pongo abelii     YINRFMTDAARREQESLKKKIQPKLSLTLSSSVSRGNVSTPPRHSSGSLTPPVTPPITPS  119
Mus musculus     YINRFMTDAARREQESLKKKIQPKLSLTLSSSVSRGNVSTPPRHSSGSLTPPVTPPITPS  119
                 *************:*:****.*******.*  ..:**..*:*****.**.***********
```

<div align="right">ZnF2</div>

```
Danio rerio      SSFRSSTPTGSEYDEEEAEYEESDSDESWTTESAISSEYILSSMCMNGGDEKPFACPVPG  179
Xenopus laevis   SSFRSSTPTGSEYDEEEVDYEESDSDESWTTESAISSEAILSSMCMNGGDEKPFACPVPG  180
Gallus gallus    SSFRSSTPTGSEYDEEEVDYEESDSDESWTTESAISSEAILSSMCMNGGDEKPFACPVPG  179
Homo sapiens     SSFRSSTPTGSEYDEEEVDYEESDSDESWTTESAISSEAILSSMCMNGGEEKPFACPVPG  179
Pongo abelii     SSFRSSTPTGSEYDEEEVDYEESDSDESWTTESAISSEAILSSMCMNGGEEKPFACPVPG  179
Mus musculus     SSFRSSTPTGSEYDEEEVDYEESDSDESWTTESAISSEAILSSMCMNGGEEKPFACPVPG  179
                 *****************..:***************** ***********.**********
```

ZnF2   ZnF3

```
Danio rerio      CKKRYKNVNGIKYHAKNGHRTQIRVRKPFKCRCGKSYKSSQGLRHHTINFHPPVSAEIIR  239
Xenopus laevis   CKKRYKNVNGIKYHAKNGHRTQIRVRKPFKCRCGKSYKTAQGLRHHTINFHPPVSAEIIR  240
Gallus gallus    CKKRYKNVNGIKYHAKNGHRTQIRVRKPFKCRCGKSYKTAQGLRHHTINFHPPVSAEIIR  239
Homo sapiens     CKKRYKNVNGIKYHAKNGHRTQIRVRKPFKCRCGKSYKTAQGLRHHTINFHPPVSAEIIR  239
Pongo abelii     CKKRYKNVNGIKYHAKNGHRTQIRVRKPFKCRCGKSYKTAQGLRHHTINFHPPVSAEIIR  239
Mus musculus     CKKRYKNVNGIKYHAKNGHRTQIRVRKPFKCRCGKSYKTAQGLRHHTINFHPPVSAEMIR  239
                 ********************************.:*****************.**

Danio rerio      KLQQ  243
Xenopus laevis   KMQQ  244
Gallus gallus    KMQQ  243
Homo sapiens     KMQQ  243
Pongo abelii     KMQQ  243
Mus musculus     KMQQ  243
                 *:**
```

Figure A.3: Cross-species alignment of the JAZF1 amino acid sequence. Clustal Omega-based alignment [387] of JAZF1 protein sequences from six organisms (*Danio rerio*, *Xenopus laevis*, *Gallus gallus*, *Homo sapiens*, *Pongo abelii*, *Mus musculus*). Putative zinc finger motifs based on the human JAZF1 amino acid sequence are highlighted with colors (ZnF1 marked in blue, ZnF2 in green, ZnF3 in brown). Asterisk (*) represents fully conserved residues, colon (:) represents conserved strongly similar residues and period (.) represents conserved weakly similar residues.